INFORMATION TO USERS

This manuscript has been reproduced from the microfilm master. UMI films the text directly from the original or copy submitted. Thus, some thesis and dissertation copies are in typewriter face, while others may be from any type of computer printer.

The quality of this reproduction is dependent upon the quality of the copy submitted. Broken or indistinct print, colored or poor quality illustrations and photographs, print bleedthrough, substandard margins, and improper alignment can adversely affect reproduction.

In the unlikely event that the author did not send UMI a complete manuscript and there are missing pages, these will be noted. Also, if unauthorized copyright material had to be removed, a note will indicate the deletion.

Oversize materials (e.g., maps, drawings, charts) are reproduced by sectioning the original, beginning at the upper left-hand corner and continuing from left to right in equal sections with small overlaps.

Photographs included in the original manuscript have been reproduced xerographically in this copy. Higher quality 6" x 9" black and white photographic prints are available for any photographs or illustrations appearing in this copy for an additional charge. Contact UMI directly to order.

Bell & Howell Information and Learning
300 North Zeeb Road, Ann Arbor, MI 48106-1346 USA

UMI®
800-521-0600

The Investigation of Photoaquation Mechanisms
of Cr(III) Am(m)ine Complexes

by

Garth Irwin
B.Sc. (Hons), University of Otago, New Zealand, 1992

A Dissertation Submitted in Partial Fulfillment of the
Requirements for the Degree of

DOCTOR OF PHILOSOPHY

in the Department of Chemistry

We accept this dissertation as conforming
to the required standard

Dr. Alexander D. Kirk, Supervisor (Department of Chemistry)

Dr. David Harrington, Department Member (Department of Chemistry)

Dr. Terence Gough, Department Member (Department of Chemistry)

Dr. Arthur Watton, Outside Member (Department of Physics)

Dr. William L. Waltz, External Examiner (Department of Chemistry, University of Saskatchewan)

Supervisor: Dr. Alexander D. Kirk

Abstract

The photoaquation mechanisms for a series of Cr(III) am(m)ine complexes have been investigated using laser flash photolysis with conductivity detection. The observation of transient increases in solution conductivity at pH > 4 and a conductivity decay lifetime longer than the doublet emission decay lifetime at pH < 3, have confirmed an intermediate in the photoaquation of *cis*-Cr(cyclam)$(NH_3)_2^{3+}$. Transient increases in solution conductivity characteristic of an intermediate species were also observed for $Cr(en)_3^{3+}$, $Cr(tn)_3^{3+}$ and $Cr(sen)^{3+}$ at pH > 4.

The conductivity changes occurring in solution have been modelled for possible photoaquation mechanisms for the am(m)ine complexes, based on numerical integration of the rate expressions for all relevant mechanistic species. The comparison of these results with experimental data indicates that the intermediates observed for $Cr(en)_3^{3+}$, $Cr(tn)_3^{3+}$ and $Cr(sen)^{3+}$ are the initially formed photoproducts, $Cr(NN)_2(N\text{-}N)(OH_2)^{3+}$, where NN = a bidentate ligand or a sen arm. These species can undergo two processes, protonation of the dangling amine arm, or deprotonation of the aquo group. At low pH the first process dominates and conductivity decays due to proton uptake are observed. As the pH of the solution increases, the second process becomes competitive, and transient increases in solution conductivity are observed when this becomes the faster process.

The modelled results for *cis*-Cr(cyclam)$(NH_3)_2^{3+}$ indicate that the photoaquation occurs via two modes; i) direct loss of ammonia, and ii) loss and recoordination of a cyclam to displace ammonia, with both modes generating the observed photoproduct, *cis*-Cr(cyclam)$(NH_3)(OH_2)^{3+}$. The modelling indicates that

0.67 of the overall photochemistry occurs via the cyclam loss mode. The intermediate has been identified as the initial product of the cyclam loss mode, $Cr(cyc\text{-}N)(NH_3)_2(OH_2)^{3+}$. The rate of reaction observed via this mode is limited by the recoordination of the cyclam amine. As this is slower than the rate of doublet decay, the conductivity lifetimes observed at pH < 3 are longer than the doublet lifetime. The slow rate of recoordination also delays the release and subsequent protonation of ammonia, allowing for competitive deprotonation of the aquo group at pH > 4, and generating the observed transient increases in solution conductivity. The relevance of these results to Cr(III) chemistry in general, including possible ^2E state reaction mechanisms is discussed.

The photoaquation of $Cr(CN)_6^{3-}$ was investigated using laser flash photolysis with conductivity detection. Theory predicts that the signal magnitudes observed for this complex should be constant throughout the pH range 2.7 - 5.3. Experimental results showed that the observed signals dropped from a maximum of 120 mV at pH 2.75 to 45 mV at pH 5.25. Possible explanations for this pH dependence are presented.

The stereochemistry of the thermal and photoaquation products of *rac*- & Λ-$Cr(sen)^{3+}$ has been investigated using capillary electrophoresis. Two products were found in the photoaquation reactions, *trans*-$Cr(sen\text{-}NH)(OH_2)^{4+}$ and a product resulting from loss of a secondary amine. The thermal reaction produced *trans*-$Cr(sen\text{-}NH)(OH_2)^{4+}$ as the major product with virtually no *cis*-$Cr(sen\text{-}NH)(OH_2)^{4+}$ enantiomers being observed. Efficient racemization of Λ-$Cr(sen)^{3+}$ to Δ-$Cr(sen)^{3+}$ was also observed in the thermal reaction, consistent with racemization occurring via bond rupture and recoordination. The photoaquation results are discussed in terms of VC theory and a reinterpretation of conflicting literature results for the thermal and photochemical aquation of $Cr(sen)^{3+}$ is presented.

Examiners:

Dr. Alexander D. Kirk, Supervisor (Department of Chemistry)

Dr. David Harrington, Department Member (Department of Chemistry)

Dr. Terence Gough, Department Member (Department of Chemistry)

Dr. Arthur Watton, Outside Member (Department of Physics)

Dr. William L. Waltz, External Examiner (Department of Chemistry, University of Saskatchewan)

TABLE OF CONTENTS

List of Figures

List of Tables

List of Abbreviations

cycb	rac-5,5,7,12,12,14-hexamethyl-1,4,8,11-tetraazacycloteradecane
15aneN5	1,4,7,10,13-pentaazacyclopentadecane
18aneN6	1,4,7,10,13,16-hexaazacyclooctadecane
sen	4,4',4"-ethylidynetris(3-azabutan-1-amine)
bipy	2,2'-bipyridine
cyclam	1,4,7,11-tetraazacyclotetradecane
tet	N,N'-bis(2-aminoethyl)-1,3-diaminopropane
tren	β,β',β"-triaminotriethylamine
en	ethylenediamine
tn	1,3-diaminopropane
phen	1,10-phenanthroline
DETA	diethylenetriamine
Tris	tris(hydroxymethyl)aminomethane
DMSO	dimethyl sulfoxide
DMS	dimethyl sulfide
THF	tetrahydrofuran
tosyl	p-tolyl-sulfonyl
HPLC	high performance liquid chromatography
LFP	laser flash photolysis
NMR	nuclear magnetic resonance
UV/Vis	ultra violet and visible
CE	capillary electrophoresis
AOM	Angular Overlap Model
LF	ligand field

CT	charge transfer
VC	Vanquickenborne-Ceuleman's
BISC	Back intersystem crossing
GSI	Ground state intermediate
$\Delta V^{\ddagger}$	Volume of Activation
EOS	electroosmotic

Ligand Structures

en

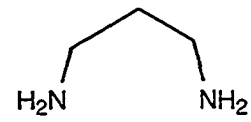

tn

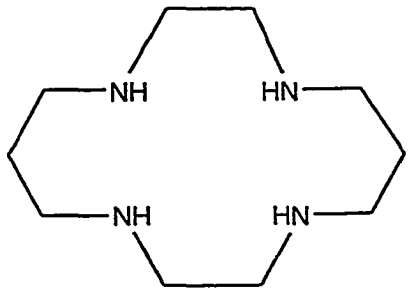

cyclam

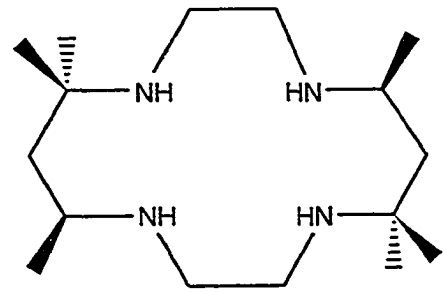

cycb

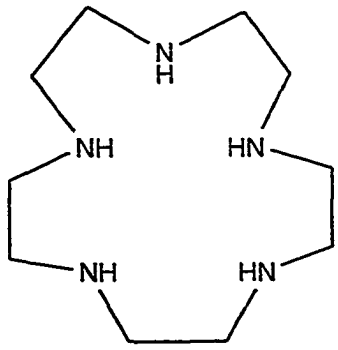

15aneN5

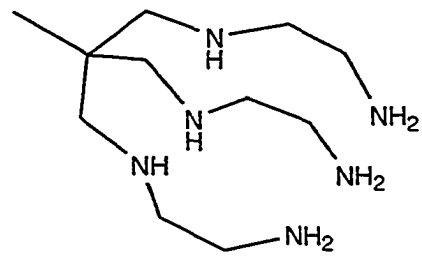

sen

Acknowledgments

There are many people who have provided the support, advice and insights that were required of this thesis and are deserving of thanks and recognition. First and foremost has to be my supervisor, Sandy Kirk. I have learnt a great deal during my time with Sandy and I wish him all the best in his retirement.

A big thanks to Rupa Fernando, LeZhen Cai and Ian Mackay, previous members of the Kirklab "family", who have provided much encouragement over the years. Ian's support in particular cannot be understated.

Cornelia Bohne and Luis Netter also deserve a vote of thanks for their technical support, advice and guidance over the years. Jack Barnes also, for teaching me the fundamentals of lasers.

I owe a great debt of gratitude to the workshop and stores people for keeping my research running when I couldn't. In particular to Terry Wiley and Terry Davies for their assistance with the conductivity apparatus, Bod Dean for computer and printer gliches, Sean Adams for a constant supply of Carius tubes and also to Roy Bennet and Dick Robinson for their assistance with numerous problems over the years.

And dare I forget the departmental secretaries. If it wasn't for Susanne Reiser, Carol Jenkins and Sandra Harris who knows what bureaucratic nightmares would have befallen me.

Thanks to Steve Rettig (deceased) and the UBC X-ray facility for kindly running our crystal structures.

Last, but not least, I would like to thank my Outdoor Support Network; Sandy Briggs, Pedro Montoya, Peter and Daniella Loock, Dave Berry, Daniel and Sophia Donnecke and in particular, Kimberley.

This dissertation is dedicated to

Friends and Family

Ad Summum

CHAPTER ONE

INTRODUCTION

1.1 General

When a molecule absorbs light energy it typically results in the excitation of an electron from one orbital to another of higher energy, forming an electronically excited state. It is the reactions and physical processes that depopulate excited states that are of interest to photochemists. For this reason photochemistry is often referred to as "the chemistry of excited states".

As they typically have different orbital occupancies, excited states often have different bond lengths and bond angles from those of the parent ground state. A change in orbital occupancy also results in different redox potentials, with excited states being both stronger oxidizing and reducing agents than the ground state. Because of these differences it is not surprising that the chemistry observed for excited state species is often richly diverse to that occurring from the ground state. This supports viewing excited states as chemically unique species and not merely as ground state molecules with extra energy.

Of major interest is the photochemistry of transition metal complexes,[1-5] with chromium (III) complexes being some of the most well studied.[6-15] The reasons for the wealth of Cr(III) studies include; the large number of thermally stable Cr(III) complexes, their well-understood spectroscopy, relatively efficient photochemical reaction and also the fact that many emit, allowing for the study of both photochemistry and photophysics.

The photochemistry of chromium (III) complexes has been actively studied for over 30 years with a large number of papers being published. However, some of the early questions are still the source of debate in the current literature. This work examines two of these, namely the role of the doublet state in photochemical reactions and the involvement of intermediates in the photoreaction mechanisms.

1.2 Electronic States of Cr(III) Complexes

Figure 1.1 shows a typical absorbance spectrum for Cr(III) complexes, characterized by two distinct spin allowed bands in the 300 - 650 nm region. A less distinct spin forbidden band, often swamped by the tail of the lowest energy spin allowed band, occurs in the 650 - 750 nm region and is shown magnified in the inset of Figure 1.1. The absorbance bands shown are labelled with the appropriate electronic transitions, introducing the states of most relevance to this thesis. The tail of a spin and symmetry allowed charge transfer (CT) band is also shown in Figure 1.1, appearing at the higher energy wavelengths.

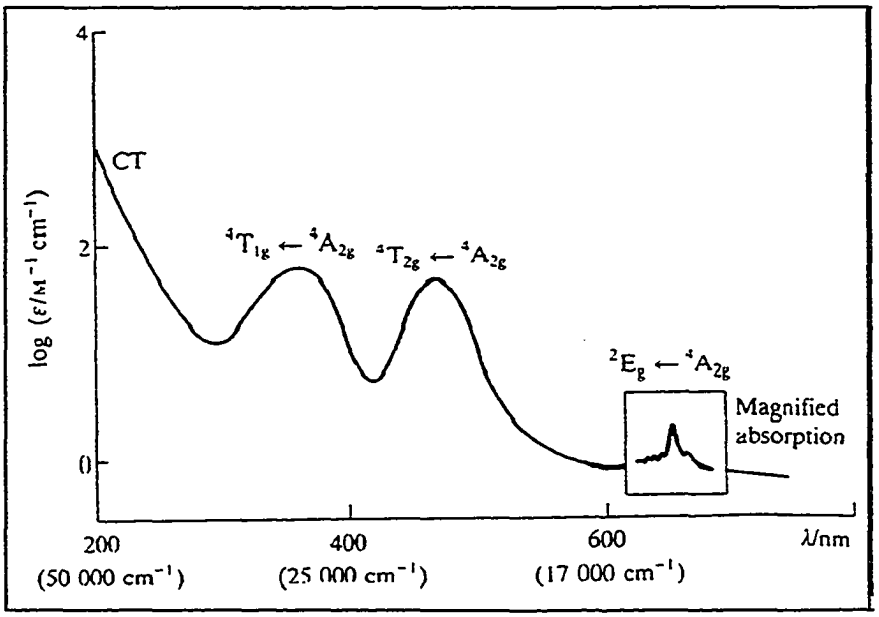

Figure 1.1 Electronic Absorption Spectrum for $Cr(NH_3)_6^{3+}$

The ground state electronic configuration for Cr(III) complexes is t_{2g}^3 with the three d electrons occupying separate orbitals and having parallel spins. Assuming octahedral symmetry, this results in a $^4A_{2g}$ ground state. Spin inversion of a single

electron within the t_{2g} manifold gives the lowest energy doublet state, ^2E_g, with the lowest energy excited quartet state being the $^4T_{2g}$ state, resulting from an in plane redistribution of electron density from a t_{2g} to an e_g^* orbital e.g. d_{xy} -> d_{x2-y2}. The higher energy $^4T_{1g}$ state also results from an e_g^*<- t_{2g} transition but involves an out of plane redistribution of electron density e.g. d_{xz} -> d_{z2} and other permutations.

As the pairing energy does not vary greatly among Cr(III) complexes the energy of the ^2E_g <- $^4A_{2g}$ transition is reasonably constant, with the variations observed resulting from the nephelauxetic effect. This transition is both symmetry and spin forbidden, resulting in a very low molar absorptivity, $\varepsilon < 1$ M^{-1} cm^{-1}. As both the $^4A_{2g}$ and ^2E_g states have a t_{2g}^3 electron configuration they have similar metal-ligand bond distances and angles, resulting in sharp absorbance and emission bands along with a small Stoke's shift.

The energy of the $^4T_{2g}$ <- $^4A_{2g}$ transition depends upon the energy difference between the t_{2g} and e_g^* orbital sets and therefore reflects the field strength of the coordinated ligands. This transition is spin allowed but symmetry forbidden with typical molar absorptivities being in the range of 10 to 100 M^{-1} cm^{-1}. As one electron occupies an antibonding e_g^* orbital, the $^4T_{2g}$ state is distorted relative to the $^4A_{2g}$ ground state. Analysis of the solid state emission spectrum for $Cr(NH_3)_6^{3+}$ shows the distortion to be tetragonal,[16] with a 12 pm bond lengthening of the Cr-N bonds in the equatorial plane and a 2 pm shortening of the axial Cr-N bonds. No fluorescence is observed from the $^4T_{2g}$ state in solution, preventing determination of the 0-0 energy. However, based on low-temperature spectroscopy this value is often estimated using the 5% rule,[16] i.e. the 0-0 energy corresponds to the wavelength at which the absorbance is 5% of the band maximum.

Two different types of CT transitions can occur within the complex; ligand to metal (LMCT) where a ligand electron is promoted to a vacant metal based orbital and metal to ligand (MLCT) where a metal electron is promoted to a vacant ligand

orbital, typically π^*. A third charge transfer transition, which is not localized to the complex, can also occur and involves an electron being transferred to the solvent (CTTS). Ligand-ligand (LL) transitions where the transition is localized on the coordinated ligand, e.g. π-π^*, are also possible.

1.3 Photophysical Processes of Cr(III) Complexes

In section 1.2 the electronic states of Cr(III) were labelled based on the octahedral microsymmetry of $Cr(NH_3)_6^{3+}$. As many of the complexes discussed are of lower symmetry the parity labels are omitted for the remainder of this thesis, referring instead to the ^2E_g and $^4T_{2g}$ states as ^2E and $^4T_2$ respectively.

Electronically excited states are thermodynamically unstable with respect to the ground state and excess energy can be dissipated via a number of deactivation processes. These processes are illustrated in the following Jablonski diagram which is specific to Cr(III), including the possible reaction pathways occurring from the $^4T_2$ and ^2E states.

Excitation of the complex generates the Franck - Condon (FC) states which are both electronically and vibrationally excited. Vibrational relaxation (VR) results in excess vibrational energy being rapidly dissipated through collisions with the solvent. Internal Conversion (IC) allows for the system to cross from a higher energy state to another of the same multiplicity. Although neither process is represented on the above diagram the combination of VR and IC allows the system to rapidly relax to the lowest energy, thermally equilibrated excited (thexi) states.

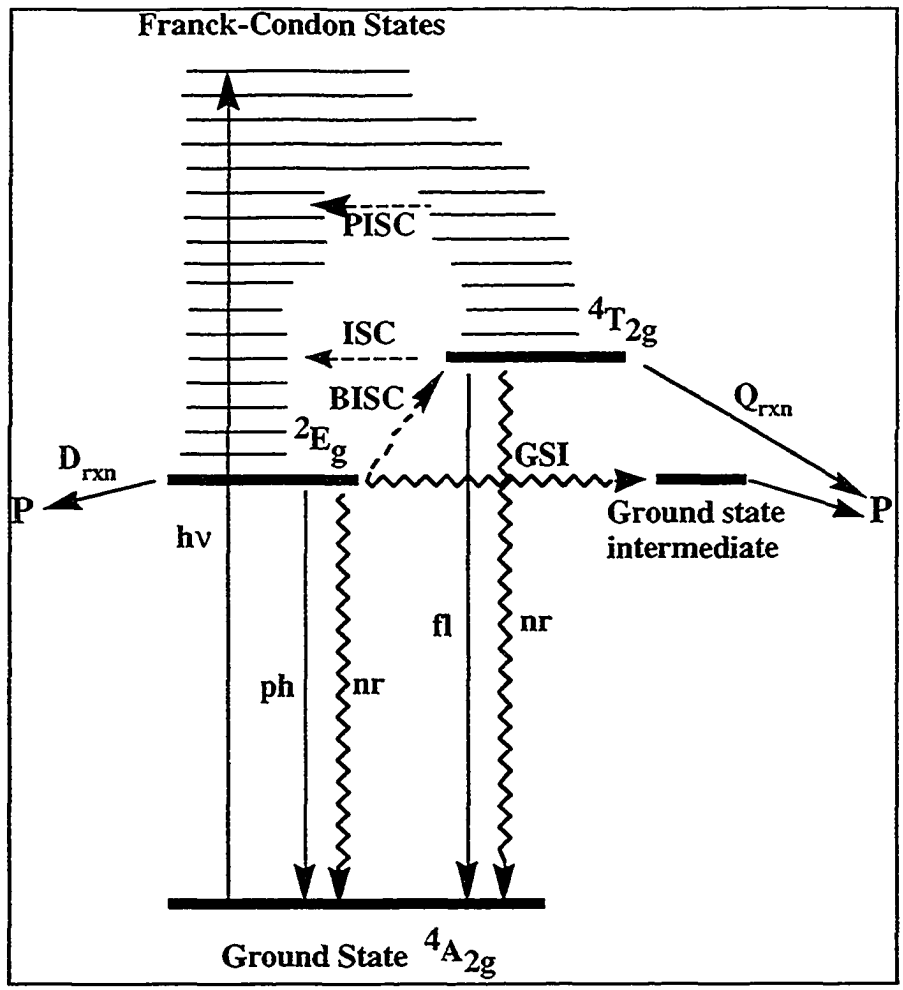

Figure 1.2 Representative Jablonski Diagram for Cr(III) Complexes

It has traditionally been assumed that the ^2E state is formed via intersystem crossing (ISC) from the equilibrated $^4T_2$ state, i.e. after VR and IC processes have occurred. Experimental evidence[17-19] indicates that ISC may be competitive with VR and IC, occuring from higher energy quartet states. This is represented in Figure 1.2 as prompt intersystem crossing (PISC).

Deactivation of the thermally equilibrated excited (thexi) states can occur via both non radiative and radiative decay. Non radiative decay involves IC or ISC from

the $^4T_2$ and ^2E states respectively, followed by vibrational relaxation to the thermally equilibrated ground state. Radiative decay (emission) occurring from the $^4T_2$ state is spin allowed and labelled fluorescence (fl) with the spin forbidden emission from the ^2E state being labelled phosphorescence (ph). As stated previously, fluorescence is not observed for Cr(III) complexes in solution, indicating that non radiative decay and/or photochemical reactions occurring from the $^4T_2$ state are highly efficient.

The photochemistry of Cr(III) complexes occurs on both prompt (sub-ns) and slow (μs) timescales, originating in the $^4T_2$ and ^2E states respectively. Direct reaction from these two states are shown as Q_{rxn} and D_{rxn} respectively. Experimental evidence[20-22] indicates that reaction does not occur directly from the ^2E state and two main alternatives have been proposed. The first is back intersystem crossing (BISC) to the $^4T_2$ state followed by quartet reaction with the second being crossing to a reactive ground state intermediate (GSI).[23-27] The relative merits of these two mechanisms have been the subject of a long lasting debate and will be discussed in more detail in section 1.9.

1.4 Cr(III) Photochemical Reactions

The type of photochemical reaction observed following irradiation of Cr(III) complexes is determined to a large extent by the band irradiated. Irradiation into the ligand field bands typically results in substitutional and isomerization reactions. Charge transfer excitation can result in photoredox reactions but efficient internal crossing to the ligand field states often occurs, resulting in predominantly substitution and photoisomerization reactions, although with a reduced quantum yield relative to LF excitation.[12,28]

The work presented in Chapters Three and Four focuses on the photoaquation reactions that occur following ligand field irradiation of Cr(III) ammine complexes in aqueous solution, where L = an am(m)ine ligand;

$$CrL_6^{n+} + H_2O \text{ ---> } CrL_5(OH_2)^{n+} + L$$

In Chapter Four the photochemical and thermal racemization reactions of $Cr(sen)^{3+}$ are also investigated.

$$\Delta\text{-}Cr(sen)^{3+} \text{ -----> } \Lambda\text{-}Cr(sen)^{3+}$$

Thermal reactions of Cr(III) complexes in aqueous solution also result in substitution of a coordinated ligand by water. The thermal chemistry of Cr(III) complexes has been the subject of a number of reviews[15,29-32] including reviews specific to fluorodiamine complexes[33] and Cr(III) cyanoam(m)ines.[12]

In the case of heteroleptic complexes, the ligand preferentially substituted in thermal reactions often contrasts with that substituted photochemically[34]. Early photolytic studies of Cr(III) complexes often referred to the photochemistry observed as being "anti-thermal".[15,35]

1.5 Adamson's Rules for Ligand Labilization

In 1967 Adamson introduced a set of empirical rules which proved highly successful in predicting the ligand labilized in the photosubstitution reactions of a number of Cr(III) and Co(III) complexes.[34]

Rule 1: "Consider the six ligands to lie in pairs at the ends of three mutually perpendicular axes. The axis having the weakest average ligand field strength will be the one labilized."

Rule 2: " If the axis contains two different ligands, then the ligand of greater field strength aquates"

These rules can be summarized in the simple statement that the strong field ligand on the weak field axis is preferentially labilized.

Although Adamson's rules still provide a useful rule of thumb for predicting the preferentially labilized ligand for Cr(III) complexes, a number of exceptions have been found. In an effort to provide a theoretical basis for both Adamson's rules, and to account for the observed exceptions, a number of theoretical models have been developed with the I* model of Vanquickenborne and Ceuleman's being the most successful.

1.6 Theoretical Models for Ligand Labilization

The $^4T_2$ state has two features likely to facilitate reaction; an electron occupying an antibonding e_g* orbital destabilizes the ligands within that plane and a vacant t_{2g} orbital makes the metal centre more accessible to nucleophilic attack. These features were recognized in the development of the following models, all based on reaction via the $^4T_2$ state.

1.6.1 Early Models

The earliest models predicting the preferentially labilized ligand for the photochemistry of various transition metal complexes, including Cr(III) were developed in a series of papers by Zink.[36-39] Although the possible influence of π-bonding effects were noted, the model predicted the leaving ligand based solely on σ-antibonding interactions. A methodology for predicting the relative extent of destabilization for each ligand was introduced based on valence state ionization energies of the ligands. It was also noted that the ligand experiencing the greatest destabilization would not necessarily have the weakest excited state bond strength and be the one preferentially labilized.

A model introduced by Wrighton et al. recognized the importance of both σ- and π-bonding effects, with three classes of ligand being introduced; σ-donor only, σ- and π-donor, and σ-donor, π-acceptor.[40] The relative ligand labilization within a particular excited complex was then predicted according to the π-bonding characteristics of the individual ligands, with destabilization increasing in the order π-donor < σ-donor < π-acceptor.

1.6.2 Vanquickenborne and Ceulemans' I* Model

The I* model, developed by Vanquickenborne and Ceulemans,[41] allows relative ligand bond strengths to be calculated for any given excited state. The basis for these calculations lie in the σ- and π- parameters derived for each ligand using the Angular Overlap Model (AOM).

The AOM[42] allows the relative d-orbital energies to be calculated for a complexed metal based upon the σ- and π-interactions with the coordinated ligands. For an octahedral complex the following equations are obtained, defining the destabilization energy for each individual orbital on the basis of its σ- and π-interactions;

$$E(d_{z2}) = E(d_{x2-y2}) = 3\sigma$$

$$E(d_{xy}) = E(d_{xz}) = E(d_{yz}) = 4\pi$$

In Ligand Field Theory the splitting energy between the t_{2g} and e_g orbital sets in an octahedral complex is assigned the value 10 Dq. Comparison with the individual d orbital energies obtained from the AOM model shows that 10 Dq = 3σ-4π.

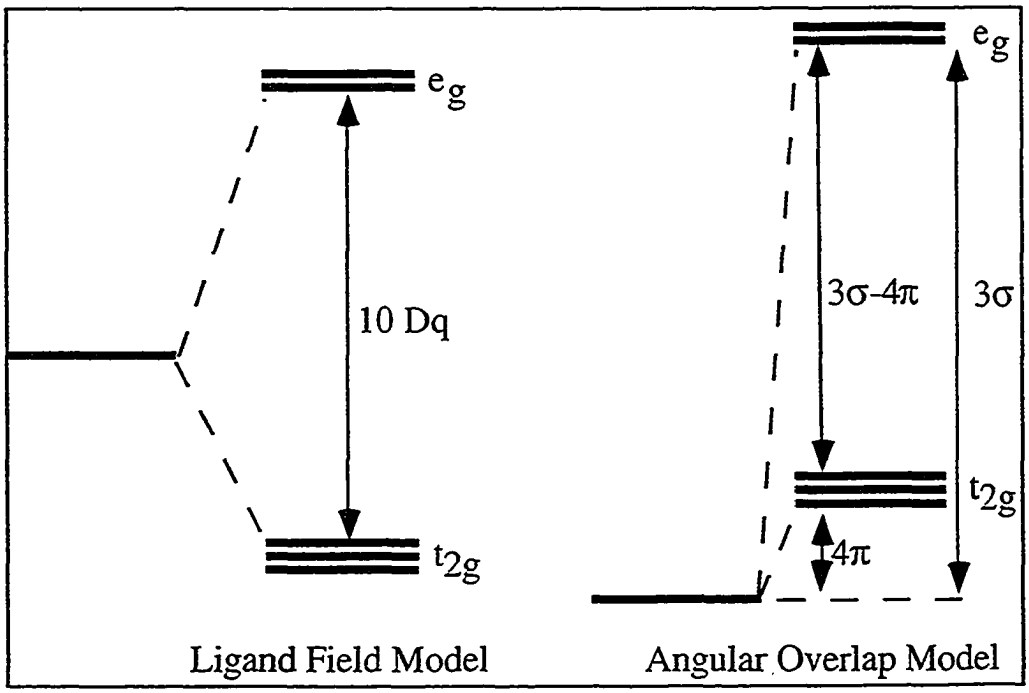

Figure 1.3 Comparison of the Ligand Field and AOM models

Similar expressions for the individual d orbital energies can be obtained using the AOM model for complexes of lower symmetry which are then related to the more complicated splitting energies observed for these complexes.

The I* model builds on the AOM model, recognizing that the individual M-L bond energies will depend on the d orbital occupancy. The total "bond energy" is defined as,

$$I_T = \Sigma\, h_i E_i$$

where h_i = number of holes in the ith orbital

E_i = energy of the ith orbital.

Because the AOM is based on additive ligand effects, the total bonding energy can be partitioned into individual ligand contributions e.g. for the simplest case of an octahedral complex $I\,(M\text{-}L) = I_T/6$.

The greatest advantage of the I* model over the earlier models is that it calculates relative excited state bond strengths, whereas earlier models estimated the relative extent of ligand destabilization. The I* model has been highly successful in predicting the ligand labilized for a series of Co(III) and Cr(III) complexes,[35] and accounts for many of the exceptions to Adamson's rules. However some exceptions to the I* model do occur, most notably with am(m)ine complexes containing fluoro[43,44], aquo[15,45] and cyano ligands.[46,47]

1.7 Photostereochemistry of Cr(III) Complexes

Photochemical reactions of Cr(III) complexes occur with stereochemical change, contrasting with thermal reactions which are typically stereoretentive. Early attempts to explain the stereochemical changes observed for Cr(III) photochemistry were empirical in nature, leading to the trans attack edge displacement mechanism. Theoretical models, which have proven highly successful in predicting the photoproduct stereochemistry for Cr(III) complexes, have been developed by Vanquickenborne and Ceulemans using a group theoretical approach.

1.7.1 Kirk's Rule and the Trans Attack Edge Displacement Mechanism

Results obtained in the photoaquations of a series of trans diacidotetram(m)ine complexes led to the proposal that; "the entering ligand will stereospecifically occupy a position corresponding to entry into the coordination sphere trans to the leaving ligand".[11]

Identification of the preferential plane of excitation and application of Kirk's rule led to the development of the trans attack, edge displacement mechanism which is illustrated in Figure 1.4 for a generic *trans*-CrL_4X_2 complex. In this example excitation is assumed to occur within the xz plane i.e. d_{xz} --> $d_{x^2-z^2}$. Assuming that X* is the leaving ligand, nucleophilic attack by the solvent occurs within the xz plane along one of the two edges trans to X*. This results in L migrating to the site occupied by X*, giving the cis product.

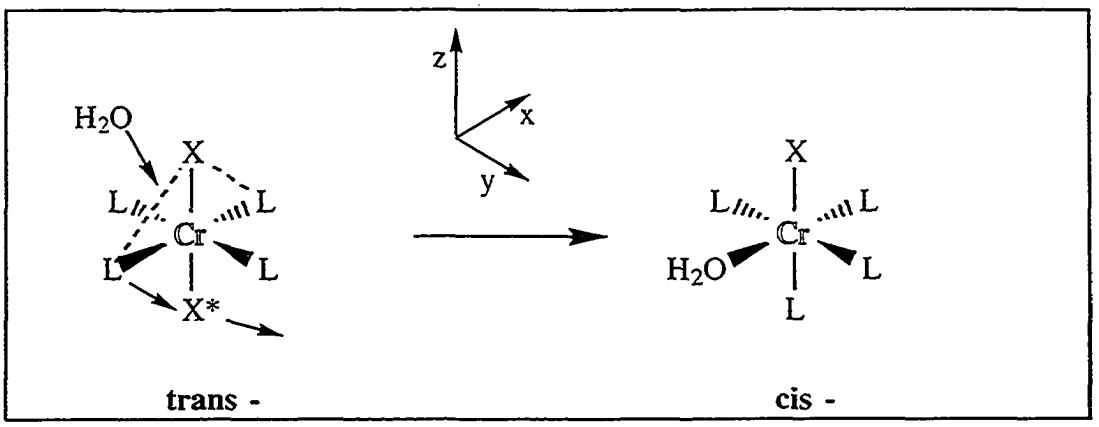

Figure 1.4 Trans attack edge displacement mechanism for Cr(III) photochemistry

Both Kirk's rule and the trans attack edge displacement are empirical, accounting for the stereochemical changes observed in Cr(III) photochemistry without providing a theoretical basis for preferential solvent attack trans to the leaving ligand. However this mechanism still provides a useful means for predicting the photoproduct stereochemistry for photolysis of Cr(III) complexes.

1.7.2 Vanquickenborne and Ceuleman's Theory of Photostereochemistry

Similar to Woodward and Hoffman's[48-51] approach for the reactions of organic molecules, Vanquickenborne and Ceuleman's developed a model based on state correlation diagrams calculated for different reaction modes.[35,52]

The model assumes that photoreaction occurs from the lowest energy quartet state and involves a series of steps:

i) dissociation of the labilized ligand to give a five coordinate, square pyramidal (SP) intermediate.

ii) rearrangement of the SP intermediate to give a trigonal bipyramidal (TBP) intermediate.

iii) attack by the nucleophile on the TBP intermediate to give the final product.

Although presented as a series of consecutive steps, the authors viewed these processes occurring in a more concerted manner.

The model is illustrated below for a generic diacidotetram(m)ine complex, trans-CrA_4XY, where A = am(m)ine ligand and X,Y = acido ligands. Assuming that acido ligands have weaker field strengths than am(m)ine ligands requires that excitation be localized within the xz or yz plane. If Y is the ligand with the weakest excited state bond it is preferentially labilized, resulting in the SP intermediate shown below in Figure 1.5. The SP intermediate can rearrange to give two possible TBP intermediates of C_{2v} and C_{3v} symmetry, corresponding to X being axial or equatorial respectively. Vanquickenborne and Ceuleman's calculated the energy changes occurring for these two processes and showed that rearrangement was energetically favourable if it involved motions within the plane of labilization, resulting in the TBP of C_{2v} symmetry. A large energy barrier towards the required ligand motions prevented formation of the C_{3v} TBP intermediate.

After formation of the C_{2v} TBP intermediate, solvent attack can occur either cis or trans to X as shown below in Figure 1.6. Calculating the energy changes for each process showed that cis attack was energetically favourable. Solvent attack trans to X was unfavourable as the photoproduct was formed in an energetically prohibitive excited state.

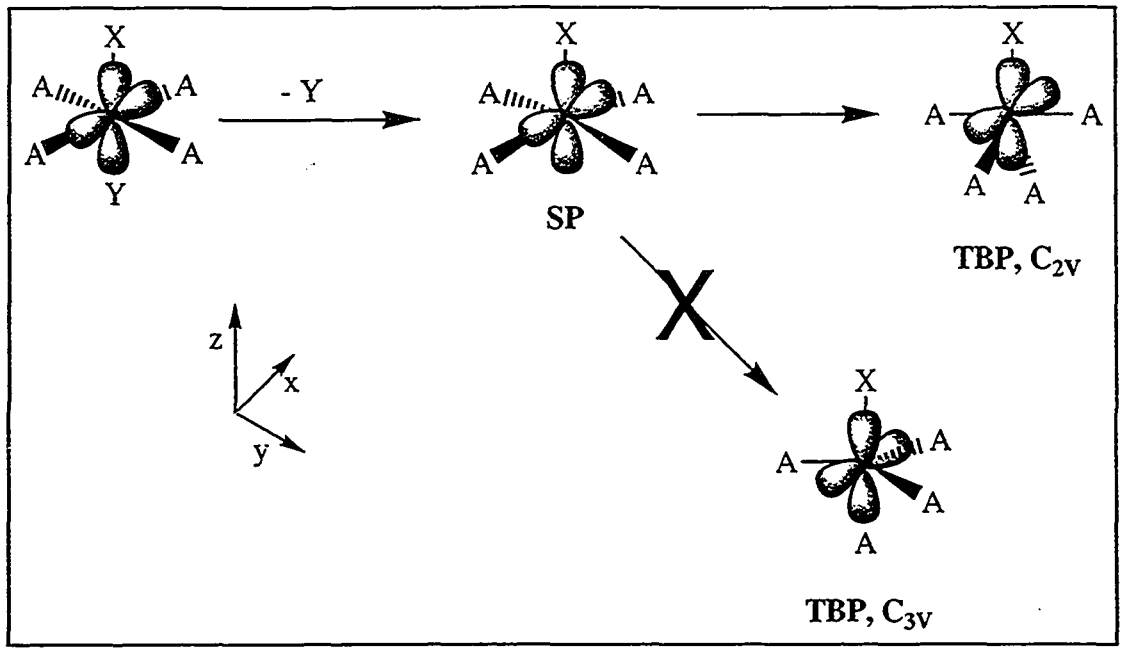

Figure 1.5 Formation of SP and TBP intermediates in the VC model

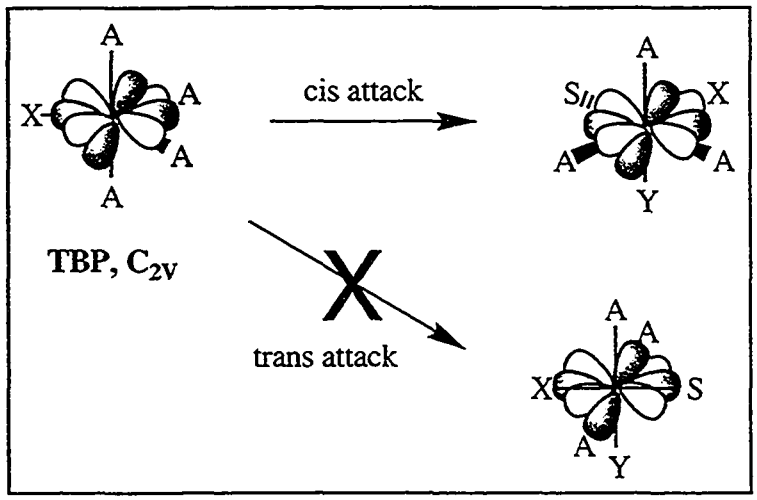

Figure 1.6 Cis and trans solvent attack on a TBP intermediate

Although this model was highly successful in accounting for the product stereochemistry observed in the majority of Cr(III) photoaquation reactions, exceptions were found. This led Vanquickenborne and Ceulemans to extend their model to include dynamic Jahn-Teller effects.[53] This proved successful in accounting for the product stereochemistries observed in the photoaquations of $Cr(NH_3)_5F^{2+}$ [54,55] and *cis-* & *trans*-$Cr(NH_3)_4F^{2+}$,[56] three complexes which were exceptions to the original VC theory.

1.7.3 Comments on VC Models

The theories developed by Vanquickenborne and Ceuleman's have been very successful in accounting for the photoproduct stereochemistry observed for Cr(III) photoaquation reactions. However the dissociative nature of the modelled mechanism conflicts with experimental evidence, including volume of activation studies,[57-61] which indicate an associative mechanism. Attempts to construct similar models for an associative mechanism have been complicated by the lack of discrimination between energy levels of possible seven coordinate intermediates and no basis for preferential ligand loss or stereochemical change can be presented. A pictorial representation for an associative mechanism has been introduced by Kirk.[8] This indicates that photoaquation via an asymmetric pentagonal bipyramidal intermediate could give the same photoproduct stereochemistry as that predicted by the original VC theory as shown in Figure 1.7.

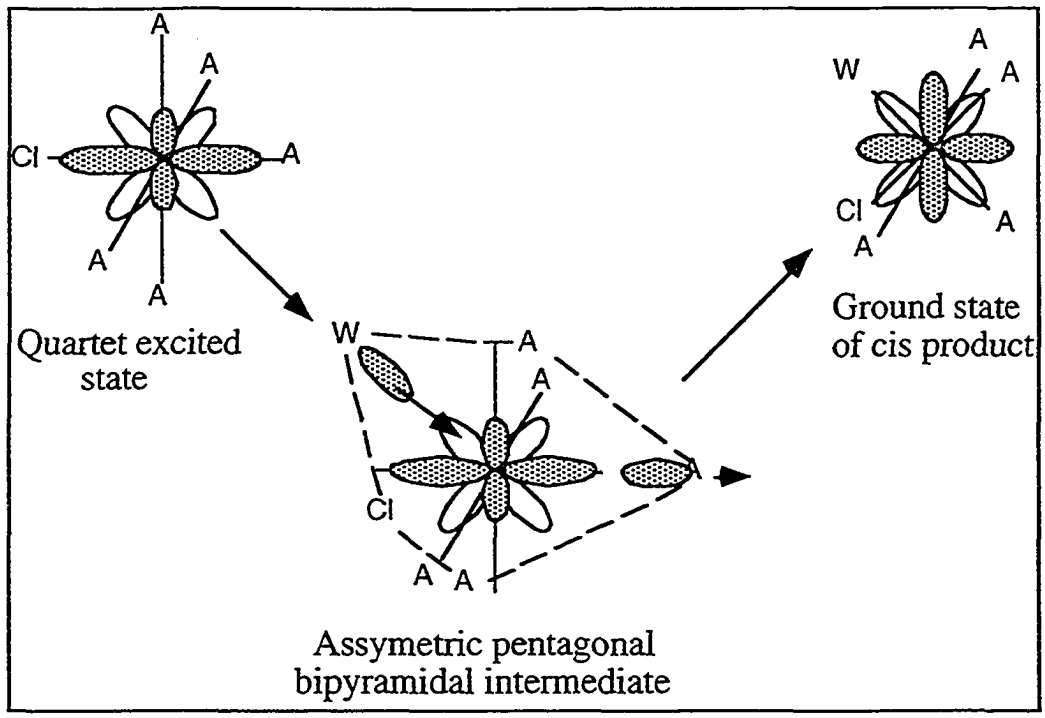

Figure 1.7 Alternative photoaquation mechanism via an asymmetric pentagonal bipyramidal intermediate

Reproduced with permission from reference 8.

1.8 Effect of Macrocyclic Ligands

An early study of $Cr(tren)F_2^+$,[62] indicated that photoaquation did not occur with loss of the tertiary tren amine. This indicated that constrained amines could not participate in Cr(III) photochemistry and was supported by results obtained in the photolysis of *trans*-$Cr(cyclam)X_2^{n+}$ complexes.

Although *cis*-$Cr(cyclam)X_2^{n+}$ complexes photoaquate with relatively high quantum yields,[63] *trans*-$Cr(cyclam)X_2^{n+}$ complexes are photoinert.[64-66] The quantum yields observed for the trans complexes are typically less than 0.01,

contrasting with the values of 0.1 - 0.3 obtained for the cis complexes and 0.2 - 0.5 for non macrocyclic $CrN_4X_2^{n+}$ complexes.

The efficient photochemistry observed for *cis*-$Cr(cyclam)X_2^{n+}$ complexes is still consistent with the trans attack, edge displacement mechanism if solvent attack and ligand migration occurs within the "cis pocket". This would not require involvement of the cyclam amines as illustrated below in Figure 1.8.

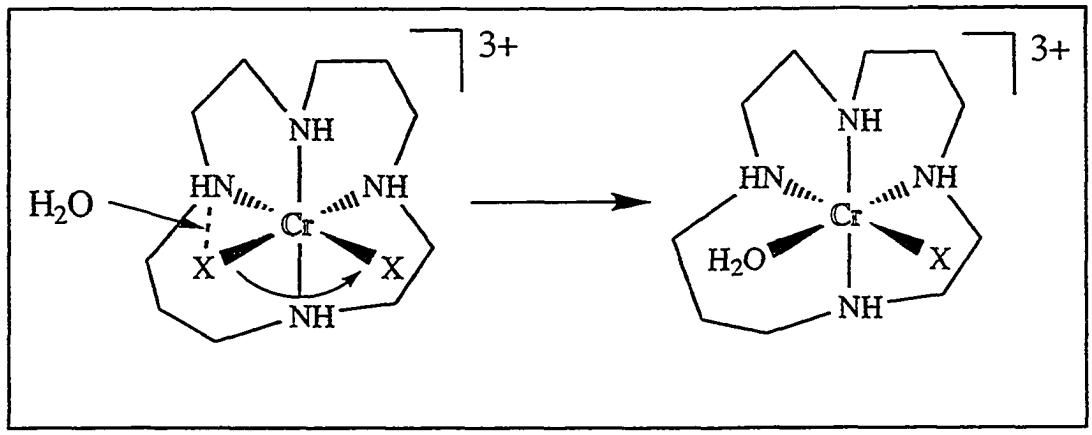

Figure 1.8 Trans attack edge displacement within the cis pocket of *cis*-$Cr(cyclam)X_2^{n+}$

Figure 1.8 illustrates that the proposed mechanism still occurs with "stereochemical change" as the retained X ligand migrates from its original position to that vacated by the leaving X. The overall sterochemistry of the complex is retained as cis-reactants -> cis-products.

The trans attack edge displacement model, illustrated above for *cis*-$Cr(cyclam)X_2^{n+}$, shows that stereochemical change occurs when the solvent attacks trans to the leaving ligand and an auxiliary ligand migrates to the vacated site. The photoinertness of *trans*-$Cr(cyclam)X_2^{n+}$ complexes and other macrocyclic complexes

has been attributed to macrocyclic ligands being immobile and unable to participate in a trans attack and edge displacement mechanism. This indicates that stereochemical change is not just a feature of Cr(III) photochemistry but may actually be a requirement.[10]

Based on these results it has been assumed that all secondary and tertiary amines of macrocyclic ligands are too constrained to participate in Cr(III) photochemical reactions which require ligand mobility and stereochemical change.[67] However, a recent photoaquation study of $Cr(sen)^{3+}$ indicates that four photoproducts are present[68] with only three of these being accounted for by loss of a primary amine. This indicates that the photoaquation of $Cr(sen)^{3+}$ also occurs with loss of a secondary amine. This possibility is investigated in more detail in Chapter Four.

Results obtained in this work indicate that photoaquation of *cis*-$Cr(cyclam)(NH_3)_2^{3+}$ occurs via loss of a secondary amine and this is discussed in more detail in Chapter Three.

1.9 The Role of the Doublet State

As stated in section 1.3, the slow component observed in Cr(III) photoreactions originates in the ^2E state, having with the same lifetime as that of doublet emission. Three mechanisms have been proposed for reaction via the ^2E state;

i) Direct reaction of the ^2E state,

ii) Back intersystem crossing (BISC) to the quartet excited state followed by reaction,

iii) Crossing to a reactive ground state intermediate (GSI) or transition state.

The weight of experimental evidence discounts direct reaction from the doublet state. This includes; no reaction occurs via the ^2E state for complexes that have a large ^2E-$^4T_2$ energy gap[20,69,70] and direct irradiation of the doublet state does not enhance quantum yields.[21,22,60,61,71] Calculations based on activation volumes obtained for Cr(III) complexes show that these are inonsistent with reaction directly from the ^2E state.[72] Support in the current literature is divided between the two alternatives, reaction via BISC or GSI. The arguments for and against these two mechanisms are considered in more detail in the following sections.

1.9.1 Back Intersystem Crossing and Quartet Reaction

A preference for photoreaction involving the $^4T_2$ state was first proposed by Adamson[34] and, as previously stated, was a key feature of the first theoretical models introduced by Zink, Wrighton et al. and Vanquickenborne and Ceulemans. An early study by Wasgestian[20] revealed that reaction from the doublet state did not occur for $Cr(CN)_6^{3-}$, a complex with a large ^2E - $^4T_2$ energy gap. This indicated that reaction from the ^2E state could only occur if the $^4T_2$ state was energetically accessible.

Two key studies by Riccieri et al.[47] along with Cimolino and Linck[73] indicated that reaction via the ^2E and $^4T_2$ states occurred via a common pathway or at least via a common intermediate. Riccieri et al. found that the same photoproduct ratios were obtained for the quenchable and unquenchable photoreactions of *trans*-$Cr(NH_3)_4(CN)(NCS)^+$. Cimolino and Linck showed that the quantum yields of Λ-*cis*-$Cr(en)_2(enH)(OH_2)^{3+}$, Δ-*cis*-$Cr(en)_2(enH)(OH_2)^{3+}$ and *trans*-$Cr(en)_2(enH)(OH_2)^{3+}$, the photoproducts of Λ-$Cr(en)_3^{3+}$, were the same upon

doublet and quartet irradiation. In both studies the authors concluded that the quartet and doublet reactions were occurring via the same pathway, with reaction from the ^2E state involving back intersystem crossing to the reactive $^4T_2$ state.

1.9.2 Crossing to a Reactive Ground State Intermediate

This model, proposed by Endicott,[23] was partly in response to the original VC models of Cr(III) photostereochemistry. Whereas the VC model was based on reaction from the $^4T_2$ state the emphasis of Endicott's paper was in evaluating possible reaction modes from both the ^2E and $^4T_2$ excited states. The energies of possible doublet and quartet state intermediates, both 5 and 7 coordinate, were calculated using AOM calculations. The results suggested that ground state intermediates were thermally accessible from the ^2E and $^4T_2$ states, for either an associative or dissociative mechanism. The argument was presented that reaction from both states could occur via the same intermediate for either mechanism. An associative mechanism was favoured, with a face-capped trigonal prismatic intermediate believed to be most consistent with the stereochemical changes observed experimentally.

More recent arguments favouring the GSI mechanism over BISC have focused on the energy gap between the ^2E and $^4T_2$ states. An apparent activation energy of 33 ± 2 kJ mol^{-1} was found for deactivation of the ^2E state in a series of polypyridyl complexes, $Cr(III)(PP)_nX_{6-2n}$, where PP = 1,10 - phenanthroline, 2,2' - bipyridine and X = NH_3, en/2, acac$^-$/2, CN^-, SCN^-.[27] This contrasted with the ^2E - $^4T_2$ energy gap calculated for these complexes based on low temperature spectroscopy, which varied between 64 and 128 kJ mol^{-1}. These results indicated that BISC could not be the process depopulating the ^2E state as the observed

activation energy was smaller than the ^2E - $^4T_2$ energy gap. It was argued that the results were more consistent with thermally activated surface crossing to a reactive ground state intermediate.

This argument was expanded in a subsequent paper where apparent activation energies, for doublet state deactivation, were contrasted with the ^2E - $^4T_2$ energy gap for a series of $Cr(III)N_4X_2$ macrocyclic complexes[24]. It was found that for the majority of these complexes the apparent activation energies were smaller than the calculated energy gaps. Complexes where $X = Cl^-$ and Br^- proved to be the exception to this trend with $Ea > \Delta E$. It was acknowledged that, for these complexes, BISC may be the dominant mechanism deactivating the ^2E state. However an argument was presented against BISC deactivating the ^2E state of $Cr(NH_3)_5Cl^{2+}$, a complex which also has $Ea > \Delta E$. As no delayed fluorescence was observed from the doped solid at 77K, this was taken as evidence against BISC populating the $^4T_2$ state. It was also stated in this paper that it was not obvious how the BISC mechanism could accommodate the observed solvent dependence of the ^2E lifetimes. Once again the authors favoured ^2E decay occurring via surface crossing to either five or seven coordinate ground state intermediates for the majority of these complexes.

More recent papers have built further on this argument including studies of *cis*- & *trans*-$CrN_4(CN)^{2+}$ complexes[25] and $Cr(sen)^{3+}$.[26] The latter study proposed that the trigonal distortion induced by the sen ligand in $Cr(sen)^{3+}$ assisted deactivation from the ^2E state via a ground state, D_{3h}, trigonal prismatic intermediate.

1.9.3 Comments on BISC versus GSI

When considering the arguments both for and against BISC and GSI it becomes apparent that proponents of the two mechanisms have become firmly entrenched in their views. To some extent the two camps can be defined by what they believe to be the most important feature of Cr(III) photochemistry; the ^2E - $^4T_2$ energy gap or the stereochemical changes occurring with photoreaction.

In addressing the relative merits of the two mechanisms it is worth considering the following questions:

Are the stereochemical changes observed for Cr(III) photochemistry consistent with reaction from the ^2E or $^4T_2$ state?

Are the ^2E - $^4T_2$ energy gaps calculated from low temperature spectroscopy representative of the ^2E - $^4T_2$ energy gap in solution?

It is well established that the thermal reactions of Cr(III) complexes are stereoretentive and that photochemical reaction occurs with stereochemical change. To account for these differences, reaction from the ^2E state via the GSI mechanism must involve a different ground state intermediate to that thermally accessible. As the ^2E and ^4A ground state have the same t_{2g}^3 electron configuration it is uncertain why solvent attack, and subsequent intermediate formation, would differ for these states. The d-electron densities of the ^2E and ^4A ground state, along with the $^4T_2$ state are illustrated in Figure 1.9.

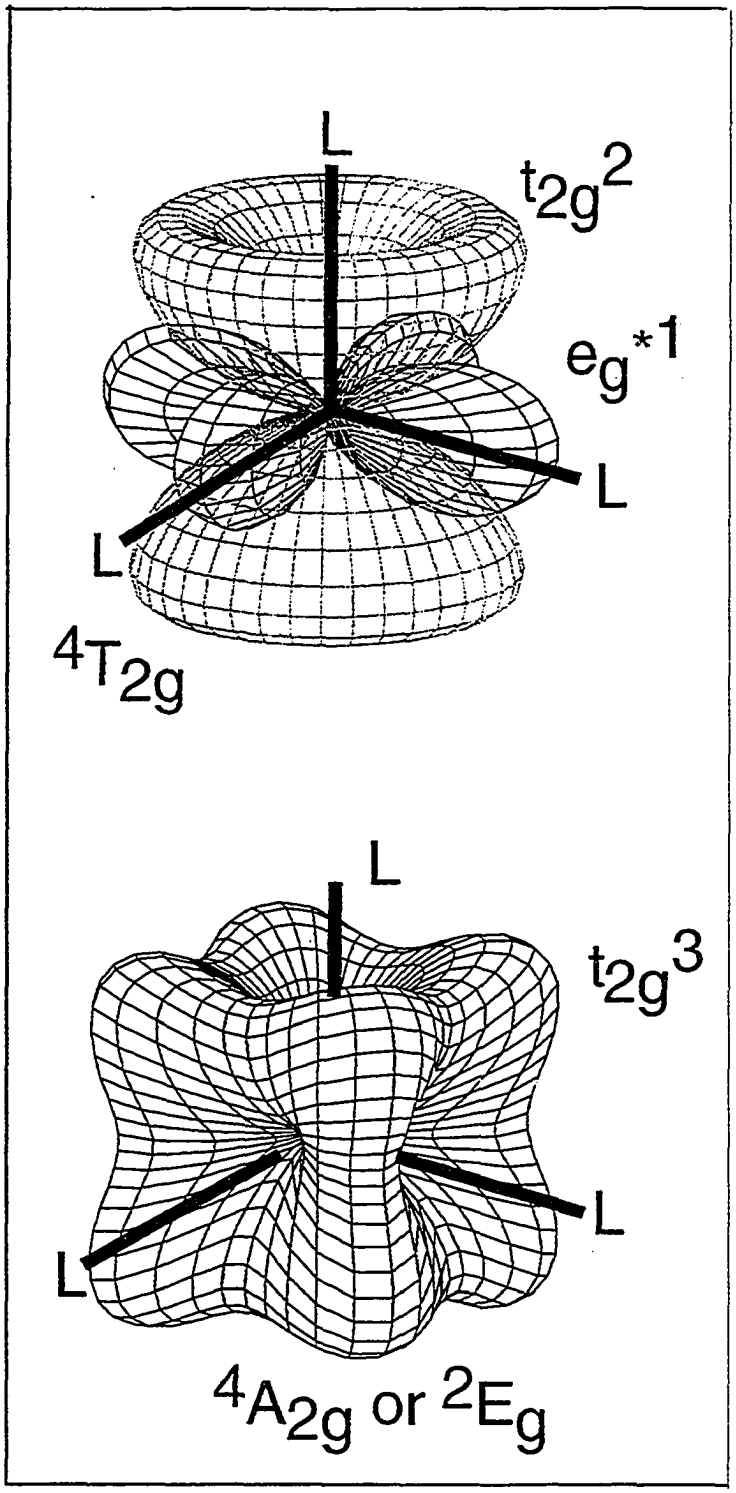

Figure 1.9 d-electron distributions for the ^4A, ^2E and $^4T_2$ states of Cr(III)

Reproduced with permission from Reference 7.

As Figure 1.9 illustrates, the d-electron distributions of the ^2E and ground states are identical and do not show any reason for the mode of solvent attack to differ between these two states. In contrast, the vacant t_{2g} orbital of the $^4T_2$ state is readily accessible to nucleophilic attack by a solvent molecule. As stated in section 1.6, this feature of the $^4T_2$ state, along with the destabilizing effect of the e_g* electron had been noted by Zink, who favoured the $^4T_2$ being the reactive state. The successful *modelling of Cr(III) photoproduct stereochemistries* by Vanquickenborne and Ceulemans based on the $^4T_2$ state provides further support for reaction via this state, with ^2E reaction involving BISC to the $^4T_2$ state.

Other inconsistencies with reaction via the GSI mechanism arise when considering Cr(III) complexes which are photoinert, e.g. *trans*-Cr(cyclam)X_2^{n+} complexes, or which do not react from the doublet state, as in the case of $Cr(CN)_6^{3-}$. Thermal substitution reactions are observed for these complexes indicating that reaction via ground state intermediates can occur. What then prevents these intermediates from being accessible to the ^2E state?

The major argument against BISC is based on the apparent activation energy for doublet deactivation being smaller than the ^2E - $^4T_2$ energy gap. Of these two values only the apparent activation energy is obtained in the solution phase. The ^2E - $^4T_2$ energy gap is typically calculated based on low temperature spectroscopy results. It is therefore questionable that the value obtained for the ^2E - $^4T_2$ energy gap is representative of that actually existing in the solution phase.

Another argument that has been presented to discredit BISC is that delayed fluorescence is not observed at low temperatures from complexes where $Ea < \Delta E$. However as fluorescence is typically not observed from the $^4T_2$ state directly, it seems illogical to base such an argument against BISC on the absence of delayed fluorescence.

The effects of solvation on Cr(III) excited state energies may be central in proving or disproving BISC as the mechanism for ^2E deactivation. Endicott has stated that it is uncertain how BISC can accommodate the observed solvent dependence of doublet deactivation but presents few details as to why the GSI mechanism would be more consistent. Kirk has taken an opposing view regarding the possible effects of solvent on BISC. In a recent paper[74] he suggests that solvation may effectively decrease the ^2E - $^4T_2$ energy gap, making BISC from the ^2E to the $^4T_2$ state energetically accessible.

The relationship between solvation and BISC efficiency is currently not well understood and is beyond the scope of this thesis. Current advances in computational chemistry and molecular mechanics may allow for more insight into the effect of solvation on the energies of electronic states.

Based on the relative merits of the two mechanisms discussed above this thesis favours BISC as the process depopulating the ^2E state. The main reasons for this are twofold; the stereochemical changes observed with photolysis are consistent with reaction from the $^4T_2$ state and no convincing argument has been presented for the ^2E - $^4T_2$ energy gaps obtained at low temperature being representative of the energy gap in solution.

1.10 Volume of Activation Studies

The effect of pressure on photochemical and photophysical processes of inorganic complexes can provide insight into the reaction and deactivation mechanisms of the excited states involved.

The volume of activation, $\Delta V^{\ddagger}$, is defined as;

$$\Delta V^{\ddagger}(X) = -RT\left[\frac{\delta \ln(X)}{\delta P}\right]_T$$

where X is the kinetic parameter of interest. This is typically the reciprocal of the observed lifetime, τ^{-1}, or the quantum yield of the photochemical reaction, $\emptyset_{rxn}$. If X is the actual rate constant for an independent process then the pressure dependence of this parameter gives a real $\Delta V^{\ddagger}(X)$. As both observed lifetimes and quantum yields are dependent on a number of processes their pressure dependence gives apparent volumes of activation, reflecting a composite of the $\Delta V^{\ddagger}$ values for the individual processes occuring.

Early pressure dependence studies of Cr(III) complexes focused on whether volumes of activation obtained from the pressure dependence of quantum yields were consistent with associative or dissociative mechanisms.[58,59]

Angermann et al. estimated $\Delta V^{\ddagger}$ ($\emptyset_{rxn}$) values of -16.0 cm^3 mol^{-1} and + 24.8 cm^3 mol^{-1} for purely associative and dissociative Cr(III) photoaquation mechanisms respectively.[58,59] These values were estimated for a neutral leaving ligand, i.e. in the absence of electrostriction effects. The values obtained for $Cr(NH_3)_5X^{2+}$, where X = Cl^-, Br^-, NCS^-, had a mean value of - 11.7 cm^3 mol^{-1} for the minor reaction mode, loss of X. For this set of complexes along with $Cr(NH_3)_6^{3+}$, an average value of -6.4 cm^3 mol^{-1} was obtained for the loss of ammonia. These $\Delta V^{\ddagger}$ values were regarded as being consistent with an associative interchange mechanism, I_a, operating in the photosubstitution reaction.

Where $\Delta V^{\ddagger}$ (τ^{-1}) values have been obtained they often contrast with the volumes of activation obtained from the quantum yield. e.g. for $Cr(NH_3)_5(NCS)^{2+}$

$\Delta V^{\ddagger}(\tau^{-1}) = +7.0\ cm^3\ mol^{-1}$.[72] Different volumes of activation obtained for the two processes is a good indication that they may not be occurring from the same state.

Waltz and co-workers have investigated the $\Delta V^{\ddagger}(\tau^{-1})$ and $\Delta V^{\ddagger}(\emptyset)$ values obtained for various Cr(III) complexes in terms of possible excited state pathways.[60,61,72] The positive $\Delta V^{\ddagger}(\tau^{-1})$ values obtained for the ^2E emission lifetimes suggests that ^2E deactivation involves expansion, consistent with BISC to the distorted $^4T_2$ state. In their study of pressure and solvent effects on the lifetime and quantum yield of $Cr(NH_3)_6^{3+}$ it was demonstrated that the $\Delta V^{\ddagger}(\tau^{-1})$ and $\Delta V^{\ddagger}(\emptyset_{rxn})$ values of $+4.3\ cm^3\ mol^{-1}$ and $-6.0\ cm^3\ mol^{-1}$ $\Delta V^{\ddagger}(\emptyset_{rxn})$ were both consistent with decay of the ^2E state via BISC.

1.11 The Question of Intermediates

From the preceding sections it becomes apparent that various intermediates have been proposed for the photolysis reactions of Cr(III) complexes.

The original models of Vanquickenborne and Ceulemans involved five coordinate square pyramidal and trigonal bipyramidal intermediates. As stated earlier this conflicts with experimental evidence suggesting an associative mechanism, leading to Kirk's proposal of an asymmetric pentagonal bipyramidal intermediate.

Møensted and Møensted have independently proposed a pentagonal bipyramidal intermediate based on their thermal and photochemical studies of Cr(III) aquo complexes.[15]

Photoaquation and photoanation studies of $Cr(NH_3)_6^{3+}$ by Wasgestian[75] led to the proposal of an interchange mechanism involving a trigonal prismatic intermediate.

The papers of Endicott have evoked decay and/or reaction via various ground state intermediates including: five coordinate square pyramidal and trigonal bipyramidal, six coordinate trigonal prismatic and seven coordinate face capped trigonal prismatic intermediates. The original paper also made reference to the possibilities of seven coordinate face capped octahedral and pentagonal bipyramidal intermediates.

To date little experimental evidence has indicated the presence of photolytic intermediates. A number of studies on the photoaquation of $Cr(phen)_3^{3+}$ and $Cr(bpy)_3^{3+}$ have indicated that these complexes react photochemically and thermally via a seven coordinate intermediate.[76-78] More recent photolysis studies of these complexes using conductivity detection,[79,80] suggest that the seven coordinate intermediate decays to a six coordinate intermediate containing a monodentate polypyridyl ligand. Two competing processes were proposed to occur from the six coordinate species; recoordination of the detached polypyridyl ligand, explaining the observed photoracemization, and solvent attack displacing the monodentate ligand to give the observed di-aquo products.

The most conclusive evidence for a photolytic intermediate has been presented in Waltz and co-worker's papers on the photoaquation of *cis*-$Cr(cyclam)(NH_3)_2^{3+}$.[60,81] As this was the inspiration for the work presented in Chapter Three, the results and implications of this study are discussed in more detail in the introduction to that chapter.

1.12 Photoracemization of Cr(III) complexes

As mentioned above, the photoracemization of Cr(III) polypyridyl complexes may occur via a six coordinate intermediate containing a monodentate polypyridyl ligand. A detailed discussion on photoracemization studies of Cr(III) complexes has been presented in a recent review.[7] In general, three photoracemization mechanisms have been proposed with the first being detachment and recoordination of a bidentate ligand. The other two involving twisting motions of the ligands, Bailar and Ray-Dutt twists. These mechanisms are illustrated below in Figure 1.10

As ii) and iii) in Figure 1.10 illustrate, the Bailar and Ray-Dutt twists are similar but differ in the symmetry axis around which the twisting motion occurs and the number of ligands which twist. Both involve a trigonal prismatic intermediate and, for the asymmetric bidentate ligands shown in Figure 1.10, the Bailar twist results in photoracemization with the Ray-Dutt twist resulting in both photoracemization and geometric isomerization.

The relative merits of these mechanisms are explored in more detail in Chapter Four in relation to the thermal and photolytic racemization of $Cr(sen)^{3+}$.

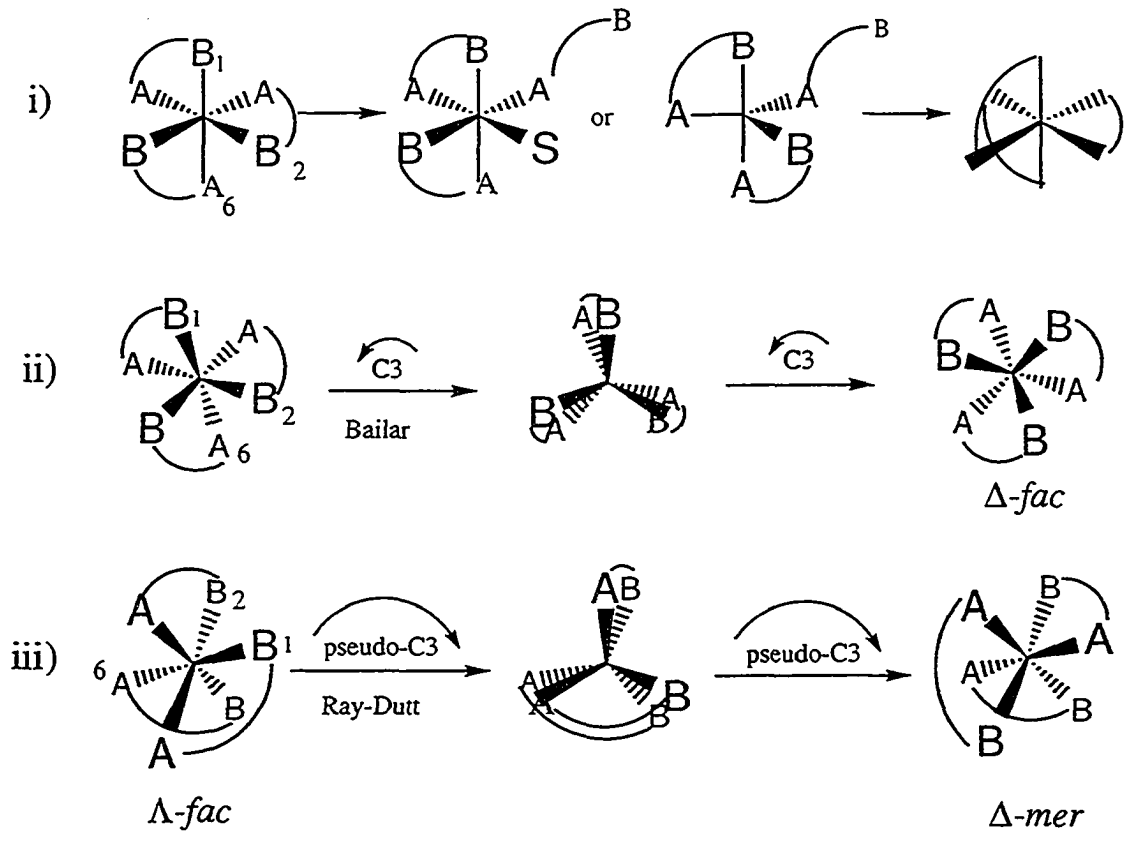

Figure 1.10 Possible photoracemization mechanisms for Cr(III) complexes
i) ligand detachment and recoordination, ii) Bailar twist,
iii) Ray-Dutt twist
Reproduced with permission from reference 7.

1.13 Conductivity Detection as a Probe for Cr(III) Photochemistry

Photolysis reactions of Cr(III) complexes are difficult to monitor using normal optical detection techniques because of the small differences in photoproduct and starting material absorptivities, typically $\Delta\varepsilon < 100\ M^{-1}\ cm^{-1}$. Conductivity detection provides a viable alternative for photoreactions that involve relatively large

changes in solution conductivity. Particularly suited for study using conductivity detection are reactions that involve proton uptake, proton release, or consumption of hydroxide; this is due to the large molar conductivities of the H^+ and OH^- ions.

The use of conductivity detection also provides a convenient method for determining the proportion of Cr(III) photochemistry which occurs via the $^4T_2$ and ^2E states. The prompt and slow changes in solution conductivity that occur due to reaction via these two states are observed directly using conductivity detection. In the past these ratios have typically been obtained through quenching studies and required determination of the photoproduct yield in the presence and absence of quencher.

The only research group that has made extensive use of conductivity detection in the study of Cr(III) photochemistry is that of Waltz, with a series of papers being published.[60,79-83]

Details on the design and development of our apparatus are presented in Chapter Two along with typical experimental conditions. The background theory of conductivity detection is investigated in Chapter Three.

1.14 Summary and Research Objectives

The elucidation of Cr(III) photoaquation mechanisms, including the possible involvement of chemical intermediates, is a central theme in the work presented in this thesis. Instrumental techniques and synthetic procedures used in our studies are presented in Chapter Two. Chapter Three focuses on the photoaquation studies of Cr(III) am(m)ine complexes and our search for intermediates similar to that observed in the photoaquation of *cis*-Cr(cyclam)$(NH_3)_2^{3+}$. In Chapter Four our research into the thermal and photolytic aquation and racemization mechanisms of $Cr(sen)^{3+}$ is reported.

CHAPTER TWO

EXPERIMENTAL

2.1 Laser Flash Photolysis with Conductivity Detection

2.1.1 Laser Source

The laser source employed in the flash photolysis experiments is a Q-switched Quanta-Ray GCR-11 pulsed Nd-Yag laser. The laser pulse is 5-10 ns in duration (as specified) and is approximately 6 mm in diameter. The tripled pulse energy at 355 nm is measured by a Molectron J50 thermal detector, with an output of 2 V J^{-1}, which is connected to a Tektronix 2445 oscilloscope. Typical laser pulse energies are 40 mJ, or expressed in amount of 355 nm photons, 1.01 x 10^{-7} moles.

2.1.2 Conductivity Cell

A cutaway representation of the conductivity cell is shown in Figure 2.1. The central compartment of the cell is cut into a teflon block with the upper and lower faces being rounded to enhance solution flow. This also prevents trapping of air bubbles at the exit port. The cell compartment is closed off, front and back, by suprasil quartz windows, 26 mm in diameter and 2 mm thick which are held in place by brass faceplates. The faceplates are connected by screws which run through the teflon block. Sufficient tightening of these screws ensures that no leaks occur at the quartz windows without the use of o-rings.

Within the cell compartment are three platinum electrodes which are spaced 7.5 mm apart. These electrodes are 0.5 mm in diameter and run the width of the cell compartment. The laser pulse enters the cell perpendicular to the electrodes and is centered between the two upper electrodes by a rounded rectangular aperture cut into

the front faceplate. The axial dimensions of this aperture are 5.4 x 4.0 mm. The truncated laser pulse then exits the cell via a 6 mm diameter window in the rear faceplate.

Stainless steel adapters allow for the attachment of Viton tubing (size 16) which connects the cell to the solution reservoir. The solution is typically pumped through the system at a flow rate of 10 - 40 ml per minute by a peristaltic pump.

Although seemingly a minor detail, the use of Viton tubing proved to be of major importance in the development of the conductivity apparatus. With the original apparatus, conductivity changes had been observed upon irradiation of "blank" solutions, pH 3-5 perchloric acid solutions which did not absorb at the irradiation wavelength of 355 nm. Replacing the original tubing with viton removed these artifacts and it is surmised that they originated in photoactive plasticizer which was leaching from the original tubing.

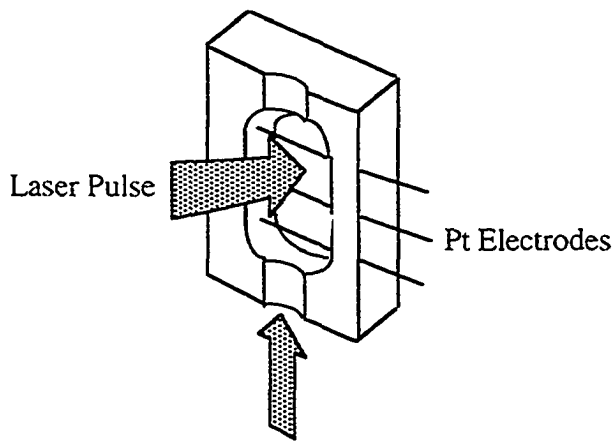

Central compartment = 20.4 x 7.6 x 8.8 mm
Teflon block = 56 x 42 x 8.8mm

Figure 2.1 Schematic representation of the conductivity cell.

2.1.3 Signal Detection and Data Processing

A schematic representation of the signal detection and processing system is presented in Figure 2.2. The two outer platinum electrodes are connected to 50 ohm resistors which are both connected to a grounded 50 ohm variable resistor. The inherent resistance of the solution present between the inner and outer two electrodes completes the circuit forming a Wheatstone bridge.

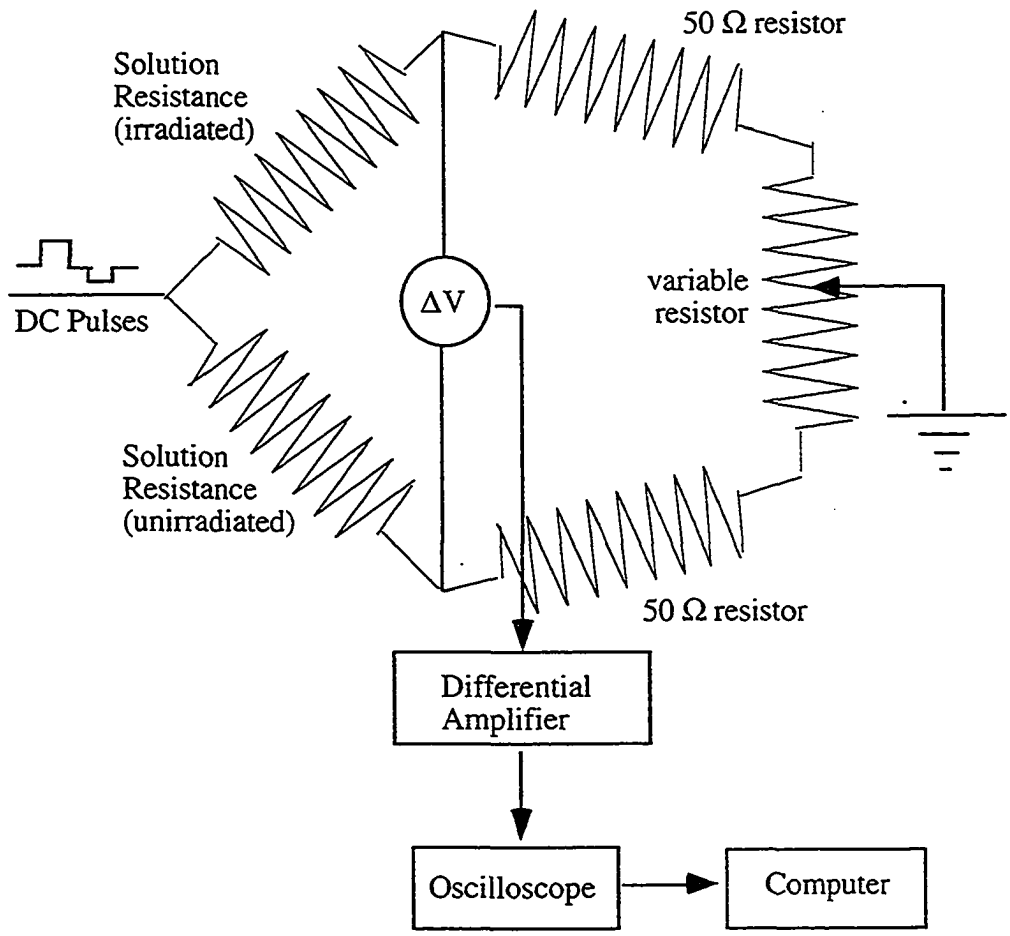

Figure 2.2 Schematic representation of the conductivity signal detection and data processing system.

Applying a 120V DC pulse of variable duration between the inner electrode and ground causes current to flow through the two arms of the bridge. The length of the DC pulse is typically 4-8 ms in duration, with the length of the pulse being adjusted to give the flattest possible baseline signal. Any difference in the currents flowing through the two arms is detected as a potential difference across the bridge. This signal is amplified by a variable gain differential amplifier (gain 10, 20, 50), digitized by a Tektronix TDS 520 oscilloscope and transferred to a Macintosh IIci computer via a GPIB and I/O data acquisition board. In the absence of a laser pulse the observed potential difference across the Wheatstone bridge is minimized through adjustment of the 50 ohm variable resistor.

Photochemical reaction occurring after laser excitation results in time dependent changes occurring in the solution resistance between the upper two electrodes. This in turn generates a time dependent difference in the current flowing through the two arms of the bridge which is then detected, amplified and recorded accordingly.

Following a literature procedure,[84] it was found that baseline fluctuations could be minimized by the introduction of a second DC pulse of opposite polarity to the first. In our experiments the second DC pulse is introduced approximately 10 ms after the trailing edge of the first DC pulse. The magnitude and length of the second pulse are variable; optimum values were found to be approximately 40 V and 8 ms respectively. The stabilizing effect of the second pulse is attributed to a reduction in H_2 and O_2 bubble formation at the electrode surfaces due to electrolysis of the acidic, aqueous solutions. Formation and detachment of gas bubbles causes fluctuations in the effective surface area of the electrodes affecting current flow and leading to baseline instability.

The computer programs for sequencing, data acquisition and data analysis have been developed here based on Labview (National Instruments) by Luis Netter with the current version employing Labview 4.1.

2.1.4 Timing

The timing sequences for the laser pulsing, DC pulsing, oscilloscope triggering and data acquisition are controlled by a custom built dual delay generator and AC synchronizer in conjunction with a Stanford Research Systems DG535 digital delay pulse generator. The delay synchronizer controls millisecond delays with the DG535 being responsible for nanosecond delays. The timing of the laser pulse relative to the 120 V DC pulse is variable and is adjusted to occur at the flattest portion of the baseline signal observed in the absence of a laser pulse. This typically occurs 1-3 ms after the leading edge of the DC pulse. Laser pulsing occurs at a 1 Hz repetition rate but data acquisition occurs approximately every 3 seconds. This allows ample time for both the introduction of fresh solution to the cell and recovery of the electrode surface from electrolysis effects.

2.1.5 Typical Experimental Conditions

Typical experimental conditions involve perchloric acid solutions, pH 2.5 - 5.3, which are approximately 1mM in complex. The pH is measured using an Acumet 910 pH meter, with an Ingold Lot glass electrode. The pH meter is calibrated with the use of appropriate buffer solutions. Data collection for each individual solution involves 3-5 repeat measurements, each consisting of 5-10 signal averaged

shots. As the solution reservoir is large, relative to the volume irradiated, continual flowing of solution ensures that secondary photolysis effects are minimal; the overall extent of photolysis rarely exceeds 2% and comparison of uv/vis spectra taken before and after photolysis confirms minimal changes in solution composition have occurred. Temperature within the laser laboratory is maintained at 20 °C and solutions are given adequate time to equilibrate to room temperature in the dark before data acquisition.

2.1.6 Data Evaluation and Curve Fitting

All evaluation of experimental data and curve fitting of conductivity traces has been done using Igor Pro 3.0 (Wavemetrics, Inc) and the associated fitting procedures. The exponential and biexponential fitting procedures are iterative with the calculated chi-square values for each iteration being minimized using the Levenberg-Marquardt algorithm.

Simple modifications to the Igor fitting procedures were made for calculation of the fraction of doublet photoreaction from conductivity traces displaying a biexponential decay. One macro involved fitting the latter two thirds of these traces with an exponential fit and extrapolating to the onset of the laser pulse. The fraction of doublet photoreaction was then calculated from the ratio of the extrapolated decay magnitude to the overall experimental change in conductivity. An alternative method involved fitting the whole experimental trace to a double exponential function, $y = A_1e^{-k_1t} + A_2e^{-k_2t}$. The fraction of doublet photoreaction was then calculated from the pre-exponential factors obtained; $F_D = \frac{A_1}{(A_1 + A_2)}$.

It was found that experimental traces that contained a transient increase in conductivity followed by a decay, could not be fitted using the IgorPro biexponential

fitting function. The problem seemed to be an inability to automatically determine initial values for a trace containing both a growth and a decay i.e. where A_1 and A_2 were not both positive or negative values. A customized fitting function was written, Rise/Decay, which enabled the fit of these traces to a biexponential function, $y = A_1e^{-k_1t} - A_2e^{-k_2t}$. The Rise/Decay function determines appropriate initial values for A_1 and A_2 from the experimental trace of interest before conducting the actual fit.

2.2 Instruments and Techniques

2.2.1 Elemental Analysis

Elemental analysis for C, H and N content was performed by Canadian Microanalytical Services Ltd., Delta, Vancouver, B.C.

2.2.2 UV/Vis Spectroscopy

UV-Vis spectra were obtained using a Cary-1 or Cary-5 UV/Vis/NIR spectrophotometer coupled with a Compaq Deskpro 386s micro computer, or alternatively a Cary 50 UV/Vis spectrometer coupled to a Viewsonic P655 PC and operated using Win UV software.

2.2.3 Emission Lifetime Measurements

Emission lifetimes were measured using a PTI nitrogen laser as the excitation source, delivering a pulse of approximately 7 ns in duration, with a pulse energy of about 1 mJ. The emission is monitored using a Jarrel-Ash 82-410 monochromator in conjunction with a Hamamatsu R928 GaAs photomultiplier. The lifetimes are evaluated from the slope of a weighted least squares logarithmic plot of the decay over 1024 data points.

2.2.4 Continuous Photolysis

These experiments used the 488 nm or 458 nm output of a SpectroPhysics 2000 Argon Ion laser as the light source. The Cr(III) solutions were typically 5.0 mM in complex and made from pH 2.7 - 3.2 $HClO_4$ solutions. To avoid secondary photolysis effects the irradiatied solution was constantly stirred using a magnetic flea in the 1.0 cm cuvette. Typical laser powers were 30 - 40 mW and photochemical conversion of the starting material was kept less than 15%. The laser output intensity was monitored directly using a Scientific 36-5002-365 Digital power and Energy Indicator.

2.2.5 NMR

^{1}H, ^{13}C and ^{13}C DEPT NMR spectra were obtained on a Bruker B-ACS60 300 MHz NMR spectrophotometer. Chemical shifts were internally referenced to the residual solvent shifts.

2.2.6 Conductivity Measurements

Solution conductance measurements were made using an Orion 3025 conductivity electrode in conjunction with a Radiometer Copenhagen CD83 conductivity meter. The electrode cell constant was checked by measuring the conductance of KCl and NaCl solutions of known conductance, made up in deionised water.

2.2.7 Capillary Electrophoresis

Capillary electrophoresis experiments were run using an Applied Biosystems 270A - HT high throughput capillary electrophoresis system with UV/vis detection. The capillary used was a Supelco CElect™ - UVT 50 which has a 50 μm inner diameter and is transparent down to 200 nm. Different capillary lengths were used during the course of the experiments with a typical total length being 45 - 50 cm and the distance between the injection point and the detector being 27 cm. Electrophoresis buffers used were 50 - 100 mM *d*-tartrate solutions, pH 3.0 - 6.0. The applied voltage was varied for each buffer and care was taken to keep the resulting current below 30 μA as this resulted in better baseline stability. Although the apparatus allows for both electrophoretic or vacuum aspiration (5.0" Hg) loading of the sample onto the column, the latter was used exclusively.

Electropherograms were recorded using a Shimadzu C-R5A Chromatopac integrator. Migration times were reproducible within ± 1% on a given day but, due to changes in capillary properties, displayed a larger drift over several days.

2.2.8 Reversed Phase HPLC

Reversed phase HPLC experiments were conducted using a Varian 5000 liquid chromatograph with a 25 cm octadecylsilane RP-HPLC column. Both HPLC grade methanol and deionized water were used as the eluents and contained 25 mM tetraethylammonium as the competing ion and 25 mM hexanesulfonate as the ion interaction agent. The relative ratio of MeOH to H_2O varied with the complex studied and the typical flow rate was 1.5 mL min^{-1}. Unless otherwise stated the pH of both the MeOH and H_2O the solutions were adjusted to pH 3.0.

2.3 Materials

All chemicals used were analytical grade and purchased from Aldrich, BDH Chemicals, Fischer Scientific or Parish Chemicals and used without further purification.

2.4 Synthesis of Cr(III) Complexes

2.4.1 Synthesis of Cr(III) complexes used in LFP/Conductivity Studies

The perchlorate salts of the complexes $Cr(en)_3^{3+}$ [22], $Cr(tn)_3^{3+}$,[85] $Cr(sen)^{3+}$,[68] and *trans*-$Cr(2,3,2\text{-tet})(CN)_2^{+}$ [67] have been the subject of previous studies by this group and samples were available for use in this work. The UV/Vis

spectra and emission lifetimes obtained for these complexes were in agreement with literature values, confirming their purity.

$Cr(NH_3)_6^{3+}$ [86] and *cis*-$Cr(cyclam)(NH_3)_2^{3+}$ [87] were prepared following literature procedures and recrystallized as their perchlorate salts. Comparison of λ_{max}, ε_{max} and emission lifetimes with literature values confirmed the purity of these complexes.

The complexes *cis- & trans*-$[Cr(tn)_2(NH_3)_2](ClO_4)_3$ were obtained via *trans*-$Cr(tn)_2F_2^+$, prepared by a modification [88] of the analogous preparation for *trans*-$Cr(en)_2F_2^+$.[89] The product was converted to *trans*-$Cr(tn)_2(Cl)_2^+$ by overnight stirring in 38% HCl. Ammonolysis of the resulting *trans*-$Cr(tn)_2(Cl)_2^+$ yielded a mixture of *cis- & trans*-$[Cr(tn)_2(NH_3)_2]Cl_3$. These isomers were separated as the perchlorate salts by fractional recrystallization. Although the two isomers have identical λ_{max} values and similar ε_{max} values[85,86] they have significantly different emission lifetimes. Lifetime comparison to literature values indicated the first batch of crystals obtained to be pure *trans-* isomer and the third batch to be pure *cis-* isomer.

$K_3Cr(CN)_6$ was prepared and recrystallized by literature methods[90] and the purity confirmed by comparison of λ_{max} and ε_{max} values.

2.4.2 Synthesis of $[Cr(sen)]X_3$ used in CE Studies

2.4.2.1 Synthesis of sen

The sen ligand, 4,4',4" ethylidenetris(3-azabutan-1-amine), was prepared via established procedures,[91] with the exception of the conversion of 1,1,1-tris(toluenesulfonatomethyl)ethane to 1,1,1-tris(bromomethyl)ethane.[92]

Firstly 1,1,1-tris(toluenesulfonatomethyl)ethane was prepared by tosylation of 1,1,1-tris(hydroxymethyl)ethane in pyridine. This was then converted to 1,1,1-tris(bromomethyl)ethane by overnight refluxing in DMF with 4 equivalents of sodium bromide. Refluxing 1,1,1-tris(bromomethyl)ethane in anhydrous ethylenediamine for 48 hours under nitrogen produced crude sen. Purification involved elution of the crude oil though a Dowex 50W-X2 cation exchange column with 4M HCl and evaporation of the eluant to give the hydrochloride salt, sen.6HCl.

2.4.2.2 Synthesis of $[Cr(sen)]X_3$

The literature procedures for preparing crude $[Cr(sen)]Cl_3$ are based on standard synthetic procedures for complexing amine ligands to Cr(III). $CrCl_3.6H_2O$ is converted to $Cr(S)_3Cl_3$, where S = DMF[26] or DMSO,[68] by boiling in the appropriate solvent. Addition of the free ligand with stirring to the warm solution and further heating produces the crude product as either a yellow or red precipitate. Recrystallization from water with saturated sodium bromide gave yellow crystals for both preparations. However, repeated attempts at both procedures failed to produce $[Cr(sen)]Cl_3$ in this work.

In our attempts sen.6HCl was converted to the free base by dissolving in the appropriate volume of 25% sodium methoxide in methanol. Precipitated sodium chloride formed was filtered off and the filtrate evaporated to give the free ligand as a yellow oil. If residual sodium chloride was present the ligand was purified by dissolving in the minimum of absolute ethanol, filtering off the insoluble sodium chloride and evaporation of the filtrate.

Reaction of the free ligand with $Cr(DMSO)_3Cl_3$ in DMSO resulted in a black solution containing DMS, readily identified by its odour. This would indicate

that the ligand and/or the Cr(III) complex were being oxidized by DMSO. Although not investigated further, it is worth noting that this problem had also been experienced by the author of the literature preparation.[93] The attempted synthesis via $Cr(DMF)_3Cl_3$ resulted in a yellow, gum-like residue which was water insoluble, and a red solution. The UV/Vis spectrum of this solution did not indicate the presence of $Cr(sen)^{3+}$. The reasons for the failure of this preparation were not investigated.

$[Cr(sen)]Cl_3$ was successfully prepared following a literature procedure for $[Cr(stn)]Cl_3$. [94]The free ligand was prepared as described above and refluxed in dry ethanol with a stoichiometric amount of $Cr(py)_3Cl_3$, [95] two equivalents of triethylamine and a catalytic amount of zinc dust. The crude complex was recrystallized from warm (60°) water by the dropwise addition of concentrated HCl. $[Cr(sen)]Br_3$ and $[Cr(sen)](ClO_4)_3$ were recrystallized from $[Cr(sen)]Cl_3$ by dissolving in warm water and dropwise addition of the appropriate concentrated acid and purified by subsequent recrystallization. UV/vis spectra gave λ_{max} and ε_{max} values in agreement with literature values.

2.4.2.3 Resolution of $[Cr(sen)]Cl_3$

(+)-$[Cr(sen)]Cl_3$ was obtained following the literature procedure for the enantiomeric resolution of $[Cr(en)_3]Cl_3$ using d-tartaric acid.[96] Enantiomeric purity was confirmed by capillary electrophoresis using a chiral buffer, 100mM d-tartrate, pH 4.1. A single peak was observed indicating an enantiomeric excess greater than 95%.

(+)-$[Cr(sen)]Cl_3$ was converted to (+)-$[Cr(sen)]Br_3$ and (+)-$[Cr(sen)](ClO_4)_3$ and subsequently purified as outlined above for the racemic

material. Capillary electrophoresis of these resolved salts also gave a single electrophoresis peak, indicating an enantiomeric excess greater than 95%.

2.4.3 Attempted Syntheses

2.4.3.1 *cis*-$Cr(cycb)(NH_3)_2^{3+}$

The macrocyclic ligand C-racemic-5,7,7,12,14,14-hexamethyl-1,4,8,11-tetraazacyclotetradeane (cycb) was prepared following a literature preperation[97,98] Sea green [*cis*-$Cr(cycb)Cl_2^{3+}$]Cl was synthesized by adding the DMF solution of the ligand to a DMF solution of $CrCl_3(DMF)_3$ and refluxing.[98]

[*cis*-$Cr(cycb)Cl_2^{3+}$]Cl was reacted with liquid ammonia in a Carius tube for two days. During this time the insoluble sea green starting material changed to a pink-red powder. After opening the Carius tube, excess ammonia was allowed to evaporate and the product was recrystallized as the perchlorate salt by dissolving in 50°, 0.1 M $HClO_4$ followed by dropwise addition of concentrated $HClO_4$ and cooling. Subsequent purification was obtained by recrystallizing as the perchlorate salt from 1 x 10^{-3} M $HClO_4$.

Microanalysis of the deep red crystals gave C,H,N ratios consistent with the formula $[Cr(cycb)(NH_3)_2Cl](ClO_4)_2.HClO_4$. This indicated that the tetradentate cycb ligand was only coordinated by three amines with the fourth present as a hydroperchlorate salt. Two ammonia and one chloro ligands occupy the remaining three coordination sites.

C,H,N percentages for $[Cr(cycb)(NH_3)_2Cl](ClO_4)_2.HClO_4$

Found (Theoretical): **C** 27.21 (27.25), **H** 6.23 (6.14), **N** 11.73 (11.91)

2.4.3.2 Cr(15aneN5)(Cl)$^{2+}$

The ligand 1,4,7,10,13-pentaazepentadecane was purchased as the pentaachloride salt (15aneN5.5HCl) from Parish Chemicals. Note that this ligand is no longer commercially available.

The attempted synthesis of Cr(15aneN5) was based on the literature preparation of *cis*-Cr(cyclam)$(NH_3)_2^{3+}$.[87] 15aneN5.5HCl (400mg, 9.9 x10^{-4} moles) was dissolved in 10ml DMF (partially soluble) and boiled to remove any water present. $Cr(DMF)_3Cl_3$ was generated *in situ* by boiling $CrCl_3.6H_2O$ (260mg, 9.9 x10^{-4} moles) dissolved in 15 ml DMF and concentrating to 10 mL. The solutions were cooled and mixed before refluxing for 1hour. A deep red powder formed over this time. This was filtered off and recrystallized as the perchlorate salt by dissolving in the minimum of 50°, 1 x10^{-3} M $HClO_4$, followed by dropwise addition of concentrated $HClO_4$ and cooling. This recrystallization was repeated, giving deep red x-ray quality crystals. Yield: 150 mg

The crystal structure of the product was determined by Steve Rettig (deceased) of the UBC X-ray facility and is given in Appendix 4. The structure that was determined was *trans*-$[Cr(15aneN5)Cl_2]ClO_4.HClO_4$. Four of the 15aneN5 amines occupy the equatorial plane with the fifth detached and present in the crystal as a hydroperchlorate salt. Two chloro ligands occupy the axial positions.

CHAPTER THREE

LASER FLASH PHOTOLYSIS WITH CONDUCTIVITY DETECTION STUDIES AND KINETIC MODELLING OF THE PHOTOAQUATION OF Cr(III) AM(M)INE COMPLEXES

3.1 Introduction

Laser flash photolysis studies using conductivity detection techniques have provided evidence for a long-lived, aquated intermediate in the photoaquation of *cis*-$Cr(cyclam)(NH_3)_2^{3+}$.[81] The characteristic features of this study were that;

i) within the pH range studied, the conductivity decay lifetimes ($\tau = 1/k_{cond}$) were always longer than those measured by emission techniques ($\tau = 1/k_{emiss} = 1.3\mu s$), with the closest agreement being $\tau_{cond}/\tau_{emiss} = 2.7$ at $pH < 3$.

ii) the conductivity decay lifetimes increased with increasing pH in contrast to the emission lifetimes which were independent of pH.

iii) at $pH > 4$ an observable rise in conductivity preceded the decay, consistent with proton loss to the bulk solution by an aquated Cr(III) species.

Based on these results, Waltz et al. proposed a mechanism involving photolysis via an aquated intermediate. Waltz's proposed mechanism is presented in Figure 3.1, with the addition of the appropriate rate constants.

The original communication of these results showed that the intermediate was a ground state species, but did not discuss possible structures. In a subsequent paper[60] Friesen et al. investigated the pressure dependence of the doublet lifetime and quantum yield of *cis*-$Cr(cyclam)(NH_3)_2^{3+}$. Their results were consistent with BISC and with reaction occurring from the $^4T_2$ state. It was reinforced that the intermediate was an aquated ground state species and two possible structures were presented; a seven coordinate species or a six coordinate species with a detached cyclam amine.

In papers discussing possible ^2E deactivation pathways for Cr(III) complexes, Endicott and co- workers[24-26] cite the work of Waltz and Friesen as supporting a seven coordinate ground state intermediate. A seven coordinate

intermediate was consistent with Endicott's proposal that reaction from the ^2E state involves crossing to the ground state surface and reaction via a ground state intermediate.

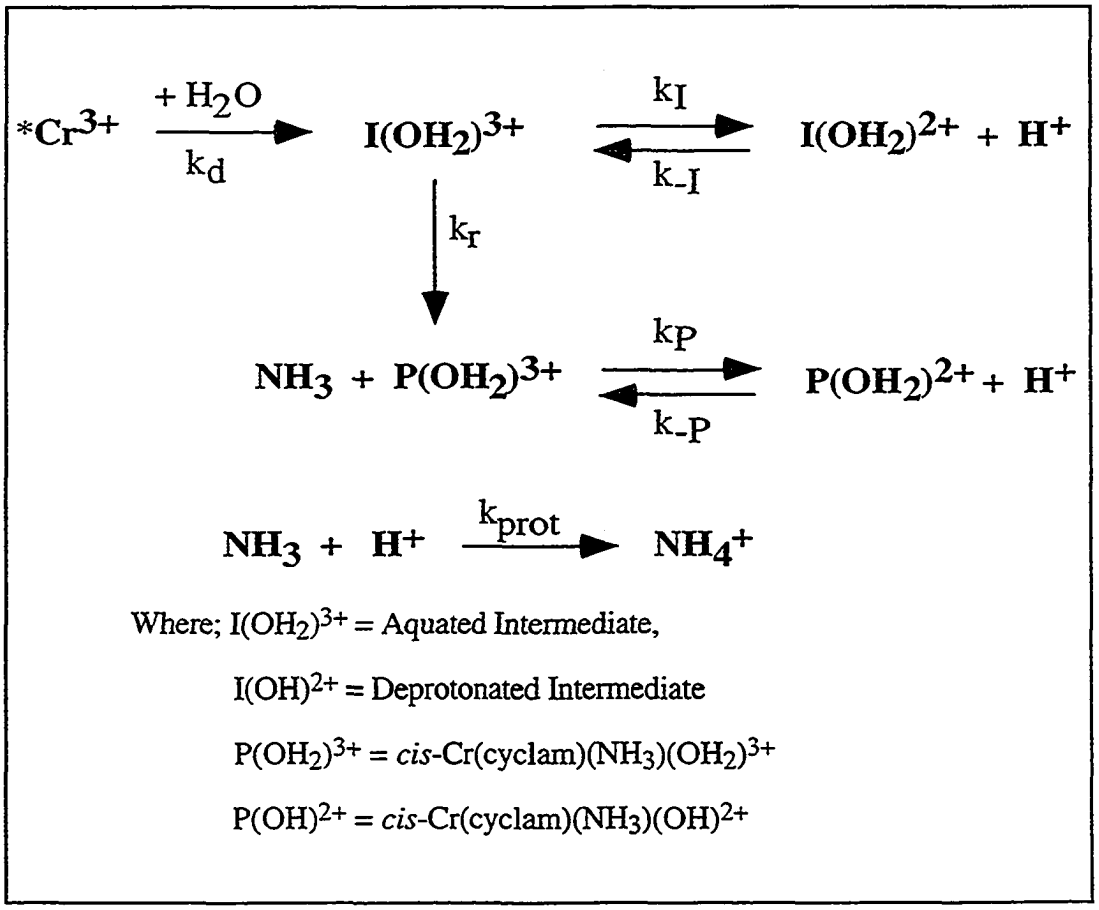

Figure 3.1. Proposed literature mechanism for the photolysis of *cis*-$Cr(cyclam)(NH_3)_2^{3+}$.

We were interested in whether intermediates would be observed in the photoaquation of other Cr(III) am(m)ine complexes and also whether intermediate formation was dependent upon ligand structure. We also hoped that the structure of

the *cis*-Cr(cyclam)$(NH_3)_2^{3+}$ intermediate could be determined, possibly providing insight into the reaction mechanism.

For these purposes the photoaquations of $Cr(NH_3)_6^{3+}$, *cis*-$Cr(tn)_2(NH_3)_2^{3+}$, *trans*-$Cr(tn)_2(NH_3)_2^{3+}$, $Cr(en)_3^{3+}$, $Cr(tn)_3^{3+}$ and $Cr(sen)^{3+}$ were investigated over the pH range 2.6 - 5.2, using laser flash photolysis with conductivity detection. The photoaquation of *cis*-Cr(cyclam)$(NH_3)_2^{3+}$ was also reinvestigated over this pH range.

Although some of the am(m)ine complexes had been the subject of similar studies, no results had been reported at pH levels greater than 4.[82] We believed that this would be the pH range of most interest as transient conductivity increases were observed for *cis*-Cr(cyclam)$(NH_3)_2^{3+}$ only at pH > 4.

Based on Waltz's results we regarded experimental evidence for such intermediates to be;

i) conductivity lifetimes longer than doublet emission lifetimes at pH < 3 and/or

ii) the observation of transient increases in solution conductivity preceding a decay at higher pH.

3.2 Laser Flash Photolysis/Conductivity Studies

3.2.1 Background theory of LFP/Conductivity

The conductivity apparatus used in this work was detailed in section 2.1. The changes in solution conductivity that occur with photolysis are monitored through the changes in potential difference which results across the two arms of a

Wheatstone bridge. A representation of a Wheatstone Bridge is presented in Figure 3.2 where R_S = the resistance of the unirradiated solution, R_S* = the resistance of the irradiated solution and R_E = the resistance of the external resistors. G_S, G_S* and G_E are the corresponding conductances.

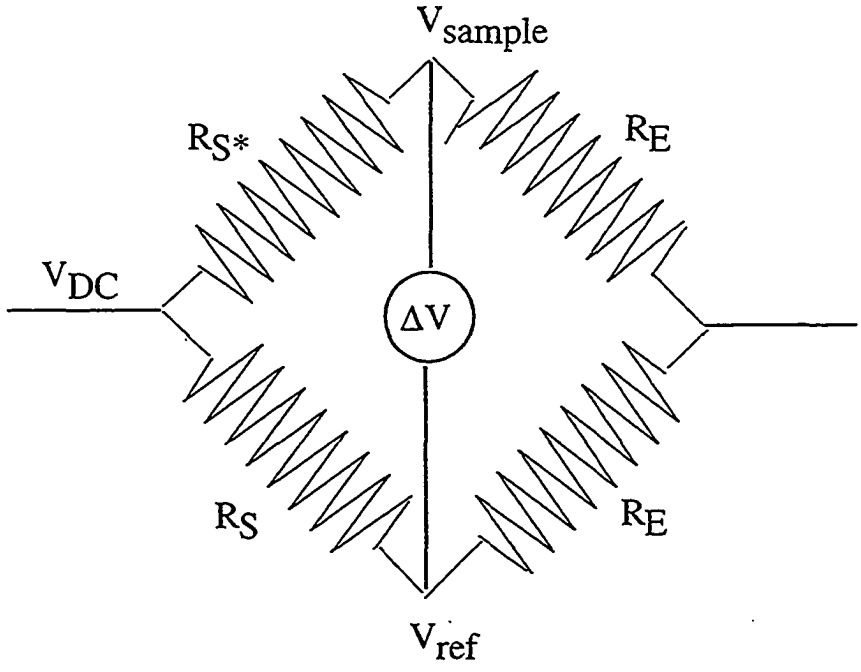

Figure 3.2 Representation of a Wheatstone Bridge

Using either conductance or resistance values, equations can be derived which predict the magnitude of the potential difference changes which develop across the bridge resulting from photochemical reaction.

In the early literature pertaining to the development of conductivity detection techniques, and its application to both pulse radiolysis and laser flash photolysis, the following equation predicting signal magnitude was introduced;[99]

$$\frac{\Delta V}{V_{DC}} = \frac{\Delta G}{(G_E+G_S+\Delta G)} \qquad (3.1)$$

where V_{DC} corresponds to the voltage of the applied DC pulse and $\Delta G = G_S - G_S^*$.

In a later paper this equation was modified,[100] instead being presented as;

$$\frac{\Delta V}{V_{DC}} = \frac{\Delta G}{(G_E+G_S)} \qquad (3.2)$$

The derivation of Equations 3.1 and 3.2 and the reasons for preferring equation 3.2 were not presented in detail in the relevant papers. The derivations of these equations have been reproduced in this work and are presented in Appendix 1.2.

We chose to derive a similar equation on resistance values, with the following equation being obtained;

$$\frac{\Delta V}{V_{DC}} = \frac{R_S.R_E}{(R_S+R_E)^2} \cdot \frac{\Delta K}{K} \cdot F_{H_2O} \qquad (3.3)$$

The derivation of Equation 3.3 is presented in Appendix 1.1. Our preference for this equation is that it reveals that the overall signal magnitudes observed to be dependent upon three factors;

$\frac{\Delta K}{K}$ - the ratio of change in conductivity to the initial solution conductivity within the irradiated volume,

$\frac{R_S.R_E}{(R_S+R_E)^2}$ - the sensitivity factor of the Wheatstone bridge which is dependent upon the R_S : R_E ratio. The closer these two resistances values are to

being equal, the greater the potential difference observed across the bridge for any given change in solution conductivity.

F_{H_2O} - the fraction of photoproduct in its aquo form. This term accounts for the different conductivity changes that occur depending on whether the photoproduct is in the aquo or hydroxo form and therefore depends upon the pK_a of the photoproduct.

$$CrN_6^{3+} + H^+ \rightarrow CrN_5(OH_2)^{3+} + NH_4^+ \Leftrightarrow CrN_5(OH)^{2+} + NH_4^+ + H^+$$

$$\Delta\lambda \approx -240\ S.cm^2\ mol^{-1} \qquad \Delta\lambda \approx 0$$

Comparisons of the signal magnitudes calculated for typical experimental conditions using Equations 3.2 and 3.3 are presented in Table 3.1. The details of the calculations are presented in Appendix 1.3, but are based on hypothetical 1.0 mM Cr(III) solutions, $A = 0.10$, $\emptyset = 0.5$ and with the photoproduct remaining as the aquated product, i.e. $F_{H_2O} = 1$.

Theoretical signal magnitudes can be calculated for the hypothetical solution as all relevant resistance and conductance values are known. This also allows for the calculation of theoretical signal magnitudes in the absence of the approximations used in Equations 3.2 and 3.3. These "absolute" values are also presented in Table 3.1.

Table 3.1 shows that the values obtained using both Equations 3.2 and 3.3 are in good agreement with the calculated absolute signal magnitudes. These calculations are also significant in indicating that signal magnitude is relatively independent of pH over the range pH 3 - 5, in the absence of a photoproduct acid-base equilibrium.

	Equation 3.2	Equation 3.3	Absolute
pH 3	38.6 mV	37.2 mV	38.8 mV
pH 4	39.3 mV	38.4 mV	37.8 mV
pH 5	39.4 mV	38.6 mV	37.1 mV

Table 3.1 Conductivity signal magnitudes calculated for theoretical equations

3.2.2 Testing of the Apparatus and Calibration Studies

To confirm the reliability of the conductivity system, calibration experiments were conducted. Decay lifetimes, fraction of doublet photoaquation, and estimated quantum yields were obtained using the conductivity apparatus for a series of Cr(III) am(m)ine complexes and compared with literature values.

As outlined in section 3.2.1, magnitudes of the observed conductivity signals are predicted to be independent of pH throughout the range pH 3 - 5. This was investigated by comparing the signal magnitudes obtained for 1.0mM solutions of $Cr(CN)_6^{3-}$ within this pH region. The photoaquation product of $Cr(CN)_6^{3-}$ has been identified by Jeftíc et al. to be $Cr(CN)_5(OH_2)^{2-}$.[101] The pKa of $Cr(CN)_5(OH_2)^{2-}$ was determined to be 9.0 indicating that this complex will not dissociate to give $Cr(CN)_5(OH)^{3-}$ within the pH range 3 - 5.

For the photoaquation of $Cr(CN)_6^{3-}$, F_{H_2O} remains constant (=1) throughout the pH range 3 - 5. It would then be expected that signal magnitudes

observed for this complex will be constant within this pH range. This is also based on the assumption that the quantum yield of $Cr(CN)_6^{3-}$ is pH independent.

3.2.2.1 Photolysis of Cr(III) am(m)ines

Solutions of the am(m)ine complexes $Cr(NH_3)_6^{3+}$, $Cr(en)_3^{3+}$, $Cr(tn)_3^{3+}$, *cis*-$Cr(tn)_2(NH_3)_2^{3+}$, *trans*-$Cr(tn)_2(NH_3)_2^{3+}$ and *cis*-$Cr(cyclam)(NH_3)_2^{3+}$ were photolyzed on the same day. The measured pH for each solution was 2.72, except for $Cr(tn)_3^{3+}$ which was pH 2.58 and all solutions were allowed to equilibrate to the laboratory temperature of 22°.

Conductivity decay lifetimes were obtained from the fitting of the experimental data using both single and double exponential fits. These are compared with both experimental doublet emission lifetimes obtained at 20° and literature values in Table 3.2.

Taking into consideration the two degree difference in temperature, which using a typical activation energy of 45 kJ mol^{-1} [74] predicts the 20° lifetimes to be about 80% of the corresponding 22° values, there is good agreement between the experimental conductivity decay and doublet emission lifetimes. The exception is *cis*-$Cr(cyclam)(NH_3)_2^{3+}$ which confirms Waltz's findings. Both sets of experimental data are consistent with literature values with the exceptions of *cis*-$Cr(tn)_2(NH_3)_2^{3+}$, *trans*-$Cr(tn)_2(NH_3)_2^{3+}$ and $Cr(tn)_3^{3+}$.

Complex	Conductivity Decay Lifetime / μs (22°)	Doublet Emission Lifetime / μs (20°)	Literature Lifetime / μs
$Cr(NH_3)_6^{3+}$	2.08 ± 0.06 (5)	2.39 ± 0.06 (5)	2.2[102]
$Cr(en)_3^{3+}$	1.613 ± 0.008 (4)	1.805 ± 0.016 (5)	1.85[102]
$Cr(tn)_3^{3+}$	1.48 ± 0.17 (4)	2.04 ± 0.10 (5)	1.6[82], 2.6[85]
t-$Cr(tn)_2(NH_3)_2^{3+}$	3.86 ± 0.17 (4)	4.58 ± 0.19 (5)	4.6[85]
c-$Cr(tn)_2(NH_3)_2^{3+}$	2.70 ± 0.08 (4)	3.36 ± 0.08 (5)	3.3[85]
c-$Cr(cyc)(NH_3)_2^{3+}$	3.96 ± 0.11 (4)	1.66 ± 0.04 (3)	1.7[66]

The figure in brackets represents the number of measurements.

Table 3.2 Comparison of experimental and literature lifetimes for a series of Cr(III) am(m)ine complexes

The literature lifetimes for *cis*- and *trans*-$Cr(tn)_2(NH_3)_2^{3+}$, along with the 2.6 μs lifetime for $Cr(tn)_3^{3+}$, were obtained by a previous graduate student of this group.[85] Examination of the raw data, and in particular the temperature dependent lifetime experiments, showed that errors were made in tabulating the lifetimes in the thesis and hence in the resulting paper. The correct lifetimes obtained in Ibrahim's study are 2.2 μs at 20°C for $Cr(tn)_3^{3+}$, 4.6 μs at 19.5°C for *trans*-$Cr(tn)_2(NH_3)_2^{3+}$ and 3.3 μs at 19.5°C for *cis*-$Cr(tn)_2(NH_3)_2^{3+}$. For *cis*-$Cr(tn)_2(NH_3)_2^{3+}$ and *trans*-$Cr(tn)_2(NH_3)_2^{3+}$, the correct values are in agreement with the experimental lifetimes obtained in our work. However the 2.2 μs value for $Cr(tn)_3^{3+}$ is suspiciously long compared to both the experimental values obtained by us, 1.48 μs for conductivity decay at 22°C and 2.04 μs for emission at 20°C, and the alternative literature lifetime of 1.6 μs.

Fractions of doublet state reaction were determined using the two procedures outlined in section 2.1.6 and are compared with literature values in Table 3.3. The values obtained for the two methods agree within experimental uncertainties for each complex. With the exception of $Cr(en)_3^{3+}$, the experimental F_D values are in good agreement with literature values. The value of 0.82 - 0.85 obtained for *cis*-$Cr(tn)_2(NH_3)_2^{3+}$ is an original result.

	Fraction of Photoreaction via the Doublet State, F_D		
Complex	Single Exponential Fit	Double Exponential Fit	Literature
$Cr(NH_3)_6^{3+}$	0.758 ± 0.010 (4)	0.766 ± 0.007 (4)	0.74*, 0.69[103]
$Cr(en)_3^{3+}$	0.842 ± 0.008 (4)	0.817 ± 0.020 (4)	0.67*, 0.70[104], 0.60[105]
$Cr(tn)_3^{3+}$	0.82 ± 0.06 (4)	0.73 ± 0.14 (3)	0.78*, 0.67[106]
t-$Cr(tn)_2(NH_3)_2^{3+}$	0.84 ± 0.03 (4)	0.822 ± 0.024 (4)	0.85[85]
c-$Cr(tn)_2(NH_3)_2^{3+}$	0.857 ± 0.027 (4)	0.82 ± 0.03 (4)	---
c-$Cr(cyc)(NH_3)_2^{3+}$	0.89 ± 0.04 (4)	0.897 ± 0.027 (4)	> 0.90

The figure in brackets represents the number of measurements.

* Obtained using conductivity detection in reference 84

Table 3.3 Comparison of experimental and literature fractions of doublet state photoreaction for a series of Cr(III) am(m)ine complexes.

The literature value of 0.67 for $Cr(en)_3^{3+}$ was also obtained using LFP with conductivity detection but a value of 0.6 has been reported using quenching experiments.[105] A protonation rate constant of 3.6×10^9 M^{-1} s^{-1} was obtained for the dangling amine of the $Cr(en)_3^{3+}$ photoproduct in the first study, significantly smaller than the protonation rate constant obtained for free ammonia, 4.3×10^{10} M^{-1} s^{-1}.[107]

The prompt photocomponent can only be observed using conductivity detection under pH conditions where protonation of the labilized amine is faster than the rate of doublet decay. Because of its smaller protonation rate constant, the prompt component of $Cr(en)_3^{3+}$ becomes indistinguishable at a lower pH than for complexes which directly aquate ammonia. It is likely that the prompt component was less well resolved at our experimental pH of 2.72 than in the literature study at pH 2.6. This would result in the fit of our data underestimating the contribution of the prompt component, explaining a larger F_D value. This could easily be checked by repeating our experiment at a lower pH. However pH levels less than 2.7 have been avoided to prevent current overload of the DC pulse power supply of the conductivity apparatus.

Quantum yields were estimated for each complex based upon the relative magnitude of the observed conductivity changes relative to that of $Cr(NH_3)_6^{3+}$, assuming that the incident laser pulse energy was constant for each complex.

$$\emptyset = \frac{n_{photoproducts}}{n_{photons\ absorbed}}$$

$$\emptyset \propto \frac{\text{conductivity decay magnitude}}{F_A}$$

$$= k \frac{\text{conductivity decay magnitude}}{F_A} \qquad (3.4)$$

where F_A is the fraction of light absorbed by the complex at the excitation wavelength of 355nm; $F_A = 1\text{-}10^{-A}$ and assumes a constant incident laser pulse energy for each complex.

Using the tabulated values for F_A, Ø and observed decay magnitude for $Cr(NH_3)_6^{3+}$, a value of 4.1×10^{-4} was obtained for k. Quantum yields were then estimated for the other am(m)ine complexes by applying this value to the measured decay magnitudes and F_A values. The quantum yields obtained are compared to literature values in Table 3.4.

Complex	Signal Magnitude / mV	F_A $(1\text{-}10^{-A})$	Estimated Quantum Yield	Literature Quantum Yield
$Cr(NH_3)_6^{3+}$	87.1 ± 1.2 (4)	0.078	--	0.46[103]
$Cr(en)_3^{3+}$	103 ± 4 (4)	0.142	0.30	0.37[73]
$Cr(tn)_3^{3+}$	50.1 ± 1.6 (4)	0.106	0.19	0.14[85]
t-$Cr(tn)_2(NH_3)_2^{3+}$	55 ± 3 (4)	0.097	0.23	0.34[85]
c-$Cr(tn)_2(NH_3)_2^{3+}$	62 ± 4 (4)	0.091	0.28	0.24[85]
c-$Cr(cyc)(NH_3)_2^{3+}$	53.0 ± 0.5 (4)	0.167	0.13	0.16[81], 0.2[66]

The figure in brackets represents the number of measurements.

Table 3.4 Comparison of experimental and literature quantum yields for a series of Cr(III) am(m)ine complexes.

The agreement between the estimated quantum yields and literature values is poor, with percent differences ranging between 19% for $Cr(en)_3^{3+}$ and 33% for

trans-$Cr(tn)_2(NH_3)_2^{3+}$. This is not surprising as Equation 3.4 is only a crude approximation, based on each solution having the same conductivity and the assumption that each photoaquation reaction produces the same conductivity change per mole as for $Cr(NH_3)_6^{3+}$, i.e. that $\frac{R_S.R_E}{(R_S+R_E)^2}$ is the same for each complex and that $\frac{\Delta K}{K}$ is the same per mole of photoproduct.

Overall the experimental lifetimes and fractions of doublet photoreaction obtained for the Cr(III) am(m)ine complexes were in agreement with literature values. This confirmed that the apparatus was producing reliable and accurate kinetic data.

3.2.2.2 Photolysis of $Cr(CN)_6^{3-}$.

$Cr(CN)_6^{3-}$ solutions, each approximately 1.0 mM in concentration, were photolyzed over the pH range 2.7 - 5.1. The experimentally obtained conductivity decay magnitudes obtained were corrected for the slight variations in solution absorbance and are plotted against pH in Figure 3.3.

In section 3.2.2. it was outlined that the signal magnitudes obtained for $Cr(CN)_6^{3-}$ are expected to be constant within the pH range 3 - 5. As shown in Figure 3.3, this was not observed experimentally; decay magnitudes decreased gradually from a maximum value of 120 mV at pH 2.75 to 111mV at pH 4.25, with a more dramatic decrease then occurring with a 45 mV signal being obtained at pH 5.25.

Possible explanations for the observed pH dependence of the $Cr(CN)_6^{3-}$ signal magnitudes focus on the physical arrangement of the cell, and the possibility of water competing with H_3O^+ to protonate the labilized base.

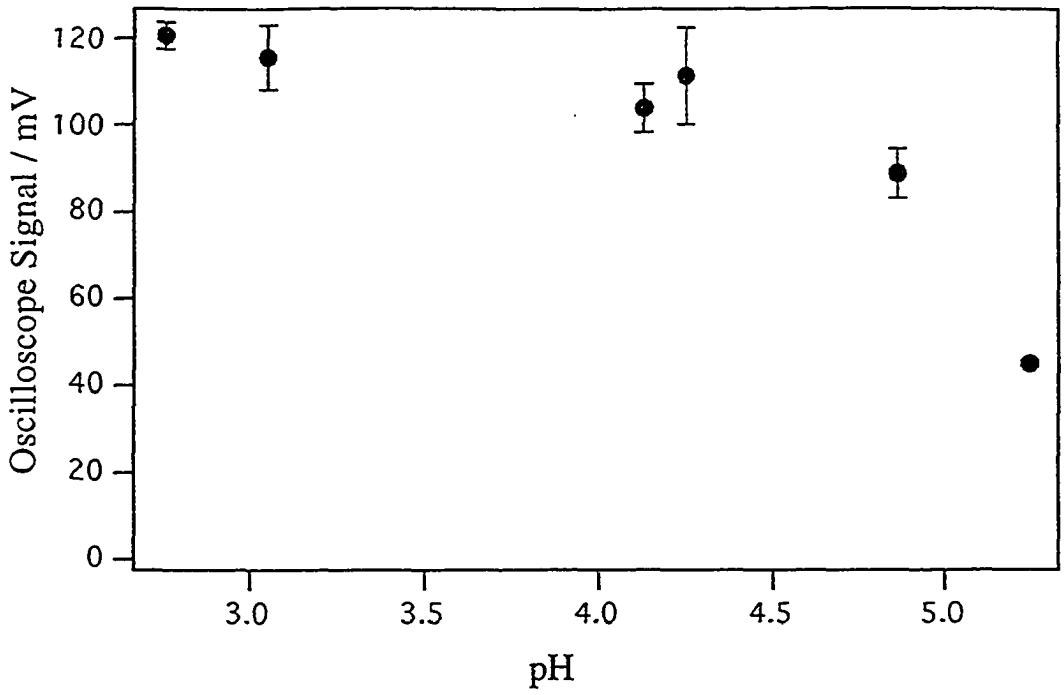

Figure 3.3 Conductivity decay magnitudes obtained for the photolysis of 1.0 mM $Cr(CN)_6^{3-}$ at various pH.

The possibility of thermal hydrolysis occurring within the microsecond timescales of the photoaquation process enhancing the observed signals at low pH can be discounted. Although $Cr(CN)_6^{3-}$ undergoes thermal hydrolysis with both acid independent and acid assisted pathways[108] the rate constants for both are small, $k_0 = 1.1 \times 10^{-5}\ s^{-1}$ and $k_{H+} = 3.2 \times 10^{-3}\ s^{-1}$. Minimal thermal hydrolysis would be expected within the timescale of our experiments for solutions between pH 2.7 and 5.1. This was confirmed by the comparison of the uv/vis spectra of $Cr(CN)_6^{3-}$ solutions taken before and after a series of laser flash experiments which showed little variation.

A possible dependence of quantum yield upon pH for $Cr(CN)_6^{3-}$ in acidic conditions has not been investigated. Two independent studies at pH 8.6[109] and pH 6.75[110] both gave quantum yields of 0.16 at 25°, showing that, within this pH range at least, the quantum yield is constant. This may not be relevant to acidic conditions

where it is possible that protonation of a coordinated cyanide could assist photochemical loss. This is a possibility that warrants further investigation although other results, discussed below, also indicate that signal magnitudes obtained with our apparatus display a pH dependence.

Based on the assumption, presented in section 3.2.1, that no overall conductivity change occurs when the $CrN_5(OH_2)^{3+}$ photoproduct dissociates to give $CrN_5(OH)^{2+}$, the pKa of the photoproduct should correspond to the pH at which the observed signal magnitude is half the maximum signal. Using our conductivity results we have been unable to obtain pKa values for *cis*-$Cr(cyclam)(NH_3)(OH_2)^{3+}$, $Cr(NH_3)_5(OH_2)^{3+}$ and $Cr(en)_2(enH)(OH_2)^{3+}$ which are in agreement with literature values. These complexes are the photoaquation products of *cis*-$Cr(cyclam)(NH_3)_2^{3+}$, $Cr(NH_3)_6^{3+}$ and $Cr(en)_3^{3+}$ respectively.

In their study of *cis*-$Cr(cyclam)(NH_3)_2^{3+}$, Waltz and Lilie estimated a pKa value of 4.0 for *cis*-$Cr(cyclam)(NH_3)(OH_2)^{3+}$, based on the above reasoning. A similar analysis of our results gave a significantly lower pKa value of 3.7. Similar treatment of experimental results for $Cr(NH_3)_6^{3+}$ and $Cr(en)_3^{3+}$ gave photoproduct pKa values of 4.4 and 3.7. These values are both significantly lower than the pKa values of the known photoproducts, $Cr(NH_3)_5(OH_2)^{3+}$ and $Cr(en)_2(enH)(OH_2)^{4+}$ which are 5.1-5.2[30] and 4.4[111] respectively.

The observed conductivity signals for the above complexes are expected to decrease as the pH is increased due to F_{H_2O} becoming smaller as the photoproduct acid-base equilibrium shifts to the right. The more acidic the photoproduct, the smaller the conductivity signals expected at any given pH. If the apparatus also generates signals which decrease in magnitude as the pH increases, this therefore gives the appearance of the photoproduct being a stronger acid. The discrepancies described are therefore consistent with the apparatus generating signals that are pH dependent.

One possibility is that insufficient H_3O^+ is present within the irradiated volume to protonate all of the photoreleased base at the higher pH conditions, giving smaller signals than at lower pH. Calculations based on a 1.0 mM $Cr(CN)_6^{3-}$ solution and typical photolysis conditions do not support this. Even at pH 5.25 there is sufficient H_3O^+ available within the irradiated volume, 1.2×10^{-9} mole, to protonate all of the liberated cyanide, 9.9×10^{-10} mole. Obviously this fails to account for the experimental observation that at pH 5.25 the conductivity decay magnitude is only 37% of that observed at pH 2.75.

The dependence of observed signal magnitude upon incident laser pulse energy for a 1.84 mM $Cr(CN)_6^{3-}$ solution at pH 5.06 showed that depletion of H_3O^+ was not the cause. This solution was deliberately made more concentrated than normal experimental conditions to exaggerate any possible effects due to depletion of H_3O^+, be it localized or occurring throughout the irradiated volume. As Figure 3.4 shows, the decay magnitudes increased linearly with incident laser pulse energy. This was not consistent with depletion of H_3O^+ occuring within the irradiated volume.

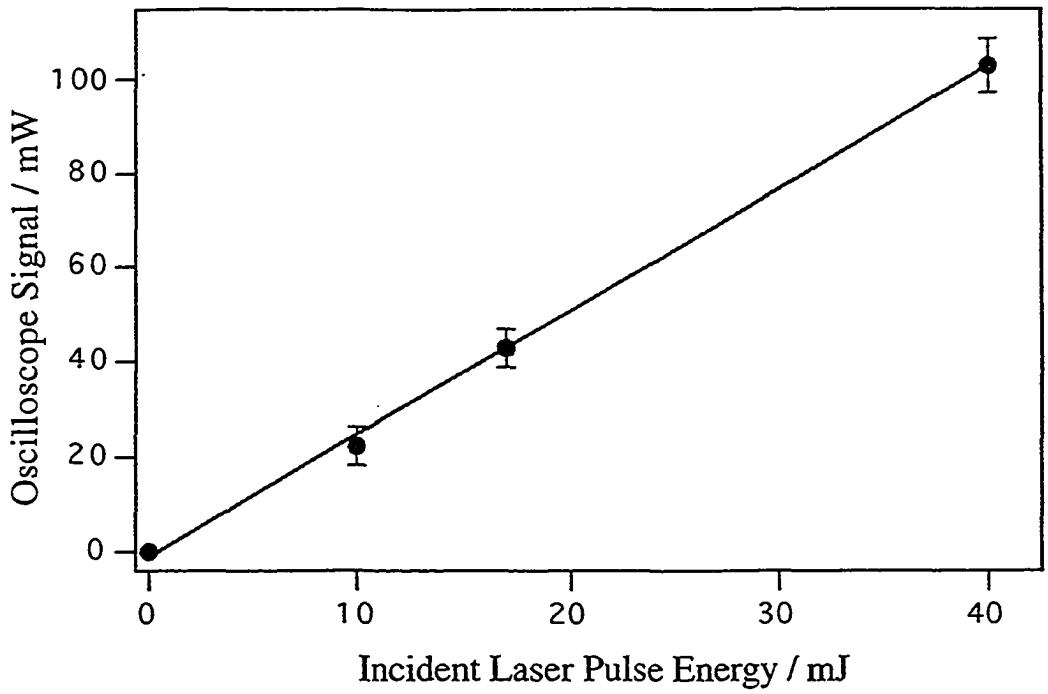

Figure 3.4 Dependence of decay magnitudes upon incident laser pulse energy for the photolysis of a 1.84 mM $Cr(CN)_6^{3-}$ solution at pH 5.06.

Another possible explanation involves the effect of solution conductivity on the electric field lines generated by the applied DC pulse. Due to the electrodes being circular these field lines arc between the central and outer electrodes. A decrease in solution conductivity causes the curvature of these arcs to increase, possibly leading to edge effects if the field lines intersect the cell wall. Such edge effects could result in decreased current flow at higher pH and a decrease in the potential difference observed across the arms of the Wheatstone bridge.

An investigation into edge effects and their possible influence on signal magnitude would require the construction of cells with alternative electrode arrangements. The use of plate electrodes would ensure that electric field lines are always parallel to the cell walls but such an arrangement is likely to impede solution flow through the cell. Reference to an arrangement using platinum plate electrodes with holes cut to allow solution flow has been found in the literature.[112]

The theoretical equations presented in section 3.2.1 are based upon highly idealized conditions and may not reflect the experimental situation. Both Equations 3.2 and 3.3 assume that photoinduced conductivity changes are occurring throughout the entire solution volume between the two electrodes. This effectively generates a new block resistor between the reference electrodes with conductance G_S* and resistance R_S*. In reality the conductivity changes only occur within the irradiated volume and outside of this there is actually no change in solution conductance.

The possible effect of this on signal magnitude is most evident when the extreme scenario is considered, the irradiation of an infinitesimal volume by a highly focused laser beam. If the solution is regarded as a block, irradiating an infinitesimal volume would result in little overall change in the composition and therefore resistance of this block. This would result in little difference in the current flowing through the two arms of the bridge and therefore small signals would be expected.

For our apparatus approximately 50% of the solution between the electrodes is irradiated. It is difficult to predict to what extent the experimental signal will deviate from that calculated for the idealized conditions. Although other factors may also contribute to this discrepancy, comparison of theoretical and experimental signal magnitudes show that the experimental signal is only 5% of that calculated. As detailed in Section 3.2.1, a 38 mV signal is calculated for a 1.0 mM $Cr(NH_3)_6^{3+}$ solution at pH 3, contrasting with the 87 mV signal obtained experimentally with an amplified gain of 50.

The above discussion indicates that the current cell design may not be the most efficient. Maximum sensitivity is predicted to occur when all of the solution between the electrodes is irradiated but our design has only 50% of the solution being irradiated. Optimum conditions would involve irradiating the maximum volume of solution without the laser pulse hitting the electrodes.

The decrease in signal magnitude with pH is not a result of a decrease in background solution conductivity at higher pH. As Figure 3.5 shows, the conductivity signals obtained for a pH 5.06 $Cr(CN)_6^{3-}$ solution did not change significantly when KCl was added to give overall conductivities comparable to the experimental situation at lower pH values.

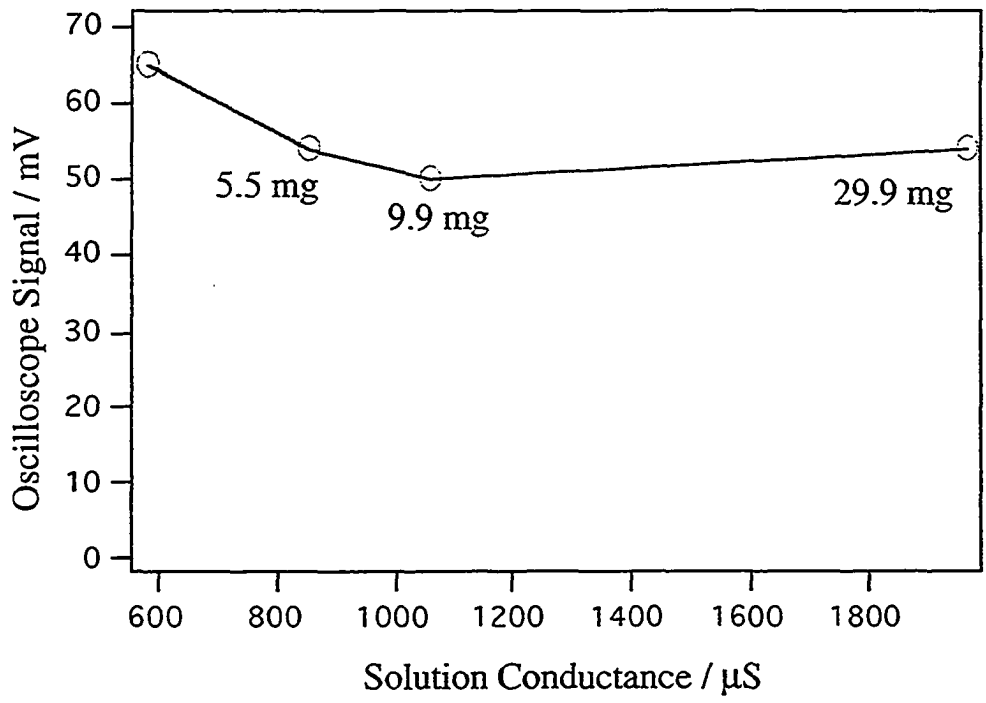

Figure 3.5 Dependence of signal magnitude for pH 5.06, 1.0 mM $Cr(CN)_6^{3-}$ solutions upon added solid KCl

*The solid KCl was added to the 50 mL solution reservior.

Figure 3.5 shows that a slight decrease in signal magnitude was actually observed as the solution conductivity was increased through the addition of KCl. This suggests that the decrease in H_3O^+ and not the associated decrease in solution conductivity causes the observed decay magnitudes to decrease with increasing pH. As stated earlier this is not the result of H_3O^+ being depleted by the labilized base.

The conductivity changes predicted by equations 3.1 - 3.3 assume that the labilized base is protonated exclusively by H_3O^+. Estimates of the changes in molar conductivity associated with this process show that a decay in solution conductivity occurs when the photoproduct is formed in its aquo form and that no overall change occurs when the photoproduct is formed in its hydroxo form;

$$CrL_6^{3+} + H_3O^+ \text{ ---> } CrL_5(OH_2)^{3+} + LH^+ \text{ <=> } CrL_5(OH)^{2+} + LH^+ + H_3O^+$$
$$\Delta\lambda \approx -350 \text{ S cm}^2 \text{ mol}^{-1} \qquad \Delta\lambda \approx 0$$

As pH increases the concentration of H_3O^+ drops and it is likely that water will be able to compete with H_3O^+ to protonate the labilized base. If protonation by water occurs this results in different estimates for the changes in molar conductivity. Formation of the aquated photoproduct results in an overall increase in molar conductivity whereas no overall change occurs with formation of the hydroxo form;

$$CrL_6^{3+} + 2H_2O \text{ --> } CrL_5(OH_2)^{3+} + LH^+ + OH^- \text{ <=> } CrL_5(OH)^{2+} + LH^+ + H_2O$$
$$\Delta\lambda \approx 290 \text{ S cm}^2 \text{ mol}^{-1} \qquad \Delta\lambda \approx 0 \text{ S cm}^2 \text{ mol}^{-1}$$

The results observed for the photolysis of $Cr(CN)_6^{3-}$ are consistent with protonation of the labilized base by water becoming competitive with protonation by H_3O^+ at higher pH as the concentration of H_3O^+ declines. At pH < 3 large decays in solution conductivity are observed, consistent with the labilized base being protonated exclusively by H_3O^+. As protonation by water becomes competitive, the associated increase in solution conductivity will offset the decrease that results from H_3O^+ protonation. The greater the extent of water protonation the larger this offset will

become, resulting in conductivity decays that decrease in magnitude as the pH is increased.

At this stage we are unable to provide a definite explanation as to why the decay magnitudes observed in the photolysis of $Cr(CN)_6^{3-}$ display a pH dependence, although a number of possibilities have been presented. However we favour the final possibility presented, that competitive protonation of the labilized base by water occurs as the pH increases. This is based on the linear dependence of signal magnitude upon incident laser pulse energy and the fact that the signals were dependent upon pH and not conductivity.

3.2.3 Variable pH studies of Cr(III) am(m)ine complexes.

Representative conductivity traces obtained in the photolysis of $Cr(NH_3)_6^{3+}$, $Cr(sen)^{3+}$ and *cis*-$Cr(cyclam)(NH_3)_2^{3+}$ are given in Figures 3.6 - 3.8. Data collection on the oscilloscope is timed to start before triggering of the laser and all experimental traces display a flat baseline signal preceding the laser induced changes in solution conductivity. The delay generator has a digital output and the triggering of the laser pulse is timed to occur 13 points after data collection begins. As data is collected for 100 points, with point 0 corresponding to t = 0, the time interval between points becomes a function of the experimental timescale. This results in traces obtained on different timescales having the appearance of different onset times for the photoinduced conductivity changes when plotted on the same graph, as shown in Figures 3.7 and 3.8. For the purposes of both fitting and data evaluation, the experimental traces are rescaled so that t=0 corresponds to point 13, the onset of the photoinduced changes in solution conductivity.

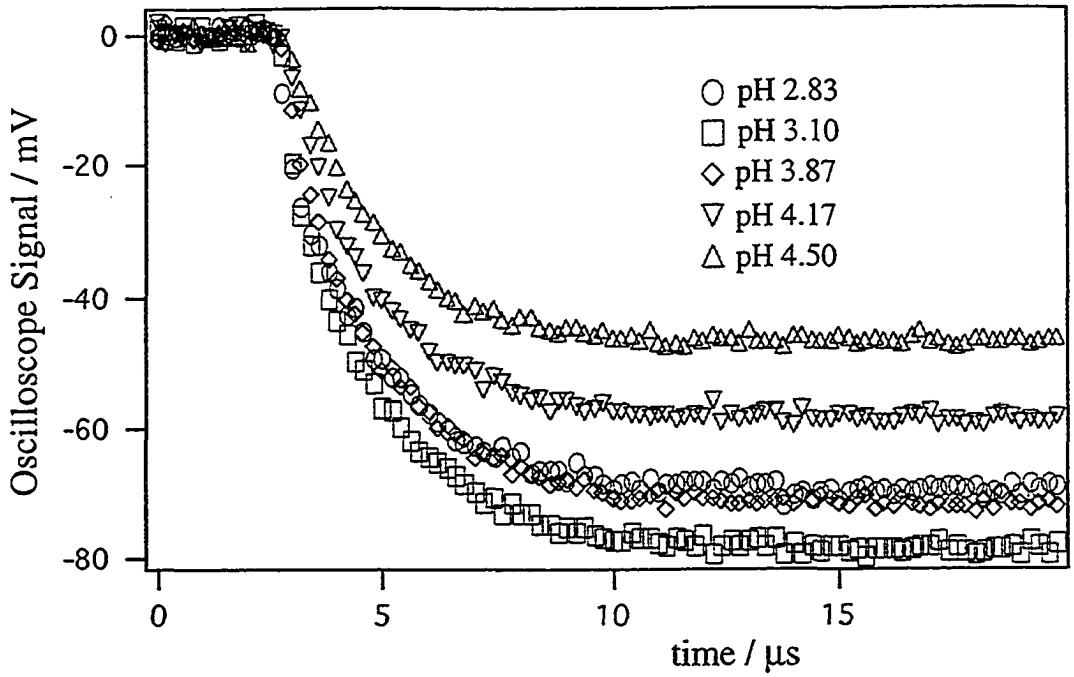

Figure 3.6 Conductivity traces obtained for the laser flash photolysis of $Cr(NH_3)_6^{3+}$ at various pH values.

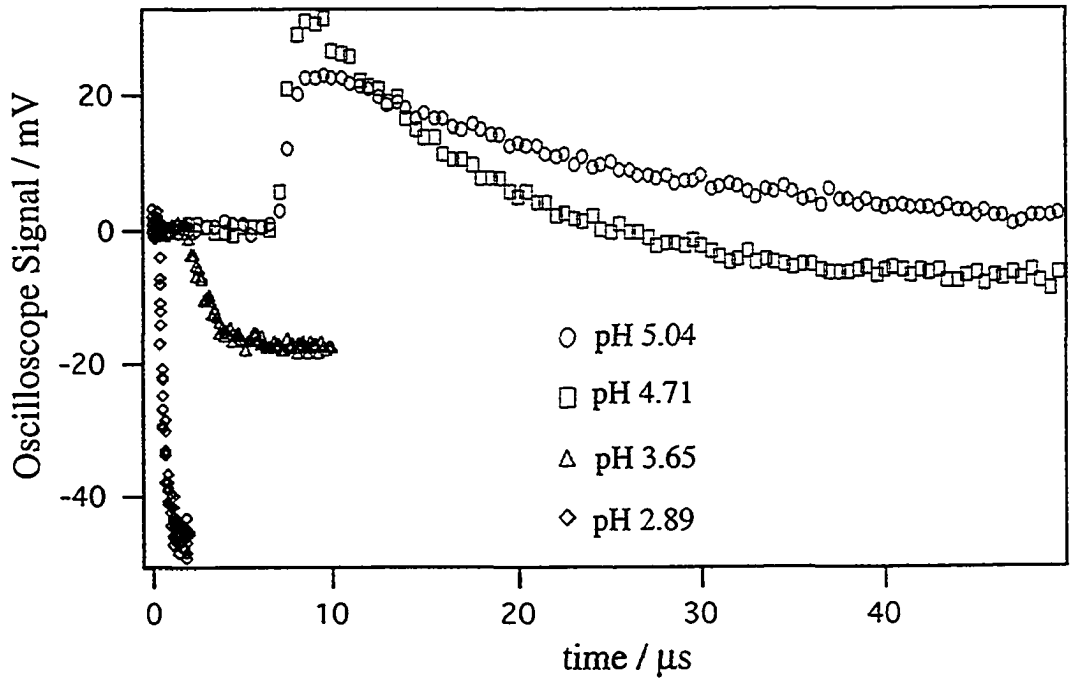

Figure 3.7 Conductivity traces obtained for the laser flash photolysis of $Cr(sen)^{3+}$ at various pH values

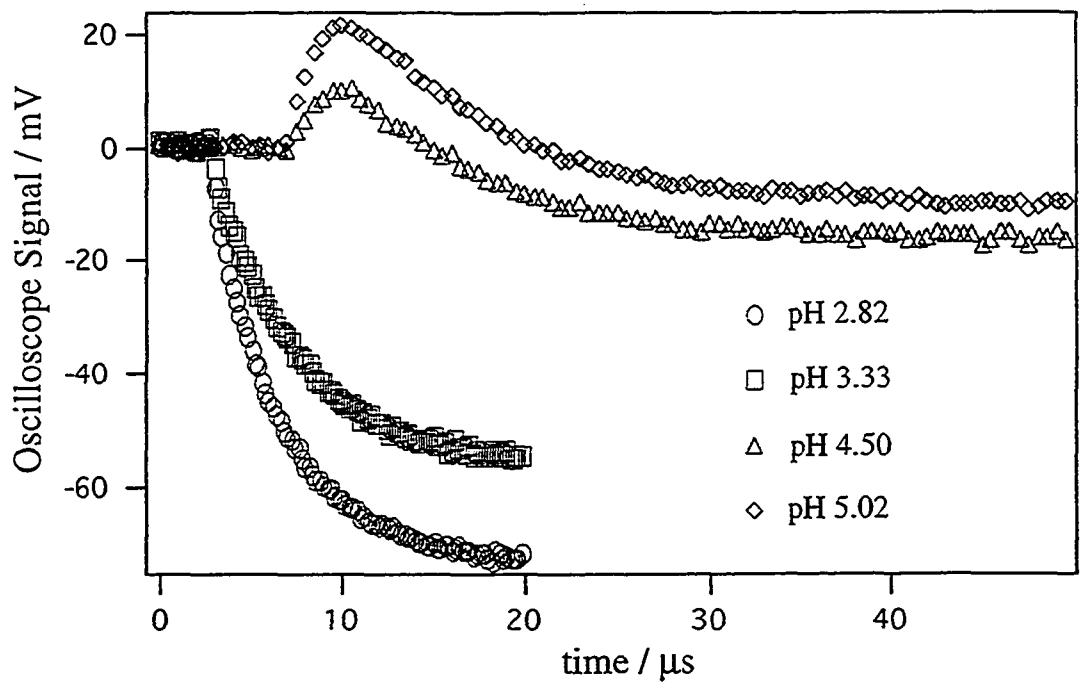

Figure 3.8 Conductivity traces obtained for the laser flash photolysis of *cis*-Cr(cyclam)$(NH_3)_2^{3+}$ at various pH values

A summary of the results obtained for all of the am(m)ine complexes is provided in Table 3.5 which also lists the dominant photoaquation process for each complex. The emphasis of this summary is on whether conductivity decay lifetimes longer than emission lifetimes were obtained at pH < 3, and if transient increases in solution conductivity were observed at any pH. As outlined earlier, these are the two conductivity based results regarded as characteristic of photolytic intermediates.

The am(m)ine complexes displayed exponential decreases in solution conductivity at pH < 3 with the observed lifetimes being in agreement with their respective doublet emission lifetimes. The only exception was *cis*-Cr(cyclam)$(NH_3)_2^{3+}$ which had a longer conductivity lifetime, confirming Waltz's results.

Complex	τ cond > τ emiss at pH < 3	Transient Conductivity Increases	Dominant Photoaquation
cis-$Cr(cyclam)(NH_3)_2^{3+}$	Yes	Yes, pH > 4	NH_3
$Cr(NH_3)_6^{3+}$	No	No	NH_3
cis-$Cr(tn)_2(NH_3)_2^{3+}$	No	No	NH_3
trans-$Cr(tn)_2(NH_3)_2^{3+}$	No	No	NH_3
$Cr(en)_3^{3+}$	No	Yes, pH > 4	en
$Cr(tn)_3^{3+}$	No	Yes, pH > 4	tn
$Cr(sen)^{3+}$	*	Yes, pH > 3.5	sen

* Observed decay is protonation limited due to fast doublet decay.

Table 3.5 Summary of conductivity based photolysis results for Cr(III) am(m)ine complexes.

Decay lifetimes were found to increase with pH for $Cr(en)_3^{3+}$, $Cr(tn)_3^{3+}$, and $Cr(sen)^{3+}$, with this trend being confirmed for *cis*-$Cr(cyclam)(NH_3)_2^{3+}$. For $Cr(NH_3)_6^{3+}$, *cis*-$Cr(tn)_2(NH_3)_2^{3+}$, and *trans*-$Cr(tn)_2(NH_3)_2^{3+}$, the decay lifetimes first became shorter as the pH increased from 2.6 - 4.3. Above pH 4.3 the lifetimes obtained for these complexes then increased with increasing pH. This trend was most evident for *cis*- and *trans*-$Cr(tn)_2(NH_3)_2^{3+}$ and is illustrated in Figure 3.9.

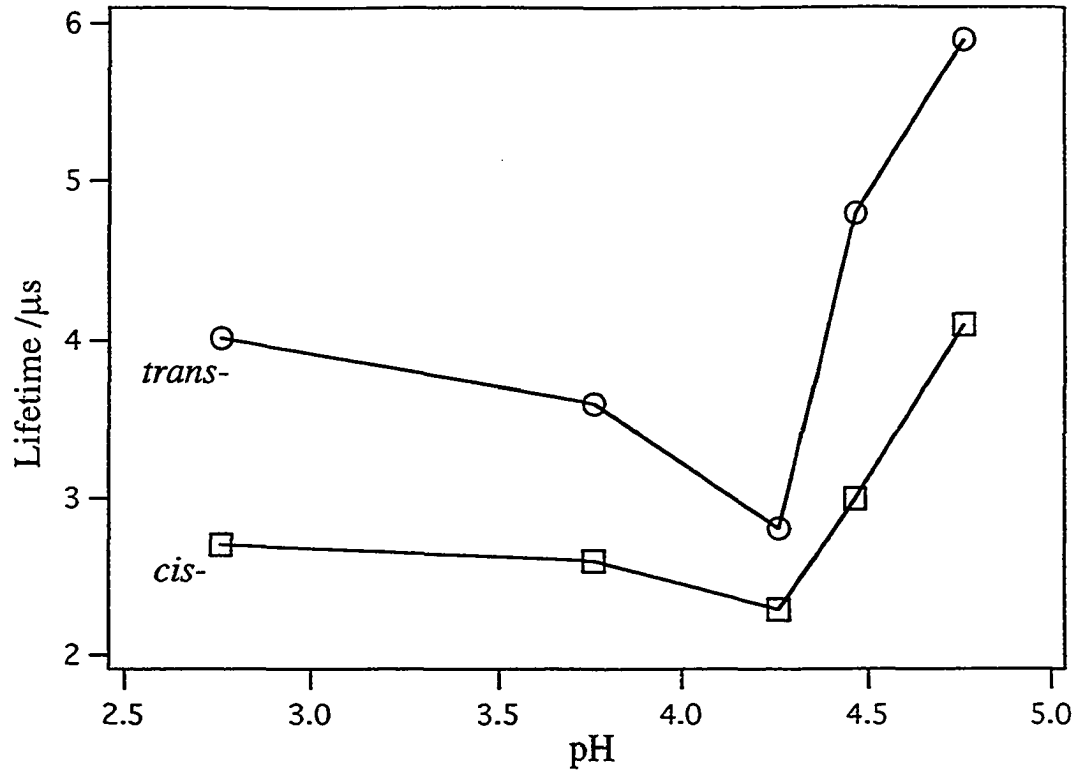

Figure 3.9 Variation of conductivity decay lifetimes with pH in the photolysis of *cis*- & *trans*-$Cr(tn)_2(NH_3)_2^{3+}$.

A significant result was the observation of transient conductivity increases in the photoaquation of $Cr(en)_3^{3+}$, $Cr(tn)_3^{3+}$ and $Cr(sen)^{3+}$ and confirmed here for *cis*-$Cr(cyclam)(NH_3)_2^{3+}$. The common feature of these complexes, with the exception of *cis*-$Cr(cyclam)(NH_3)_2^{3+}$, is that they photoaquate to give a dangling amine arm. The magnitudes of the transient increases in conductivity increased with pH for each complex. Apart from *cis*-$Cr(cyclam)(NH_3)_2^{3+}$, no transient increases were observed over the pH range 2.6-5.0 for any of the complexes which photoaquate with ammonia loss.

The conductivity traces obtained at pH 3.85 for *cis*-$Cr(cyclam)(NH_3)_2^{3+}$ displayed a reproducible "kink", shown in Figure 3.10. The fact that this "kink" was

reproducible, observed at different timescales, and absent in traces obtained for the other am(m)ine complexes at this pH, precluded it from being artifactual. The significance of this result is discussed in more detail in section 3.5.4.

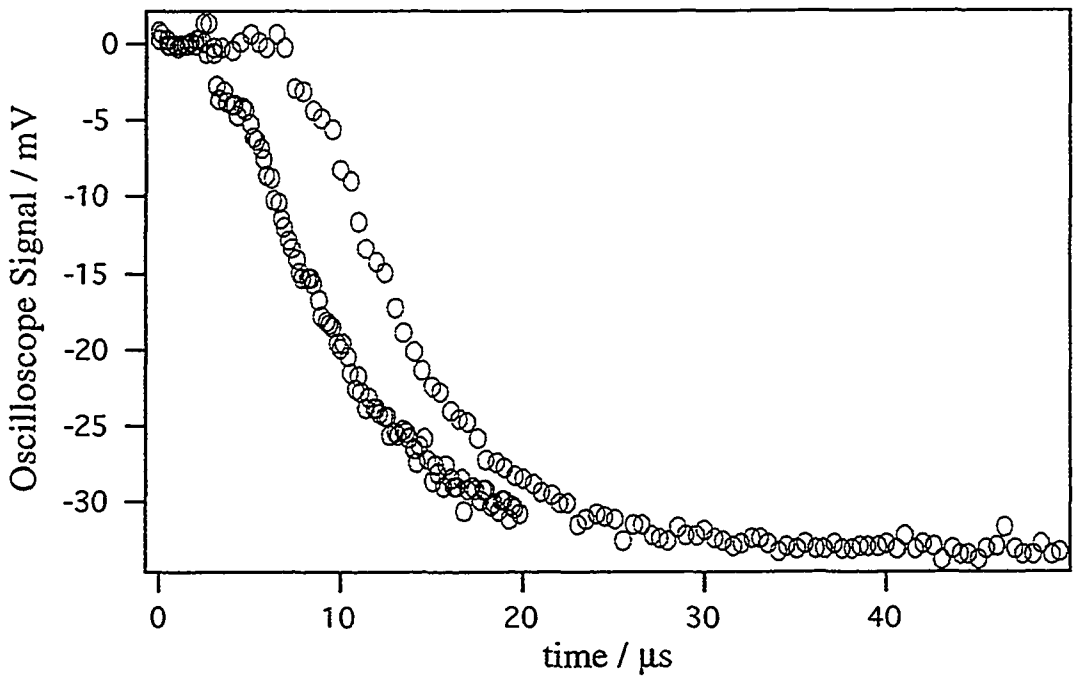

Figure 3.10 Conductivity traces for the laser flash photolysis of *cis*-$Cr(cyclam)(NH_3)_2^{3+}$ at pH 3.85.

3.3 Kinetic modelling of photoaquation mechanisms

3.3.1 Basis of modelling

Our first modelling studies were based on the mechanism proposed by Waltz and Lilie for the photoaquation of *cis*-$Cr(cyclam)(NH_3)_2^{3+}$. Differential rate equations were derived for each mechanistic species and numerical integration of these equations gave the time dependent changes in concentration occurring for each

species in solution. Time dependent changes in solution conductivity were then calculated from the concentration changes using relevant molar conductivity values. The changes in H_3O^+ and OH^- concentration occuring due to the autoionization of water were not included in the modelling as no significant changes occur due to this process within the microsecond timescales of the modelled photoreactions. The results discussed in section 3.2.2 indicates that water competes with H_3O^+ at higher pH to protonate the labilized base. At the time of the modelling studies this possibility was not recognized and therefore was not included. This is unlikely to affect the results below pH 4.5, but may explain why poor fits were obtained between modelled changes and experimental data, at higher pH values for complexes which photoaquated with a high quantum yield.

Modelling of the experimental data was regarded as being successful if a single set of variables could be used to model the experimental traces obtained at all pH values for any given complex. Based on this criterion it was found that experimental results could not be successfully modelled using Waltz's mechanism for any of the am(m)ine complexes studied, including *cis*-Cr(cyclam)$(NH_3)_2^{3+}$. This led to the modelling of alternative photoaquation mechanisms which will be discussed in more detail in section 3.4. A key feature is that all modelled mechanisms include prompt and slow components occurring from the $^4T_2$ and ^2E states. Reaction from the ^2E state is modelled as involving BISC to the $^4T_2$ state followed by prompt reaction.

It was intended for Equation 3.3 to be incorporated into the kinetic modelling with the theoretical mV signals resulting across the Wheatstone bridge then being calculated for comparison with the experimental data. However, as discussed in section 3.2.2.2, the results obtained for $Cr(CN)_6^{3-}$ indicate that Equation 3.3 is not representative of the experimental situation. The equation predicts that conductivity

signal magnitudes are independent of pH in the absence of a photoproduct acid - base equilibrium, which is not observed experimentally.

A valid comparison of experimental and modelled data is still possible by plotting the experimental mV signals and modelled changes in solution conductivity on the same graph but using independent scaling. Time profiles of the modelled and experimental changes can then be directly compared as can the relative ratio of conductivity rises and decays for traces which display a transient increase in solution conductivity. Fitting the modelled and experimental traces and comparison of the exponential rate constants obtained confirmed a good match between the two sets of data.

Modelling of each photoaquation mechanism involves a large number of variables. Many of these values can be obtained from the literature, or are measurable, so can not strictly be regarded as variables. In the following discussion the modelling variables have been classified into three groups and the details regarding how the values are obtained are discussed. Details of the actual modelling, including the integrated rate expressions and other calculations involved, are detailed in Appendix 2 for each modelled mechanism.

3.3.2 Modelling Variables

3.3.2.1 Physical and chemical parameters

To calculate the concentrations of excited state species occurring in solution it is necessary to know the solution absorbance, incident laser pulse energy and volume of solution irradiated. The volume irradiated is a known quantity with the molar absorptivity at 355 nm being measured for each complex. Incident laser pulse

energy was measured before each set of photolysis experiments were conducted and is corrected for the truncation of the laser pulse by the cell window.

The concentrations of photoproducts formed by reaction via the excited states are dependent upon the quantum yield and the absorption for each complex;

$$[\text{Prods}] = \emptyset\,[^*\text{Cr(III)}]$$

$$= \emptyset \frac{F_A\, n_{photons}}{\text{Vol Irrad}}$$

where; $F_A = 1\text{-}10^{-A}$

$$n_{photons} = \frac{E_{pulse}}{E_{355\ photon}}$$

A = solution absorbance at 355 nm

E_{pulse} = energy of the 355 nm laser pulse

Solution absorbance and incident laser pulse energy were measured for each set of experiments. The modelled incident laser pulse energy was corrected for truncation by the cell window. Volume irradiated was calculated from the cell dimensions.

3.3.2.2 Rate constants and pKa values

The modelling assumes that the thermally equilibrated ^2E and $^4T_2$ states are formed instantaneously from the Franck - Condon states. Prompt reaction from the $^4T_2$ is also viewed as giving instantaneous formation of the initial photoproduct. Reaction from the ^2E state is modelled as occurring with the rate of doublet decay which is obtained experimentally or else from the literature.

Protonation rate constants of 4.3×10^{10} M^{-1} s^{-1} and 3.6×10^{9} M^{-1} s^{-1} were obtained from the literature for ammonia[107] and a monodentate ethylenediamine ligand[83] respectively. The protonation rate for the monodentate ethylenediamine ligand was used to estimate the rates for the similar dangling amine arms generated in the photolysis of $Cr(tn)_3^{3+}$ and $Cr(sen)^{3+}$.

The pK_a values for $Cr(NH_3)_5(OH_2)^{3+}$ and $Cr(en)_2(enH)(OH_2)^{3+}$, the photoproducts of $Cr(NH_3)_6^{3+}$ and $Cr(en)_3^{3+}$ are 5.1[30] and 4.4[111] respectively. These were used to estimate the pKa values modelled for the photoproducts of the other am(m)ine complexes studied.

The use of the Debye-Smoluchowski and Fuoss equations in calculating ion-pair formation yields and ion diffusion rate constants has been investigated in detail by a previous member of this research group.[113,114] Computer models were developed in Cai's work which readily calculate the values of k_{diff}, k_{-diff} and K_{IP} for any ion pair. Based on hydrodynamic radii[115] of 900 pm for H^+ and 400 pm for both $Cr(NH_3)_6^{3+}$ and ClO_4^-, k_{diff} values of $4 - 6 \times 10^9$ $M^{-1}s^{-1}$ were calculated for approach of a proton to a Cr^{3+} species. Using the same radius as for $Cr(NH_3)_6^{3+}$, but adjusting for charge gave k_{diff} values of $5 - 7 \times 10^9$ $M^{-1}s^{-1}$ for approach of a proton to a Cr^{2+} species. Assuming that protonation is a diffusion controlled process, these k_{diff} values can be used to estimate k_{-a} in the modelling. The k_a values were obtained from the pK_a and k_{-a} values as $k_a = k_{-a}\ 10^{-pKa}$.

3.3.2.3 Molar conductivities

Central to the modelling of the transient conductivity changes are the molar conductivity values of the am(m)ine complexes and photoproducts. Limiting molar conductivity values were obtained experimentally for the Cr(III) am(m)ine complexes

by measuring the conductivities of a series of successive dilutions. The limiting molar conductivities were determined for each complex from a plot of molar conductivity against the square root of concentration. The conductivity electrode was calibrated with standard NaCl and KCl solutions before making these measurement.

To check the accuracy of this procedure, the limiting molar conductivity of $Co(NH_3)_6^{3+}$ was determined and compared to the literature value of 305.7 x 10^{-4} S m^2 mol^{-1} at 25°C.[116] The limiting conductivity value obtained for $[Co(NH_3)_6]Cl_3$ was 460 x 10^{-4} S m^2 mol^{-1}, measured at 18°C. Correcting for temperature and subtracting the anionic contribution gave a calculated value of (294 ± 13) x 10^{-4} S m^2 mol^{-1} at 25°C for the $Co(NH_3)_6^{3+}$ cation, within 4% of the literature value. The values for the Cr(III) complexes were similarly corrected for temperature and the anionic contribution subtracted using the values tabulated in Table 3.6. The limiting molar conductivities calculated for the Cr(III) am(m)ine cations at 20°C are presented in Table 3.6.

Complex	Counterion, λ° at 20° C / S m^2 mol^{-1}	Cation λ° at 20° C / S m^2 mol^{-1}
$Co(NH_3)_6^{3+}$	Cl^-, 69 x 10^{-4}	(265 ± 22) x 10^{-4}
$Cr(NH_3)_6^{3+}$	NO_3^-, 64 x 10^{-4}	(252 ± 5) x 10^{-4}
$Cr(en)_3^{3+}$	ClO_4^-, 61 x 10^{-4}	(172 ± 6) x 10^{-4}
$Cr(tn)_3^{3+}$	Cl^-, 69 x 10^{-4}	(155 ± 11) x 10^{-4}
cis-$Cr(tn)_2(NH_3)_2^{3+}$	ClO_4^-, 61 x 10^{-4}	(227 ± 27) x 10^{-4}
trans-$Cr(tn)_2(NH_3)_2^{3+}$	ClO_4^-, 61 x 10^{-4}	(202 ± 7) x 10^{-4}
$Cr(sen)^{3+}$	Br^-, 70 x 10^{-4}	(300 ± 13) x 10^{-4}
cis-$Cr(cyc)(NH_3)_2^{3+}$	ClO_4^-, 61 x 10^{-4}	(202 ± 8) x 10^{-4}

Table 3.6 Calculated limiting molar conductivities for Cr(III) a(m)ine complexes at 20°C.

The expected trend in limiting molar conductivity was observed for the Cr(III) am(m)ine complexes with conductivities decreasing as the size of the complex increased. The exception to this was $Cr(sen)^{3+}$ which gave the largest limiting molar conductivity, $(300 \pm 13) \times 10^{-4}$ S m^2 mol^{-1} even though this is predicted to be the largest complex. At the time of these studies there was insufficient $Cr(sen)^{3+}$ available to validate this result.

The molar conductivity values of photoproducts and intermediate species can not be determined experimentally. These were therefore estimated based on their charge relative to that of the parent am(m)ine complex, assuming that no significant changes in ionic volume occur for these species when changing the charge. Trivalent intermediate and product Cr(III) species were therefore assumed to have the same limiting molar conductivity as their parent am(m)ine, with divalent and tetravalent Cr(III) species having molar conductivities 0.67 and 1.33 of the parent value respectively.

It was recognized that ionic conductivity is highly dependent upon the ionic strength of the solution so the limiting values obtained are not representative of the molar conductivities under experimental conditions. The Onsager equation indicated that 86% of the limiting values was a reasonable estimate for the molar conductivities for the 3^+ ions in solution. Although it was recognized that the effect of ionic strength is charge dependent, this 86% value of the limiting molar conductivities was applied to the other ionic species relevant to the modelling.

3.4 Comparison of Modelled and Experimental Results

It was necessary to confirm that realistic changes in solution conductivity were being produced by the modelling. This was confirmed by checking that the

final concentrations obtained in the modelling gave quantum yield and pKa values that agreed with the input values. Any discrepancy between modelled and input values indicates errors in the modelled equations and was investigated. For all modelled results presented here agreement between modelled and input values is within 0.5%.

3.4.1 Waltz's Mechanism for Photoaquation of *cis*-Cr(cyclam)$(NH_3)_2^{3+}$

This mechanism was presented in Figure 3.1. The values used in the modelling of *cis*-Cr(cyclam)$(NH_3)_2^{3+}$ with this mechanism included; the literature value for ammonia protonation, 4.3 x 10^{10} M^{-1} s^{-1}, Waltz's estimated pKa values of 4.6 and 4.0 for pK_I and pK_P respectively, and values for k_{-I} and k_{-P} of 4 x 10^9 M^{-1} s^{-1} estimated using the Debye - Smoluchowski equation.

Reasonable fits to the experimental data were obtained at pH > 3.5 using the above values, the literature doublet decay rate of 625 000 s^{-1} and k_r = 250 000 s^{-1}. The significance of k_r = 250 000 s^{-1} is that it corresponds to the reciprocal of the conductivity decay lifetime observed at pH < 3 i.e. $1/\tau_{cond}$. However at pH < 3.5 we were unable to fit the experimental data with these parameters and a representative result obtained at pH 2.82 is illustrated in Figure 3.11a

To fit the data at pH < 3.5 it was necessary to make $k_r >> k_d$, and for k_d to equal 250 000 s^{-1}. Figure 3.11b shows how these values produced a good fit to the experimental data at pH 2.82. Obviously this was an unacceptable situation and it was also found this set of parameters could not reproduce the transient increases observed experimentally at pH > 4.0. Modifications were made to Waltz's mechanism to include a prompt photocomponent and reaction from $I(OH)^{2+}$ to give $P(OH)^{2+}$ but did not improve the fit between the modelled and experimental data.

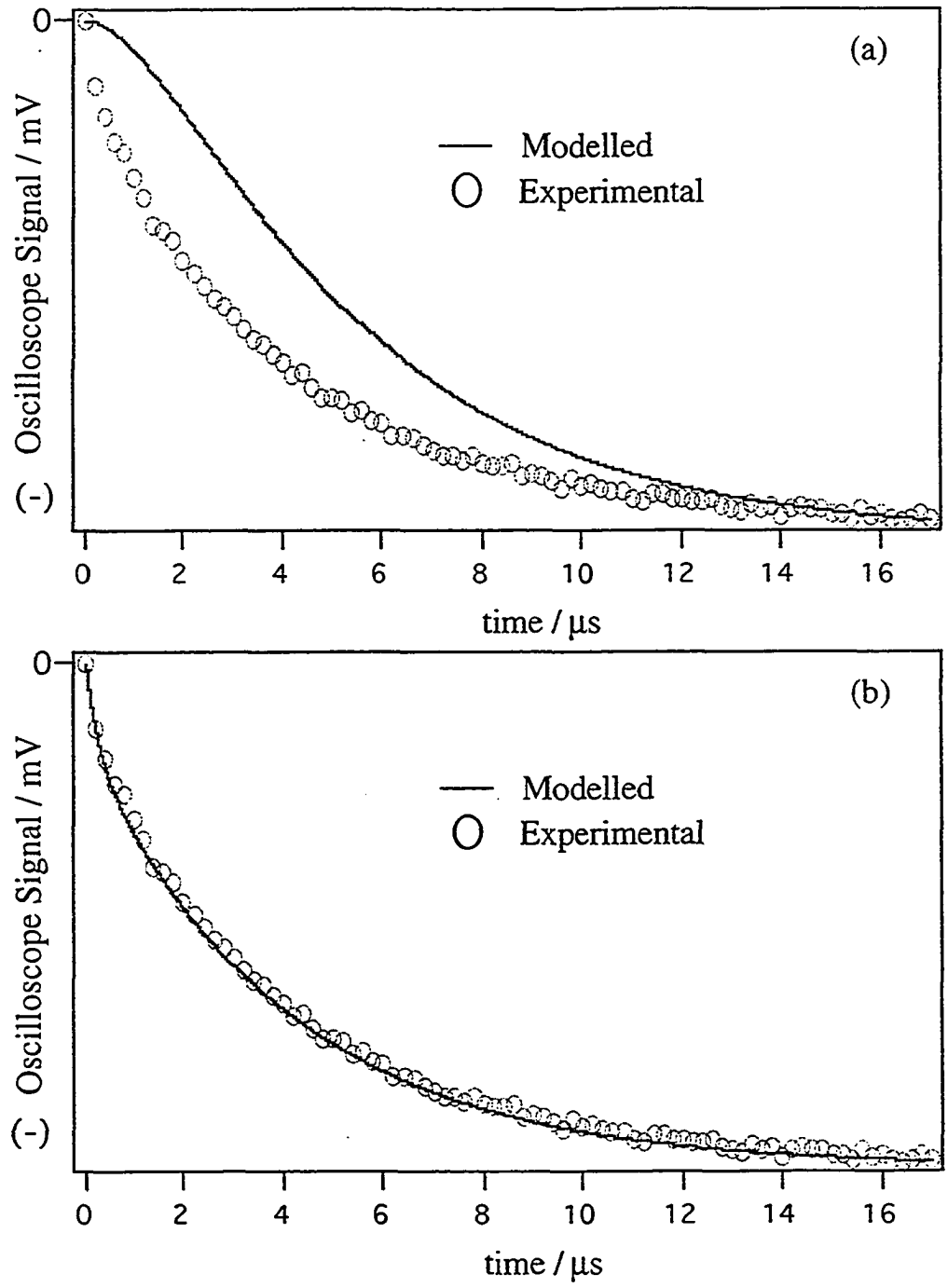

Figure 3.11 Comparison of modelled and experimental conductivity changes for the photolysis of *cis*-Cr(cyclam)$(NH_3)_2^{3+}$ at pH 2.82.

(a) $k_d = 625\ 000\ s^{-1}$, $k_r = 250\ 000\ s^{-1}$

(b) $k_d = 250\ 000\ s^{-1}$, $k_r = 5 \times 10^6\ s^{-1}$

As we were unable to fit the experimental data for the photoaquation of the Cr(III) am(m)ine complexes studied using the literature mechanism, it was necessary to consider alternative mechanisms. It was found that, with the exception of *cis*-$Cr(cyclam)(NH_3)_2^{3+}$, the complexes could be modelled based upon the type of am(m)ine labilized and the results are presented in the following sections.

3.4.2 $Cr(NH_3)_6^{3+}$, *cis*-$Cr(tn)_2(NH_3)_2^{3+}$ and *trans*-$Cr(tn)_2(NH_3)_2^{3+}$.

The common feature of these three complexes is that they photoaquate with ammonia loss as the dominant mode. The ammonia loss yields, $\Phi(NH_3)$, are 0.46, 0.21, 0.31 for $Cr(NH_3)_6^{3+}$,[103] *cis*-$Cr(tn)_2(NH_3)_2^{3+}$ and *trans*-$Cr(tn)_2(NH_3)_2^{3+}$ [85] respectively. The photoaquation of *cis*- & *trans*-$Cr(tn)_2(NH_3)_2^{3+}$ also involves a tn mode, $\Phi(tn) = 0.03$ for both complexes.[85]

The experimental results for *cis*-$Cr(tn)_2(NH_3)_2^{3+}$ and *trans*-$Cr(tn)_2(NH_3)_2^{3+}$ were successfully modelled by ignoring the minor tn mode and using the same mechanism as for $Cr(NH_3)_6^{3+}$. This mechanism involves photoaquation directly to the products via both prompt and slow photocomponents as shown in Figure 3.12.

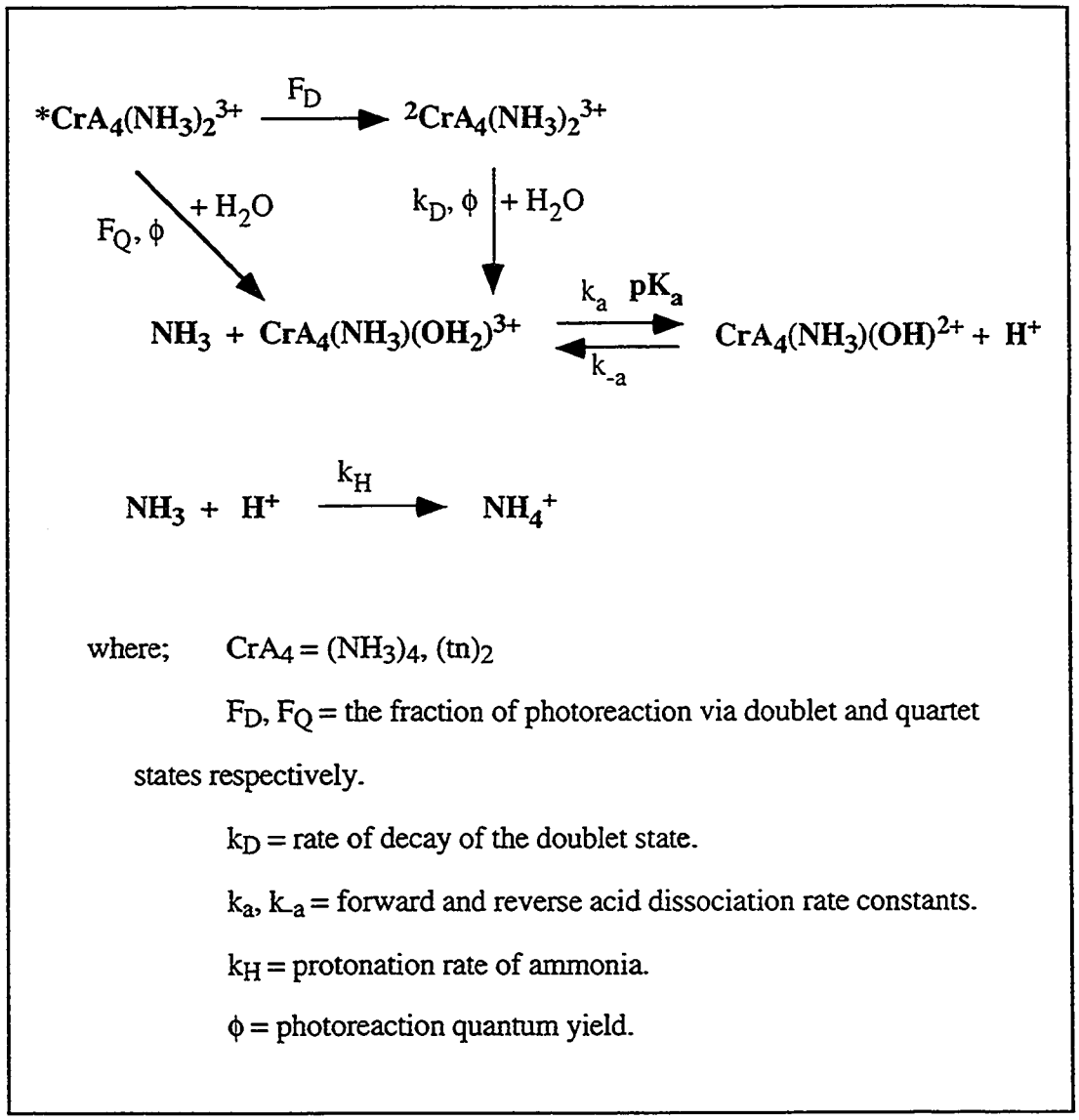

Figure 3.12 Modelled mechanism for $Cr(NH_3)_6^{3+}$, *cis*-$Cr(tn)_2(NH_3)_2^{3+}$ and *trans*-$Cr(tn)_2(NH_3)_2^{3+}$.

The good agreement between experimental and modelled conductivity changes for $Cr(NH_3)_6^{3+}$ at pH 2.82 and pH 4.72 is illustrated in Figure 3.13. A comparison of the lifetimes obtained from fitting experimental and modelled traces is given in Figure 3.14. For traces displaying both prompt and slow decays the lifetime

of the slow component occurring via the ^2E state is presented. This comparison shows that a good agreement between modelled and experimental results was obtained throughout the pH range 2.82 - 4.72. Similar figures are presented for *cis-* & *trans*-$Cr(tn)_2(NH_3)_2^{3+}$ in Appendix 3.1.

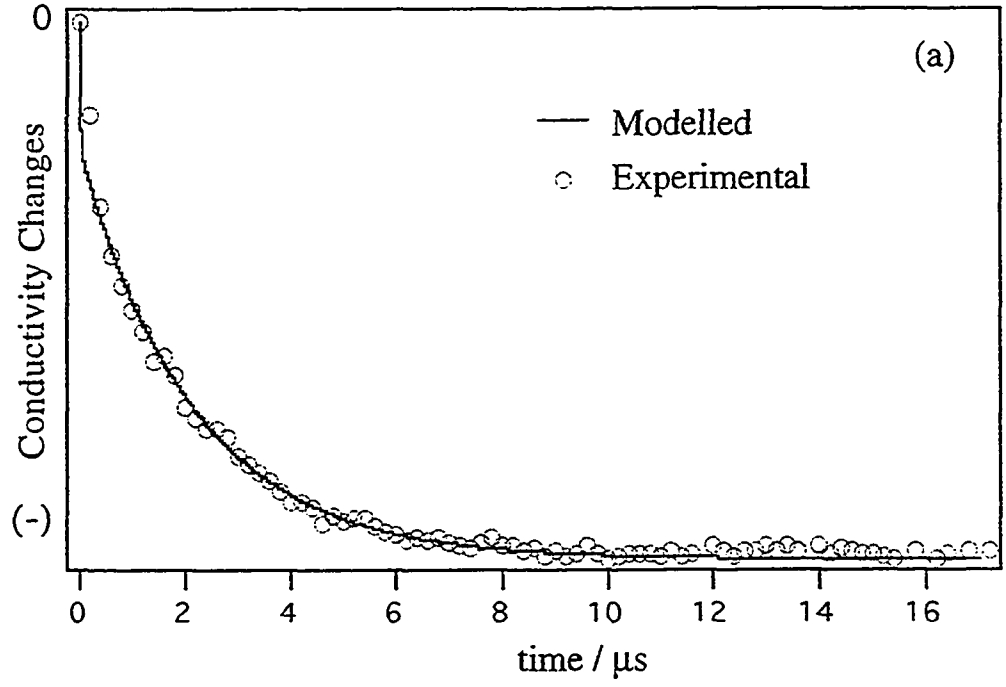

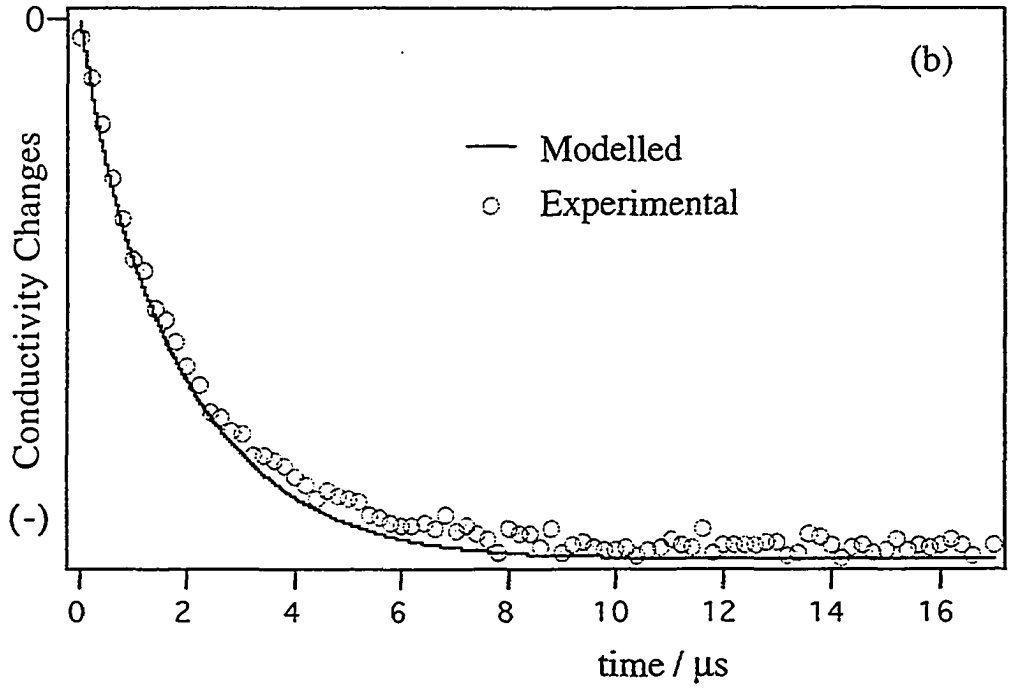

Figure 3.13 Comparison of modelled and experimental conductivity changes for $Cr(NH_3)_6^{3+}$; (a) pH 2.82, (b) pH 4.72.

Decay lifetimes that became shorter as the pH increased were obtained experimentally for $Cr(NH_3)_6^{3+}$, *cis*-$Cr(tn)_2(NH_3)_2^{3+}$ and *trans*-$Cr(tn)_2(NH_3)_2^{3+}$. This trend was reproduced in the modelled conductivity changes. Although evident in the results presented for $Cr(NH_3)_6^{3+}$ in Figure 3.14, this is better illustrated by the results obtained for *trans*-$Cr(tn)_2(NH_3)_2^{3+}$, Figure 3.15.

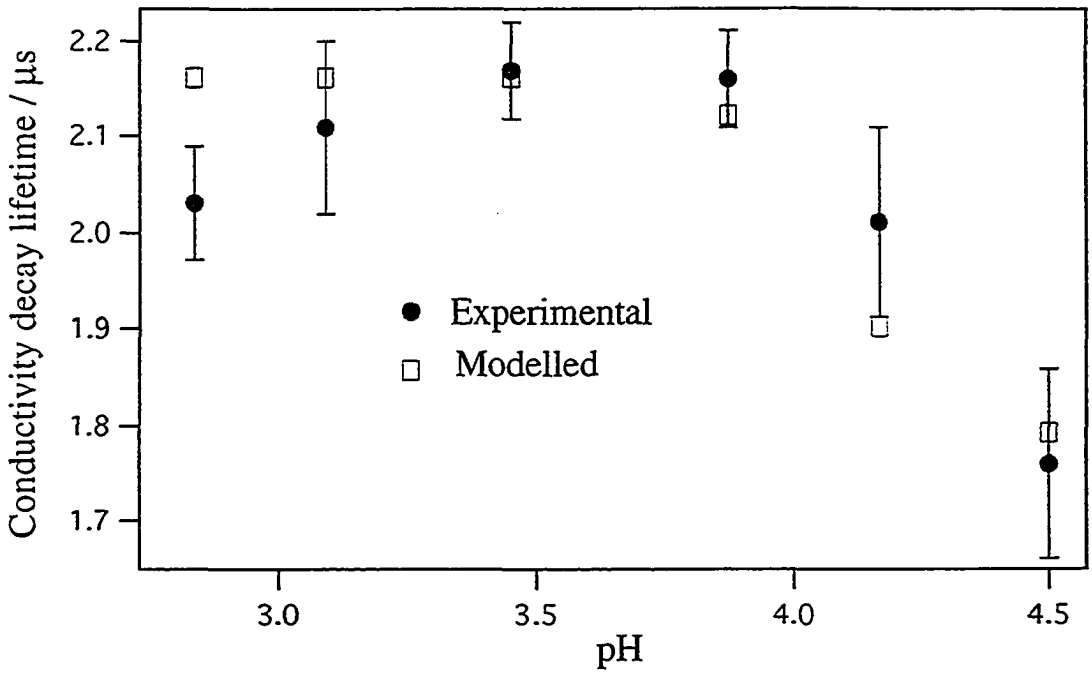

Figure 3.14 Comparison of modelled and experimental lifetimes for $Cr(NH_3)_6^{3+}$ at various pH values

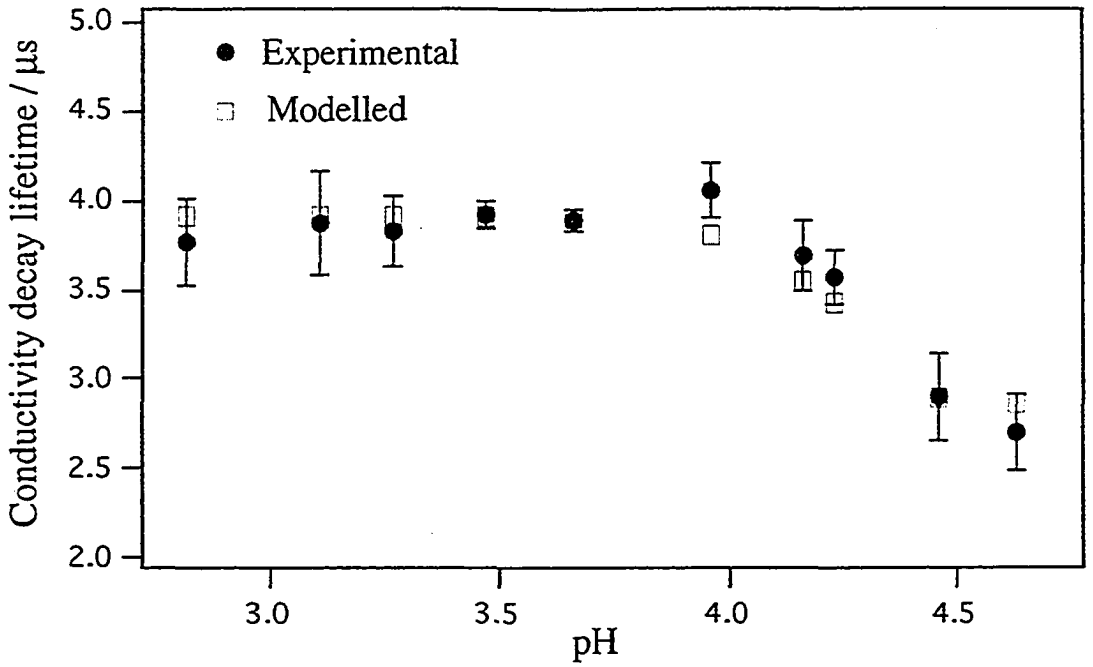

Figure 3.15 Comparison of modelled and experimental lifetimes for *trans*-$Cr(tn)_2(NH_3)_2^{3+}$ at various pH values.

The relevant rate constants, and other variables used in the modelling of $Cr(NH_3)_6^{3+}$, *cis*-$Cr(tn)_2(NH_3)_2^{3+}$ and *trans*-$Cr(tn)_2(NH_3)_2^{3+}$ are given in Table 3.7. Common to all three were the variables $k_H = 4.3 \times 10^{10}$ M^{-1} s^{-1}, $\lambda_{H^+} = 301 \times 10^{-4}$ S m^2 mol^{-1} and $\lambda_{NH4^+} = 63 \times 10^{-4}$ S m^2 mol^{-1}.

The pKa, k_a and k_{-a} values for the photoproducts of *cis*- & *trans*-$Cr(tn)_2(NH_3)(OH_2)^{3+}$ are intuitively expected to be similar to those of $Cr(NH_3)_5(OH_2)^{3+}$. This was supported by the modelling, with best fits to the experimental data being obtained for *cis*- & *trans*-$Cr(tn)_2(NH_3)_2^{3+}$ using pKa values of 5.0 and 5.2 for the respective photoproducts and with k_a and k_{-a} values within 30% of those modelled for $Cr(NH_3)_6^{3+}$.

Variable	$Cr(NH_3)_6^{3+}$	*cis*-$Cr(tn)_2(NH_3)_2^{3+}$	*trans*-$Cr(tn)_2(NH_3)_2^{3+}$
F_D	0.76	0.83	0.83
F_Q	0.24	0.17	0.17
Φ	0.46	0.21	0.31
ε_{355} / M^{-1} cm^{-1}	40	50	50
k_D / s^{-1}	4.63×10^5	3.75×10^5	2.50×10^5
λCr^{3+} / $\times 10^{-4}$ S m^2 mol^{-1}	217	195	173
λCr^{2+} / $\times 10^{-4}$ S m^2 mol^{-1}	145	130	116
pK_a	5.1	5.0	5.2
k_a / M^{-1} s^{-1}	7×10^9	5×10^9	6×10^9
k_a / s^{-1}	4.4×10^4	5.0×10^4	3.8×10^4

Table 3.7 Values used for the adjustable variables in the modelling of $Cr(NH_3)_6^{3+}$, *cis*-$Cr(tn)_2(NH_3)_2^{3+}$ and *trans*-$Cr(tn)_2(NH_3)_2^{3+}$.

3.4.3 $Cr(en)_3^{3+}$, $Cr(tn)_3^{3+}$ and $Cr(sen)^{3+}$.

The common feature of these three complexes is that they photoaquate to give products which contain a dangling amine arm. It was recognized that the initially formed photoproduct, $Cr(NN)_2(N\text{--}N)(OH_2)^{3+}$, was transient in nature and had competing decay processes; protonation of the dangling amine to give $Cr(NN)_2(N\text{--}NH)(OH_2)^{4+}$, and deprotonation of the co-ordinated water to give $Cr(NN)_2(N\text{--}$

N)$(OH)^{2+}$. The complete mechanism modelled for the photoaquation of $Cr(en)_3^{3+}$, $Cr(tn)_3^{3+}$ and $Cr(sen)^{3+}$ is illustrated in Figure 3.16.

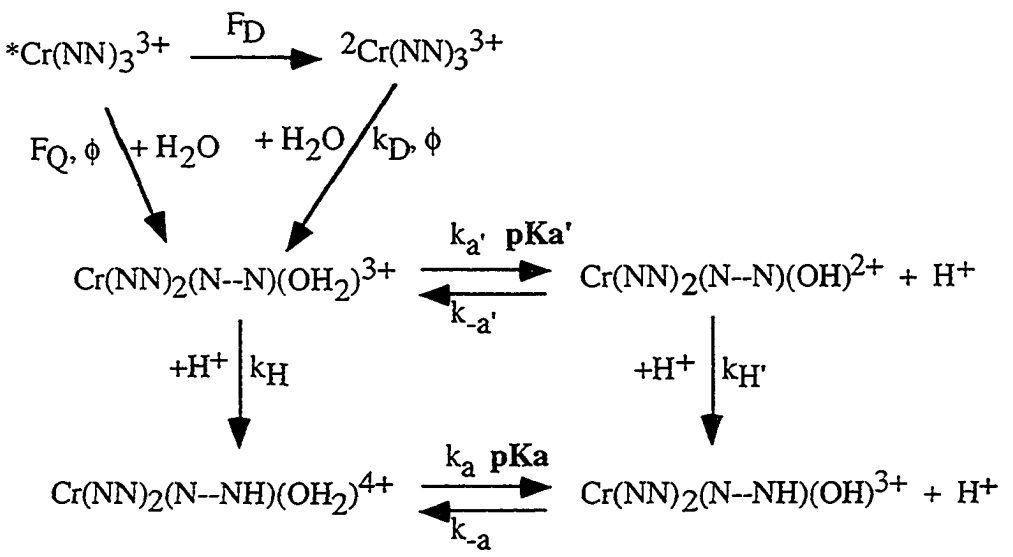

Where; NN = bidentate en or tn

N--N = monodentate en or tn

N--NH = protonated monodentate en or tn

F_D, F_Q = fraction of photoreaction via the doublet and quartet states

k_D = rate of decay of the doublet state.

k_a,k_{-a} = forward and reverse acid dissociation rate constants.

k_H, $k_{H'}$ = protonation rate for the dangling amine in 3^+ and 2^+ species

*$(NN)_3$ is also an appropriate representation of the sen ligand viewing it as three 1,2-diaminoethane arms capped by a neopentyl group.

Figure 3.16 Modelled mechanism for the photoaquation of $Cr(en)_3^{3+}$, $Cr(tn)_3^{+}$ and $Cr(sen)^{3+}$.

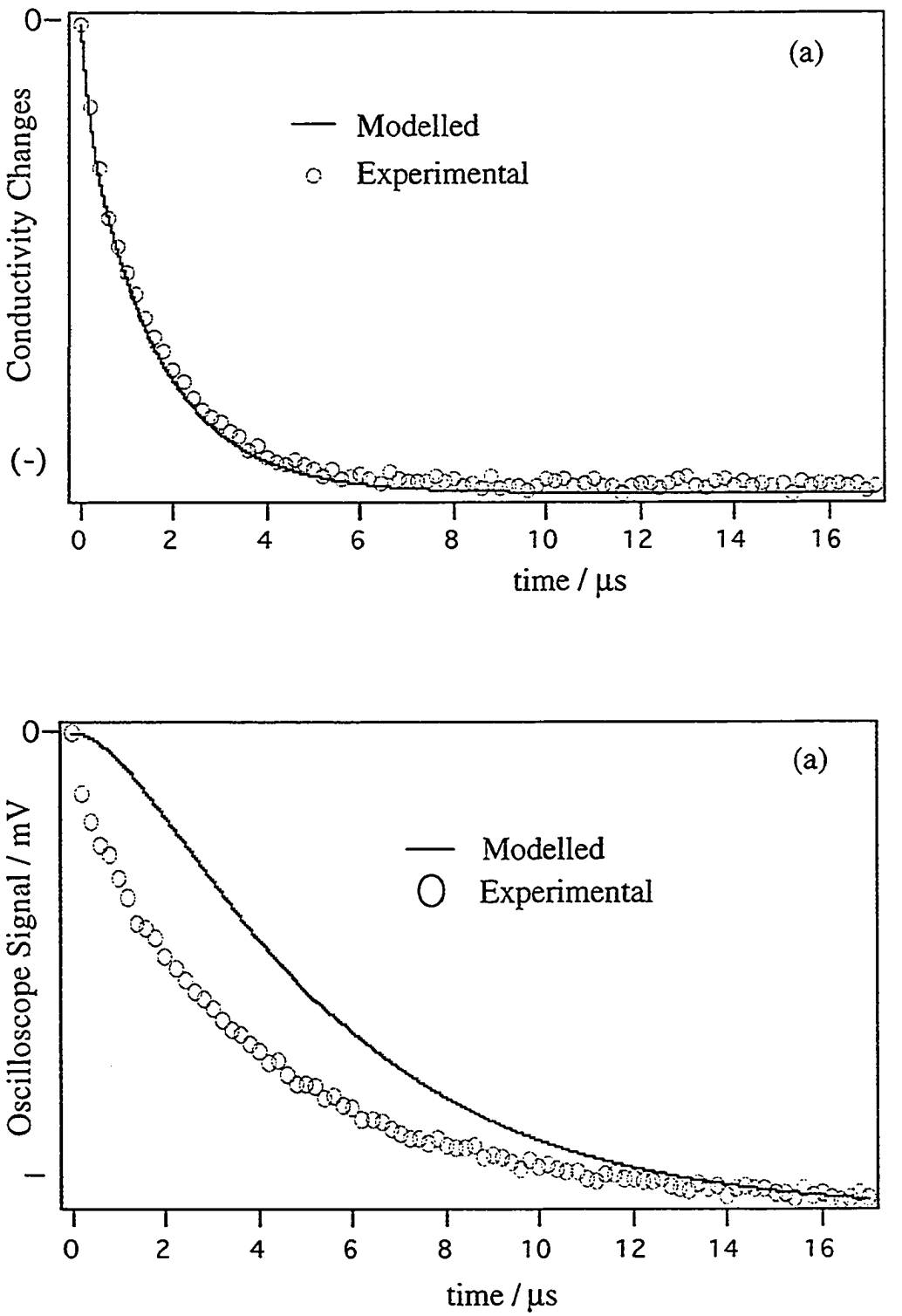

Figure 3.17 Comparison of modelled and experimental conductivity changes for $Cr(en)_3^{3+}$; (a) pH 2.74, (b) pH 4.56.

Figure 3.17 shows the comparison of modelled and experimental results for $Cr(en)_3^{3+}$ at pH 2.74 and 4.56. Similar results are presented for $Cr(tn)_3^{3+}$ and $Cr(sen)^{3+}$ in Appendix 3.2. As Figure 3.17 shows a good fit to the experimental data was obtained at pH 2.74 but at pH 4.56 the ratio of the transient rise to the overall decay for the modelled data is smaller than that observed experimentally.

The disparity between the modelled and experimental rise:decay ratios at pH 4.56 could be corrected by changing the modelled parameters, e.g. by decreasing the pKa values listed in Table 3.8 for either the intermediate, $Cr(en)_2(en\text{-}N)(OH_2)^{3+}$, or the final product, $Cr(en)_2(en\text{-}NH)(OH_2)^{3+}$. However doing this resulted in the fit between modelled and experimental data at other pH values deteriorating.

This highlights a problem with modelling such a large number of parameters. It is extremely difficult to obtain an optimal set of variables which produce a perfect fit between modelled and experimental data at all pH studied. A good fit at one pH may require a slight variation in one or more parameters to produce an equally good fit at another pH. Theoretically it would be possible to obtain optimal values by minimizing the fit between modelled and experimental data over the whole pH range studied. To do so would require extensive computing capabilities and with such a large number of variables does not carry any great expectation of success in finding a global minimum.

It has been accepted that manual optimization of the parameters is unlikely to produce a perfect fit at every pH. However the modelled mechanism appears to be valid as experimental trends are reproduced in the modelled results; decays are observed at pH < 4 and transient rises, which increase in magnitude with pH, are observed above pH 4. The decay lifetimes obtained for the experimental and modelled data are compared in Figure 3.18. These are in good agreement, supporting both the validity of the modelled mechanism and the values used in the modelling.

Traces displaying a simple decay were fitted using a single exponential decay with traces containing a transient rise being fitted by a double exponential function.

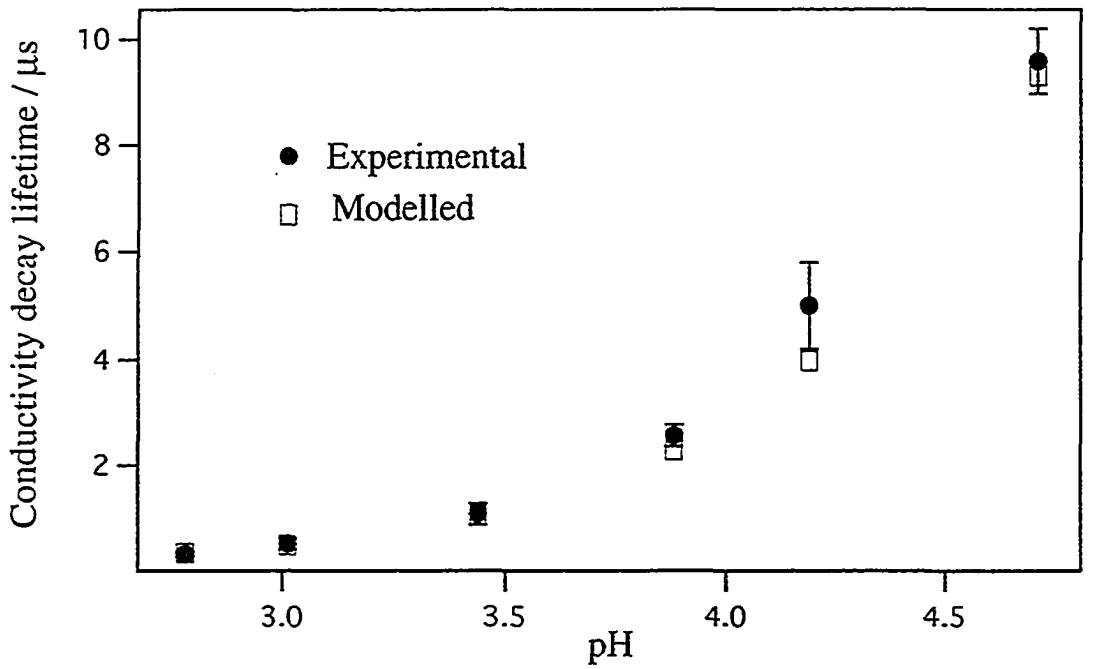

Figure 3.18 Comparison of modelled and experimental decay lifetimes for $Cr(en)_3^{3+}$ at various pH values.

The values for the modelled variables for each complex are given in Table 3.8. Modelled rate constants for protonation of the dangling amines, generated in the photoaquation of $Cr(en)_3^{3+}$, $Cr(tn)_3^{3+}$ and $Cr(sen)^{3+}$, were based upon the literature value of 3.6×10^9 M^{-1} s^{-1} obtained for $Cr(en)_2(en\text{-}N)(OH_2)^{3+}$.[83] The best fits to the experimental data were obtained with slower protonation rate constants for $Cr(tn)_3^{3+}$ and $Cr(sen)^{3+}$ than for $Cr(en)_3^{3+}$, with modelled k_H values of 2.0×10^9 M^{-1} s^{-1} and 2.2×10^9 M^{-1} s^{-1} respectively. Presumably this can be rationalized by greater steric hindrance to protonation in these bulkier complexes.

Variable	$Cr(en)_3^{3+}$	$Cr(tn)_3^{3+}$	$Cr(sen)^{3+}$
F_D	0.75	0.80	1.0*
F_Q	0.25	0.20	--
Φ	0.33	0.15	0.1
ε_{355} / M^{-1} cm^{-1}	50	50	70
k_D / s^{-1}	6.27×10^5	5.90×10^5	**
k_H / M^{-1} s^{-1}	3.6×10^9	2.2×10^9	2.2×10^9
$k_{H'}$ / M^{-1} s^{-1}	5.4×10^9	3.3×10^9	4.2×10^9
λCr^{3+} / x 10^{-4} S m^2 mol^{-1}	148	133	258
λCr^{2+} / x 10^{-4} S m^2 mol^{-1}	99	99	172
λCr^{4+} / x 10^{-4} S m^2 mol^{-1}	198	178	344
$pK_{a'}$	4.1	3.9	3.7
$k_{-a'}$ / M^{-1} s^{-1}	5.0×10^9	6.0×10^9	9×10^9
$k_{a'}$ / s^{-1}	4.0×10^5	7.6×10^5	1.8×10^6
pK_a	4.4	4.4	4.1
k_{-a} / M^{-1} s^{-1}	3.5×10^9	4.0×10^9	7.0×10^9
k_a / s^{-1}	1.4×10^5	1.7×10^5	7.0×10^5

** As the doublet lifetime of $Cr(sen)^{3+}$ is sub-ns this was modelled as instantaneous formation of the initial photoproduct.

Table 3.8 Values used for adjustable variables in the modelling of $Cr(en)_3^{3+}$, $Cr(tn)_3^{3+}$, and $Cr(sen)^{3+}$.

Protonation of the dangling amine in the $Cr(NN)_2(N\text{--}N)(OH)^{2+}$ intermediates is expected to be faster than that of $Cr(NN)_2(N\text{--}N)(OH_2)^{3+}$ on the basis of charge so for all three complexes modelled $k_{H'}$ values were greater than the corresponding k_H value. Best fits to the experimental data were obtained with a $k_{H'}/k_H$ ratio of 1.5 for $Cr(en)_3^{3+}$ and $Cr(tn)_3^{3+}$ and a higher ratio of 1.9 for $Cr(sen)^{3+}$.

$Cr(en)_3^{3+}$ photoaquates to give 35% *cis*-$Cr(en)_2(en\text{-}NH)(OH_2)^{3+}$ and 65% *trans*-$Cr(en)_2(en\text{-}NH)(OH_2)^{3+}$.[73] Only the pKa of the thermal hydrolysis product of $Cr(en)_3^{3+}$, presumably the cis isomer, has been reported in the literature.[111] For the purposes of modelling a single photoproduct was assumed and the literature pKa value of 4.4 for the cis isomer was used in the modelling.

$Cr(tn)_3^{3+}$ photoaquates to give approximately 40% *cis*-$Cr(tn)_2(tn\text{-}NH)(OH_2)^{4+}$ and 60% *trans*-$Cr(en)_2(en\text{-}NH)(OH_2)^{3+}$, based on relative peak areas obtained from an HPLC analysis of a photolyzed solution.[85] Two conflicting pKa values have been obtained from the literature for $Cr(tn)_2(tn\text{-}NH)(OH_2)^{4+}$. A value of 3.7[106] was obtained for a photolyzed $Cr(tn)_3^{3+}$ solution, presumed to be a 40:60 cis:trans mixture, whereas a value of 4.7[45] was found for the product of thermally hydrolyzed $Cr(tn)_3^{3+}$ solution, presumably the cis isomer. Although the cis and trans isomers would be expected to have different pKa values, a difference of one pKa unit seems unlikely. For modelling purposes, a single photoproduct with a pKa of 4.4 was assumed, the same as for $Cr(en)_2(en\text{-}NH)(OH_2)^{4+}$.

The photolysis of $Cr(sen)^{3+}$ has not been investigated extensively in the literature and no pKa values for the photoproduct(s) were found. Best fits to the modelling were obtained with a pK_a of 4.1, indicating a slightly more acidic photoproduct than for $Cr(en)_3^{3+}$ and $Cr(tn)_3^{3+}$.

For all three complexes best fits to the experimental data were obtained with $Cr(NN)_2(N\text{--}N)(OH_2)^{3+}$ intermediates being more acidic than the $Cr(NN)_2(N\text{--}NH)(OH_2)^{4+}$ products.

The modelled k_{-a} values for the photoproducts and intermediates of $Cr(en)_3^{3+}$ and $Cr(tn)_3^{3+}$ were within the ranges estimated using the Debye Smoluchowski equation for approach of a proton to 3^+ and 2^+ species respectively. However, for $Cr(sen)^{3+}$ the modelled k_{-a} values for both the intermediate, $9 \times 10^9\ M^{-1}\ s^{-1}$, and photoproduct, $7 \times 10^9\ M^{-1}\ s^{-1}$, were outside the estimated ranges of $5\text{-}7 \times 10^9\ M^{-1}\ s^{-1}$, and $4\text{-}6 \times 10^9\ M^{-1}\ s^{-1}$ respectively. The modelled k_a values for the $Cr(sen)^{3+}$ intermediate, $1.8 \times 10^6\ s^{-1}$, and photoproduct, $7.0 \times 10^5\ s^{-1}$, were both significantly greater than corresponding values for the $Cr(en)_3^{3+}$ and $Cr(tn)_3^{3+}$ intermediates and photoproducts.

As mentioned in section 3.3.2.3, the limiting molar conductivity obtained for $Cr(sen)^{3+}$ was suspiciously high compared to those obtained for the other Cr(III) am(m)ine complexes. As the modelling is highly dependent on the input molar conductivity values, the modelled conductivities for $Cr(sen)^{3+}$ were replaced by those used to model the $Cr(en)_3^{3+}$ results. No significant changes to the pK_a, k_a and k_{-a} values were required in order to fit the $Cr(sen)^{3+}$ experimental results. This indicated that the more acidic intermediate and photoproduct pKa values required in the modelling of $Cr(sen)^{3+}$ did not result from the high molar conductivity values obtained experimentally.

3.4.4 *cis*-Cr(cyclam)$(NH_3)_2^{3+}$.

The experimental results for *cis*-Cr(cyclam)$(NH_3)_2^{3+}$ could not be modelled using either the literature mechanism, Figure 3.1, or that used in the modelling of the other complexes which photoaquate with ammonia loss, Figure 3.12.

The "kink" observed in the conductivity traces at pH 3.85 , Figure 3.10, is evidence for two distinct photoaquation processes occurring on different timescales. Both modes must result in overall loss of an ammonia ligand as the only photoproduct observed experimentally is *cis*-Cr(cyclam)$(NH_3)(OH_2)^{3+}$. We proposed that the photoaquation of *cis*-Cr(cyclam)$(NH_3)_2^{3+}$ involved two modes; i) direct ammonia loss and ii) labilization of a cyclam amine which recoordinates to displace an ammonia ligand.

As stated in section 3.1 the possibility of cyclam loss had been proposed by Friesen et al.[60] Based on a greater ligand field strength, preferential loss of a cyclam amine is predicted by the AOM model. Our proposed mechanism for the photoaquation of *cis*-Cr(cyclam)$(NH_3)_2^{3+}$ is presented in Figure 3.19.

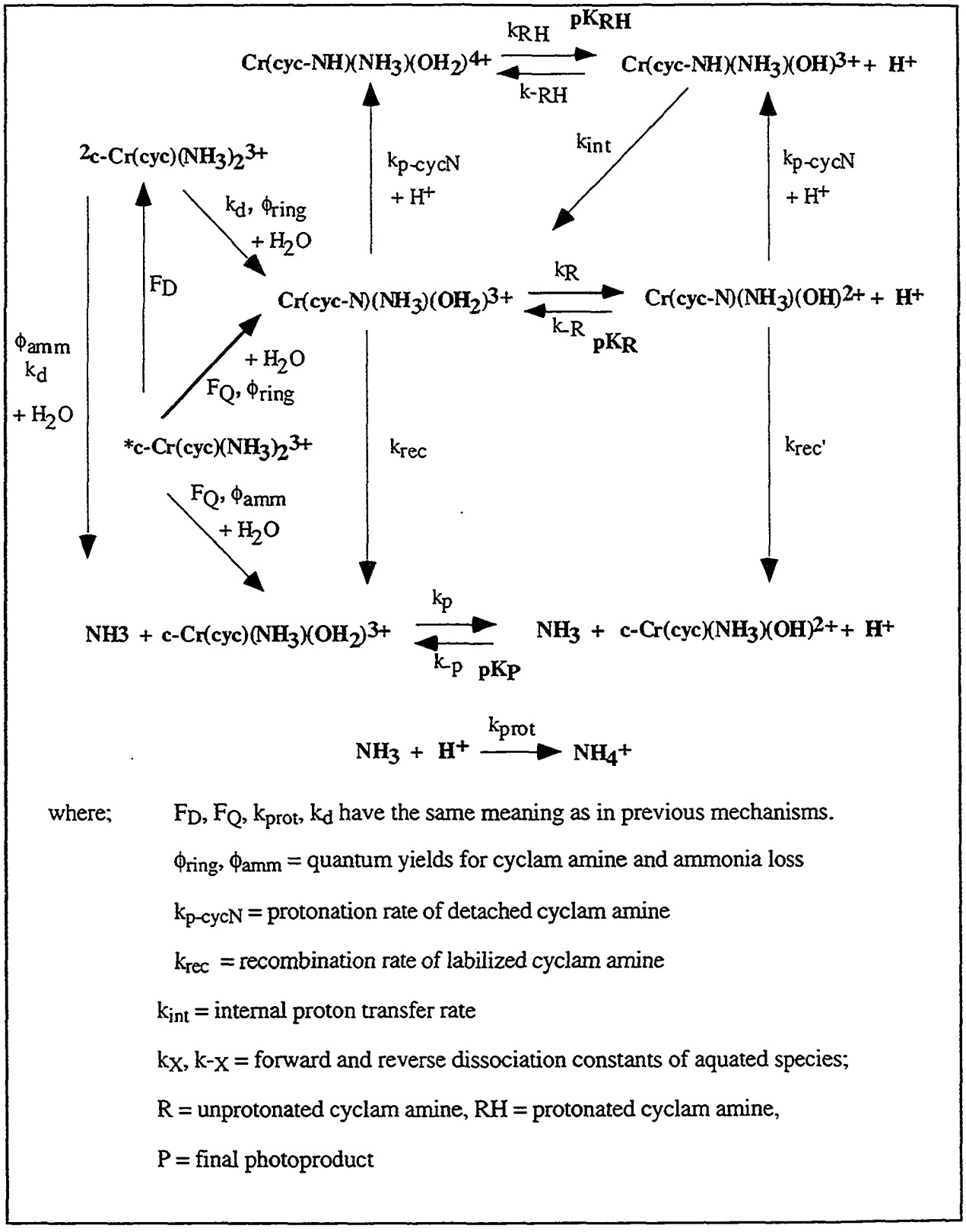

where; F_D, F_Q, k_{prot}, k_d have the same meaning as in previous mechanisms.

ϕ_{ring}, ϕ_{amm} = quantum yields for cyclam amine and ammonia loss

$k_{p\text{-}cycN}$ = protonation rate of detached cyclam amine

k_{rec} = recombination rate of labilized cyclam amine

k_{int} = internal proton transfer rate

k_X, $k\text{-}_X$ = forward and reverse dissociation constants of aquated species;

R = unprotonated cyclam amine, RH = protonated cyclam amine,

P = final photoproduct

Figure 3.19 Modelled mechanism for the photoaquation of cis-$Cr(cyclam)(NH_3)_2^{3+}$.

This mechanism includes the assumption that a labilized cyclam amine is not able to recoordinate if protonated. Our initial modelling indicated that approximately 10% of the cyclam loss intermediate would become trapped by protonation of the labilized amine at pH < 3 if this was the case. To confirm this experimentally *cis*-Cr(cyclam)$(NH_3)_2^{3+}$ solutions were photolyzed and examined using HPLC analysis. A single photoproduct, *cis*-Cr(cyclam)$(NH_3)(OH_2)^{3+}$, was observed. This suggested that cyclam loss intermediates are not trapped by protonation, even at pH 2.0. An HPLC study by Kirk and Heyd [63] had indicated two photoproducts but the minor product was attributed to secondary photolysis as their solutions were photolyzed to approximately 20% conversion. Our photolysis was conducted under more acidic conditions and involved the use of more acidic HPLC buffers, pH 2.0 vs pH 5.0 of Kirk and Heyd. It would therefore be predicted that our conditions would be more likely to trap a cyclam loss intermediate. As only one product was observed this supports cyclam loss intermediates not being trapped by protonation under our experimental conditions.

The intramolecular proton transfer process between the protonated amine and hydroxy group of the Cr(cyc-NH)$(NH_3)_2(OH)^{3+}$ intermediate was introduced to prevent the modelled build up of protonated cyclam loss intermediates. This provides an exit channel for the protonated cyclam species as the unprotonated amine is then able to recoordinate to give the observed products. Intramolecular proton transfer has been shown to occur in the photogenerated conversion of 1,1-diaryl alkenes to quinone methides,[117] with proton transfer being mediated by a chain of three water molecules operating in a Grotthus type mechanism.

Using the mechanism shown in Figure 3.19, good fits to the experimental data were obtained at almost all pH values studied, including at pH 3.85, where the "kink" observed experimentally was reproduced by the modelled results. Figure 3.20 shows the comparison of modelled and experimental data at pH 2.82, 3.85 and 4.50.

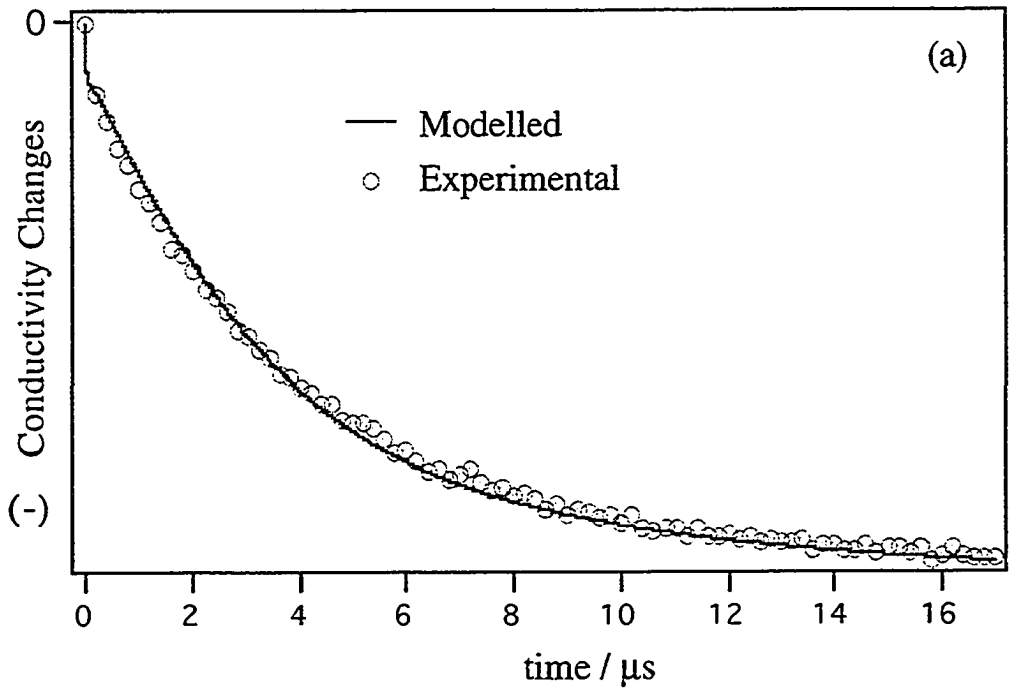
0
(-)
Conductivity Changes
(a)
Modelled
Experimental
0
2
4
6
8
10
12
14
16
time / μs

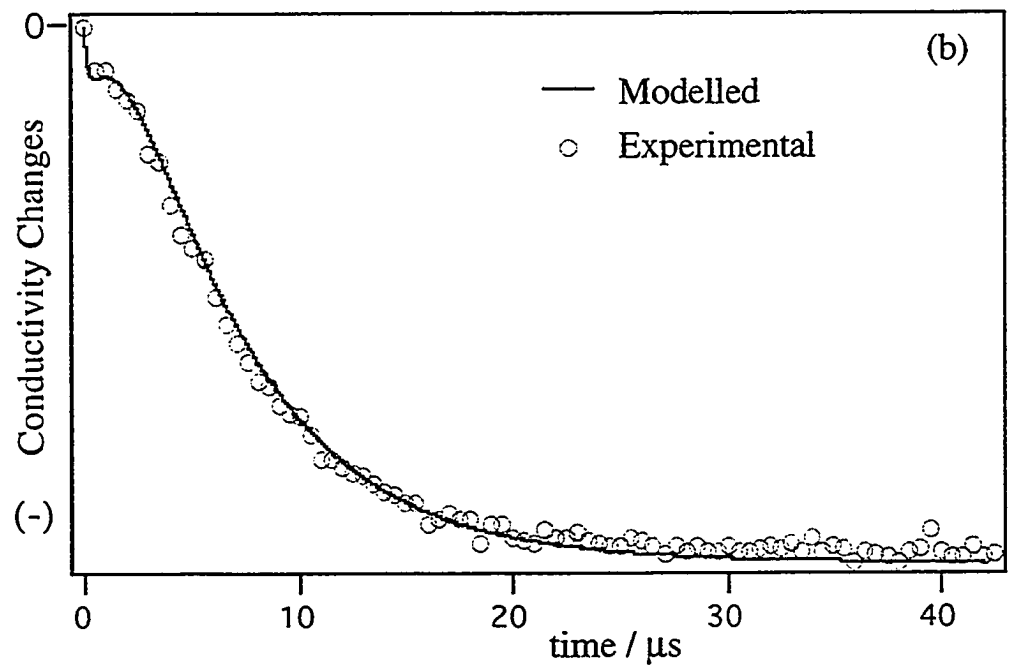
0
(-)
Conductivity Changes
(b)
Modelled
Experimental
0
10
20
30
40
time / μs

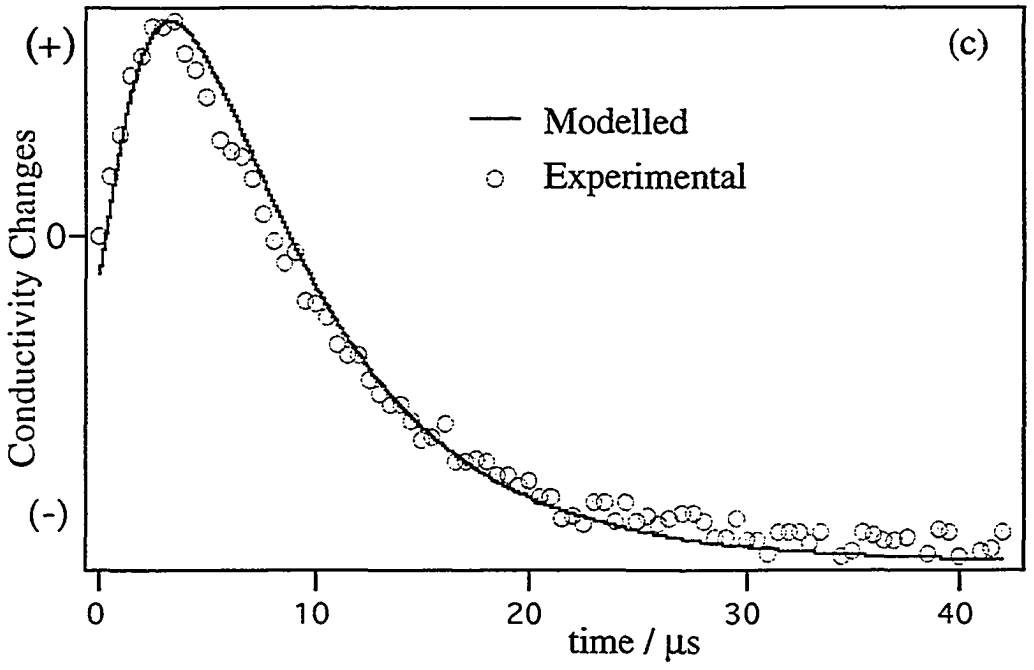

Figure 3.20 Comparison of modelled and experimental conductivity changes for *cis*-Cr(cyclam)$(NH_3)_2^{3+}$; (a) pH 2.82, (b) 3.85, (c) 4.50.

The only exception to the good fits between experimental and modelled data was found at pH 3.33 where a slight kink, similar to that observed at pH 3.85, was observed in the modelled trace but not the experimental. However the decay lifetimes obtained from experimental and modelled data at this pH were in good agreement. Similarly good agreements between the experimental and modelled lifetimes were obtained over the whole pH range studied as shown in Figure 3.21. All traces which displayed a decay were fitted using a single exponential fit, with those displaying a transient increase being fitted with a biexponential function.

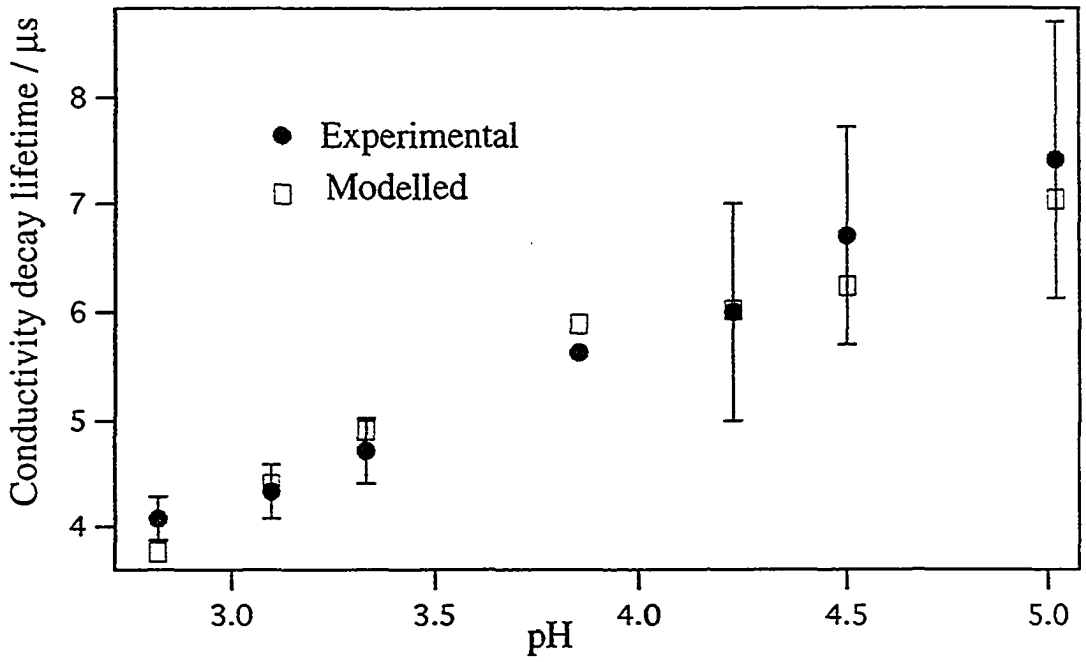

Figure 3.21 Comparison of modelled and experimental decay lifetimes for *cis*-$Cr(cyclam)(NH_3)_2^{3+}$ at various pH values

The relevant variables used in the modelling of *cis*-$Cr(cyclam)(NH_3)_2^{3+}$ are listed in Table 3.9. The best fits of the modelled results to experimental data were obtained with a much lower photoproduct pK_a than those modelled for $Cr(NH_3)_6^{3+}$, *cis*-$Cr(tn)_2(NH_3)_2^{3+}$ and *trans*-$Cr(tn)_2(NH_3)_2^{3+}$, complexes which also photoaquate to give a $CrN_4(NH_3)(OH_2)^{3+}$ photoproduct.

The effect of the cyclam ligand on the pK_a values of coordinated waters is evident in di-aquo complexes of Cr(III); *cis*-$Cr(NH_3)_4(OH_2)_2^{3+}$ has a pKa of 5.0,[118] with the pKa of the analogous cyclam complex *cis*-$Cr(cyclam)(OH_2)_2^{3+}$ being 4.2.[119] The trend of lower pKa values for complexes containing cyclam ligands is even more pronounced for the trans isomers. *Trans*-$Cr(NH_3)_4(OH_2)_2^{3+}$ has a pKa of 4.4, compared to 3.0 for *trans*-$Cr(cyclam)(OH_2)_2^{3+}$. These results suggest that the modelled pKa value of 4.2 is reasonable for *cis*-$Cr(cyclam)(NH_3)(OH_2)^{3+}$. Modelled pK_a, k_a and k_{-a} values for protonated and

unprotonated ring loss intermediates, $Cr(cyc\text{-}NH)(NH_3)_2(OH_2)^{4+}$ and $Cr(cyc\text{-}N)(NH_3)_2(OH_2)^{3+}$ are similar to those used in the modelling of $Cr(sen)^{3+}$.

Variable	Modelled value	Variable	Modelled value
F_D	0.70	pK_P	4.2
Φ_{total}	0.10	k_{-P} / $M^{-1}.s^{-1}$	7.0×10^9
F_{cvc}	0.67	k_P / s^{-1}	4.4×10^5
ε_{355} / M^{-1} cm^{-1}	90	pK_R	4.1
k_d / s^{-1}	6.25×10^5	k_{-R} / M^{-1} s^{-1}	6.0×10^9
$k_{p\text{-}cycN}$ / M^{-1} s^{-1}	8×10^7	k_R / s^{-1}	9.5×10^5
k_{prot}/ M^{-1} s^{-1}	4.3×10^{10}	pK_{RH}	3.8
λCr^{3+} / $\times 10^{-4}$ S m^2 mol^{-1}	174	k_{-RH} / M^{-1} s^{-1}	4.0×10^9
λCr^{2+} / $\times 10^{-4}$ S m^2 mol^{-1}	116	k_{RH} / s^{-1}	3.2×10^5
λCr^{4+} / $\times 10^{-4}$ S m^2 mol^{-1}	232	k_{rec} / s^{-1}	2.35×10^5
k_{int} / s^{-1}	5.0×10^8	$k_{rec'}$ / s^{-1}	1.35×10^5

Table 3.9 Modelling variables relevant to the photoaquation of *cis*-$Cr(cyclam)(NH_3)_2^{3+}$

The modelling required a large rate constant for intramolecular proton transfer with the maximum value that could be incorporated being 5.0×10^8 s^{-1}. In the cited study involving conversion of 1,1- diaryl alkenes to quinone methides,

Stern-Volmer analysis indicated that three waters mediated the proton transfer. Quenching rates of 3.2×10^8 M^{-3} s^{-1} and 1.5×10^8 M^{-3} s^{-1} were obtained for two of the compounds. This indicates that intramolecular proton transfer within these compounds is very rapid, supported by the observation that zwitterionic intermediates resulting from the intramolecular proton transfer are produced within the timescale of the laser pulse, 10ns.

A conductivity lifetime longer than the emission lifetime at pH < 3 indicated that recoordination of the labilized cyclam amine was slower than the rate of doublet decay. Therefore the 250 000 s^{-1} decay rate constant observed at pH < 3 was chosen as the initial estimate for k_{rec}. This value of k_{rec} was initially modelled as the cyclam recoordination rate in both the $Cr(cyc\text{-}N)(NH_3)_2(OH_2)^{3+}$ and $Cr(cyc\text{-}N)(NH_3)_2(OH)^{2+}$ intermediates. Best fits to the experimental data were obtained with k_{rec} = 235 000 s^{-1} for recoordination in the 3^+ intermediate and $k_{rec'}$ = 135 000 s^{-1} for recoordination in the 2^+ intermediate, .

The 8.0×10^7 M^{-1} s^{-1} value modelled for the protonation rate constant of the labilized cyclam amine, $k_{p\text{-}cycN}$, was based entirely on the best fits of modelled to experimental data. This protonation rate constant is significantly smaller than the values modelled for the protonation of dangling amine arms, 2.0 - 3.6 x10 M^{-1} s^{-1}. Although we have no literature values with which to compare the 8.0×10^7 M^{-1} s^{-1} value, a slower protonation rate would be expected based on the increased steric hindrance of a dangling cyclam ring compared to a dangling amine arm.

Modelled values for the fraction of prompt photoreaction via the quartet state, F_Q (= 1-F_D), and fraction of photoreaction via cyclam loss, F_{cyc}, were obtained from the best fits of the modelled results to the experimental data for *cis*-$Cr(cyclam)(NH_3)_2^{3+}$. A F_Q value less than 0.10 had been estimated for *cis*-$Cr(cyclam)(NH_3)_2^{3+}$ by Waltz based on exponential fits of the conductivity data

obtained at pH < 3. Our modelled value of 0.33 is therefore in better accord with values obtained for analogous Cr(III) complexes.

3.5 Discussion and Related Studies

The comparison of modelled and experimental results has provided insight into the photoaquation mechanisms of the Cr(III) am(m)ine complexes studied, explaining many of the puzzling experimental observations including;

i) the observed conductivity lifetimes decreasing with pH for $Cr(NH_3)_6^{3+}$, *cis*-$Cr(tn)_2(NH_3)_2^{3+}$ and *trans*-$Cr(tn)_2(NH_3)_2^{3+}$,

ii) the transient increases in solution conductivity observed for $Cr(en)_3^{3+}$, $Cr(tn)_3^{3+}$ and $Cr(sen)^{3+}$ and

iii) the conductivity decay lifetime longer than the emission lifetime at pH < 3, the kink at pH 3.85 and the conductivity rises observed at pH > 4.0 for *cis*-$Cr(cyclam)(NH_3)_2^{3+}$.

The explanations for these observations are discussed in detail in the following sections.

3.5.1 $Cr(NH_3)_6^{3+}$, *cis*-$Cr(tn)_2(NH_3)_2^{3+}$ and *trans*-$Cr(tn)_2(NH_3)_2^{3+}$.

The conductivity changes that occur in solution upon photolysis of these complexes are predominantly the result of proton uptake by labilized ammonia. At pH 3, protonation of the labilized ammonia is pseudo first order as no appreciable changes in H_3O^+ concentration occur due to proton uptake. However at pH 5,

significant changes in H_3O^+ concentration do occur on proton uptake by the labilized ammonia. This is alleviated to some extent by the buffering action of the photoproduct, but protonation still becomes second order as the pH increases, dependent upon both the concentration of both photoreleased ammonia and H_3O^+. Modelled results indicate that the observed rate constant, k_{obs}, ($= k_{prot}.[H_3O^+]$), drops from an initial value of 430 000 s^{-1} to approximately 50 000 s^{-1} during the course of the photoaquation at pH 5. Fitting the experimental traces at higher pH to a single exponential therefore results in a biased fit, with faster decay rates being obtained as the pH increases.

The effects of non first order protonation on the observed conductivity decay lifetimes are only observed when significant depletion of H_3O^+ occurs, i.e. for complexes that have relatively large quantum yields. The quantum yields for $Cr(NH_3)_6^{3+}$, *cis*-$Cr(tn)_2(NH_3)_2^{3+}$ and *trans*-$Cr(tn)_2(NH_3)_2^{3+}$, are all relatively large 0.46, 0.27 and 0.30 respectively. A similar effect is not observed for $Cr(en)_3^{3+}$ even though it also has a high quantum yield, 0.37. The reason for this is that the observed decays in solution conductivity for $Cr(NH_3)_6^{3+}$, *cis*-$Cr(tn)_2(NH_3)_2^{3+}$ and *trans*-$Cr(tn)_2(NH_3)_2^{3+}$ are the direct result of ammonia protonation. For $Cr(en)_3^{3+}$ other processes are also occuring and the observed conductivity changes are no longer determined solely by protonation of the labilized amine.

3.5.2 $Cr(en)_3^{3+}$, $Cr(tn)_3^{3+}$ and $Cr(sen)^{3+}$.

The successful modelling of the experimental data obtained for $Cr(en)_3^{3+}$, $Cr(tn)_3^{3+}$ and $Cr(sen)^{3+}$ shows that the competing processes that occur from $Cr(NN)_2(N\text{--}N)(OH_2)^{3+}$ determine the profile of the conductivity trace.

At low pH, the dominant process is protonation of the dangling amine and an exponential decay in solution conductivity is observed. For $Cr(en)_3^{3+}$ and $Cr(tn)_3^{3+}$ this decay is rate limited at pH < 3 by the decay of the doublet state but becomes protonation limited as pH increases above this level. For $Cr(sen)^{3+}$, which has a sub-ns doublet decay lifetime, the conductivity decays are protonation limited at all pH.

For all three complexes the rate of amine protonation decreases and deprotonation of the co-ordinated water becomes competitive with amine protonation as the pH is increased above pH 3.5. When deprotonation of the aquo group becomes the faster of the two processes, transient increases in solution conductivity are observed. The increase in solution conductivity is only transient in nature as the proton uptake by released base eventually exceeds the proton release and an overall decrease in solution conductivity is observed.

It is debatable whether $Cr(NN)_2(N\text{--}N)(OH_2)^{3+}$ should be called a metastable photoproduct or an intermediate. From a photochemical viewpoint it is the direct product of the photoreaction, favouring the term metastable photoproduct. In terms of the overall chemistry occurring it is an intermediate, not present in the final solution under acidic conditions. For this latter reason we favour calling $Cr(NN)_2(N\text{--}N)(OH_2)^{3+}$ an intermediate. It should be noted however that $Cr(NN)_2(N\text{--}N)(OH_2)^{3+}$ is not a ground state intermediate in the sense used by Endicott.

3.5.3 *cis*-Cr(cyclam)$(NH_3)_2^{3+}$.

The successful modelling of the experimental results obtained for *cis*-Cr(cyclam)$(NH_3)_2^{3+}$ suggests that approximately 67% of the photoaquation occurs via loss and recoordination of a cyclam amine to displace ammonia. This mechanism leads to the unusual features observed in the photolysis studies of this complex using LFP with conductivity detection.

A conductivity decay lifetime longer than the emission decay of *cis*-Cr(cyclam)$(NH_3)_2^{3+}$ results from the large fraction of photoaquation that occurs via the cyclam loss mode. For this mode, recoordination of the cyclam amine, and not doublet decay, is rate limiting. Slow recoordination of the cyclam amine also delays the release and subsequent protonation of ammonia, allowing for competitive deprotonation of the co-ordinated water from the intermediate. This results in the transient increases observed in solution conductivity as the pH increases above 4.

The "kink" observed in the experimental trace at pH 3.85 results from the prompt photochemistry occurring via direct ammonia loss. At pH < 3.85 this is observable on a prompt timescale and corresponds to the initial drop in conductivity observed in the experimental trace. Proton uptake resulting from the prompt component that leads to cyclam loss is rate limited by recoordination of the cyclam amine and occurs on a "slow" timescale. The initial fast decay observed at pH 3.85 corresponds to about 10% of the overall decay in solution conductivity. The decays observed at lower pH values also give a 10% prompt component. This value is consistent with the modelled values for F_Q and F_{cyc}, i.e.

$$F_Q \text{ observed} = (1-F_{cyc}) \times F_Q = 0.33 \times 0.3 \times 100 = 9.9\%.$$

It was recognized that other values of F_{cyc} and F_Q could be possible as long as the observable fraction of prompt remained at 10%, e.g. with $F_Q = 0.15$ and $F_{cyc} = 0.33$, consistent with the F_Q values obtained for *cis* & *trans*-$Cr(tn)_2(NH_3)_2^{3+}$. Modelled conductivity changes obtained with these values of F_{cyc} and F_Q did not, however, reproduce the experimental results. In particular, no significant kink was observed at pH 3.85 and the modelled decays at pH < 3.5 were significantly faster than those observed experimentally.

As stated in section 3.4.4, preferential loss of cyclam is predicted by the AOM due to cyclam having a greater ligand field strength than ammonia. Both the direct ammonia loss and cyclam loss modes are consistent with the trans attack, edge displacement mechanism as illustrated in Figure 3.22.

Direct ammonia loss involves attack of the incoming water along an edge trans to the labilized ammonia but within the plane containing the two ammonia ligands. Migration of the second ammonia ligand, to the site vacated by the first, gives the observed photoproduct, cis-$Cr(cyclam)(NH_3)(OH_2)^{3+}$. For cyclam loss, attack of a water trans to the labilized cyclam amine results in an ammonia ligand migrating to the vacated site. Recoordination of the cyclam amine then displaces ammonia, resulting in the same photoproduct as direct ammonia loss, *cis*-$Cr(cyclam)(NH_3)(OH_2)^{3+}$.

As the AOM and trans attack edge displacement mechanism are both based on reaction from the $^4T_2$ state, the proposed photoaquation mechanism for *cis*-$Cr(cyclam)(NH_3)_2^{3+}$ is therefore also consistent with reaction via the $^4T_2$ state. This supports reaction originating in the ^2E state occurring via BISC to the $^4T_2$ state in the photoaquation of *cis*-$Cr(cyclam)(NH_3)_2^{3+}$.

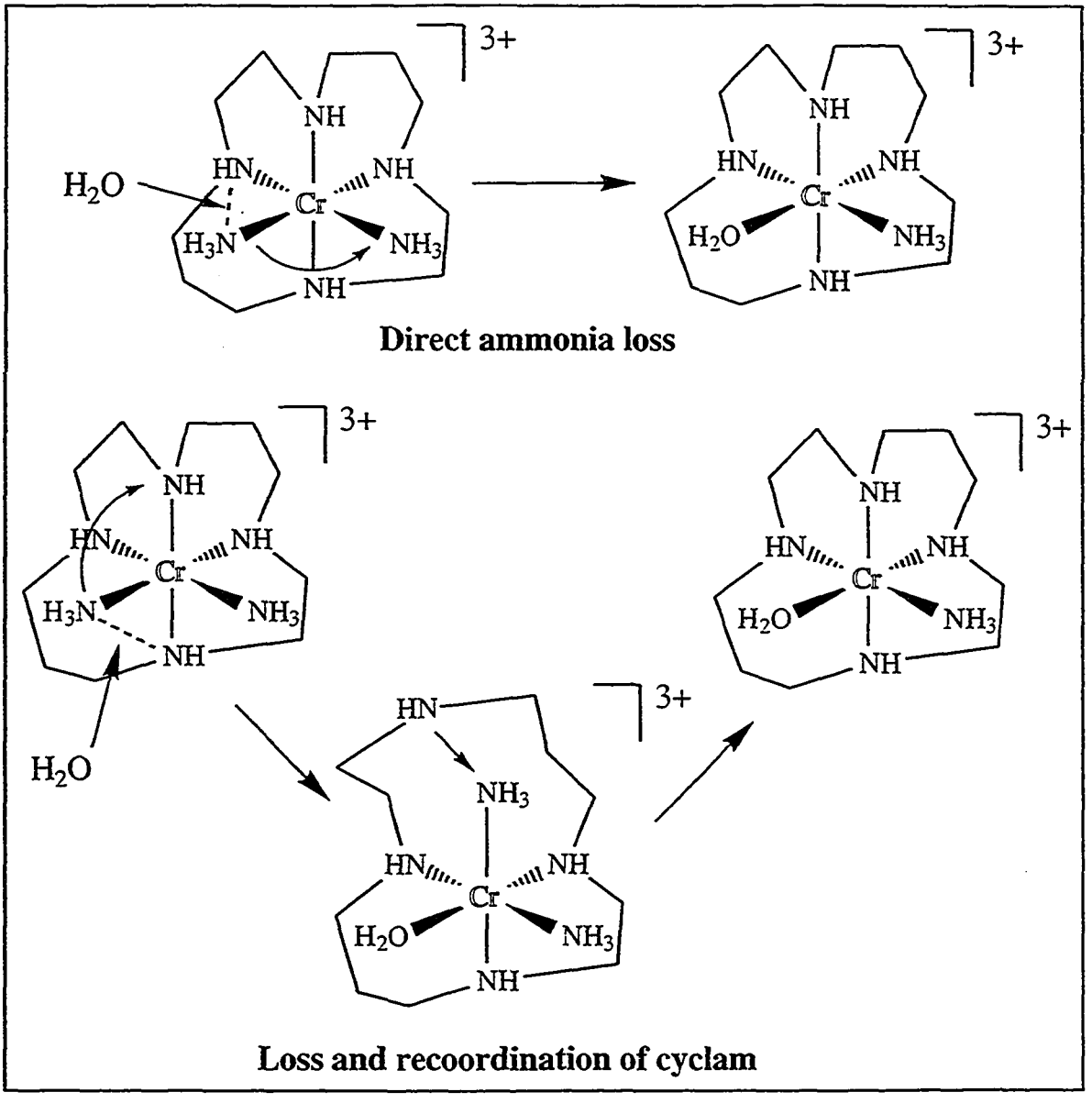

Figure 3.22 Pictorial representation of the two photoaquation modes modelled for *cis*-Cr(cyclam)$(NH_3)_2^{3+}$.

3.5.4 Related Studies

Our proposal that *cis*-Cr(cyclam)$(NH_3)_2^{3+}$ photoaquates via cyclam loss and recoordination leads to other, more general, questions which are discussed in the following sections. Do other Cr(III) cyclam complexes photoaquate via cyclam loss and recoordination? Can an intermediate containing a labilized cyclam amine be trapped? Are general assumptions that Cr(III) complexes do not photoaquate with loss of secondary amines valid?

3.5.4.1 Photoaquation of *cis*-Cr(cyclam)X_2^+ complexes

The photoinertness of *trans*-Cr(cyclam)X_2^{n+} complexes has been attributed to the cyclam ligand lacking the mobility required for photoaquation via a trans attack edge displacement mechanism. A similar lack of mobility has been assumed for the ligand when folded in *cis*-Cr(cyclam)X_2^{n+} complexes; the photochemistry observed is instead believed to occur within the "cis pocket" with no actual involvement of the cyclam ligand.

Our proposed mechanism for *cis*-Cr(cyclam)$(NH_3)_2^{3+}$ does not require the cyclam ligand to be stereomobile; labilization and recoordination of the cyclam amine occurs without any overall change in coordination of the cyclam ligand. Therefore it would be expected that other *cis*-Cr(cyclam)X_2^{n+} complexes may photoaquate via this mechanism. To investigate this, the photoaquations of *cis*-Cr(cyclam)F_2^+, *cis*-Cr(cyclam)Cl_2^+ and *cis*-Cr(cyclam)$(NCS)_2^+$ were investigated using LFP with conductivity detection.

An early study of *cis*-Cr(cyclam)F_2^+[44] showed that, although preferential cyclam loss was predicted by the AOM model, fluoride loss was observed experimentally. The authors recognized that these findings were consistent with a cyclam amine being labilized and recoordinating to displace fluoride, but discounted this reaction mode in favour of direct fluoride loss. As the experiments were conducted in acidic solutions they believed that the labilized cyclam amine would be protonated and unable to recoordinate.

Our successful modelling of the *cis*-Cr(cyclam)$(NH_3)_2^{3+}$ conductivity data indicates that protonation of the detached amine may not prevent recoordination for two reasons. Firstly, protonation of the detached amine is slow due to steric hindrance and at moderate pH is comparable to the rate of recoordination. Secondly, the detached amine may not become trapped in the protonated form due to prompt intramolecular proton transfer between the protonated amine and coordinated hydroxo group in moderately acidic conditions.

These results prompted the reinvestigation of the photolysis of *cis*-Cr(cyclam)F_2^+ using conductivity detection.

A representative conductivity trace obtained for *cis*-Cr(cyclam)F_2^+ at pH 2.94 is shown in Figure 3.23. No signals were observed above background noise at higher pH conditions. Based on these results no evidence is found for *cis*-Cr(cyclam)F_2^+ photoaquating via cyclam loss and recoordination.

The traces obtained at pH 2.94 display a decay in solution conductivity which occurs with a sub-microsecond lifetime. Monitoring the conductivity changes over longer time periods confirmed that no subsequent changes were occurring on microsecond or longer timescales. Fast decays are inconsistent with loss and recoordination of a cyclam amine; the results obtained for *cis*-Cr(cyclam)$(NH_3)_2^{3+}$ indicate that this occurs on the microsecond timescale. Observation of a sub microsecond decay is instead consistent with fast doublet decay and protonation of

the photoreleased fluoride being rate limiting. A sub-ns doublet lifetime was subsequently confirmed for *cis*-Cr(cyclam)F_2^+ by measuring the decay in doublet emission intensity.

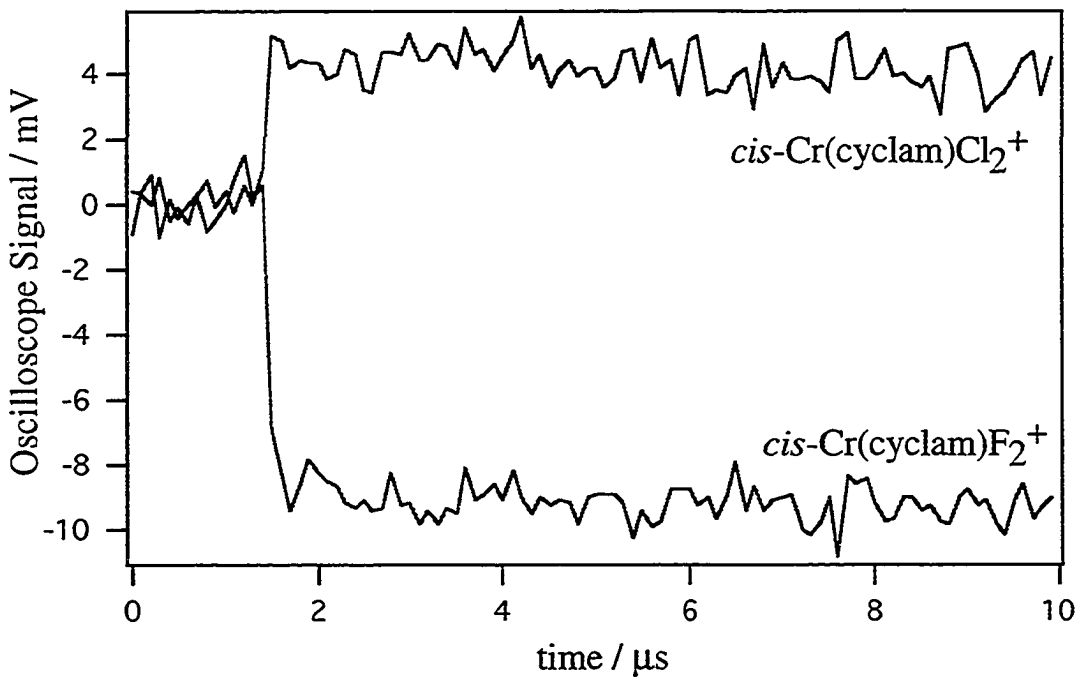

Figure 3.23 Representative conductivity traces for *cis*-Cr(cyclam)F_2^+ (pH 2.94) and *cis*-Cr(cyclam)Cl_2^+ (pH 3.45)

The quantum yield obtained by Kane-Maguire for *cis*-Cr(cyclam)F_2^+ is 0.24, yet the observed conductivity decay is only 10% of those typically observed for Cr(III) hexamine complexes with similar quantum yields. One explanation for this is that not all of the photoreleased fluoride is being protonated in solution, consistent with F^- being a weak base. However, the literature pKa of HF[120] is 3.45 and it would be expected that 70% of the free fluoride would be protonated at pH 2.94. This would result in signal magnitudes 7 times greater than those observed.

Although not investigated further, these results indicate that the literature quantum yield of *cis*-Cr(cyclam)F_2^+ may be in error.

With only direct fluoride loss being observed, *cis*-Cr(cyclam)F_2^+ becomes an exception to the I* theory which predicts preferential amine loss. Other fluoro ammine complexes also proven to be exceptions to the I* theory, including *trans*-$Cr(tn)_2F_2^+$,[43] and $Cr(tren)F_2^+$.[44]

A representative conductivity trace obtained for *cis*-Cr(cyclam)Cl_2^+ at pH 3.45 is also displayed in Figure 3.23. Similar to *cis*-Cr(cyclam)F_2^+, no discernible signals were observed at higher pH for this complex. The traces obtained at pH 3.45 displayed very small increases in solution conductivity, less than 5 mV, which occurred on the sub microsecond timescale.

The small increases in solution conductivity are consistent with formation of the 2^+ product, *cis*-Cr(cyclam)$(OH_2)Cl^{2+}$, and the release of chloride. No proton uptake occurs due to chloride being non basic. As for *cis*-Cr(cyclam)F_2^+, the absence of any conductivity changes on a microsecond timescale indicates that the photoaquation of *cis*-Cr(cyclam)Cl_2^+ does not occur with cyclam loss and recoordination.

Representative conductivity traces obtained for *cis*-Cr(cyclam)$(NCS)_2^+$ are presented in Figure 3.24. These were obtained at a higher than normal laboratory temperature of 25.5°C. Prompt and slow increases in solution conductivity were observed over the pH range 2.6 - 5.0, with the overall signal magnitude increasing as pH increased. An increase in solution conductivity is consistent with formation of the 2^+ product *cis*-Cr(cyclam)$(NCS)(OH_2)^{2+}$, and release of SCN^- . No proton uptake is observed due to NCS^- being non-basic.

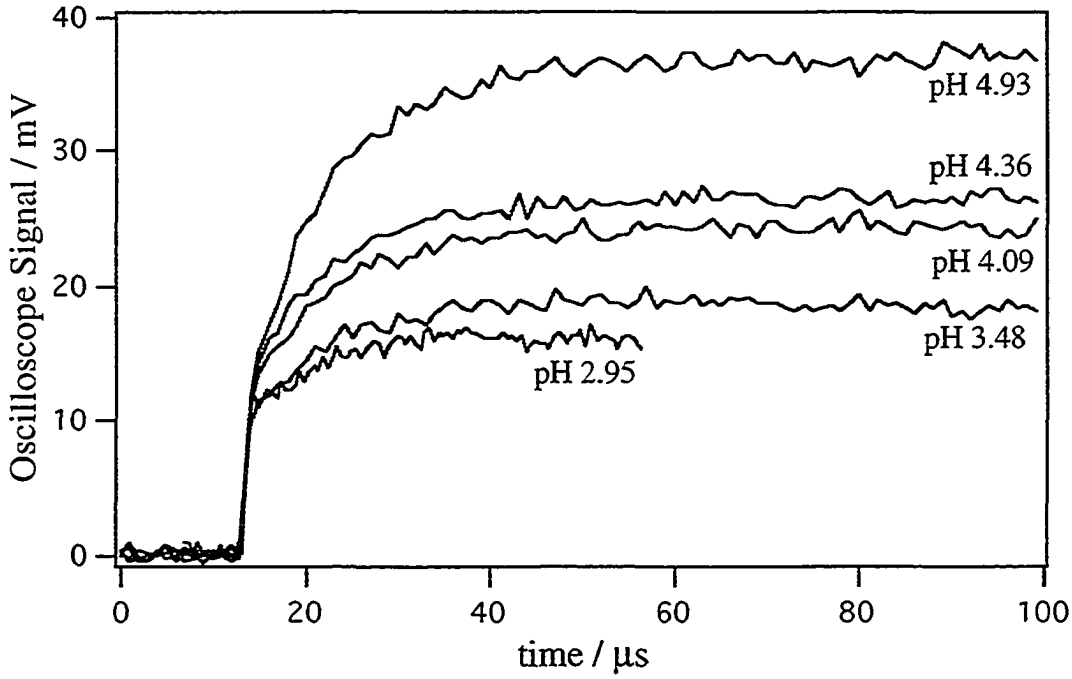

Figure 3.24 Representative conductivity traces obtained for *cis*-$Cr(cyclam)(NCS)_2^+$ at various pH values

The magnitude of the prompt conductivity increase does not vary with pH but the magnitude of the slow component increases as pH is increased. The overall increase in conductivity with increasing pH results from the acid - base equilibrium of the photoproducts,

$$cis\text{-}Cr(cyclam)(NCS)(OH_2)^{2+} <=> cis\text{-}Cr(cyclam)(NCS)(OH)^{+} + H^{+}$$

As pH increases this equilibrium shifts to the right, releasing protons to solution and generating a larger increase in solution conductivity.

Lifetimes obtained for the slow growth component are constant over the whole pH range, 9 ± 1 µs. Taking into consideration the temperature difference

between the two studies, this value is in reasonable agreement with the doublet emission lifetime obtained at 21.5°C, 11.33 ± 0.10 μs measured at 728 nm .

The measured growth lifetimes clearly indicate that the slow photocomponent originates in the doublet state but two possibilities can be presented for the origin of the prompt component, either the $^4T_2$ or CT state.

As the tail of the CT band overlaps the higher energy $^4T_2$ band of *cis*-Cr(cyclam)$(NCS)_2^+$, irradiation at 355nm results in both LF and CT excitation. The fact that a consistent prompt:slow ratio is not obtained over the whole pH range argues against the prompt component originating in the $^4T_2$ state as this would require reaction from either the $^4T_2$ or ^2E state to be pH dependent. The alternative possibility is that the prompt component results from a pH independent amount of redox chemistry originating in the CT states.

If the photoaquation of *cis*-Cr(cyclam)$(NCS)_2^+$ does occur via cyclam loss and recoordination, it is unlikely to be observed using these techniques. The rate of doublet decay for this complex, 1.1 x 10^5 s^{-1} is slower than the rate constant of 2.0 x 10^5 s^{-1} estimated for cyclam recoordination, based on the modelling of the *cis*-Cr(cyclam)$(NH_3)_2^{3+}$ experimental data. Therefore doublet decay will be rate limiting for *cis*-Cr(cyclam)$(NCS)_2^+$ at all pH.

Photolysis studies of *cis*-Cr(cyclam)F_2^+, *cis*-Cr(cyclam)Cl_2^+ and *cis*-Cr(cyclam)$(NCS)_2^+$ do not support photoaquation occurring via cyclam loss and recoordination. The prompt conductivity changes observed for *cis*-Cr(cyclam)F_2^+ and *cis*-Cr(cyclam)Cl_2^+ definitely preclude cyclam loss and recoordination for these two complexes. The slow rate of doublet decay for *cis*-Cr(cyclam)$(NCS)_2^+$ would prevent cyclam loss and recoordination being observed for this complex so cannot be discounted.

3.5.4.2 *cis*-Cr(cyclam)$(CN)_2^+$, *cis*-Cr(cycb)$(NH_3)_2^{3+}$ and Cr(15aneN5)$(NH_3)^{3+}$

No evidence was found for photoaquation via cyclam loss and recoordination for *cis*-Cr(cyclam)F_2^+, *cis*-Cr(cyclam)Cl_2^+ and *cis*-Cr(cyclam)$(NCS)_2^+$. Attention was then focused on other macrocyclic complexes with *cis*-Cr(cyclam)$(CN)_2^+$, *cis*-Cr(cycb)$(NH_3)_2^{3+}$ and Cr(15aneN5)$(NH_3)^{3+}$ being of particular interest.

Based on the strength of the Cr-CN bond strength, *cis*-Cr(cyclam)$(CN)_2^+$ is predicted to be the cis-cyclam complex most likely to produce a stable detached amine species. Labilization of a cyclam amine and trans attack, edge displacement by a water molecule would result in a cyanide ligand migrating to the vacated site. The strength of the Cr-CN bond may be sufficient to prevent recoordination of the amine, trapping the cyclam loss species Cr(cyc-NH)$(CN)_2(OH_2)^{2+}$.

Literature attempts at synthesizing *cis*-Cr(cyclam)$(CN)_2^+$ [24] have been unsuccessful with only the trans isomer being produced. This was attributed to both basic conditions catalyzing the cis -> trans isomerization and the trans isomer having a greater thermodynamic stability. Our attempts at synthesizing *cis*-Cr(cyclam)$(CN)_2^+$ through thermal and photoanation reactions also resulted in exclusive formation of the trans isomer. However possible synthetic strategies have not been explored in detail and this remains a complex whose photolysis study is of great interest.

The cycb ligand differs from cyclam in having 6 methyl groups substituted at the 5,5,7,12,12,14 positions. Although it is difficult to predict the effect of the

substituent methyls it is not unreasonable to expect that *cis*-$Cr(cycb)(NH_3)_2^{3+}$ would photoaquate with a mechanism similar to that of *cis*-$Cr(cyclam)(NH_3)_2^{3+}$.

Reference to a failed attempt at synthesizing *cis*-$Cr(cycb)(NH_3)_2^{3+}$ [119] was found in the literature but no details were given as to the procedure itself. The authors believed that their lack of success was due to steric hindrance with the cycb methyls preventing two ammonia ligands from occupying the cis pocket. *Cis*-$Cr(cycb)(OH_2)_2^{3+}$ and *cis*-$Cr(cycb)(OH)_2^{+}$ have been successfully isolated with the crystal structure of *cis*-$Cr(cycb)(OH)_2^{+}$ complex showing little evidence for such steric interactions between the hydroxo ligands and cycb methyl groups.[121]

As ammonia is not significantly larger than water or hydroxo, we believed that ammonia ligands would be able to occupy the cis pocket and that synthesis of *cis*-$Cr(cyclam)(NH_3)_2^{3+}$ would be possible. Some support for this hypothesis has been gained through preliminary molecular modelling investigations using Hyperchem. The N-Cr-N bond angles for the cycb ligand and the X-Cr-X bond angles for the ligands in the cis pocket were virtually identical for models of *cis*-$Cr(cycb)(OH_2)_2^{3+}$ and *cis*-$Cr(cycb)(NH_3)_2^{3+}$. The modelled X-Cr-X angles were also very similar to those found in the crystal structure of *cis*-$Cr(cycb)(O_2CO)^{+}$.[121]

The attempted synthesis of *cis*-$Cr(cycb)(NH_3)_2^{3+}$ involved the ammonolysis of the sea-green complex [*cis*-$Cr(cycb)Cl_2$]Cl in a Carius tube. This complex is surprisingly insoluble in most solvents, including water, and it has been suggested that the three chlorides may be coordinated with a macrocyclic amine detached, resulting in the neutral complex $Cr(cycb\text{-}N)Cl_3$. Regardless of the structure it was hoped that ammonolysis would give *cis*-$Cr(cycb)(NH_3)_2^{3+}$, similar to the preparation of *cis*-$Cr(cycb)(OH)_2^{+}$ by base hydrolysis of [*cis*-$Cr(cycb)Cl_2$]Cl .

After 48 hours ammonolysis resulted in the formation of a red powder. Excess ammonia was allowed to evaporate and recrystallization of the powder as the perchlorate salt gave deep red crystals. Microanalysis of the crystals generated C, H,

N percentages consistent with the formula $[Cr(cycb\text{-}NH)(NH_3)_2Cl](ClO_4)_3$, indicating that the cycb macrocycle was coordinated by three amines, with the fourth present in the crystal as a hydroperchlorate salt. The remaining three coordination sites are occupied by two ammonias and a chloro ligand. To date no attempt has been made to coordinate the final amine but, if successful these results indicate that *cis*-$Cr(cycb)(NH_3)_2^{3+}$ photoproducts generated by loss of a cycb amine will be thermally stable and observable.

Macrocyclic $Cr(N_5)(NH_3)^{3+}$ complexes are of interest as photoreactivity of these complexes would support photoaquation via loss and recoordination of a macrocyclic amine. If photochemistry is assumed to occur via the trans attack edge displacement mechanism this is unlikely to occur with migration of a macrocyclic amine. Labilization of a ring amine could result in trans attack with the mobile ammonia ligand migrating to the vacated site. Recoordination of the ring amine would then displace ammonia producing $Cr(N_5)(OH_2)^{3+}$. This is illustrated in Figure 3.25.

Attempts at synthesizing $Cr(15aneN5)Cl^{2+}$ by refluxing 15aneN5 with $Cr(DMSO)_3Cl_3$, generated *in situ*, were unsuccessful. The x-ray structure showed the ligand to be coordinated by four amines in the equatorial plane, with the fifth amine being uncoordinated and present as the hydroperchlorate salt. Two chloro ligands occupied the axial sites. Some difficulty has been reported in coordinating a fifth macrocyclic amine to an axial position when the macrocycle contains amine groups spaced by only two methylene groups. However this does not prevent the synthesis of $Cr(18aneN6)^{3+}$ [68] where the hexadentate ligand folds to occupy all six coordination sites even though all six amines are spaced by two methylenes. It is likely that conducting the synthesis with the pentahydrochloride salt and not the free ligand hindered coordination of the fifth amine. The stability of the observed

product, $Cr(15aneN5\text{-}NH)Cl_2^{2+}$ indicates that any photoproducts resulting from ring loss in the photoaquation of $Cr(15aneN5)(NH_3)^{3+}$ may be stable and observable under acidic conditions.

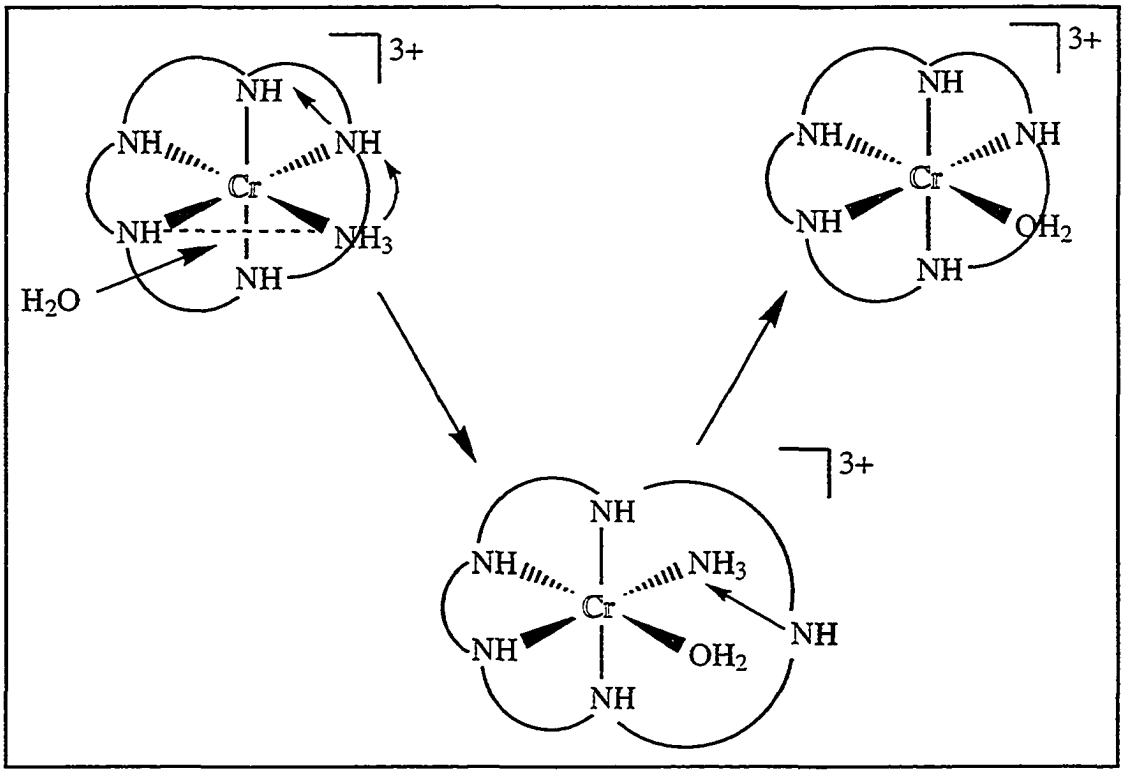

Figure 3.25 Possible photoaquation mechanism for macrocyclic $Cr(N_5)(NH_3)^{3+}$ complexes

3.5.4.3 Photoaquation of *trans*-$Cr(tet)(CN)_2^+$

The proposal that the *cis*-$Cr(cyclam)(NH_3)_2^{3+}$ intermediate contains a labilized cyclam amine is significant. This indicates that photochemical reactions of Cr(III) complexes can occur via labilization of secondary amines, a possibility that has often been discounted in the literature.

The complex *trans*-$Cr(tet)(CN)_2^+$ was specifically chosen for a literature study in the belief that it would be photoinert.[67] It was predicted that steric constraints of the tet ligand would prevent the stereochemical changes required of Cr(III) photoreactions. However efficient photoaquation was observed, $\emptyset = 0.09$, with the authors attributing this to stereoretentive loss of a primary amine occurring from a higher energy quartet state.

The possibility that loss of a secondary amine was occurring with migration of a primary amine to the vacant site, consistent with the trans attack edge displacement mechanism, was also considered. This process is illustrated in the first step of the mechanism proposed in Figure 3.26. The observed photoproduct underwent efficient conversion back to the starting material at pH 6.0 and the authors believed this was consistent with recoordination of a primary, rather than a secondary, amine. Based on the results for *cis*-$Cr(cyclam)(NH_3)_2^{3+}$ it is possible that loss of a secondary amine would be followed by recoordination to displace a primary amine. This is illustrated in the second step of the mechanism proposed in Figure 3.26 and gives the same final product as that favoured by Kirk and Fernando.

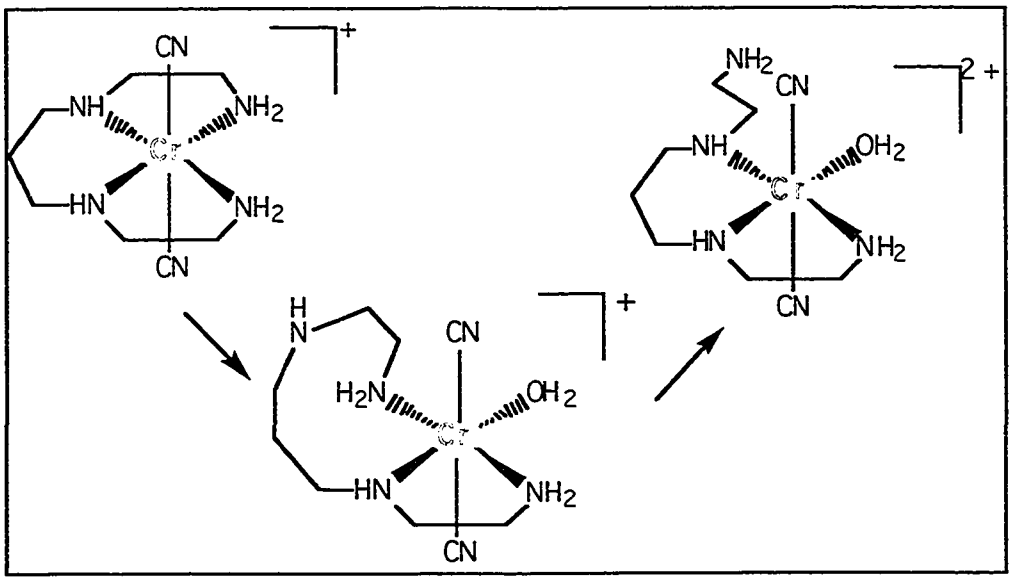

Figure 3.26 Possible photoaquation mechanism for *trans*-$Cr(tet)(CN)_2^+$

Conductivity decays observed for the photolysis of *trans*-$Cr(tet)(CN)_2^+$ do not support direct loss of a primary amine. This complex has a relatively long doublet lifetime of 30 μs and protonation of a dangling amine arm should not become rate limiting until the pH exceeds 4.6. This is based on the literature protonation rate for the dangling amine arm in $Cr(en)_2(en\text{-}N)(OH_2)^{3+}$, $k_{prot} = 3.6 \times 10^9\ M^{-1}\ s^{-1}$. However protonation of $Cr(tet\text{-}N)(CN)(OH_2)^+$ involves a 2^+ species, not a 3^+ species as for $Cr(en)_2(en\text{-}N)(OH_2)^{3+}$. The Debye-Smoluchowski equation indicates that the protonation rate constant for a 2^+ species could be as high as $7.0 \times 10^9\ M^{-1}\ s^{-1}$. Based on this value, protonation of the dangling amine would not become rate limiting until the pH exceeds 5.3.

Experimentally it was found that conductivity decay lifetimes became longer than the doublet decay lifetime when the pH was increased above 4.0. A 43 μs conductivity lifetime was obtained at pH 4.20, increasing to 67 μs at pH 5.05. Although not conclusive, these results support a process slower than protonation of a

primary amine being rate determining in the photoaquation of *trans*-$Cr(tet)(CN)_2^+$ when the pH is increased above 4.0. We favour this being loss and recoordination of a secondary amine to displace a primary amine.

3.6 Conclusions

As outlined in the introduction, the original intentions of this work were;

i) to determine whether *cis*-$Cr(cyclam)(NH_3)_2^{3+}$ was unique among Cr(III) am(m)ine complexes in having a photolytic intermediate,

ii) to explore the possible effect of ligand structure upon intermediate formation,

iii) to determine whether the observation of intermediates was consistent with photoaquation via GSI or BISC.

Our results indicate that *cis*-$Cr(cyclam)(NH_3)_2^{3+}$ is not unique among Cr(III) am(m)ine complexes in having a "photolytic" intermediate. Although this was the only complex which displayed a conductivity decay lifetime longer than its doublet emission lifetime at pH < 3, transient conductivity rises indicating intermediates were also observed for $Cr(en)_3^{3+}$, $Cr(tn)_3^{3+}$ and $Cr(sen)^{3+}$.

The intermediates observed for $Cr(en)_3^{3+}$, $Cr(tn)_3^{3+}$, $Cr(sen)^{3+}$ and *cis*-$Cr(cyclam)(NH_3)_2^{3+}$ were identified as thermally unstable, initial photoproducts. These initial photoproducts are all six-coordinate aquated species with the $Cr(en)_3^{3+}$, $Cr(tn)_3^{3+}$, $Cr(sen)^{3+}$ intermediates containing an unprotonated dangling amine.

The modelled results for *cis*-$Cr(cyclam)(NH_3)_2^{3+}$ indicate that this complex photoaquates via two modes; i) direct ammonia loss and ii) loss and recoordination of a cyclam amine to displace ammonia. Both modes generate the observed

photoproduct, *cis*-Cr(cyclam)$(NH_3)(OH_2)^{3+}$ with the cyclam loss mode accounting for 67% of the overall chemistry occurring. The intermediate occurring in the photoaquation of *cis*-Cr(cyclam)$(NH_3)_2^{3+}$ has been identified as Cr(cyc-N)$(NH_3)_2(OH_2)^{3+}$, the initial photoproduct of the cyclam loss mode.

The observation of intermediates is related to ligand structure as the protonation rate and/or recoordination rate of the labilized ligand determines whether intermediates are observed. For $Cr(en)_3^{3+}$, $Cr(tn)_3^{3+}$ and $Cr(sen)^{3+}$, conductivity rises occur when protonation of the dangling amine arm of the photoproduct becomes slower than deprotonation of the coordinated water. For *cis*-Cr(cyclam)$(NH_3)_2^{3+}$ slow recoordination of the detached cyclam amine results in both a conductivity decay lifetime longer than the emission lifetime at pH < 3 and the conductivity rises occurring at pH > 4.

Identification of the intermediate species as being unstable initial photoproducts provides little insight into whether photoaquation occurs via BISC or GSI. However these findings do not support the literature bias towards the *cis*-Cr(cyclam)$(NH_3)_2^{3+}$ results being more consistent with the GSI mechanism. Based on preferential loss of a cyclam amine, and the stereochemical changes occurring with cyclam loss and recoordination to displace ammonia, the proposed mechanism is consistent with reaction occurring from the $^4T_2$ state for *cis*-Cr(cyclam)$(NH_3)_2^{3+}$. Therefore the proposed photoaquation mechanism for *cis*-Cr(cyclam)$(NH_3)_2^{3+}$ is more consistent with BISC being the dominant process depopulating the ^2E state.

LFP/conductivity results suggest that *cis*-Cr(cyclam)F_2^+ and *cis*-Cr(cyclam)F_2^+ do not photoaquate with cyclam loss and recoordination. A slow rate of doublet decay prevents conclusions from being reached for the photoaquation of *cis*-Cr(cyclam)$(NCS)_2^+$. Conductivity results obtained for the photolysis of *trans*-

$Cr(tet)(CN)_2^+$ are consistent with labilization and recoordination of a secondary tet amine.

The attempted syntheses of *cis*-$Cr(cyclam)(CN)_2^+$, *cis*-$Cr(cycb)(NH_3)_2^{3+}$ and $Cr(15aneN5)(NH_3)^{3+}$ were unsuccessful. The products obtained in both attempts contained a stable detached ring amine. This indicates that the photoaquations of *cis*-$Cr(cyclam)(CN)_2^+$ and *cis*-$Cr(cycb)(NH_3)_2^{3+}$ may generate stable ring loss photoproducts and warrant further investigation.

CHAPTER FOUR

CAPILLARY ELECTROPHORESIS STUDY OF THE PHOTOLYSIS AND THERMOLYSIS OF *rac*-Cr(sen)$^{3+}$ AND Λ-Cr(sen)$^{3+}$

4.1 Introduction

The complex $Cr(sen)^{3+}$ is very similar in structure to $Cr(en)_3^{3+}$ if the hexadentate sen ligand is viewed as analogous to three ethylenediamine ligands capped by a neopentyl cap. Representative structures are given for these two complexes in Figure 4.1.

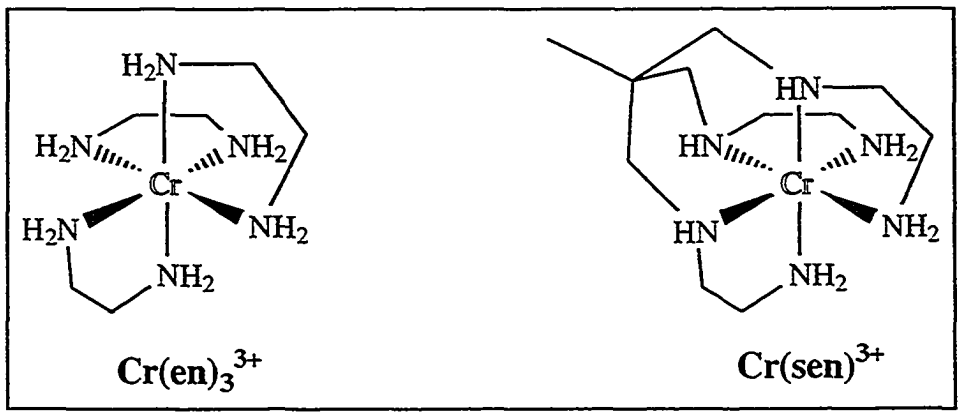

Figure 4.1 Representative structures of $Cr(en)_3^{3+}$ and $Cr(sen)^{3+}$

The photochemistry and photophysics of $Cr(en)_3^{3+}$ have been well studied; the complex photoaquates with a quantum yield of 0.37[122,123] and has a 1.6 μs doublet emission lifetime.[102] Photoaquation studies on the resolved complex, Λ-$Cr(en)_3^{3+}$, have shown that three photoproducts are formed, Λ-*cis*-$Cr(en)_2(enH)(OH_2)^{4+}$, Δ-*cis*-$Cr(en)_2(enH)(OH_2)^{4+}$ and *trans*-$Cr(en)_2(enH)(OH_2)^{4+}$ with quantum yields of 0.10, 0.03 and 0.24 respectively.[73] In a separate paper,[124] Cimolino showed that a minor photoisomerization mode was also present with Λ-$Cr(en)_3^{3+}$ photoracemizing to Δ-$Cr(en)_3^{3+}$ with a quantum yield of 0.015.

The first photochemical and photophysical study[26] of $Cr(sen)^{3+}$ showed it to have remarkably different photophysical properties to $Cr(en)_3^{3+}$. In particular, a remarkably short < 0.1 ns doublet emission lifetime was obtained. The difference in doublet lifetimes between $Cr(en)_3^{3+}$ and $Cr(sen)^{3+}$ was attributed to the trigonal strain imposed by the sen ligand in $Cr(sen)^{3+}$ promoting twisting of the complex and crossing to the ground state surface. A quantum yield of 0.10 was obtained for the photoaquation of $Cr(sen)^{3+}$ but no investigation into the number, or structure, of photoproducts was made.

A more recent study[68] has confirmed the short lifetime and 0.10 quantum yield for $Cr(sen)^{3+}$. This study also investigated the stereochemistry of the observed products in the thermolysis and photoaquation of both *rac*-$Cr(sen)^{3+}$ and the resolved enantiomer, Λ-$Cr(sen)^{3+}$, using reverse phase HPLC. Results suggested that four photoproducts were present, three resulting from loss of a primary amine and one from loss of a secondary amine. This contrasted with the single photoproduct expected based on VC theory.

The VC model (section 1.7.2) has been applied to the photoaquation of Λ-$Cr(en)_3^{3+}$ to account for the 28% Λ-*cis*-$Cr(en)_2(enH)(OH_2)^{4+}$, 7% Δ-*cis*-$Cr(en)_2(enH)(OH_2)^{4+}$ and 65% trans-$Cr(en)_2(enH)(OH_2)^{4+}$ product distribution[9]. Formation of the 2 major products is consistent with labilization of the ethylendiamine ligand with both nitrogen donors in the plane of excitation. The minor Δ-*cis*-$Cr(en)_2(enH)(OH_2)^{4+}$ product was consistent with loss of an ethylenediamine with only one nitrogen donor in the plane of excitation.

Applying the VC model to the photoaquation of $Cr(sen)^{3+}$ indicates the neopentyl cap of the sen ligand restricts the number of sites at which solvent attack can occur. Only one photoproduct is predicted, *trans*-$Cr(sen\text{-}NH)(OH_2)^{4+}$, as illustrated in Figure 4.2 which is reproduced[68] with the permission of Ian Mackay.

The three nitrogens capped by the neopentyl group are denoted by the * symbol and all three planes are equivalent due to the symmetry of the complex. Identifying a plane of excitation shows that two primary amine are labilized, labelled 1 and 2 in Figure 4.2. Secondary amines within this plane are assumed not to be labilized due to steric constraints.

Photochemical loss of amine 1 is followed by rearrangement to give a TBP intermediate. Although shown here as preceding rearrangement, protonation of the labilized amine may be a consecutive or subsequent process. Solvent attack on the TBP intermediate along the edges trans to the vacant site is blocked by the sen ligand and prevents photoproduct formation.

Loss of amine 2 is followed by rearrangement to give a TBP where an edge trans to the vacant site is open to nucleophilic attack. Attack by water then results in a single product with the aquo group trans to the labilized sen arm, *trans*-Cr(sen-NH)$(OH_2)^{4+}$.

Thermal reactions of Cr(III) complexes are predominantly stereoretentive, therefore the thermolysis of *rac*-Cr(sen)$^{3+}$ is expected to give Λ- & Δ-*cis*-Cr(sen-NH)$(OH_2)^{4+}$. Thermolysis of Λ-Cr(sen)$^{3+}$ is expected to give Λ-*cis*-Cr(sen-NH)$(OH_2)^{4+}$ as the only product. Based on the rationale that thermal reactions are stereoretentive, Mackay concluded that four photoaquation products were present in the photoaquation of Cr(sen)$^{3+}$. Although poor resolution was obtained between both the Λ- & Δ-starting materials and Λ- & Δ- cis photoproducts Mackay's results were consistent with four photoproducts. Three of these were attributed to loss of a primary amine giving; Λ-*cis*-Cr(sen-NH)$(OH_2)^{4+}$, Δ-*cis*-Cr(sen-NH)$(OH_2)^{4+}$ and *trans*-Cr(sen-NH)$(OH_2)^{4+}$, analogous to the photoproducts of Cr(en)$_3^{3+}$. The fourth product was attributed to loss of a secondary amine.

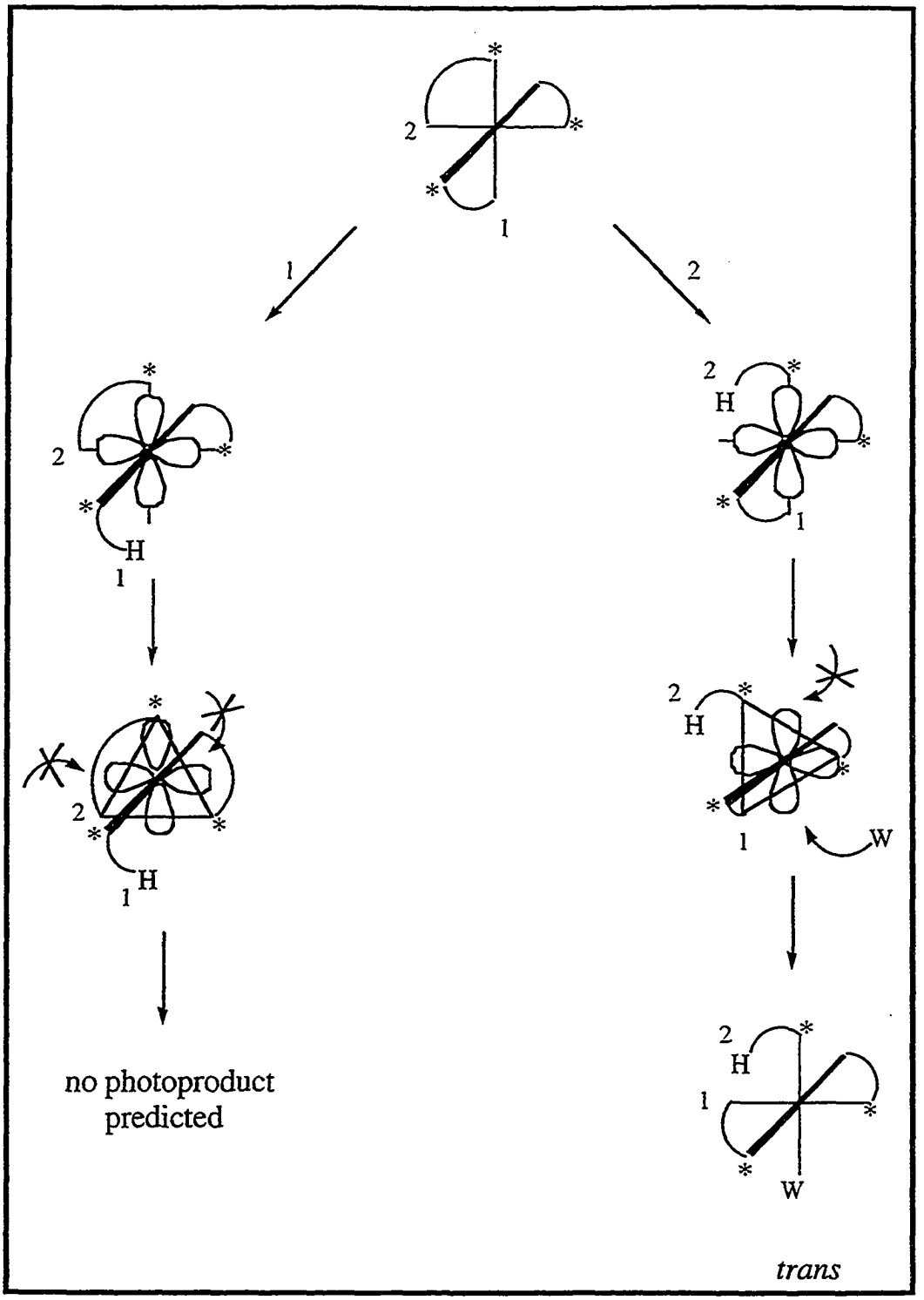

Figure 4.2 VC theory applied to the photoaquation of $Cr(sen)^{3+}$

The above work also involved preliminary investigations into the use of capillary electrophoresis as an alternative separation technique. The results of these

studies were promising with better resolution between the Λ- & Δ-starting materials being obtained than with reverse phase HPLC.

This has led to the work presented in this thesis where the thermolysis and photolysis reactions of $Cr(sen)^{3+}$ are reinvestigated using capillary electrophoresis. Of particular interest to us is confirmation of a photoproduct resulting from loss of a secondary sen amine. This would support the photoaquation mechanism involving loss of a secondary cyclam amine which was proposed for *cis*-$Cr(cyclam)(NH_3)_2^{3+}$ in Chapter Three.

4.2 Capillary Electrophoresis

4.2.1 Background

The use of thin bore capillaries allows for the use of larger voltages and current densities than other electrophoretic techniques. The large surface area to volume ratio allows for efficient dissipation of Joule heating that arises from current flow. One of the most striking features of capillary electrophoresis is the small amounts of sample required for successful analysis with typical experiments involving injection of nanolitres of sample containing as little as femtomoles of analyte.

Capillary electrophoresis has become a standard separation technique in the biochemical field and is a developing area in the separation of metal ions and metal complexes, as detailed in a recent review[125]. The effectiveness of capillary electrophoresis in separating metal ions is ably demonstrated by two studies which are referenced in this review. Baseline resolution of 26[126] and 27[127] alkali, alkali-

earth, lanthanide and transition metal ions are attained within 10 and 6 minutes respectively in these two studies.

The application of capillary electrophoresis has recently been extended to the resolution of chiral transition metal complexes using chiral buffers.[128,129]

4.2.2 Theory of Capillary Electrophoresis and Ion separation

Applying a potential difference across the capillary results in a flow of ions toward the electrodes. The electrophoretic velocity for migration of an ion, v_{app}, due to a applied potential difference is defined as;

$$v_{app} = \frac{qE}{6\pi\eta R} \qquad (4.1)$$

where; q = charge of ion, E = Electric Field Strength, η = solution viscosity,

R = ionic radius

The electrophoretic mobility, μ_{app}, is defined as the electrophoretic velocity per unit field strength;

$$\mu_{app} = \frac{q}{6\pi\eta R} \qquad (4.2)$$

Equation 4.1 implies that the migration velocity will not vary significantly for ions of the same charge and similar radii. However, as will be discussed, a number of secondary effects can act to increase the separation of metal complexes using capillary electrophoresis.

Except at very low pH conditions the wall of the fused silica capillaries contains negative sites and results in the formation of a double layer with the positive ions of the buffer. The capillary wall is immobile but the positive component, consisting of the solution containing positive buffer ions is mobile. Applying a potential across the capillary results in the positive layer migrating towards the cathode dragging the bulk solvent with it. This phenomenon is known as electroosmotic flow. The extent of electroosmotic flow is determined by pH as it is dependent on the following equilibrium,

$$Si\text{-}OH <=> Si\text{-}O^- + H^+$$

A pictorial representation of electrophoretic and electroosmotic mobilities is presented in Figure 4.3.

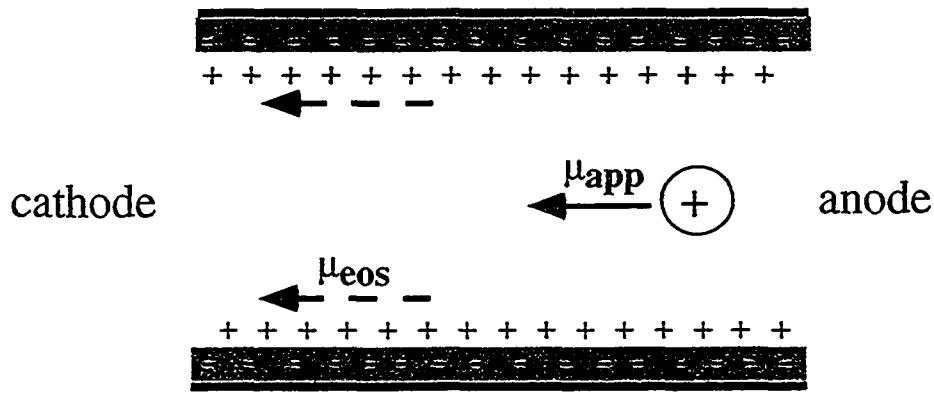

Figure 4.3 Electrophoretic and electroosmotic mobilities

Associated with electroosmotic flow is the electroosmotic velocity, v_{os}, and electroosmotic mobility, μ_{os}, which are easily determined;

$$v_{os} = \frac{L_{det}}{t_{os}} \qquad (4.3)$$

where; L_{det} = length of capillary between injection point and detector

t_{os} = migration time for relevant Cr(III) species

$$\mu_{os} = \frac{L_{tot} \cdot v_{os}}{V} \qquad (4.4)$$

where; L_{tot} = total length of capillary

V = applied voltage

The observed mobility, μ_{obs}, of an ion is the sum of the electrophoretic and electroosmotic mobilities;

$$\mu_{obs} = \mu_{os} + \mu_{app} \qquad (4.5)$$

$$\mu_{obs} = \frac{v_{obs}}{E} = \frac{L_{tot} \cdot v_{obs}}{V} \qquad (4.6)$$

$$v_{obs} = \frac{L_{det}}{t_{obs}}$$

where; t_{obs} = observed migration time for the species of interest

The extent of electroosmotic flow can be decreased through the use of electroosmotic flow modifiers. Typically these are cationic compounds which have a

high affinity for the $Si\text{-}O^-$ groups and effectively coat the capillary wall, preventing formation of a double layer.

The electophoretic mobilities of metal ions are also influenced by buffer effects, in particular ion-pairing which can occur with the buffer anions,

$$M^{n+} + A^{m-} <=> \{M\text{-}A\}^{(m-n+)}$$

Formation of an ion pair effectively decreases the charge on the ion resulting in a decrease in electrophoretic mobility. The extent to which this affects different metal ions is related to their ion pairing equilibrium constants, K_{IP}, and the relative concentrations of the metal ions and buffer anions.

As the buffers commonly employed in capillary electrophoresis are the conjugate bases of organic or inorganic acids, solution pH will affect the extent of ion pair formation via the acid base equilibrium;

$$H^+ + A^- <=> HA$$

where HA represents an acid and A^- the conjugate base. At lower pH the concentration of A^- is decreased and less ion-pair formation occurs.

For the Cr(III) photoproducts of interest to this study, pH is predicted to have a further effect on migration times. As pH increases, the acid base equilibrium of the photoproduct shifts to the right;

$$CrL_5(OH_2)^{n+} <=> CrL_5(OH)^{(n-1)+} + H^+$$

This results in an ion of lower charge and it would be predicted that longer migration times will result as the pH is increased above the pKa. However as migration times of the metal ions are a reflection of many different equilibria, including ion-pairing, the overall effect of pH may be more complicated than this.

A recent paper,[129] showed that baseline resolution was achieved for the Λ- & Δ– isomers of both $Ru(phen)_3^{2+}$ and $Ni(phen)_3^{2+}$ using buffers containing 25 mM

sodium phosphate, 100 mM potassium antimonyl *d*-tartrate at pH 7.0. It was hoped that similar peak resolution could be achieved using chiral buffers in our thermal and photoaquation studies of *rac*-$Cr(sen)^{3+}$ and Λ-$Cr(sen)^{3+}$.

4.3 Experimental Studies

4.3.1 Effect of Electroosmotic Flow and pH on Ion Migration

Electroosmotic mobilities were determined for 50 mM *d*-tartrate buffers at pH 3.5, 4.5 and 5.5 by electrophoresing an aqueous 0.1% DMSO solution with an applied voltage of 8 kV. Unless otherwise stated, adjustment of pH was made by the addition of tris(hydroxymethyl)aminomethane (TRIS). The effect of the electroosmotic flow modifier diethylenetriamine (DETA) on the observed migration times was also investigated at pH 4.5 and 5.5.

Relative separations and electrophoretic mobilities of the $Cr(en)_3^{3+}$ enantiomers and photoproducts were also investigated using the above conditions. The capillary was flushed between each set of experiments with the appropriate buffer for 30 minutes using vacuum aspiration (20" Hg) and 30 minutes electrophoretically at the operating potential.

4.3.2 Thermolysis and Photolysis of $Cr(en)_3^{3+}$ and $Cr(sen)^{3+}$

The thermolysis results for $Cr(sen)^{3+}$ that were presented in Mackay's thesis could not be reproduced in this work. Chemical changes were observed for 2 x 10^{-2} M *rac*-$[Cr(sen)]Cl_3$ and Λ-$[Cr(sen)]Cl_3$ solutions in 0.01 M $HClO_4$ within 5

minute of heating at 70° C. In this work no chemical changes were observed, even after 2 hours of heating at 70° C, for 5 x 10^{-3} M $[Cr(sen)](ClO_4)_3$ solutions in 0.001 M $HClO_4$. It was found that reflux temperatures were required to observe any chemical changes for these solutions within 10 minutes of heating.

Photolysis experiments were conducted on 5 x 10^{-3} M *rac*- and Λ-$[Cr(en)_3](ClO_4)_3$ along with 5 x 10^{-3} M *rac*- and Λ-$[Cr(sen)](ClO_4)_3$ solutions in 0.001 M $HClO_4$. Irradiation was either at 458 or 488 nm with typical laser powers of 30-35 mW as described in section 2.2.4.

4.4 Results

4.4.1 Effect of Electroosmotic Flow and pH on Ion Migration

The migration times obtained for DMSO and the $Cr(en)_3^{3+}$ starting materials and photoproducts are listed in Table 4.1. *Cis*- prod and *trans*-prod represent *cis* -$Cr(en)_2(enH)(OH_2)^{4+}$ and *trans* -$Cr(en)_2(enH)(OH_2)^{4+}$ respectively.

For $Cr(en)_3^{3+}$ and *cis* -$Cr(en)_2(enH)(OH_2)^{3+}$ the Δ and Λ isomers were resolved at each pH with typical separations being 0.05 - 0.1 min. In Table 4.1 the migration times listed for these species are those of the first enantiomer observed.

From the values listed in Table 4.1 the electroosmotic mobility was calculated for each set of conditions using the DMSO migration time and the equations outlined in section 4.2. Observed mobilities were calculated for the different Cr(III) species at each set of conditions and electrophoretic mobilities were obtained from the difference between observed and osmotic mobilities. For these experiments the relevant values of L_{det} and L_{tot} were 27.0 and 45.0 cm respectively.

	Migration Times / min			
Conditions	DMSO	$Cr(en)_3^{3+}$	*cis* - prod	*trans*-prod
pH 3.5	54.0	8.1	10.5	12.7
pH 4.5	24.0	9.5	11.9	13.0
pH 4.5 + 3.75 mM DETA	36.5	10.6	14.0	15.3
pH 5.5	13.5	7.7	8.5	10.2
pH 5.5 + 3.76 mM DETA	19.1	9.0	9.7	10.3

Table 4.1 Migration times observed for DMSO and $Cr(en)_3^{3+}$ starting materials and photoproducts at various pH.

All buffers were 50 mM in *d*-tartrate and pH was adjusted with TRIS base. The applied voltage was 8kV. Capillary length was 45 cm with the length to the detector being 27cm. Detection wavelength was 210 nm.

	Mobilities / $m^2\ s^{-1}\ V^{-1}$			
Conditions	μ_{os}	μ_{app} $Cr(en)_3^{3+}$	μ_{app} *cis* - prod	μ_{app} *trans*-prod
pH 3.5	4.7×10^{-9}	3.1×10^{-8}	2.4×10^{-8}	2.0×10^{-8}
pH 4.5	1.1×10^{-8}	2.7×10^{-8}	2.1×10^{-8}	2.0×10^{-8}
pH 4.5 + 3.75 mM DETA	6.9×10^{-9}	2.4×10^{-8}	1.8×10^{-8}	1.7×10^{-8}
pH 5.5	1.9×10^{-8}	3.3×10^{-8}	3.0×10^{-8}	2.5×10^{-8}
pH 5.5 + 3.76 mM DETA	1.3×10^{-8}	2.8×10^{-8}	2.6×10^{-8}	2.5×10^{-8}

Table 4.2 Osmotic mobilities and electrophoretic mobilities for $Cr(en)_3^{3+}$ starting materials and photoproducts at various pH

4.4.2 Photolysis of $Cr(en)_3^{3+}$

The electropherograms obtained in the photolysis of 5.0 mM Λ- and *rac*-$[Cr(en)_3]Cl_3$ in 1 x 10-3 M $HClO_4$ are presented in Figure 4.4 and 4.5 respectively. Both solutions were photolyzed at 458 nm with a laser power of 32 mW. The CE buffer conditions were 50 mM *d*-tartrate, adjusted to pH 4.06 using NaOH and the samples were electrophoresed at 12 kV with a detection wavelength of 220 nm.

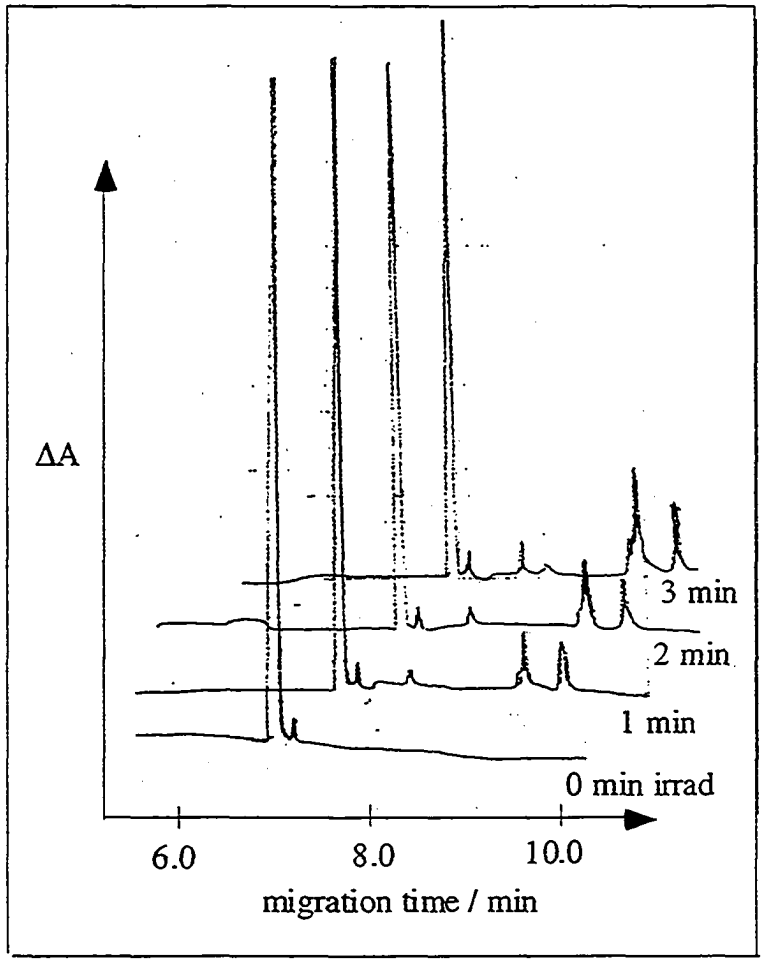

Figure 4.4 Electropherograms obtained for the photolysis of 5.0 mM Λ-$[Cr(en)_3]Cl_3$ in 1 x 10^{-3} M $HClO_4$ at increasing photolysis times. Conditions: buffer: 50 mM d-tartrate, pH 4.06; applied voltage: 12 kV; detection wavelength: 220 nm

As shown in Figures 4.4 and 4.5, baseline resolution was obtained for Λ- & Δ-$[Cr(en)_3]Cl_3$. In the photolysis of Λ-$[Cr(en)_3]Cl_3$ the starting material is observed at 6.6 minutes with a small amount of Δ- impurity following this at 6.8 minutes.

Two major photoproduct peaks are observed in the photoaquation of Λ-$[Cr(en)_3]Cl_3$, growing in at 9.3 and 9.7 minutes. A third product was evident in the shoulder observed on the leading edge of the 9.3 minute peak. Based on Cimolino's findings the two major peaks can be identified as Λ-*cis*-$Cr(en)_2(enH)(OH_2)^{4+}$ and *trans*-$Cr(en)_2(enH)(OH_2)^{4+}$. The separation between the Δ- and Λ-*cis*-$Cr(en)_2(enH)(OH_2)^{4+}$ enantiomers is expected to be small, therefore the peak and shoulder occurring at 9.3 and 9.2 minutes are consistent with Δ- and Λ-*cis*-$Cr(en)_2(enH)(OH_2)^{4+}$ respectively. The 9.7 minute peak is therefore identified as *trans*-$Cr(en)_2(enH)(OH_2)^{4+}$.

As will be discussed for the $Cr(sen)^{3+}$ results, photoanation appears to be competitive with photoaquation for the chloride salts of these amine complexes. Based on this, the minor peak observed at 7.6 minutes in the photolysis of Λ-$[Cr(en)_3]Cl_3$ is believed to be a $Cr(en)_2(enH)Cl^{3+}$ photoanation product. As *trans*-$Cr(en)_2(enH)(OH_2)^{4+}$ is the major product, this is presumably *trans*-$Cr(en)_2(enH)Cl^{3+}$. At longer photolysis times a very small peak was observed at 7.9 minutes which could be Λ-*cis*-$Cr(en)_2(enH)Cl^{3+}$ or else results from secondary photolysis.

Figure 4.5 shows the electropherograms obtained for the photoaquation of *rac*-$[Cr(en)_3]Cl_3$. The migration times are slightly longer than those obtained for Λ-$[Cr(en)_3]Cl_3$ but a consistent peak pattern is observed. The Λ- & Δ-$[Cr(en)_3]Cl_3$ starting materials are observed at 6.8 and 7.0 minutes respectively and three major photoproduct peaks are observed at 9.7, 9.9 and 10 .4 minutes, consistent with Δ-*cis*-$Cr(en)_2(enH)(OH_2)^{4+}$, Λ-*cis*-$Cr(en)_2(enH)(OH_2)^{4+}$ and *trans*-

$Cr(en)_2(enH)(OH_2)^{4+}$ respectively. The minor peak believed to be *trans*-$Cr(en)_2(enH)Cl^{3+}$ is observed at 8.0 minutes and a small peak at 8.2 minutes grows in with longer photolysis times .

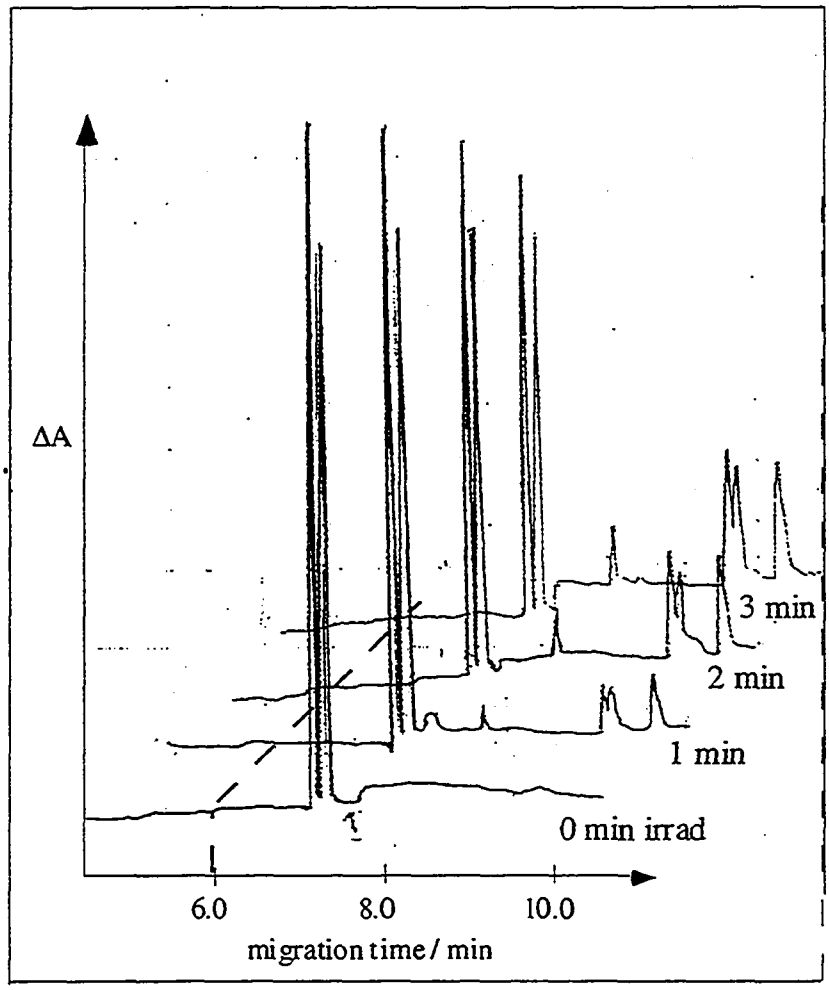

Figure 4.5 Electropherograms obtained for the photolysis of 5.0 mM racemic-$[Cr(en)_3]Cl_3$ in 1 x 10^{-3} M $HClO_4$ at increasing photolysis times.

Conditions: buffer: 50 mM d-tartrate, pH 4.06; applied voltage: 12 kV; detection wavelength: 220 nm

4.4.3 Photolysis of $Cr(sen)^{3+}$

The product peaks observed for the photolysis of *rac*-$[Cr(sen)](ClO_4)_3$ and Λ-$[Cr(sen)]Br_3$ were virtually identical in appearance as shown in Figures 4.6 and 4.7. The electrophoresis buffers were 50 mM *d*-tartrate buffers containing 4.0 mM DETA and adjusted to pH 5.0 with Tris base. The samples were electrophoresed with an applied voltage of 10 kV and a detector wavelength of 210 nm.

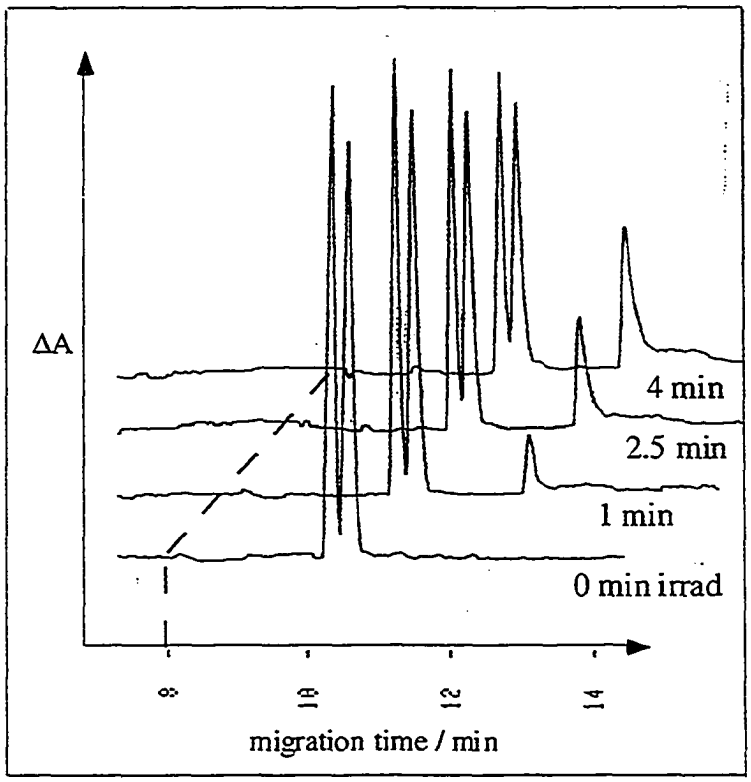

Figure 4.6 Electropherograms obtained for the photolysis of 5.0 mM *rac*-$[Cr(sen)](ClO_4)_3$ in 1 x 10^{-3} M $HClO_4$ at increasing photolysis times.

Conditions: buffer: 50 mM d-tartrate, pH 5.0; applied voltage: 10 kV;
detection wavelength: 210 nm

Figure 4.6 shows that baseline separation was not obtained for the Λ- and Δ-$Cr(sen)^{3+}$ enantiomers although the two were still clearly distinguishable, migrating at 10.3 and 10.5 minutes respectively. Photolysis of *rac*-$[Cr(sen)](ClO_4)_3$ resulted in two product peaks, a sharp peak at 12.2 minutes and a broad peak at 13 minutes.

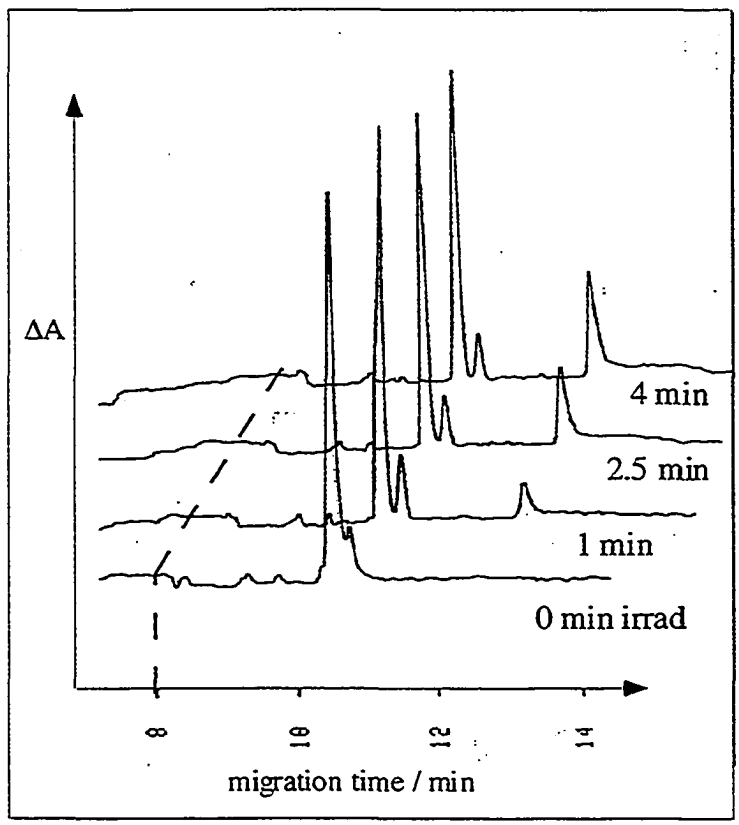

Figure 4.7 Electropherograms obtained for the photolysis of 5.0 mM Λ-$[Cr(sen)]Br_3$ in 1 x 10^{-3} M $HClO_4$ at increasing photolysis times.
Conditions: buffer: 50 mM d-tartrate, pH 5.0; applied voltage: 10 kV;
detection wavelength: 210 nm

The electropherograms obtained for Λ-[Cr(sen)]Br_3 show that a small amount of the Δ- isomer was present. Although appearing at slightly longer migration times, the same peak pattern is observed for the photolysis of Λ-[Cr(sen)]Br_3 as for *rac*-[Cr(sen)]$(ClO_4)_3$. The two $Cr(sen)^{3+}$ enantiomers appear at 10.5 and 10.8 minutes with a sharp photoproduct peak growing in at 12.4 minutes and a broad peak at 13.3 minutes.

The fact that the same sharp photoproduct peak is observed for *rac*-[Cr(sen)]$(ClO_4)_3$ and Λ-[Cr(sen)]Br_3 suggests that both photoaquate to give the same major product. Based on the predictions of VC theory this is identified as *trans*-Cr(sen-NH)$(OH_2)^{4+}$. Three possibilities can then be presented for the broad peak: i) splitting of the *trans*-Cr(sen-NH)$(OH_2)^{4+}$ peak, ii) unresolved Λ- & Δ-*cis*-Cr(sen-NH)$(OH_2)^{4+}$ and iii) a photoproduct resulting from secondary amine loss. These possibilities are discussed in more detail in section 4.5.4.

4.4.4 Thermolysis of $Cr(sen)^{3+}$

As stated in section 4.3.2, it was necessary to reflux the [Cr(sen)]$(ClO_4)_3$ solutions in order to observe any changes in chemical composition. The electropherograms obtained for the thermolysis of both *rac*- and Λ-[Cr(sen)]$(ClO_4)_3$ are presented in Figures 4.8 and 4.9 respectively. The same CE conditions were used as in the photolysis studies.

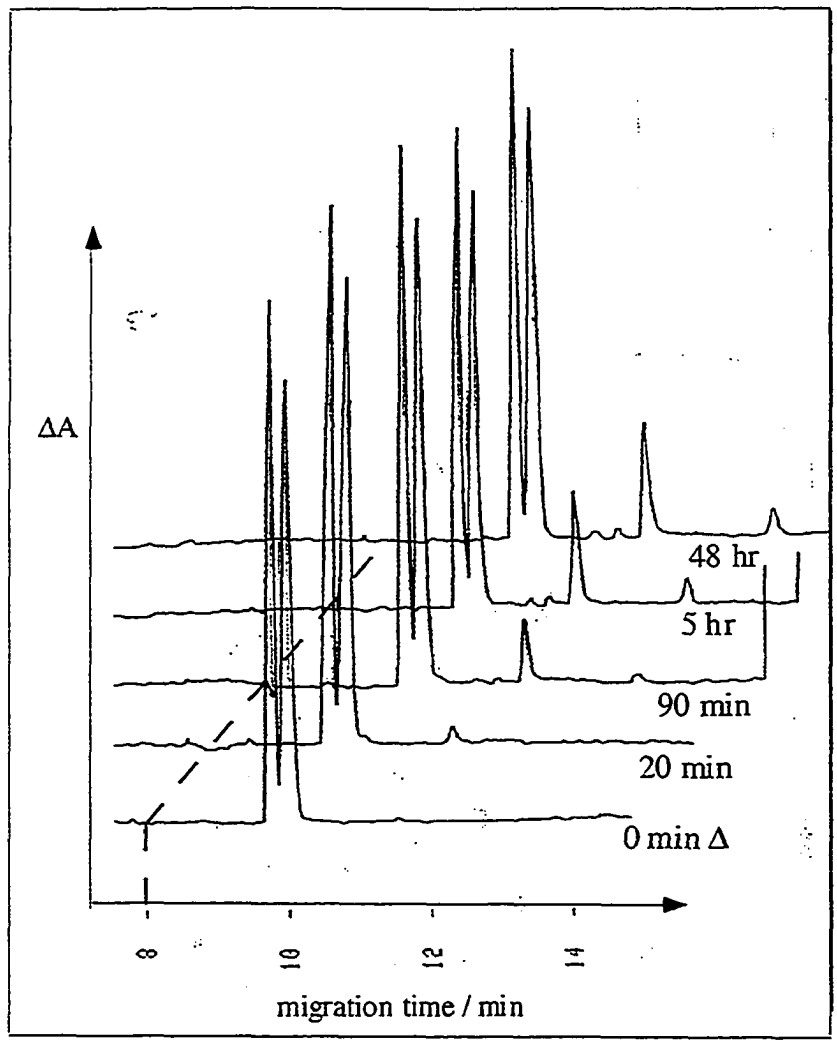

Figure 4.8 Electropherograms obtained for the thermolysis of 5.0 mM *rac*-[Cr(sen)]$(ClO_4)_3$ in 1 x 10^{-3} M $HClO_4$ at increasing thermolysis times.

Conditions: buffer: 50 mM d-tartrate, pH 5.0; applied voltage: 10 kV; detection wavelength: 210 nm

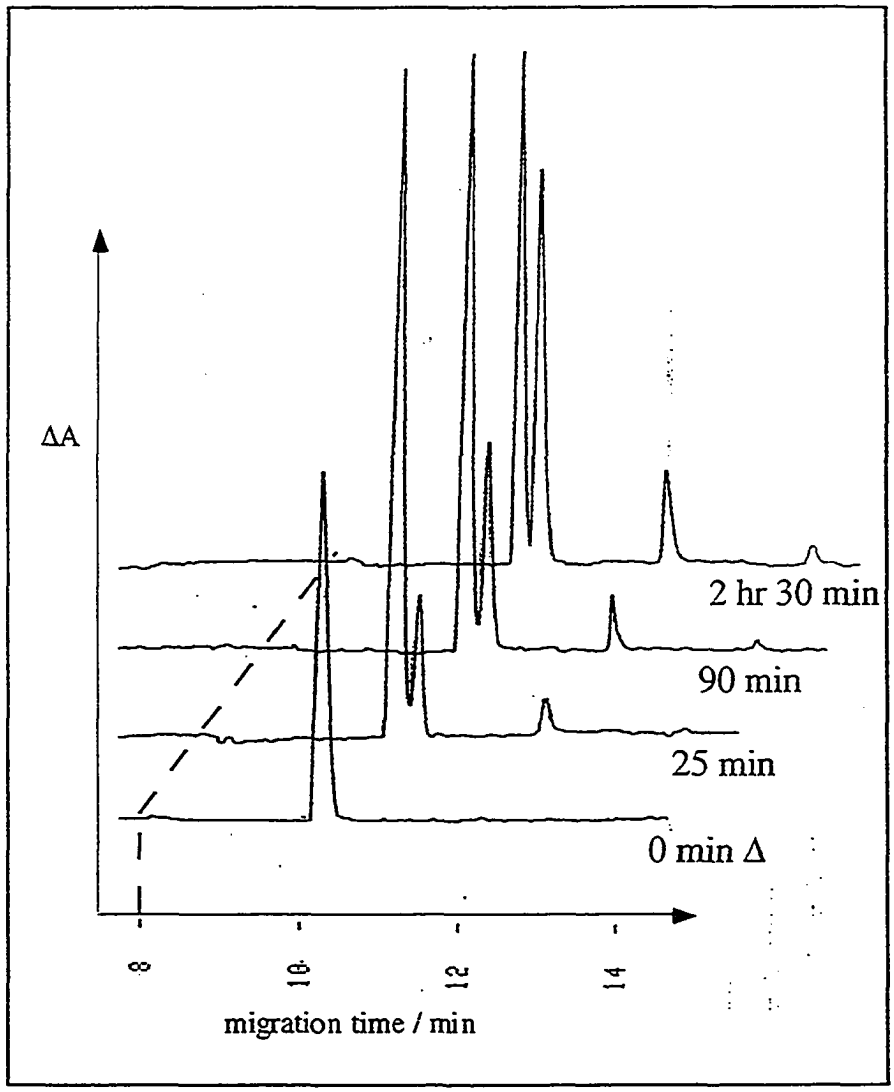

Figure 4.9 Electropherograms obtained for the thermolysis of 5.0 mM Λ-[Cr(sen)]$(ClO_4)_3$ in 1 x 10^{-3} M $HClO_4$ at increasing thermolysis times. Conditions: buffer: 50 mM d-tartrate, pH 5.0; applied voltage: 10 kV; detection wavelength: 210 nm

The thermolysis of both *rac*- and Λ-[Cr(sen)]$(ClO_4)_3$ showed the same major product observed in the photolysis experiments. As detailed in section 4.4.3

this is presumed to be *trans*-Cr(sen-NH)$(OH_2)^{4+}$. No evidence of the broad peak observed in the photolysis experiments was found in the thermolysis experiments. A small, sharper, peak did grow in at 14 minutes and this is attributed to thermal loss of a second amine and formation of Cr(sen-$(NH)_2)(OH_2)_2^{5+}$.

The starting material and photoproduct migration times obtained in the thermolysis of *rac*-[Cr(sen)]$(ClO_4)_3$ were initially shorter than those obtained in the other experiments. Initially Λ- and Δ-$Cr(sen)^{3+}$ migrated at 9.8 and 10.0 minutes and the photoproduct at 11.5 minutes. As the experiment proceeded, migration times became progressively longer with times similar to those observed in other experiments being obtained after 48 hours. This indicates that instrumental factors and/or capillary conditioning were causing the shorter migration times initially observed in this experiment.

An interesting result in the thermolysis of Λ-[Cr(sen)]$(ClO_4)_3$ was that Δ-[Cr(sen)]$(ClO_4)_3$ grew in as the thermolysis progressed. Racemization was efficient with a racemic mixture resulting after about 2.5 hours of refluxing.

Although the results presented in Figure 4.8 show a maximum thermolysis time of 48 hours for *rac*-[Cr(sen)]$(ClO_4)_3$, both solutions were continuously refluxed for a week. The electropherograms obtained after this time showed no further change in composition to those obtained for *rac*-[Cr(sen)]$(ClO_4)_3$ after 48 hours. This indicated that a stable solution composition had been reached and also demonstrates the remarkable resistance of $Cr(sen)^{3+}$ to hydrolysis in acidic solution.

4.5 Discussion

4.5.1 Effect of Electroosmotic Flow and pH on Ion Migration

The calculated μ_{os} values listed in Table 4.2 show the expected trend with pH as electroosmotic mobility increases with pH in the absence of DETA. At both pH 4.5 and 5.5 the addition of 3.75 mM DETA resulted in a 65 - 70% decrease in the electrophoretic mobility. This indicates that the addition of 3.75 mM DETA reduces the extent of electroosmotic flow but does not eliminate it.

Tartaric acid is diprotic with $pK_{a1} = 2.93$ and $pK_{a2} = 4.24$. Therefore as the buffer pH increases from 3.5 to 5.5 the amount of $tart^{2-}$ present in solution increases. Assuming that $Cr(en)_3^{3+}$ has a larger K_{IP} with $tart^{2-}$ than with $tartH^-$, longer migration times would be expected for this species at pH 5.5. This was not observed experimentally as the shortest migration time of 7.65 minutes was obtained for $Cr(en)_3^{3+}$ at pH 5.5 in the absence of DETA. The migration times observed at pH 3.5 and 4.5 were 8.10 and 9.45 minutes respectively.

The calculated electrophoretic mobilities show that this was not the result of greater electroosmotic flow at pH 5.5 as the calculated μ_{app} was greatest for $Cr(en)_3^{3+}$ at pH 5.5. The value calculated at pH 5.5 was 3.3×10^{-8} m^2 s^{-1} V^{-1}, contrasting with the values of 3.1×10^{-8} m^2 s^{-1} V^{-1} and 2.7×10^{-8} m^2 s^{-1} V^{-1} calculated at pH 3.5 and pH 4.5 respectively. Although seemingly implausible based on electrostatics, a possible explanation is that $Cr(en)_3^{3+}$ has a greater association with $tartH^-$ than with $tart^{2-}$.

It had been predicted that increasing the solution pH would result in longer migration times for *cis* -$Cr(en)_2(enH)(OH_2)^{4+}$ and *trans* -$Cr(en)_2(enH)(OH_2)^{4+}$ based on their acid-base equilibria. With a pKa of 4.4[111] the majority of these ions

exist as their 3^+ forms, *cis* -$Cr(en)_2(enH)(OH)^{3+}$ and *trans* -$Cr(en)_2(enH)(OH)^{3+}$ at pH > 4.4. Due to the decrease in ionic charge, the longest migration times and smallest mobilities are therefore expected at pH 5.5. The opposite was observed experimentally, indicating that ionic charge is not the dominant factor in the mobilities of these ions.

4.5.2 Photolysis of $Cr(en)_3^{3+}$

Our results confirmed the findings of Cimolino with three photoaquation products being observed in the photolysis of Λ-$[Cr(en)_3]Cl_3$. The ratio of Λ-*cis*-$Cr(en)_2(enH)(OH_2)^{4+}$ to Δ-*cis*-$Cr(en)_2(enH)(OH_2)^{4+}$ in our results is approximately 4 to 1, in excellent agreement with the 4 to 1 ratio obtained by Cimolino. However the 2.3 to 1 ratio of *trans*-$Cr(en)_2(enH)(OH_2)^{4+}$ to Λ-*cis*-$Cr(en)_2(enH)(OH_2)^{4+}$ obtained by Cimolino was not reproduced in our work. This ratio was estimated at 1 to 1.33 based on relative peak heights. However this is only a meaningful comparison if *cis*-$Cr(en)_2(enH)(OH_2)^{4+}$ and *trans*-$Cr(en)_2(enH)(OH_2)^{4+}$ have the same molar absorptivity at this wavelength. Our ratio of *trans*- to *cis*-$Cr(en)_2(enH)(OH_2)^{4+}$ is smaller than Cimolino's, indicating that the trans isomer has a smaller molar absorptivity than the cis isomers at 220 nm.

The $Cr(en)_3^{3+}$ complexes used in these studies were chloride salts which introduces the possibility of photoanation occurring in competition with photoaquation. The presence of a fourth peak in our results is consistent with photoanation by chloride to give *trans*-$Cr(en)_2(enH)Cl^{3+}$.

4.5.3 Photolysis of $Cr(sen)^{3+}$

As discussed in section 4.1, the VC model predicts a single photoproduct, *trans*-$Cr(sen\text{-}NH)(OH_2)^{4+}$. Based on this, the peak observed at 12.2 minutes in the photolysis of *rac*- & Λ-$Cr(sen)^{3+}$ was identified as *trans*-$Cr(sen\text{-}NH)(OH_2)^{4+}$. Three possibilities were presented in section 4.4.3 for the broad peak: i) splitting of the *trans*-$Cr(sen\text{-}NH)(OH_2)^{4+}$ peak, ii) unresolved Λ-& Δ-$Cr(sen\text{-}NH)(OH_2)^{4+}$, or iii) a product resulting from loss of a secondary amine.

Possibilities i) and ii) are not favoured based upon the thermolysis results presented in section 4.4.4. The electropherograms obtained in the thermolysis experiments showed the same major peak that was obtained photochemically. However no broad peak was observed in the thermolysis experiments even when a comparable amount of the major peak was present and the samples were electrophoresed under the same conditions. This precludes the broad peak being the result of peak splitting of the major peak.

As stated in section 4.1, thermal reactions are stereoretentive, so peaks resulting from the *cis*-$Cr(sen\text{-}NH)(OH_2)^{4+}$ enantiomers would be expected in the thermolysis electropherograms. Some evidence of these were found in two very small peaks occurring at 11.2 and 11.5 minutes in the electropherograms obtained after 7 and 48 hours refluxing of *rac*-$Cr(sen)^{3+}$. These are tentatively identified as resulting from the cis isomers as this is the same migration order observed for the *cis*- & *trans*- $Cr(en)_2(en\text{-}H)(OH_2)^{4+}$ photoproducts under similar conditions. Based on this, the peaks at 11.2 and 11.5 minutes are identified as Δ-*cis*-$Cr(sen\text{-}NH)(OH_2)^{4+}$ & Λ-*cis*-$Cr(sen\text{-}NH)(OH_2)^{4+}$ respectively.

If the peaks at 11.2 and 11.5 are due to Δ- & Λ-*cis*-$Cr(sen\text{-}NH)(OH_2)^{4+}$ this precludes the broad peak observed in the photolysis experiments from being unresolved Λ- & Δ- *cis*-photoproducts. Another argument against this being

unresolved Λ- & Δ- *cis*-Cr(sen-NH)$(OH_2)^{4+}$ is that it would be expected to also occur in the thermolysis experiments.

The above reasons eliminate possibilties i) and ii) and therefore support possibility iii), that the broad peak results from a product formed via loss of a secondary amine.

Loss of a secondary amine is consistent with a trans attack edge displacement mechanism if the attack of the solvent results in the primary amine on the same arm of the labilized amine migrating to the vacated site. Such a mechanism is consistent with Kirk and Heyd's[63] proposal that photolysis of *cis*-Cr(cyclam)$(en)^{3+}$ occurs with labilization of an ethylenediamine amine and migration of the second en amine to the site vacated by the first. The proposed mechanism for photoaquation with loss of a secondary amine in $Cr(sen)^{3+}$ is illustrated in Figure 4.10.

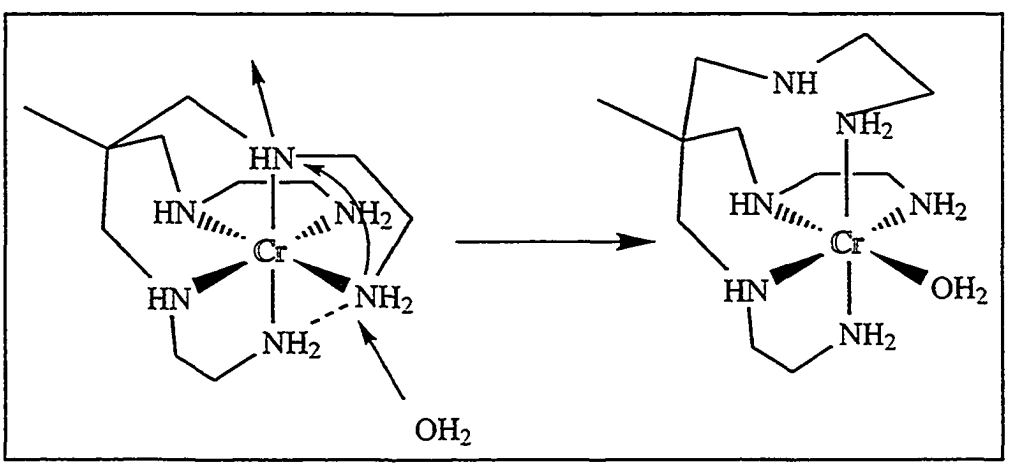

Figure 4.10 Possible mechanism for secondary amine loss in the photoaquation of $Cr(sen)^{3+}$

The effect of different electrophoresis conditions on the migration times of the photoproduct peaks of $Cr(sen)^{3+}$ is shown in Figure 4.11.

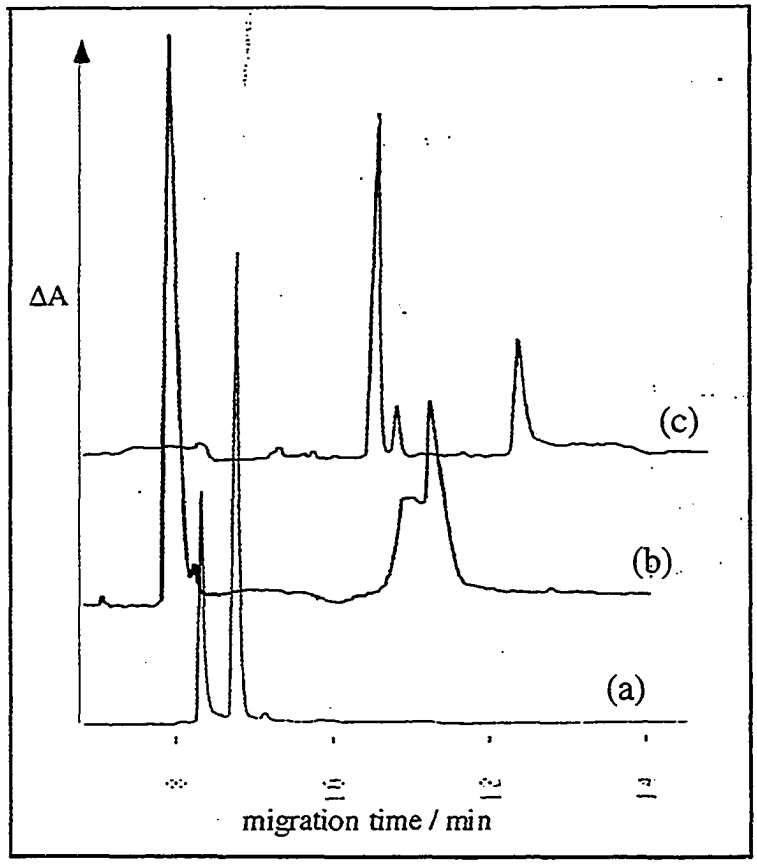

Figure 4.11 Electropherograms obtained for the photolysis of 5.0 mM Λ-$[Cr(sen)](ClO_4)_3$ in 1 x 10^{-3} M $HClO_4$.

Conditions: a) buffer: 50 mM d-tartrate, pH 6.0 (TRIS); applied voltage: 11 kV; detection wavelength: 210 nm; photolysis time: 4.5 min

b) buffer: 50 mM d-tartrate, pH 4.06 (NaOH); applied voltage: 11 kV; detection wavelength: 210 nm; photolysis time: 3 min

c) buffer: 50 mM d-tartrate, pH 5.0 (TRIS); applied voltage: 10 kV; detection wavelength: 210 nm; photolysis time: 4 min

The results presented in Figure 4.11 (c) are the same as those shown in Figure 4.7 for 5.0 mM Λ-[Cr(sen)]$(ClO_4)_3$ after 4 minutes photolysis. At pH 4.06, adjusted using NaOH, the broad peak is better resolved than at pH 5.0 and migrates before *trans*-Cr(sen-NH)$(OH_2)^{4+}$ as shown in (b). A single photoproduct peak is observed at pH 6.0 (c) which migrates before the starting material. It is possible that the two product peaks are coincident at this pH, or alternatively, that the second peak is coincident with the starting material. These results show the migration order of the two photoproduct peaks changing relative to each other at different pH conditions. This is consistent with two aquated products having different pKa values.

Our results do not support photoracemization occuring in the photolysis of Λ-[Cr(sen)]Br_3. The small peak due to residual Δ-Cr$(sen)^{3+}$ observed in the photolysis of Λ-[Cr(sen)]Br_3 did not increase with photolysis, indicating that photoracemization is a very minor process, if it occurs at all.

4.5.4 Thermolysis of Cr$(sen)^{3+}$

The fact that the thermolysis reactions reach an equilibrium indicates that all processes occurring in solution are reversible. Possible pathways for the efficient racemization of Λ-Cr$(sen)^{3+}$ are shown in Figure 4.12. Although evidence for a Cr(sen-$(NH)_2)(OH_2)_2^{5+}$ species was observed experimentally, this was a minor product and possible pathways for its formation are not included in Figure 4.12.

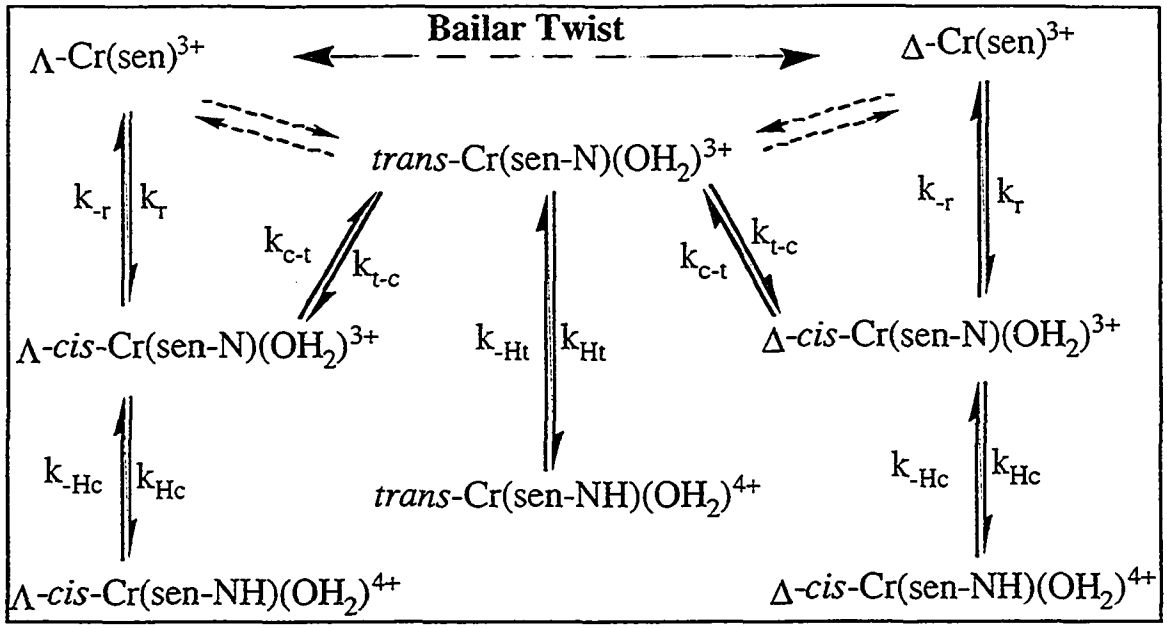

Figure 4.12 Proposed mechanism for thermolysis of $Cr(sen)^{3+}$

The key experimental observations in the thermolysis of Λ-$Cr(sen)^{3+}$ are;

i) efficient racemization occurs i.e. Λ-$Cr(sen)^{3+}$ --> Δ-$Cr(sen)^{3+}$,

ii) a significant amount of *trans* -$Cr(sen\text{-}NH)(OH_2)^{4+}$ is present at equilibrium,

iii) Λ- & Δ-*cis* -$Cr(sen\text{-}NH)(OH_2)^{4+}$ are only observed in small amounts after extensive refluxing.

The proposed mechanisms for racemization of Cr(III) trisbidentate complexes were introduced in section 1.11 and are illustrated in Figure 1.10. These proposed mechanisms involve either: bond cleavage and recoordination of the ligand, or twist mechanisms, Bailar or Ray-Dutt twists.

The experimental observation that large amounts of *trans*-$Cr(sen\text{-}NH)(OH_2)^{4+}$ are present in the equilibrium solution shows that bond cleavage is definitely occurring. Whilst this supports racemization occurring via bond cleavage

and recoordination, it does not preclude the possibility of a twist mechanism operating in concert with bond cleavage to produce Δ-Cr(sen)$^{3+}$.

Formation of *trans*-Cr(sen-NH)$(OH_2)^{4+}$ has to result from protonation of *trans*-Cr(sen-N)$(OH_2)^{3+}$, which is also the central intermediate for racemization via bond rupture. Two possible pathways for the formation of this species are shown in Figure 4.12.

The first is shown in bold arrows and is consistent with the stereoretentive nature of Cr(III) thermal reactions. Starting with Λ-Cr(sen)$^{3+}$, bond rupture of a Cr-primary amine bond results in Λ-*cis*-Cr(sen-N)$(OH_2)^{3+}$. This species can undergo three processes; protonation of the amine to give Λ-*cis*-Cr(sen-NH)$(OH_2)^{4+}$, recoordination to displace water and return to Λ-Cr(sen)$^{3+}$, or recoordination to displace a primary amine forming *trans*-Cr(sen-N)$(OH_2)^{3+}$.

Trans-Cr(sen-N)$(OH_2)^{3+}$ can either protonate to give the observed *trans*-Cr(sen-NH)$(OH_2)^{4+}$, or recoordinate to give Λ- or Δ-*cis* -Cr(sen-N)$(OH_2)^{3+}$. The analogous processes are available to Δ-*cis* -Cr(sen-N)$(OH_2)^{3+}$.

Only small amounts of *cis* -Cr(sen-NH)$(OH_2)^{4+}$ isomers are observed experimentally. This can only be consistent with the above mechanism if protonation of *cis* -Cr(sen-N)$(OH_2)^{3+}$ is significantly slower than the recoordination processes available to this species. However, observation of significant amounts of *trans* -Cr(sen-NH)$(OH_2)^{4+}$ indicates that protonation of *trans* -Cr(sen-N)$(OH_2)^{3+}$ is competitive with trans -> cis recoordination. Two explanations can be presented for these observations;

i) assuming that protonation of the cis and trans intermediates occurs with a similar rate, then cis -> trans recoordination is faster than trans -> cis i.e. $k_{c\text{-}t} > k_{t\text{-}c}$.

ii) assuming that $k_{c\text{-}t} \approx k_{t\text{-}c}$, then protonation of the amine in the trans intermediate is faster than in the cis intermediates i.e. $k_{Ht} > k_{Hc}$.

A possible reason for either i) or ii) is that intramolecular H-bonding within one of the isomers is greater than for the other, resulting in a more stable arrangement and hindering either slower recoordination or protonation. Molecular modelling of the cis and trans intermediates may provide more insight into this matter.

Although we favour the above mechanism for formation of *trans*-Cr(sen-N)$(OH_2)^{3+}$, a second mechanism is shown with dotted arrows. This shows bond cleavage of $Cr(sen)^{3+}$ occurring with stereochemical change, forming *trans* -Cr(sen-N)$(OH_2)^{3+}$ directly. The reason for the dotted mechanism being disfavoured is that it conflicts with the stereoretentive nature of Cr(III) thermal reactions. However it is consistent with only small amounts of *cis* -Cr(sen-NH)$(OH_2)^{4+}$ being observed and can not be discounted on the basis of our experimental results.

4.6 Reinterpretation of Mackay's Results

Our photolysis results for $Cr(sen)^{3+}$ indicate two products are formed, *trans*-Cr(sen-NH)$(OH_2)^{4+}$ and a product resulting from loss of a secondary amine. This contrasts with Mackay who concluded that four photoproducts were present, based on the assumption that thermolysis of $Cr(sen)^{3+}$ results in exclusive formation of the *cis*-Cr(sen-NH)$(OH_2)^{4+}$ enantiomers. However our results indicate that this is not the case with the thermal product actually being *trans*-Cr(sen-NH)$(OH_2)^{4+}$. Based on this, and other findings in this work, a reinterpretation of Mackay's results show them to be consistent with ours. Typical thermolysis and photolysis HPLC chromatograms obtained in Mackay's work are reproduced with his permission in Figure 4.13.

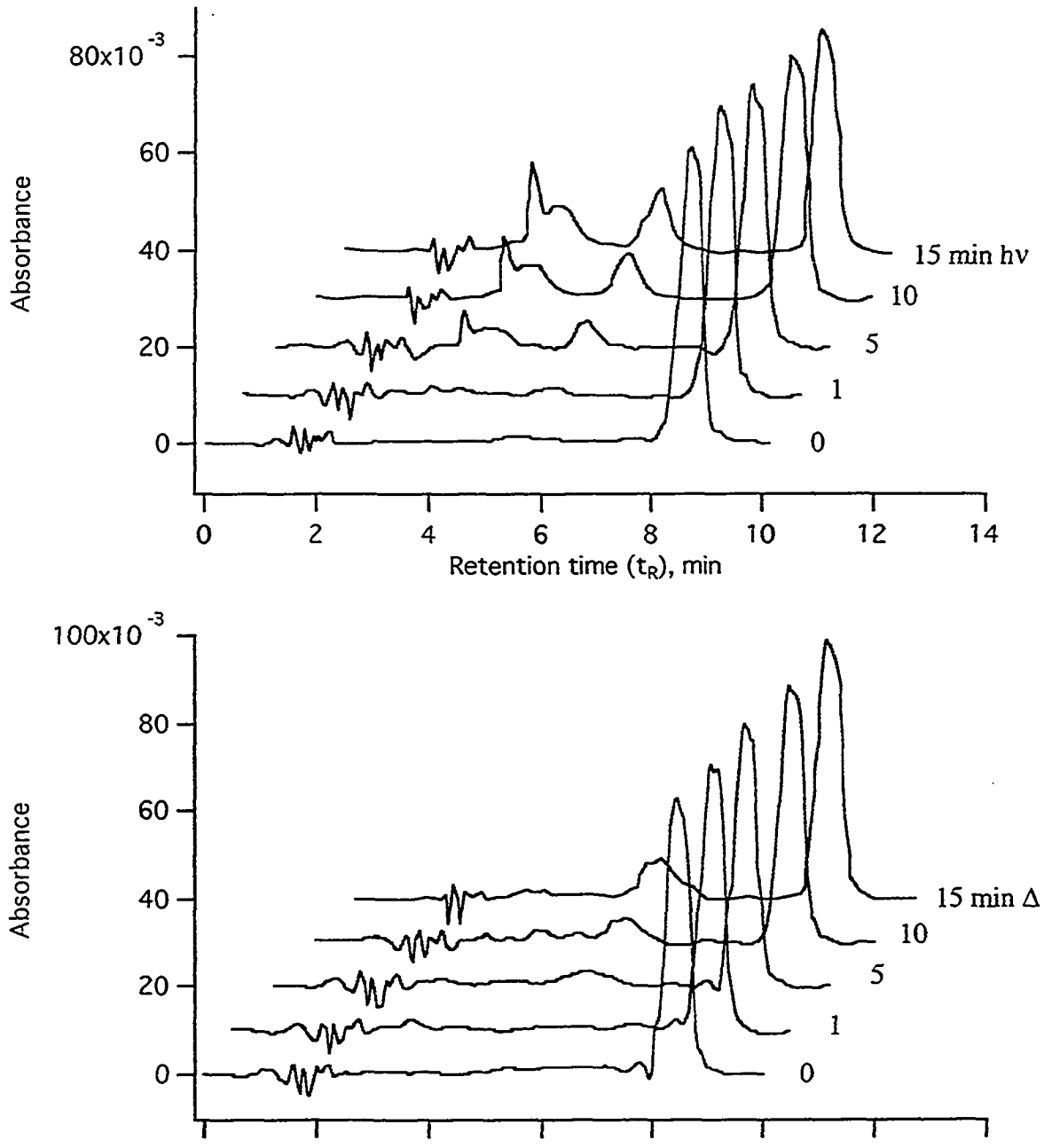

Figure 4.13 Chromatograms obtained in the photolysis (upper) and thermolysis (lower) of Λ-[Cr(sen)]Cl_3, 2 x 10^{-2} M in 0.01M $HClO_4$. Conditions: eluent; 25mM butanesulfonate, 25 mM triethylamine, 25mM *d*-tartaric acid in 7.5% MeOH, pH 3.6. Flow rate; 1.5 mL min-1 detection wavelength; 250 nm.

As shown in Figure 4.13, the thermolysis and photolysis chromatograms display a common peak at approximately 5.6 minutes which is also observed in the chromatograms obtained for the racemic complex. Based on the assumption that $Cr(sen)^{3+}$ would undergo stereoretentive thermolysis, Mackay assigned this peak to unresolved Λ- and Δ-*cis* -$Cr(sen\text{-}N)(OH_2)^{3+}$. The two peaks occuring at 3.4 and 3.9 minutes were therefore assigned to *trans*-$Cr(sen\text{-}NH)(OH_2)^{4+}$ and a product presumed to result from loss of a secondary amine.

Our results indicate that *trans*-$Cr(sen\text{-}NH)(OH_2)^{4+}$ is the major product in both the thermal and photochemical aquations. Based on this, the peak observed at 5.6 minutes in Figure 4.13 is assigned by us as *trans*-$Cr(sen\text{-}NH)(OH_2)^{4+}$. The peak at either 3.4 or 3.9 minutes is assigned as the secondary amine loss product, leaving a third peak unassigned. This indicates that three photoproducts rather than four as concluded by the author are present in Mackay's HPLC chromatograms.

The Fuoss equation indicates that substantial ion-pairing occurs in solution between $Cr(sen)^{3+}$ and counterions with $K_{IP} \approx 6$. The chloride salts of $Cr(sen)^{3+}$ were used in Mackay's experiments, suggesting the possibility of photoanation. This was supported by results obtained by us in the photolysis of $[Cr(sen)](ClO_4)_3$ samples which had only been recrystallized once from $[Cr(sen)]Cl_3$. A third peak was observed for these samples, consistent with photoanation by residual chloride.

The possibility of photanation was investigated further by photolyzing Λ-$[Cr(sen)](ClO_4)_3$ in the presence of 27 mM NaCl. The results obtained in this study are shown in Figure 4.14.

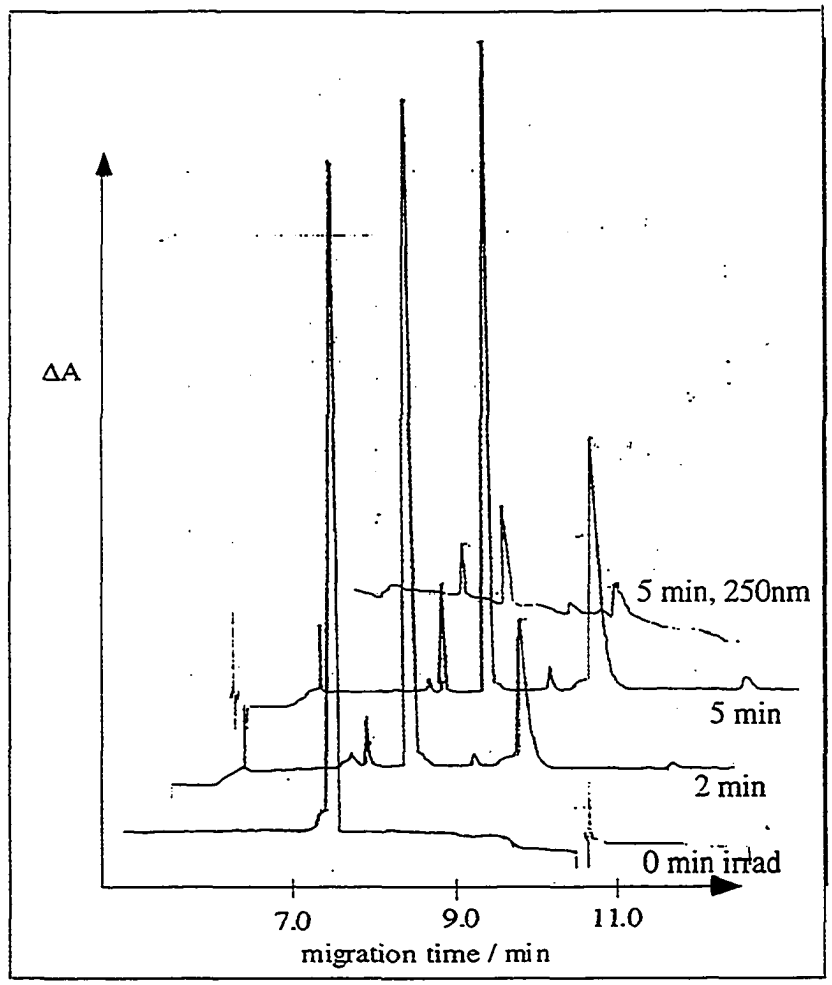

Figure 4.14 Electropherograms obtained for the photolysis of 5.0 mM Λ-$[Cr(sen)](ClO_4)_3$ + 27 mM NaCl in 1 x 10^{-3} M $HClO_4$.
Conditions: buffer: 50 mM d-tartrate, pH 4.10; applied voltage: 12 kV; detection wavelength: 210 nm

As shown in Figure 4.14, photolysis of $Cr(sen)^{3+}$ in the presence of chloride generates a new peak that migrated before the starting material at 6.8 minutes. Presumably this results from photoanation and can be identified as *trans*-$Cr(sen\text{-}NH)Cl^{3+}$. The broad peak observed in Figure 4.11, attributed to loss of a secondary amine, does not migrate after the major *trans*-$Cr(sen\text{-}NH)(OH_2)^{4+}$ under

these conditions. This is somewhat surprising as the conditions are very similar to those which produced Figure 4.11. However a shoulder is observed preceding the *trans*-Cr(sen-NH)$(OH_2)^{4+}$ peak in Figure 4.14, suggesting that the two peaks are coincident, with the broad peak underlying that of *trans*-Cr(sen-NH)$(OH_2)^{4+}$.

The HPLC buffers used in Mackay's work are highly absorbing below 240 nm and require a detection wavelength of 250 nm. Our results indicate that this is an inappropriate wavelength for these studies as it enhances the apparent contribution of anation over photoaquation. As evidence, the final trace in Figure 4.14 displays an electropherogram obtained for the solution photolyzed for 5 minutes with a detector wavelength of 250 nm instead of 210nm. All peaks decreased dramatically in size at this detection wavelength; the recorder sensitivity was 20 mV full scale deflection for the original electropherograms and 5 mV full scale deflection for detection at 250 nm. However, the shift to 250 nm detection also resulted in the peak area of the photoanation product increasing relative to that of the starting material and photoaquation peaks and is consistent with the anation product having the larger molar absorptivity at this wavelength.

4.7 Conclusions

The thermal and photoaquation reactions of $Cr(sen)^{3+}$ have been investigated using capillary electrophoresis. Only two product peaks are observed in the photolysis experiments of *rac*- & Λ-[Cr(sen)]$(ClO_4)_3$, consistent with the formation of *trans* -Cr(sen-NH)$(OH_2)^{4+}$ and a second product resulting from loss of a secondary amine. No *cis* -Cr(sen-NH)$(OH_2)^{4+}$ is formed. The results obtained by

Mackay using HPLC are also consistent with two photoaquation products with the third peak found being a chloride photoanation product, *trans* -Cr(sen-NH)Cl^{3+}.

The short doublet lifetime of $Cr(sen)^{3+}$ has been attributed by Endicott to the ligand strain facilitating distortion towards a trigonal prismatic structure which can return to the ground state or react to give the observed photoproducts. Our photolysis results indicate that *trans* -Cr(sen-NH)$(OH_2)^{4+}$ is the major photoproduct, consistent with the predictions of VC theory and reaction occuring from the $^4T_2$ state. This therefore supports deactivation of the doublet state via BISC and suggests that the trigonal strain imposed by the sen ligand assists back intersystem crossing to the quartet state rather than formation of a trigonal prismatic intermediate.

The AOM normally predicts that secondary amines will be labilized preferentially to primary amines due to their greater ligand field strength. However in the case of $Cr(sen)^{3+}$, the distortion imposed by the neopentyl cap of the sen ligand reduces the effective field strength of the secondary sen amines and results in the primary amines being preferentially labilized. Our experimental results indicate that a minor mode involving loss of a secondary amine is operating and involves migration of the primary amine on the same arm as the labilized secondary amine. This secondary amine loss product is observed photochemically but not thermally.

Thermolysis of Λ-$Cr(sen)^{3+}$ at 100 °C results in the formation of *trans* -Cr(sen-NH)$(OH_2)^{4+}$ and efficient racemization to Δ-$Cr(sen)^{3+}$. Although the presence of significant amounts of *trans* -Cr(sen-NH)$(OH_2)^{4+}$ supports racemization occurring via bond cleavage and recoordination it does not preclude a contribution to racemization via a Bailar twist. Since thermal reactions are stereoretentive Λ- & Δ-*cis* -Cr(sen-NH)$(OH_2)^{4+}$ enantiomers were expected as thermolysis products. The absence of major amounts of these indicates that either the *cis* -Cr(sen-NH)$(OH_2)^{4+}$ isomers are less stable than *trans* -Cr(sen-NH)$(OH_2)^{4+}$ or that protonation of the *cis* -Cr(sen-N)$(OH_2)^{3+}$ intermediates is significantly slower than protonation of *trans*

-Cr(sen-N)$(OH_2)^{3+}$. A detailed kinetic analysis of the racemization of Λ-Cr(sen)$^{3+}$ warrants investigation.

CHAPTER FIVE

CONCLUDING REMARKS AND FUTURE DIRECTIONS

The work has investigated the photoaquation mechanisms of Cr(III) am(m)ine complexes and has provided some new insights. Like most studies however it has, in the act of probing one problem, generated new questions and provided new challenges and goals.

This study has revealed a mechanistic feature of Cr(III) am(m)ine photoreactions that has often been overlooked; that initial photoproducts may not be thermally stable and are intermediate species, further complicating the observed photochemistry. In our work using conductivity detection this was most evident for *cis*-Cr(cyclam)$(NH_3)_2^{3+}$, but also observed for $Cr(en)_3^{3+}$, $Cr(tn)_3^{3+}$ and $Cr(sen)^{3+}$.

Our conductivity based results for *cis*-Cr(cyclam)$(NH_3)_2^{3+}$ indicate that 67% of the photolysis occurs via loss and recoordination of a cyclam amine, displacing an ammonia ligand. This is a significant result as it dispels a popular belief that secondary amines are too constrained to participate in Cr(III) photoreactions. This may be true in the sense that the secondary amines are unable to migrate to a site vacated by another ligand which is labilized. However, it does not preclude the secondary amine being labilized and a more mobile ligand migrating to the vacated site as we have proposed for *cis*-Cr(cyclam)$(NH_3)_2^{3+}$. In the case of *cis*-Cr(cyclam)$(NH_3)_2^{3+}$, the labilized cyclam amine recoordinates, displacing the ammonia which migrated to the vacant site. However for other macrocyclic complexes the secondary amine may remain detached and a search for such a species is worth pursuing, as it would provide conclusive evidence for a ring nitrogen loss mechanism.

Our conductivity based results for other *cis*-Cr(cyclam)X_2^{n+} complexes did not support photoaquation via loss and recoordination of a cyclam amine. However studies of $Cr(sen)^{3+}$, using CE analysis of the photoproducts, and *trans*-Cr(tet)$(CN)_2^{+}$ using conductivity detection, have provided evidence for loss of a

secondary amine, which in the case of *trans*-$Cr(tet)(CN)_2^+$ recoordinates to displace a primary amine of the same ligand.

We have identified complexes which may photoaquate via a similar ring loss mode to *cis*-$Cr(cyclam)(NH_3)_2^{3+}$, but will result in stable ring nitrogen loss products. The attempted syntheses of *cis*-$Cr(cycb)(NH_3)_2^{3+}$ and $Cr(15aneN5)Cl^{2+}$ gave products which contained detached macrocyclic amines. Successful synthesis of these complexes would be a good starting point in a search for ring amine loss intermediates as the photoproducts generated by loss of a ring amine in these complexes may be stable.

The synthesis of $Cr(15aneN5)(NH_3)^{3+}$ is of particular interest as photochemistry occuring with "stereochemical change" is only possible for this complex via ring loss and recoordination, or at least via ring loss if the photoproduct formed is thermally stable.

Our investigation into the thermolysis and photolysis of $Cr(sen)^{3+}$ using capillary electrophoresis has shown this technique to be highly suited to the separation of Cr(III) complexes, including the resolution of enantiomeric complexes. The results presented in this work have shown that changing pH and buffer conditions, e.g. presence of DETA, concentration of buffer, use of TRIS base to adjust pH, has notable effects on the observed migration times and migration order of Cr(III) complexes. Due to its ease of use, and the fact that successful analysis requires nanograms of analyte this technique is likely to become highly favoured in future kinetic and characterization studies of metal complexes. The potential exists for an analytical project to investigate further the effect of buffer conditions and pH on migration times so that optimum conditions, i.e fast migration times with baseline resolution, can be attained for Cr(III) and other transition metal complexes.

Our studies have confirmed that conductivity detection is highly suited to the study of Cr(III) photoreactions, particularly as it has provided new mechanistic

insights. However, as our results for $Cr(CN)_6^{3-}$ have shown, there are a number of gray areas regarding our use of this technique which need to be addressed. Is our current cell design the most sensitive and, if not, how can it be improved? Is our derived equation predicting signal magnitudes valid, particularly with respect to the assumption that it is H_3O^+ which exclusively protonates the labilized base, giving the observed conductivity changes? These matters deserve further investigation otherwise the technique remains somewhat of a "black box".

The thermolysis studies of $Cr(sen)^{3+}$ have revealed that highly efficient racemization occurs in acidic solution. This warrants further kinetic studies and some investigation into why the cis-$Cr(sen\text{-}NH)(OH_2)^{3+}$ enantiomers are not observed. The analogous ligand stn, where the ligand has 1,3 diamino arms instead of ethylenediamine arms as in sen, has been prepared although not reported in this thesis. Comparisons of $Cr(en)_x(NH_3)_{(6-2x)}^{3+}$ and $Cr(tn)_x(NH_3)_{(6-2x)}^{3+}$ complexes have shown that tn is a poorer leaving ligand than en and ammonia.[85] It would be of interest to see if similar results are found in the photolysis and thermolysis of $Cr(stn)^{3+}$ and also what effect, if any, the longer ligand arms may have on the thermal racemization of the resolved complex.

REFERENCES

(1) Sykora, J.; Sîma, J. *Coord. Chem. Rev.* **1990**, *107*, 1.

(2) Balzani, V.; Carassati, V. *Photochemistry of coordination compounds*; Academic Press London and New York, 1970.

(3) Balzani, V.; Moggi, L. *Coord. Chem. Rev.* **1990**, *97*, 313.

(4) Endicott, J. F.; Ramasami, T.; Tamilarasan, R.; Lessard, R. B.; Ryu, C. K. *Coord. Chem. Rev.* **1987**, *77*, 1.

(5) Wrighton, M. *Chem. Rev.* **1974**, *74*.

(6) Zinato, E. In *Concepts of Inorganic Photochemistry*; Adamson, A. W., Fleischauer, P. D., Eds.; John Wiley & Sons:, 1975.

(7) Kirk, A. D. *Chem. Rev.* **1999**, *99*, 1607.

(8) Kirk, A. D. *Comments Inorg. Chem.* **1992**, *14*, 89.

(9) Kirk, A. D. *J. Chem. Educ.* **1983**, *60*, 843.

(10) Kirk, A. D. *Coord. Chem. Rev.* **1981**, *39*, 225.

(11) Kirk, A. D. *Mol. Photochem.* **1973**, *5*, 127.

(12) Zinato, E. *Coord. Chem. Rev.* **1994**, *129*, 195.

(13) Endicott, J. F.; Perkovic, M. W.; Heeg, M. J.; Ryu, C. K.; Thompson, D. *Coord. Chem. Rev.* **1990**, *97*, 65.

(14) Endicott, J. F.; Lessard, R. B.; Lynch, D.; Perkovic, M. W.; Ryu, C. K. *Adv. Chem. Ser.* **1997**, 199.

(15) Mønsted, L.; Mønsted, O. *Coord. Chem. Rev.* **1989**, *94*, 109.

(16) Fleischauer, P. D.; Adamson, A. W.; Sartori, G. *Progr. Inorg. Chem.* **1972**, *17*, 1.

(17) Kane-Maguire, N. A. P.; Helwic, N.; Derrick, J. M. *Inorg. Chim. Acta* **1985**, *102*, L21.

(18) Kane-Maguire, N. A. P.; Richardson, D. E.; Toney, C. G. *J. Am. Chem. Soc.* **1976**, *98*, 3996.

(19) Kane-Maguire, N. A. P.; Phifer, J. E.; Toney, C. G. *Inorg. Chem.* **1976**, *15*, 593.

(20) Wasgestian, H. F. *J. Phys. Chem.* **1972**, *14*, 1947.

(21) Wegner, E. E.; Adamson, A. W. *J. Am. Chem. Soc.* **1966**, *88*, 394.

(22) Kirk, A. D.; Scandola, M. A. R. *J. Phys. Chem.* **1982**, *86*, 4141.

(23) Endicott, J. F. *Comments Inorg. Chem.* **1985**, *3*, 349.

(24) Lessard, R. B.; Endicott, J. F.; Perkovic, M. W.; Ochymowycz, L. A. *Inorg. Chem.* **1989**, *28*, 2574.

(25) Lessard, R. B.; Heeg, M. J.; Buranda, T.; Perkovic, M. W.; Schwartz, C. L.; Rudong, Y.; Endicott, J. F. *Inorg. Chem.* **1992**, *31*, 3091.

(26) Perkovic, M. W.; Heeg, M. J.; Endicott, J. F. *Inorg. Chem.* **1991**, *30*, 3140.

(27) Ryu, C. K.; Endicott, J. F. *Inorg. Chem.* **1988**, *27*, 2203.

(28) Sandrini, D.; Gandolfi, M. T.; Moggi, L.; Balzani, V. *J. Am. Chem. Soc.* **1978**, *100*, 1463.

(29) Archer, R. D. *Coord. Chem. Rev.* **1969**, *4*, 243.

(30) Garner, C. S.; House, D. A. In *Transition Metal Chemistry*; Carlin, R. C., Ed.; Marcel Dekker: New York, 1970; Vol. VI.

(31) House, D. A. *Coord. Chem. Rev.* **1971**, *23*, 223.

(32) Colton, R. *Coord. Chem. Rev.* **1988**, *90*, 1.

(33) Vaughn, J. W. *Coord. Chem. Rev.* **1981**, *39*, 265.

(34) Adamson, A. W. *J. Phys. Chem.* **1967**, *71*, 798.

(35) Vanquickenborne, L. G.; Ceulemans, A. *Coord. Chem. Rev.* **1983**, *48*, 157.

(36) Zink *J. Am. Chem. Soc.* **1972**, *94*, 8039.

(37) Zink, J. I. *Inorg. Chem.* **1973**, *12*, 1018.

(38) Zink, J. I. *Mol. Photochem.* **1973**, *5*, 151.

(39) Zink, J. I. *J. Am. Chem. Soc.* **1974**, *96*, 4464.

(40) Wrighton, M.; Gray, H. B.; Hammond, G. S. *Mol. Photochem.* **1973**, *5*, 165.

(41) Vanquickenborne, L. G.; Ceulemans, A. *J. Am. Chem. Soc.* **1977**, *99*, 2208.

(42) Lever, A. B. P. *Inorganic Electronic Spectroscopy*; Elsevier Publishing Company, 1984.

(43) Kirk, A. D.; Namasivayam, C.; Ward, T. *Inorg. Chem.* **1986**, *25*, 2225.

(44) Kane-Maguire, N. A. P.; Wallace, K. C.; Speece, D. G. *Inorg. Chem.* **1986**, *25*, 4650.

(45) Mønsted, L.; Mønsted, O. *Acta Chem. Scand.* **1993**, *47*, 9 .

(46) Riccieri, P.; Zinato, E.; Damiani, A. *Inorg. Chem.* **1988**, *27*, 3755.

(47) Riccieri, P.; Zinato, E.; Damiani, A. *Inorg. Chem.* **1987**, *26*, 2667.

(48) Woodward, R. B.; Hoffman, R. *J. Am. Chem. Soc.* **1965**, *87*, 2046.

(49) Woodward, R. B.; Hoffman, R. *J. Am. Chem. Soc.* **1965**, *87*, 395.

(50) Woodward, R. B.; Hoffman, R. *J. Am. Chem. Soc.* **1965**, *87*, 2511.

(51) Woodward, R. B.; Hoffman, R. *J. Am. Chem. Soc.* **1965**, *87*, 4389.

(52) Vanquickenborne, L. G.; Ceulemans, A. *J. Am. Chem. Soc.* **1978**, *100*, 475.

(53) Vanquickenborne, L. G.; Ceulemans, A.; Coussens, B.; Postelmans, D.; Pierloot, K. *Inorg. Chem.* **1992**, *31*, 539.

(54) Wong, C. F. C.; Kirk, A. D. *Inorg. Chem.* **1977**, *16*, 3148.

(55) Wright, R. E.; Adamson, A. W. *Inorg. Chem.* **1977**, *16*, 3360.

(56) Kirk, A. D.; Frederick, L. A. *Inorg. Chem.* **1981**, *20*, 60.

(57) Angermann, K.; Schmidt, R.; van Eldik, R.; Kelm, H.; Wasgestian, F. *Inorg. Chem.* **1982**, *21*, 1175.

(58) Angermann, K.; van Eldik, R.; Kelm, H.; Wasgestian, F. *Inorg. Chem.* **1981**, *20*, 955.

(59) Angermann, K.; van Eldik, R.; Kelm, H.; Wasgestian, F. *Inorg. Chim. Acta* **1981**, *49*, 247.

(60) Friesen, D. A.; Lee, S. H.; Waltz, W. L.; Vincze, L. *Inorg. Chem.* **1991**, *30*, 1975.

(61) Friesen, D. A.; Lee, S. H.; Nashiem, R. E.; Mezyk, S. P.; Waltz, W. L. *Inorg. Chem.* **1995**, *34*, 4026.

(62) Saliby, M. J.; Sheridan, P. S.; Madan, S. K. *Inorg. Chem.* **1980**, *19*, 1291.

(63) Kirk, A. D.; Heyd, D. *Inorg. Chem.* **1991**, *30*, 2453.

(64) Kutal, C.; Adamson, A. W. *Inorg. Chem.* **1973**, *12*, 1990.

(65) Kane-Maguire, N. A. P.; Crippen, W. S.; Miller, P. K. *Inorg. Chem.* **1983**, *22*, 696.

(66) Kane-Maguire, N. A. P.; Wallace, K. C.; Miller, D. B. *Inorg. Chem.* **1985**, *24*, 597.

(67) Kirk, A. D.; Fernando, S. R. L. *Coord. Chem. Rev.* **1994**, *132*, 121.

(68) Mackay, I. Ph.D. Dissertation, University of Victoria, 1998.

(69) Riccieri, P.; Zinato, E.; Aliboni, A. *Inorg. Chem.* **1990**, *25*, 5035.

(70) Riccieri, P.; Zinato, E. *Inorg. Chem.* **1997**, *36*, 2279.

(71) Kirk, A. D.; Ibrahim, A. M. *Inorg. Chem.* **1990**, *29*, 4848.

(72) Lee, S. H.; Waltz, W. L.; Demmer, D. R.; Walters, R. T. *Inorg. Chem.* **1985**, *24*, 1531.

(73) Cimolino, M. C.; Linck, R. G. *Inorg. Chem.* **1981**, *20*, 3499.

(74) Kirk, A. D.; Güdel, H. U. *Inorg. Chem.* **1992**, *31*, 4564.

(75) Krause, H. H.; Wasgestian, F. *Inorg. Chim. Acta* **1978**, *29*, 231.

(76) Jamieson, M. A.; Serpone, N.; Hoffman, M. Z. *Coord. Chem. Rev.* **1981**, *39*, 121.

(77) Bolletta, F.; Maestri, M.; Moggi, F.; Jamieson, M. A.; Serpone, N.; Henry, M. S.; Hoffman, M. Z. *Inorg. Chem.* **1983**, *22*, 2502.

(78) Maestri, M.; Bolletta, F.; Moggi, L.; Balzani, V.; Henry, M. S.; Hoffman, M. Z. *J. Am. Chem. Soc.* **1978**, *100*, 2694.

(79) Lilie, J.; Waltz, W. L. *Inorg. Chem.* **1983**, *22*, 1473.

(80) Lilie, J.; Waltz, W. L.; Lee, S. H.; Gregor, L. L. *Inorg. Chem.* **1986**, *25*, 4487.

(81) Waltz, W. L.; Lee, S. H.; Friesen, D. A.; Lilie, J. *Inorg. Chem.* **1988**, *27*, 1132.

(82) Waltz, W. L.; Lilie, J.; Lee, S. H. *Inorg. Chem.* **1984**, *23*, 1768.

(83) Waltz, W. L.; Walters, R. T.; Woods, R. J.; Lilie, J. *Inorg. Chim. Acta* **1980**, *46*, L153.

(84) Ballard, S. G. *Rev.Sci.Instrum* **1976**, *47*, 1157.

(85) Kirk, A. D.; Ibrahim, A. M. *Inorg. Chem.* **1988**, *27*, 4567.

(86) Oppegard, A. L.; Bailar, J. C. *Inorg. Synth.* **1950**, *3*, 153.

(87) Ferguson, J.; Tobe, M. L. *Inorg. Chim. Acta* **1970**, *4*, 109.

(88) Fernando, S. R. L. Ph.D. Dissertation, University of Victoria, 1993.

(89) Vaughn, J. W.; Stvan, O. J.; Magnuson, V. E. *Inorg. Chem.* **1968**, *7*, 736.

(90) Bigelow, J. *Inorg. Synth.* **1946**, 2, 203.

(91) Geue, R. J.; Searle, G. H. *Aust. J. Chem.* **1983**, *36*, 927.

(92) Subramanian, S., Personal Communication.

(93) Mackay, I., Personal Communication.

(94) Brown, K. N. Ph.D. Dissertation, Australian National University, 1994.

(95) Taft, J. C.; Jones, M. M. *J. Am. Chem. Soc.* **1960**, *82*, 4196.

(96) Glasbøl, F. *Inorg. Synth.* **1970**, *12*, 274.

(97) Hay, R. W.; Lawrence, G. A.; Curtis, N. F. *J. Chem. Soc. Perkin Trans. 1* **1975**, 591.

(98) House, D. A.; Hay, R. W.; Ali, M. A. *Inorg. Chim. Acta* **1983**, *72*, 239.

(99) Asmus, K.-D.; Janata, E. In *The Study of Fast Processes and Transient Species by Electron Pulse Radiolysis*; Baxendale, J. H., Busi, F., Eds.; D. Reidel Publishing Company:, 1982.

(100) Janata, E.; Lilie, J.; Martin, M. *Radiat. Phys. Chem.* **1994**, *43*, 353.

(101) Jeftic, L.; Feldberg, S. *J. Am. Chem. Soc.* **1970**, *92*, 5272.

(102) Walters, R. T.; Adamson, A. W. *Acta Chem. Scand. A* **1979**, *A33*, 53.

(103) Krause, H. H.; Wasgestian, F. *Inorg. Chim. Acta* **1981**, *49*, 231.

(104) Fukuda, R.; Walters, R. T.; Mäcke, H.; Adamson, A. W. *J. Phys. Chem.* **1979**, *83*, 2097.

(105) Ballardini, R.; Varani, G.; Wasgestian, H. F.; Moggi, L.; Balzani, V. *J. Phys. Chem.* **1973**, *77*, 2947.

(106) Gowin, E.; Wasgestian, F. *Inorg. Chem.* **1985**, *24*, 3106.

(107) Eigen, M. *Angew. Chem.* **1963**, *75*, 489.

(108) Wakefield, D. K.; Schaap, W. B. *Inorg. Chem.* **1969**, *8*, 512.

(109) Wasgestian, H. F. *Z.Phys.Chem* **1969**, *67*, 39.

(110) Chiang, A.; Adamson, A. W. *J. Phys. Chem.* **1968**, *11*, 3827.

(111) Andersen, P.; Berg, T.; Jacobsen, J. *Acta Chem. Scand. A* **1975**, *29*, 381.

(112) Beck, G.; Thomas, J. K. *J. Chem. Phys.* **1972**, *57*, 3649.

(113) Cai, L.-Z.; Kneeland, D. M.; Kirk, A. D. *J. Phys. Chem.* **1997**, *101*, 3871.

(114) Cai, L. Ph.D. Dissertation, University of Victoria, 1996.

(115) Harris, D. C. *Quantitative Chemical Analysis*; Fifth ed.; W. H. Freeman and Company, New York, 1999.

(116) *Handbook of Chemistry and Physics*; 70th ed.; CRC Press Inc.: Boca Raton, 1989.

(117) Fischer, M.; Wan, P. *J. Am. Chem. Soc.* **1998**, *120*, 2680.

(118) Mønsted, L.; Mønsted, O. *Acta Chem. Scand. A* **1976**, *30*, 203.

(119) Eriksen, J.; Mønsted, O. *Acta Chem. Scand. A* **1983**, *37*, 579.

(120) *The Merck Index*; Eleventh ed.; Merck & Co., Inc.: Rahway, 1989.

(121) Bang, E.; Mønsted, O. *Acta Chem. Scand. A* **1984**, *38*, 281.

(122) Kirk, A. D.; Frederick, L. A.; Wong, C. F. C. *Inorg. Chem.* **1979**, *18*, 448.

(123) Geis, W.; Schläfer, H. L. *Z. Phys. Chem.* **1969**, *65*, 107.

(124) Cimolino, M. C.; Shipley, N. J.; Linck, R. G. *Inorg. Chem.* **1980**, *19*, 3291.

(125) Timerbaev, A. R. *J. Chromatogr. A* **1997**, *792*, 495.

(126) Chen, M. *J. Chromatogr.* **1993**, *640*, 425.

(127) Shi, Y.; Fritz, J. S. *J. Chromatogr.* **1993**, *640*, 459.

(128) Watson, R. T.; Desai, N.; Wildsmith, J.; Wheeler, J. F.; Kane-Maguire, N. A. P. *Inorg. Chem.* **1999**, *38*, 2683.

(129) Shelton, C. M.; Seaver, K. E.; Wheeler, J. F.; Kane-Maguire, N. A. P. *Inorg. Chem.* **1997**, *36*, 1532.

Appendix 1

Derivation of Equations for Conductivity Apparatus

Appendix 1.1 Derivation of theoretical equation predicting conductivity signal magnitudes.

The potential difference observed across the Wheatstone bridge results from the different currents that flow through the irradiated (sample) and unirradiated (reference) solution. Diagram 3.2 and the associated text provides the defintions for the V, R and G terms used in the derivations of Equations 3.1, 3.2 and 3.3.

$$\Delta V = V_{ref} - V_{sample}$$

$$= \frac{R_S.V_{app}}{(R_S+R_E)} - \frac{R_S^*.V_{app}}{(R_S^*+R_E)}$$

$$\frac{\Delta V}{V_{app}} = \frac{R_S}{(R_S+R_E)} - \frac{(R_S+\Delta R)}{(R_S+\Delta R+R_E)} \qquad (3.3)$$

(3.3) is the rigorous equation which can be used to calculate the potential difference across the bridge arms if all resistances are known.

$$= \frac{R_S.(R_S+\Delta R+R_E) - (R_S+R_E).(R_S+\Delta R)}{(R_S+\Delta R+R_E).(R_S+R_E)}$$

$$= \frac{\Delta R R_E}{(R_S+\Delta R+R_E).(R_S+R_E)}$$

$$= \frac{\frac{\Delta R R_E}{R_S R_E}}{\frac{(R_S+\Delta R+R_E).(R_S+R_E)}{R_S R_E}}$$

$$= \frac{\frac{\Delta R}{R_S}}{\frac{(R_S+\Delta R+R_E)}{R_S}\frac{(R_S+R_E)}{R_E}} \quad \text{if } \Delta R << R_S \text{ and } R_E$$

$$= \frac{\frac{\Delta R}{R_S}}{\frac{(R_S+R_E)}{R_S} \cdot \frac{(R_E+R_S)}{R_E}}$$

$$= \frac{\frac{\Delta R}{R_S}}{\frac{(R_S+R_E)^2}{R_S R_E}}$$

$$= \frac{\Delta R}{R_S} \cdot \frac{R_S R_E}{(R_S + R_E)^2}$$

Can convert $\frac{\Delta R}{R_S}$ to equivalent expression in terms of solution conductivities.

$$\frac{\Delta R}{R_S} = \frac{(R_S^* - R_S)}{R_S}$$

$$= \frac{\frac{1}{A}\left(\frac{1}{K_S^*} - \frac{1}{K_S}\right)}{\frac{1}{A}\frac{1}{K_S}}$$

$$= \frac{\frac{\Delta K}{K_S^* . K_S}}{\frac{1}{K_S}}$$

$$\frac{\Delta R}{R_S} = \frac{\Delta K}{K_S^*}$$

$$= \frac{\Delta K}{K_S} \quad \text{if assume that } K_S^* = K_S$$

$$\frac{\Delta V}{V_{app}} = \frac{\Delta K}{K_S} \cdot \frac{R_S R_E}{(R_S+R_E)^2}$$

This equation can be modified to account for the actual photochemistry in acidic solution where the Cr(III) am(m)ine complex photoaquates to give a protonated amine and an aquated photoproduct. The overall conductivity changes observed are going to be affected by the acid base equilibria of the photoproduct.

$$CrN_6^{3+} + H^+ \rightarrow CrN_5(OH_2)^{3+} + NH^+ \Leftrightarrow CrN_5(OH)^{2+} + NH^+ + H^+$$

$$\Delta K = \text{Large} \qquad \Delta K \approx 0$$

Therefore if the aquated photoproduct acts as an acid there is no significant overall contribution to the change in solution conductivity. This can be accounted for by introducing F_{H20}, which reflects the proportion of photoproduct in the aquo form.

$$Ka = \frac{[CrN_5(OH)^{2+}]\,.[H^+]}{[CrN_5(OH_2)^{3+}]}$$

$$\frac{[CrN_5(OH)^{2+}]}{[CrN_5(OH_2)^{3+}]} = \frac{K_a}{[H^+]}$$

$$F_{H20} = \frac{[CrN_5(OH_2)^{3+}]}{([CrN_5(OH)^{2+}]+[CrN_5(OH_2)^{3+}])}$$

$$= \frac{1}{(1 + \frac{[CrN_5(OH)^{2+}]}{[CrN_5(OH_2)^{3+}]})}$$

$$= \frac{1}{(1 + \frac{K_a}{[H^+]})}$$

$$= \frac{1}{(1 + 10^{(pH - pKa)})}$$

$$\frac{\Delta V}{V_{app}} = \frac{\Delta K}{K_S} \cdot \frac{R_S R_E}{(R_S + R_E)^2} \cdot F_{H20}$$

** In the modelling detailed in Appendix 2, the equation used calculates the overall ΔK in solution based on the molar conductivities of all ions present. i.e. it does not make the assumption that $\Delta K = 0$ for the photoproduct acting as a base.

Appendix 1.2 Derivation of literature equations predicting conductivity signal magnitudes

This equation is based on the same set-up as for the equation in appendix 1.1.

$$\Delta V = V_{ref} - V_{sample}$$

$$\frac{\Delta V}{V_{app}} = \frac{R_S}{(R_S+R_E)} - \frac{(R_S+\Delta R)}{(R_S+\Delta R+R_E)}$$

Convert to conductances, G

$$R_S = \frac{1}{G_S},\ R_E = \frac{1}{G_E},$$
$$R_S^* = R_S + \Delta R = \frac{1}{(G_S+\Delta G)} = \frac{1}{G_S^*}$$

$$\frac{\Delta V}{V_{app}} = \frac{\frac{1}{G_S}}{\frac{1}{G_S} + \frac{1}{G_E}} - \frac{\frac{1}{(G_S+\Delta G)}}{\frac{1}{(G_S+\Delta G)} + \frac{1}{G_E}}$$

Term 1 Term 2

Terms 1 and 2 can be simplified individually;

Term 1;

$$\frac{\frac{1}{G_S}}{\frac{1}{G_S} + \frac{1}{G_E}} = \frac{\frac{1}{G_S}}{\frac{(G_S+G_E)}{G_S G_E}}$$

$$= \frac{G_E}{(G_S+G_E)}$$

Term 2

$$\frac{\frac{1}{(G_S+\Delta G)}}{\frac{1}{(G_S+\Delta G)}+\frac{1}{G_E}} = \frac{\frac{1}{(G_S+\Delta G)}}{\frac{(G_EG_S+\Delta G)}{G_E(G_S+\Delta G)}}$$

$$= \frac{G_E(G_S+\Delta G)}{(G_S+\Delta G)(G_E+G_S+\Delta G)}$$

$$= \frac{G_E}{(G_E+G_S+\Delta G)}$$

Recombining the two terms

$$\frac{\Delta V}{V_{app}} = \frac{G_E}{(G_S+G_E)} - \frac{G_E}{(G_E+G_S+\Delta G)}$$

$$= \frac{\Delta G G_E}{(G_S+G_E)(G_E+G_S+\Delta G)}$$

$$= \frac{\Delta G}{(G_E+G_S+\Delta G)} \cdot \frac{G_E}{(G_S+G_E)} \qquad (3.1)$$

$$= \frac{\Delta G}{(G_S+G_E)} \cdot \frac{G_E}{(G_E+G_S+\Delta G)} \qquad (3.2)$$

Simplification used for (3.1)

Assume that $G_E >> G_S$ then $\frac{G_E}{(G_S + G_E)} = 1$

$$\frac{\Delta V}{V_{app}} = \frac{\Delta G}{(G_E+G_S+\Delta G)}$$

Simplification used for (3.2),

This recognizes that ΔG is a negative value and that $(G_E + G_S + \Delta G) = G_E$ is a more valid assumption than $(G_S + G_E) = G_E$

$$\frac{G_E}{(G_E+G_S+\Delta G)} = 1$$

$$\frac{\Delta V}{V_{app}} = \frac{\Delta G}{(G_S+G_E)}$$

Appendix 1.3 Calculation of theoretical signals for photolysis of a $Cr(NH_3)_6^{3+}$ solution

Theoretical solution;

[$Cr(NH_3)_6^{3+}$] = 1.0 mM, Absorbance = 0.05, Quantum Yield = 0.50.

Relevant Terms and Equations;

G_S = Solution conductance

$$G_S = K\frac{A}{l}$$
$$= \{10^{-pH}(\lambda_{H+} + \lambda_{ClO4^-}) + [Cr^{3+}].(\lambda_{Cr3+} + 3.\lambda_{ClO4^-})\}\frac{A}{l}$$

$$R_S = \frac{l}{G_S}$$

$$\Delta G = \Delta K.\frac{A}{l}$$

Assume that the major conductivity changes are due to proton uptake by the photoreleased ammonia and the formation of an ammonium ion.

$$\Delta K = [NH_3]\,(\lambda_{NH4+} - \lambda_{H+})$$

$$[NH_3] = \frac{(F_{abs} \cdot n_{photons} \cdot \emptyset)}{Vol_{irrad}}$$

$$F_{abs} = 1\text{-}10^{-Abs}$$

$$n_{photons} = \frac{\frac{E_{pulse}}{E_{355nm\ photon}}}{N_A}$$

$$G_S^* = G_S + \Delta G$$

$$R_S^* = \frac{1}{G_S^*}$$

$$\Delta R = R_S^* - R_S$$

Calculated and measured values

$\lambda_{H+} = 350$ S cm^2 mol^{-1}, $\lambda_{Cr3+} = 165$ S cm^2 mol^{-1},

$\lambda_{ClO4^-} = 68$ S cm^2 mol^{-1} , $\lambda_{NH4+} = 73$ S cm^2 mol^{-1}

$\frac{l}{A} = 1.63$ cm^{-1} (measured),

Absorbance $= 0.1$ (theoretical)

Incident pulse energy = 34 mJ (estimated based on 6 x 4 mm window and 40 mJ pulse energy with a 6mm diameter pulse profile)

$Vol_{irrad} = 2.10 \times 10^{-4}$ L (measured)

$F_{abs} = 0.109$

$\emptyset = 0.5$ (Strictly this should be 0.46, the literature quantum yield for $Cr(NH_3)_6^{3+}$)

$n_{photons} = 1.01 \times 10^{-7}$ moles

$[NH_3] = 2.62 \times 10^{-5}$ M

$\Delta K = 7.25 \times 10^{-6}$ S cm^{-1}

$\Delta G = 4.45 \times 10^{-6}$ S

$V_{app} = 120$ V

$R_E = 75\ \Omega$, $G_E = 1.33 \times 10^{-2}$ S m^2 mol^{-1}

Using these values the values presented in the following tables were obtained.

	pH 3	pH 4	pH 5
K / S cm^{-1}	7.87×10^{-4}	4.11×10^{-4}	3.73×10^{-4}
G_S / S	4.83×10^{-4}	2.52×10^{-4}	2.29×10^{-4}
R_S / Ω	2070	3970	4370
G_S* / S	4.79×10^{-4}	2.48×10^{-4}	2.25×10^{-4}
R_S* / Ω	2090	4040	4453
ΔR / Ω	20	70	83

Table A1.1 Calculated conductance and resistance values at pH 3, pH 4 and pH 5

	pH 3	pH 4	pH 5
$\frac{\Delta K}{K}$	9.21×10^{-3}	1.76×10^{-2}	1.94×10^{-2}
$\frac{R_S R_E}{(R_S + R_E)^2}$	3.37×10^{-2}	1.82×10^{-2}	1.66×10^{-2}
Product	3.10×10^{-4}	3.20×10^{-4}	3.22×10^{-4}
Signal Magnitude	37.2 mV	38.4 mV	38.6 mV

Table A1.2 Calculated values for individual terms and overall signal magnitudes for Equation 3.1 at pH 3, pH 4 and pH 5

	pH 3	pH 4	pH 5
(3.3)	37.2 mV	38.4 mV	38.6 mV
(3.2)	38.6 mV	39.3 mV	39.4 mV
Absolute	38.8 mV	37.8 mV	37.1 mV

Table A1.3 Comparison of conductivity signal magnitudes calculated at pH 3, pH 4 and pH 5 for different equations

The tables show that both our derived equation (3.3) and that of Asmus and Janata (3.2) give signals that increase as the pH is increased from pH 3 to pH 5. However the signal magnitudes predicted by the absolute equation decrease slightly over this pH range. Presumably this is a results of the simplifications that are made in the derivation of (3.1) and (3.2).

All signals generated by the conductivity apparatus have an amplified gain of 50. Based on this the theoretical equations predict signal magnitudes of approxiamtely 2 V in the absence of a photoproduct acid-base equilibrium. The signals obtained for 1.0 mM $Cr(NH_3)_6^{3+}$ solutions are typically in the order of 100 mV. This indicates that the experimental signal magnitudes are approximately 1/20th of those predicted based on the theoretical calculations.

Appendix 2

Integrated Rate Equations for Kinetic Modelling of Mechanisms

These mechanisms are presented using the abbreviations used in the actual modelling rather than as formal rate expressions. The reason for this is that, for the author at least, the shorthand notation is easier to follow than when the equations contain the concentration symbols and correct formula for each chemical species.

Initial concentrations are calculated based on the experimental conditions, i.e solution absorbance, quantum yield of the complex, incident laser energy. The integrated rate expressions then calculate the changes in concentration occuring over a small time interval, dt, for each mechanistic species based on input values for the relevant rate constants. Each calculation is done over 12 000 iterations so dt = timescale / 12 000.

The modelled rate constants correspond to those presented for each mechanism in the text.

Appendix 2.1 Modelling of Waltz's mechanism for *cis*-$Cr(cyclam)(NH_3)_2^{3+}$ photoaquation

Definitions

delt = dt

Htot[j] = $[H_3O^+]_j$

Int_OH2[j] = $[I(OH_2)^{3+}]_j$

Int_OH[j] = $[I(OH)^{2+}]_j$

prod_OH2[j] = $[Cr(cyclam)(NH_3)(OH_2)^{3+}]_j$

prod_OH[j] = $[Cr(cyclam)(NH_3)(OH)^{2+}]_j$

amm[j] = $[NH_3]_j$

ammH[j] = $[NH_4]_j$

lamX = λ_X

delH[j] = $[H_3O^+]_{j+1} - [H_3O^+]_j$

Initial Concentrations

Htot[0] = 10^{-pH}

All other initial concentrations = 0

Integrated Rate Expessions

$Htot[j+1] = Htot[j] + delt*(k_I*I\_OH2[j] + k_P*P\_OH2[j] - k_{-I}*I\_OH[j]*Htot[j] - k_{-P}*P\_OH[j]*Htot[j] - k_{prot}*amm[j]*Htot[j])$

$I\_OH2[j+1] = I\_OH2[j] + delt*(theta*kdoub*doub[j] + k_{-I}*I\_OH[j]*Htot[j] - k_I*I\_OH2[j] - k_r*I\_OH2[j])$

$I\_OH[j+1] = I\_OH[j] + delt*(kI*I\_OH2[j] - k_{-I}*I\_OH[j]*Htot[j] - k_{r2}*I\_OH2[j])$

$P\_OH2[j+1] = P\_OH2[j] + delt*(k_r*I\_OH2[j] + k_{-P}*P\_OH[j]*Htot[j] - k_P*P\_OH2[j])$

$P\_OH[j+1] = P\_OH[j] + delt*(k_P*P\_OH2[j] + k_{r2}*I\_OH2[j] - k_{-P}*P\_OH[j]*Htot[j])$

$amm[j+1] = amm[j] + delt*(k_r*I\_OH2[j] + k_{r2}*I\_OH2[j] - k_{prot}*amm[j]*Htot[j])$

$ammH[j+1] = ammH[j] + delt*(k_{prot}*amm[j]*Htot[j])$

$delH[j+1] = Htot[j+1]-Htot[0]$

$Kappa[j+1] = lamH^+*delH[j+1] - (lamCr^{3+}-lamCr^{2+})*I\_OH[j+1] - (lamCr^{3+}-lamCr^{2+})*P\_OH[j+1] + lamNH_4^+*ammH[j+1]$

Appendix 2.2 Modelling of photoaquation with loss of ammonia

Definitions

delt = dt

Htot[j] = $[H_3O^+]_j$

prod_OH2[j] = $[Cr(N4)(NH_3)(OH_2)^{3+}]_j$ where N4 = $(tn)_2$, or $(NH_3)_4$

prod_OH[j] = $[Cr(N4)(NH_3)(OH)^{2+}]_j$

amm[j] = $[NH_3]_j$

ammH[j] = $[NH_4]_j$

lamX = λ_X

delH[j] = $[H_3O^+]_{j+1} - [H_3O^+]_j$

Initial Concentrations

Htot[0] = 10^{-pH}

Prod_OH2[0] = $\emptyset * F_Q * [*Cr(N4)(NH_3)_2^{3+}]$

amm[0] = $\emptyset * F_Q * [*Cr(N4)(NH_3)_2^{3+}]$

All other initial concentrations = 0

Integrated Rate Expessions

Htot[j+1] = Htot[j]+delt*(k_a*prod_OH2[j] - k_{-a}*prod_OH[j]*htot[j] -
k_H*amm[j]*htot[j])

prod_OH2[j+1] = prod_OH2[j] + delt*(theta*k_D*comp[j] + k_{-a}*prod_OH[j]*htot[j] -
k_a*prod_OH2[j])

prod_OH[j+1] = prod_OH[j] + delt*(k_a*prod_OH2[j] - $k_{-a}P$*prod_OH[j]*htot[j])

amm[j+1] = amm[j] + delt*(theta*k_D*comp[j] - k_H*amm[j]*htot[j])

ammH[j+1] = ammH[j] + delt*(k_H*amm[j]*htot[j])

delH[j+1] = Htot[j+1] - Htot[0]

Kappa[j+1] = lamH*delH[j+1] + lamNH4*ammH[j+1]

- (lamCr^{3+}-lamCr^{2+})*prod_OH[j+1]

Appendix 2.3 Modelling of photoaquation with loss of a dangling ammine

Definitions

delt = dt

Htot[j] = $[H_3O^+]_j$

Dang_OH2[j] = $[Cr(NN)_2(N\text{--}N)(OH_2)^{3+}]_j$ where NN = en, tn or 1/3 sen

Dang_OH[j] = $[Cr(NN)_2(N\text{--}N)(OH)^{2+}]_j$

DangH_OH2[j] = $[Cr(NN)_2(N\text{--}NH)(OH_2)^{3+}]_j$

DangH_OH[j] = $[Cr(NN)_2(N\text{--}NH)(OH)^{2+}]_j$

lamX = λ_X

delH[j] = $[H_3O^+]_{j+1}$ - $[H_3O^+]_j$

Initial Concentrations

Htot[0] = 10^{-pH}

Dang_OH2[0] = Ø*F_Q*[*$Cr(NN)_3^{3+}$]

All other initial concentrations = 0

Integrated Rate Expessions

$Htot[j+1] = Htot[j] + delt*(k_a*Dang\_OH2[j] - k_{-a}*Dang\_OH[j]*Htot[j] + k_{a'}*DangH\_OH2[j] - k_{-a'}*DangH\_OH[j]*Htot[j] - k_H*Dang\_OH2[j]*htot[j] - k_{H'}*Dang\_OH[j]*htot[j])$

$Dang\_OH2[j+1] = Dang\_OH2[j] + delt*(theta*k_D*doub[j] + k_{-a}*Dang\_OH[j]*htot[j] - k_H*Dang\_OH2[j]*Htot[j] - k_a*Dang\_OH2[j])$

$DangH\_OH2[j+1] = DangH\_OH2[j] + delt*(k_H*Dang\_OH2[j]*htot[j] + k_{-a'}*DangH\_OH[j]*htot[j] - k_{a'}*DangH\_OH2[j])$

$Dang\_OH[j+1] = Dang\_OH[j] + delt*(k_a*Dang\_OH2[j] - k_{-a}*Dang\_OH[j]*htot[j] - k_{H'}*Dang\_OH[j]*htot[j])$

$DangH\_OH[j+1] = DangH\_OH[j] + delt*(k_{a'}*DangH\_OH2[j] + k_{H'}*Dang\_OH[j]*htot[j] - k_{-a'}*DangH\_OH[j]*htot[j])$

$delH[j+1] = Htot[j+1] - Htot[0]$

$Kappa[j+1] = lamH*delH[j+1] + (lamCr^{4+} - lamCr^{3+})*DangH\_OH2[j] - (lamCr^{3+} - lamCr^{2+})*Dang\_OH[j+1]$

Appendix 2.4 Modelling of *cis*-$Cr(cyclam)(NH_3)_2^{3+}$ photoaquation

DEFINITIONS

delt = dt

$Htot[j] = [H_3O^+]_j$

$Prod\text{-}OH2[j] = [Cr(cyc)(NH_3)(OH_2)^{3+}]_j$

$Prod\text{-}OH[j] = [Cr(cyc)(NH_3)(OH)^{2+}]_j$

Int-OH2[j] = $[Cr(cyc\text{-}N)(NH_3)_2(OH_2)^{3+}]_j$

Int-OH[j] = $[Cr(cyc\text{-}N)(NH_3)_2(OH)^{2+}]_j$

IntH-OH2[j] = $[Cr(cyc\text{-}NH)(NH_3)_2(OH_2)^{4+}]_j$

IntH-OH2[j] = $[Cr(cyc\text{-}NH)(NH_3)_2(OH)^{3+}]_j$

amm[j] = $[NH_3]_j$

ammH[j] = $[NH_4]_j$

lamX = λ_X

delH[j] = $[H_3O^+]_{j+1} - [H_3O^+]_j$

Initial Concentrations

Htot[0] = 10^{-pH}

Int_OH2[0] = $\emptyset_{ring} * F_Q * [*Cr(cyc)(NH_3)_2{}^{3+}]$

Prod_OH2[0] = $\emptyset_{amm} * F_Q * [*Cr]$

amm[0] = $\emptyset_{amm} * F_Q * [*Cr]$

All other initial concentrations = 0

Integrated Rate Expressions

comp[p]=comp[p-1]-delt*k_d*comp[p-1]

Htot[j+1] = Htot[j] + delt*(k_R*Int_OH2[j] - k_{-R}*Int_OH[j]*Htot[j] +
k_{RH}*IntH_OH2[j] - k_{-RH}*IntH_OH[j]*Htot[j] - $k_{p\text{-}cycN}$*Int_OH2[j]*htot[j]
- $k_{p\text{-}cycN}$*Int_OH[j]*htot[j] - k_{-P}*Prod_OH[j]*htot[j] + k_P*Prod_OH2[j] -
k_{prot}*amm[j]*htot[j])

Int_OH2[j+1] = Int_OH2[j] + delt*($\emptyset_{cyc}$*k_d*comp[j] + k_{-R}*Int_OH[j]*htot[j] -
$k_{p\text{-}cycN}$*Int_OH2[j]*Htot[j] - k_R*Int_OH2[j] - k_{rec}*Int_OH2[j] +
k_{int}*IntH_OH[j])

$IntH\_OH2[j+1] = IntH\_OH2[j] + delt*(k_{p\text{-}cycN}*Int\_OH2[j]*htot[j] +$

$k_{-RH}*IntH\_OH[j]*htot[j] - k_{-R}*IntH\_OH2[j])$

$Int\_OH[j+1] = Int\_OH[j] + delt*(k_R*Int\_OH2[j] - k_{-R}*Int\_OH[j]*htot[j] -$

$k_{p\text{-}cycN}*Int\_OH[j]*htot[j] - k_{rec'}*Int\_OH[j])$

$IntH\_OH[j+1] = IntH\_OH[j] + delt*(k_{-R}*IntH\_OH2[j] + k_{p\text{-}cycN}*Int\_OH[j]*htot[j] -$

$k_{-RH}*IntH\_OH[j]*htot[j] - k_{int}*IntH\_OH[j])$

$Prod\_OH2[j+1] = Prod\_OH2[j] + delt*(\emptyset_{amm}*kd*comp[j] +$

$k_{-P}*Prod\_OH[j]*htot[j] - k_P*Prod\_OH2[j] + krec*Int\_OH2[j])$

$Prod\_OH[j+1] = Prod\_OH[j] + delt*(k_P*Prod\_OH2[j] - k_{-P}*Prod\_OH[j]*htot[j] +$

$k_{rec'}*Int\_OH[j])$

$amm[j+1] = amm[j] + delt*(\emptyset_{amm}*kd*comp[j] - k_{prot}*amm[j]*htot[j] +$

$k_{rec}*Int\_OH2[j] + k_{rec'}*Int\_OH[j])$

$ammH[j+1] = ammH[j] + delt*(k_{prot}*amm[j]*htot[j])$

$delH[j+1] = Htot[j+1] - Htot[0]$

$Kappa[j+1] = lamH*delH[j+1] + (LamdCr^{4+}\text{-}lamdCr^{3+})*IntH\_OH2[j] -$

$(lamdCr^{3+}\text{-} lamdCr^{2+})*Int\_OH[j+1] + 70*ammH[j+1] -$

$(lamdCr^{3+}\text{-}lamdCr^{2+})*Prod\_OH[j+1]$

Appendix 3

Comparison of Modelled and Experimental Conductivity Changes

The Figures in Appendix 3 present the experimental traces, comparison of modelled and experimental conductivity changes and the comparison of modelled and experimental lifetimes for the complexes that were not detailed in the main text.

Appendix 3.1 *cis*-$Cr(tn)_2(NH_3)_2^{3+}$

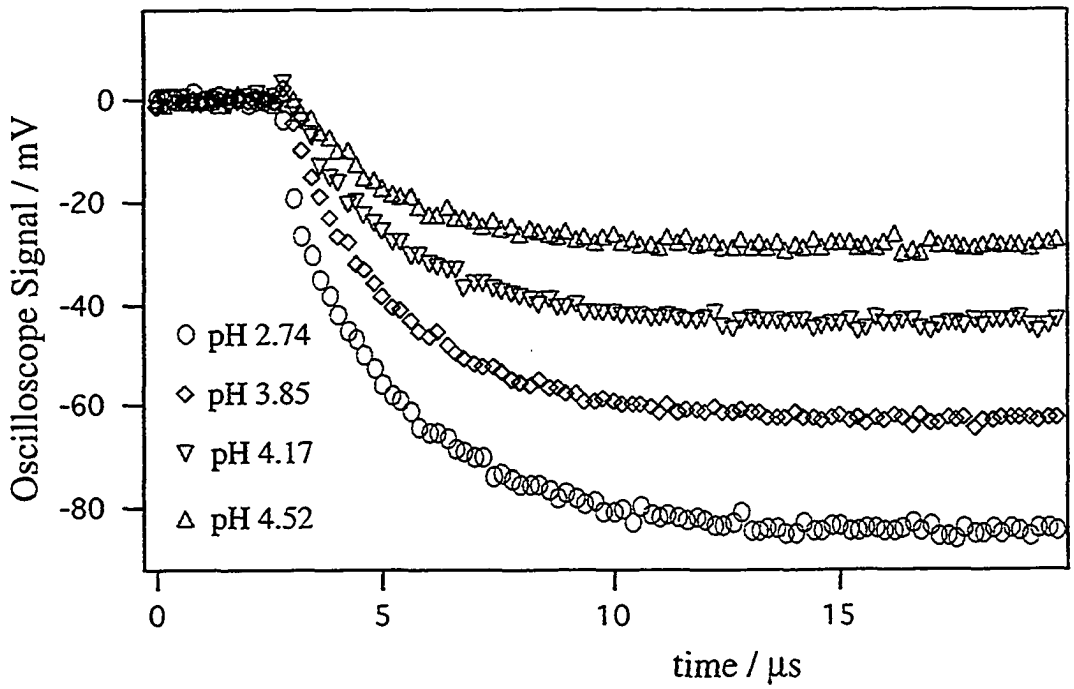

Figure A3.1 Conductivity traces obtained for the laser flash photolysis of *cis*-$Cr(tn)_2(NH_3)_2^{3+}$ at various pH values

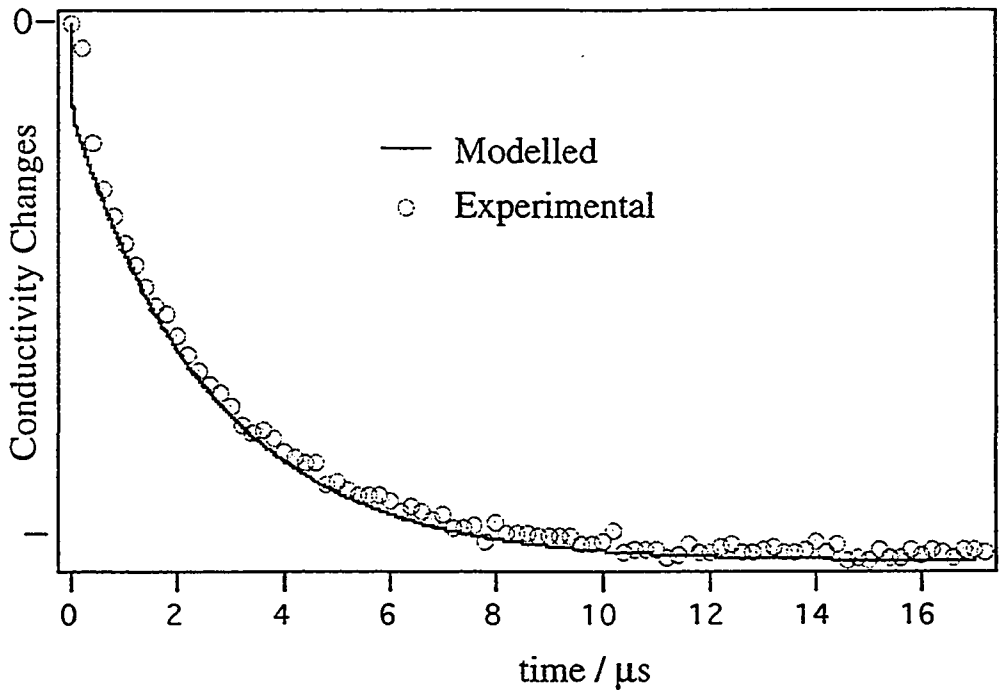

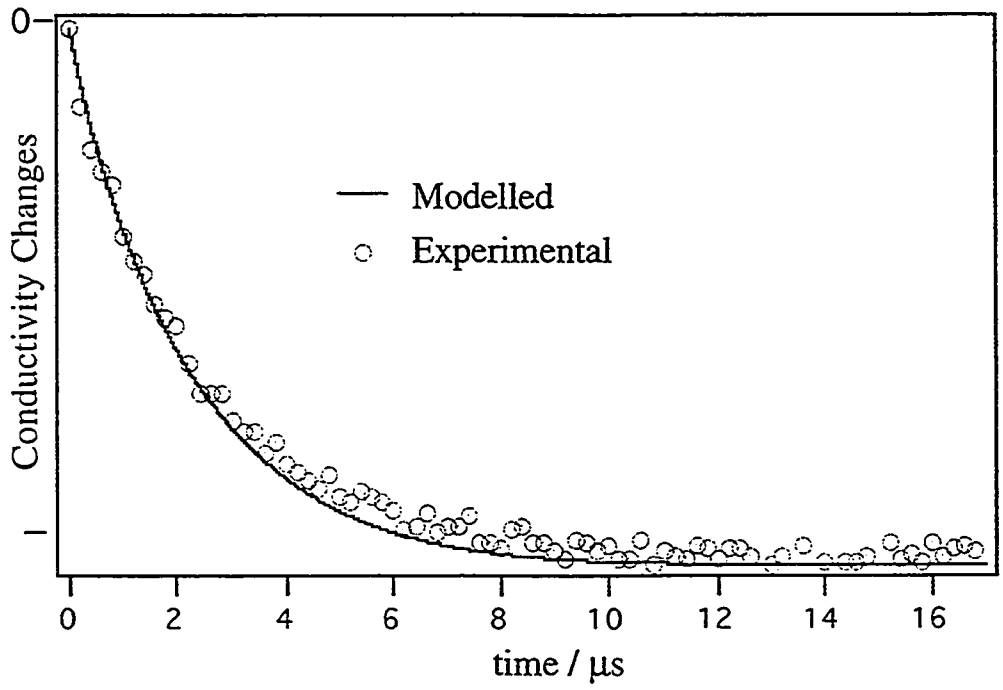

Figure A3.2 Comparison of modelled and experimental conductivity changes for *cis*-$Cr(tn)_2(NH_3)_2^{3+}$ at pH 2.74 and 4.17

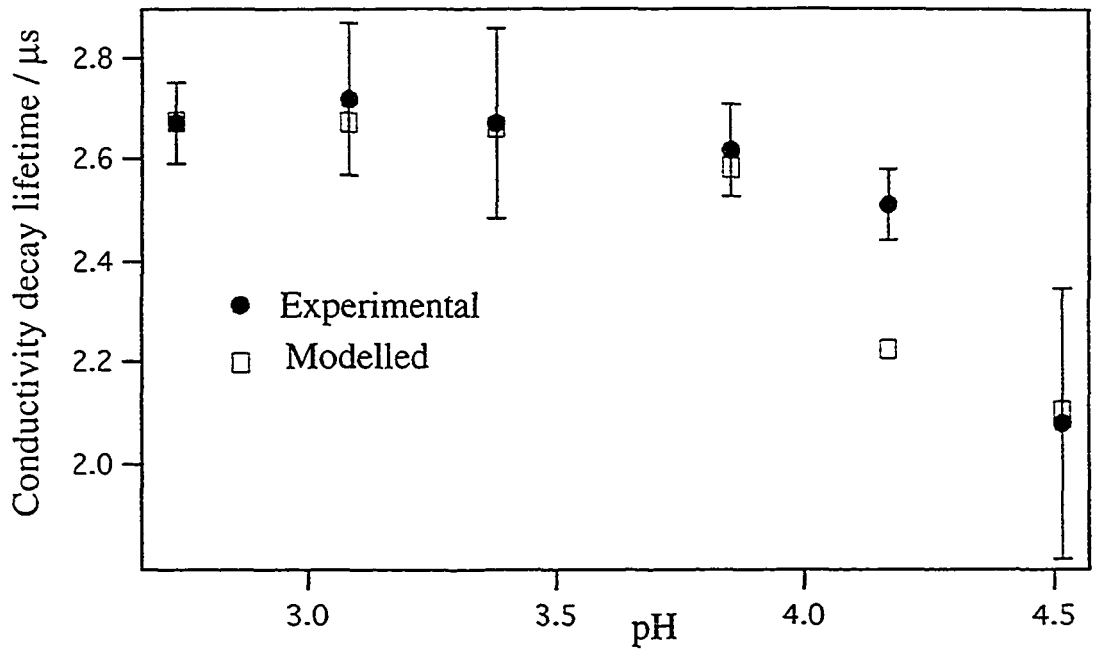

Figure A3.3 Comparison of modelled and experimental decay lifetimes for *cis*-$Cr(tn)_2(NH_3)_2^{3+}$ at various pH values.

Appendix 3.2 *trans*-$Cr(tn)_2(NH_3)_2^{3+}$

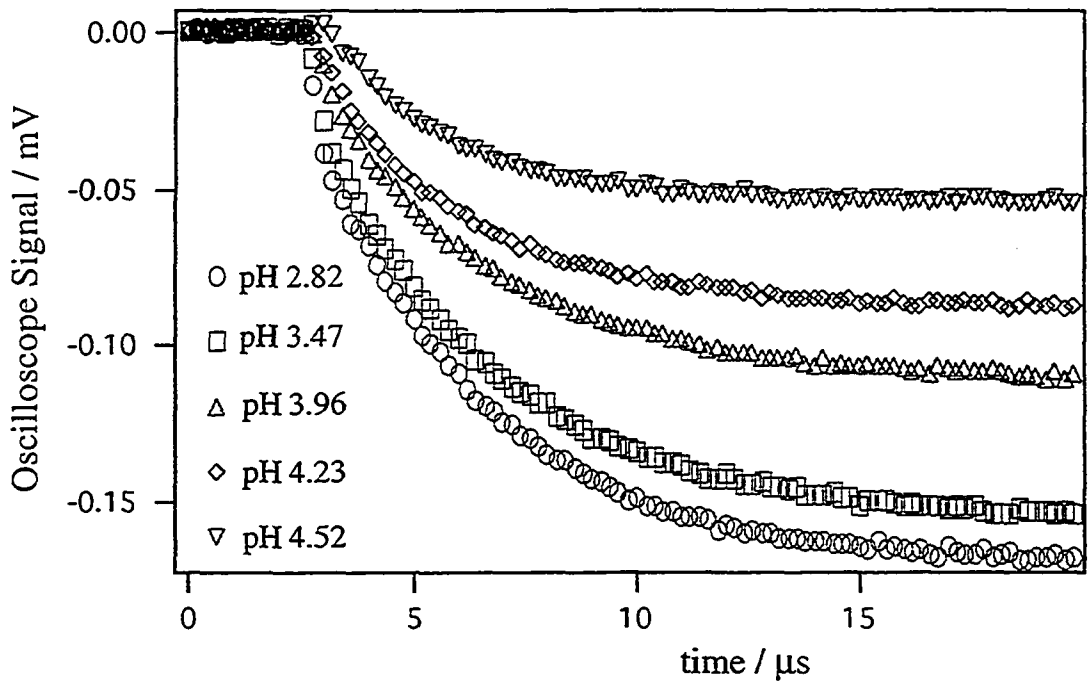

Figure A3.4 Conductivity traces obtained for the laser flash photolysis of *trans*-$Cr(tn)_2(NH_3)_2^{3+}$ at various pH values

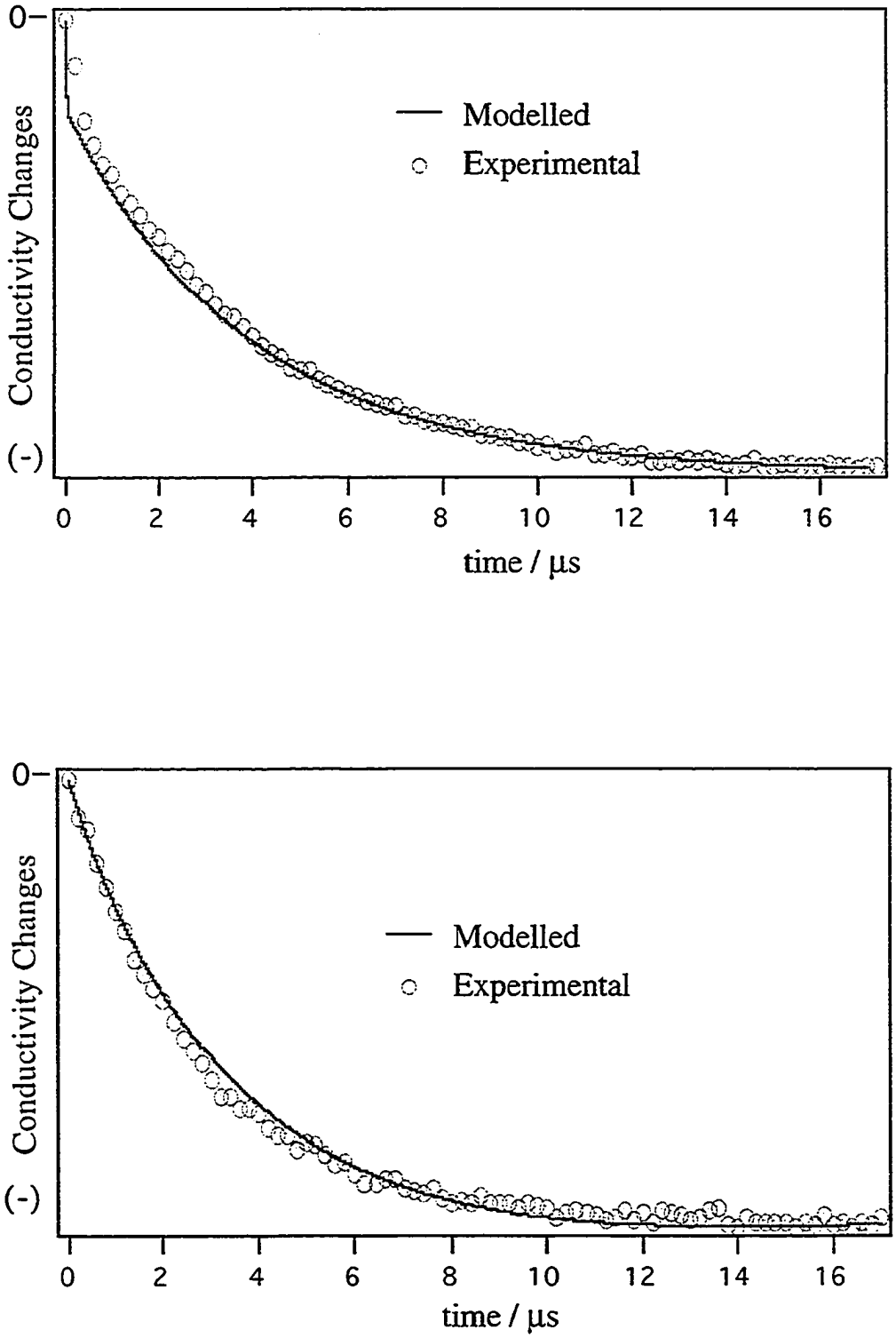

Figure A3.5 Comparison of modelled and experimental conductivity changes for *trans*-$Cr(tn)_2(NH_3)_2^{3+}$ at pH 2.82 and 4.46

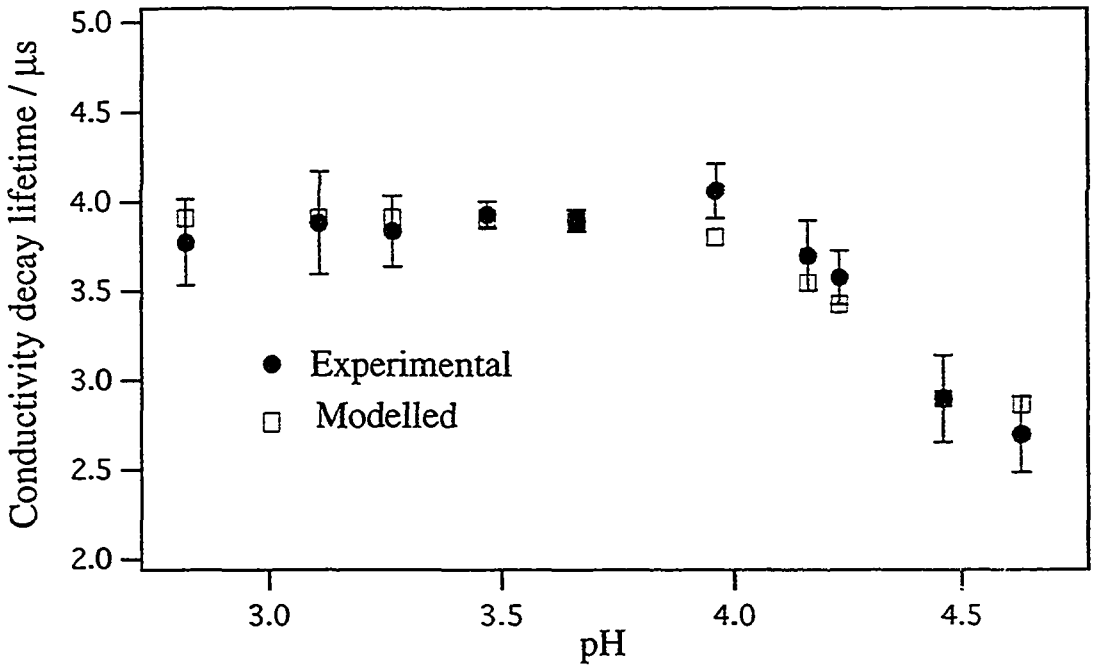

Figure A3.6 Comparison of modelled and experimental decay lifetimes for *trans*-$Cr(tn)_2(NH_3)_2^{3+}$ at various pH values.

Appendix 3.3 $Cr(tn)_3^{3+}$

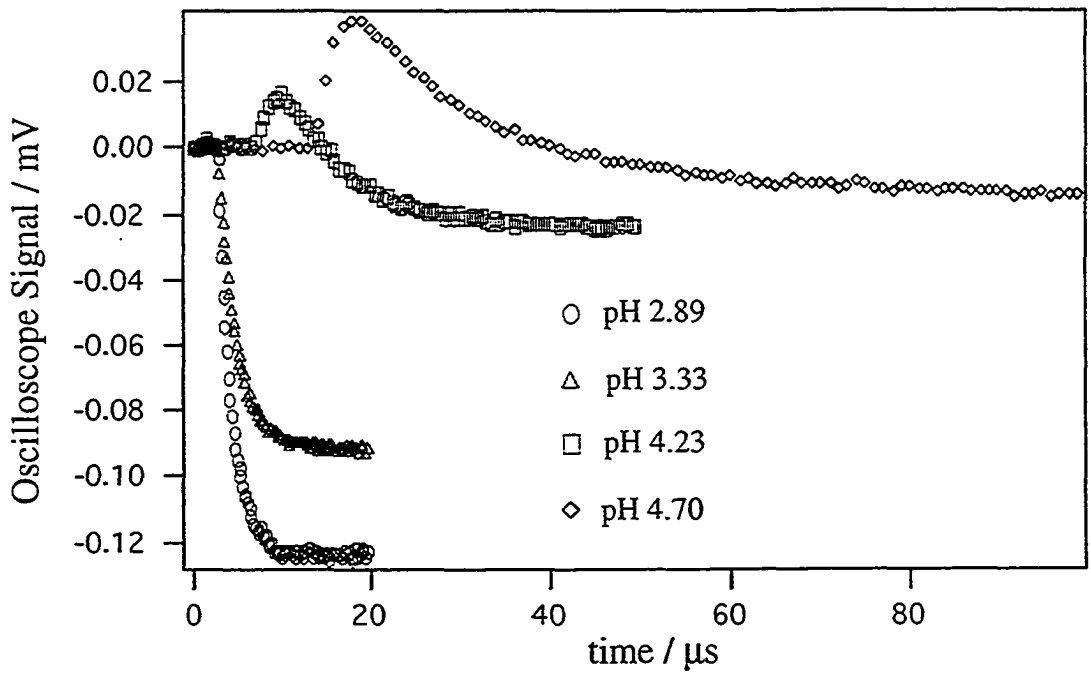

Figure A3.7 Conductivity traces obtained for the laser flash photolysis of $Cr(tn)_3^{3+}$ at various pH values

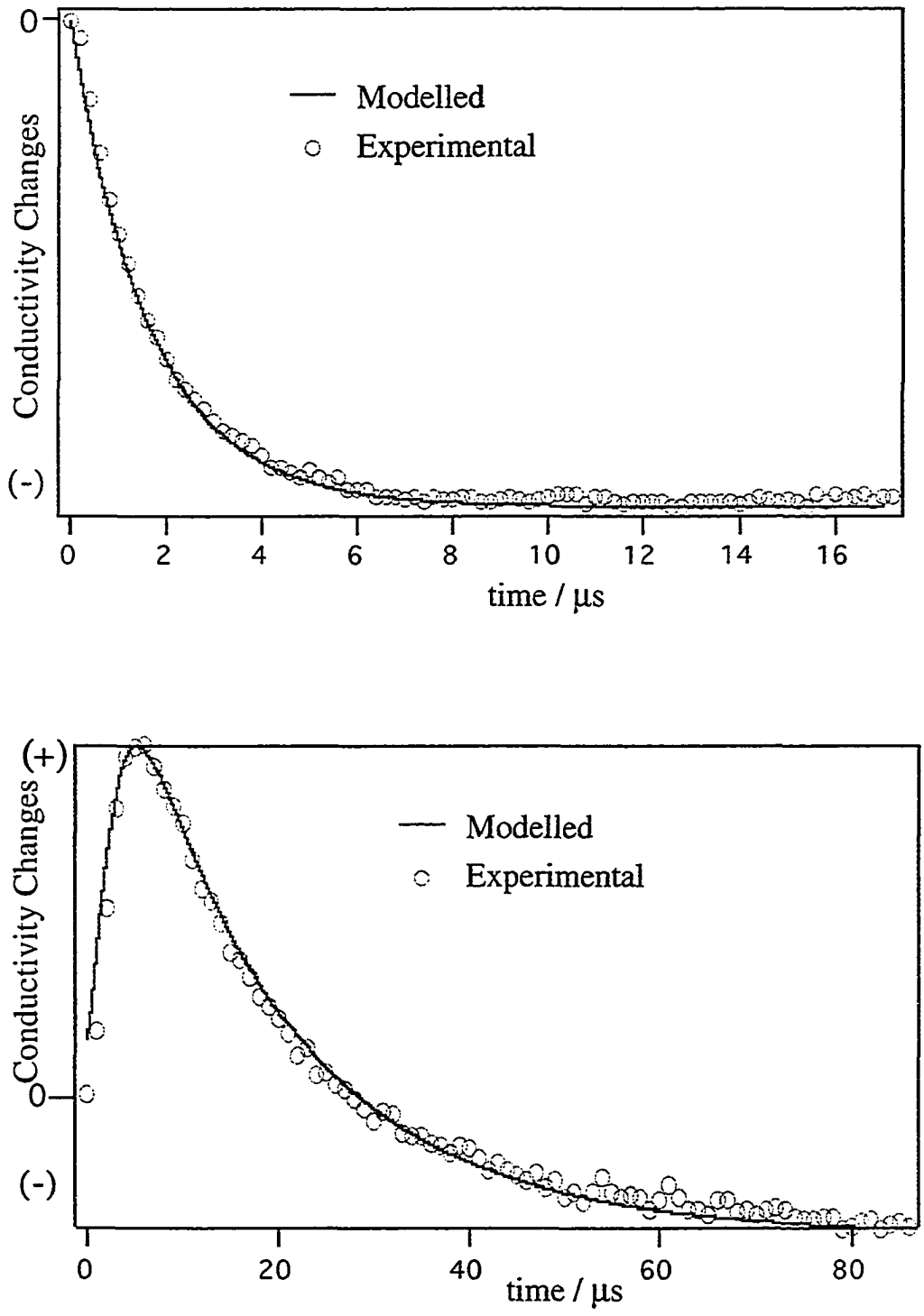

Figure A3.8 Comparison of modelled and experimental conductivity changes for $Cr(tn)_3^{3+}$ at pH 2.89 and 4.70

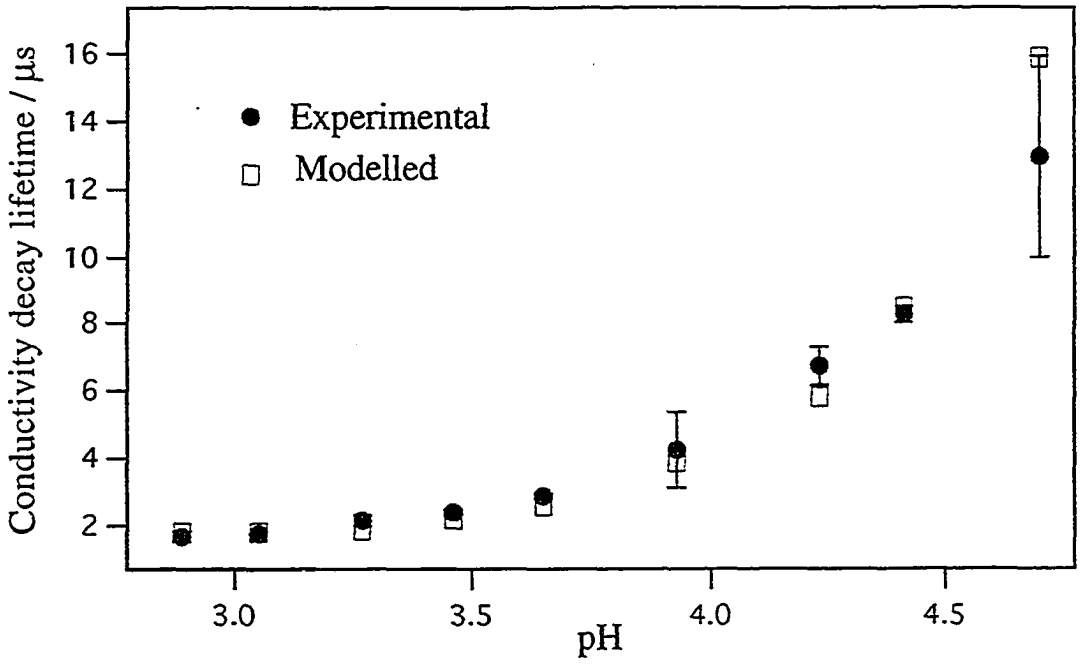

Figure A3.9 Comparison of modelled and experimental decay lifetimes for $Cr(tn)_3^{3+}$ at various pH values.

Appendix 3.4 $Cr(sen)^{3+}$

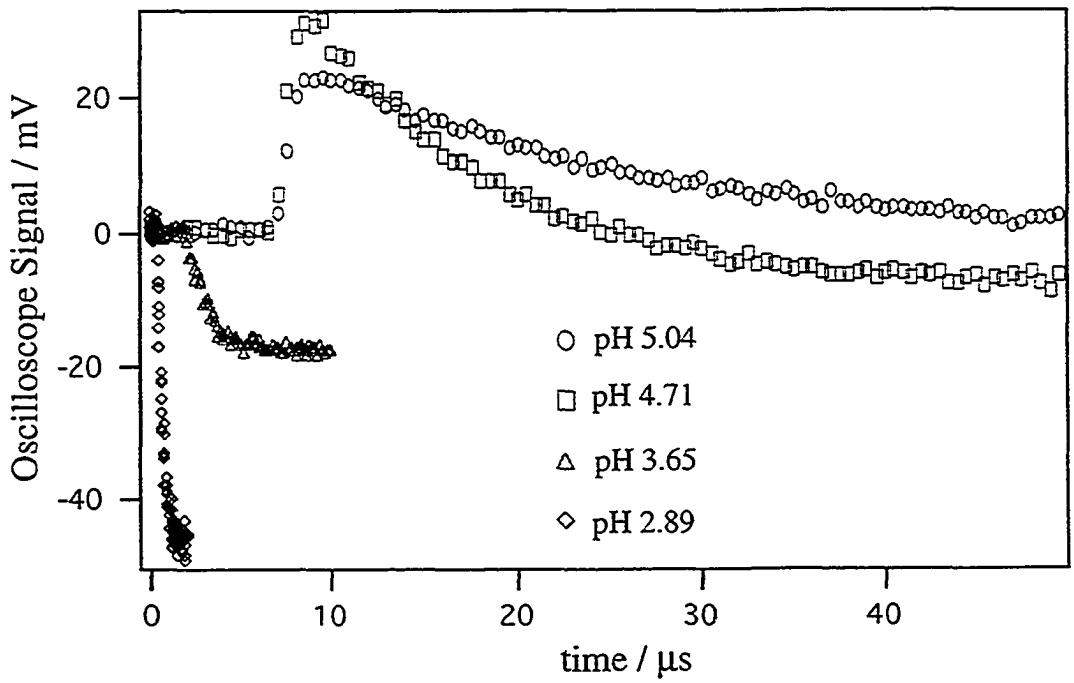

Figure A3.10 Conductivity traces obtained for the laser flash photolysis of $Cr(sen)^{3+}$ at various pH values

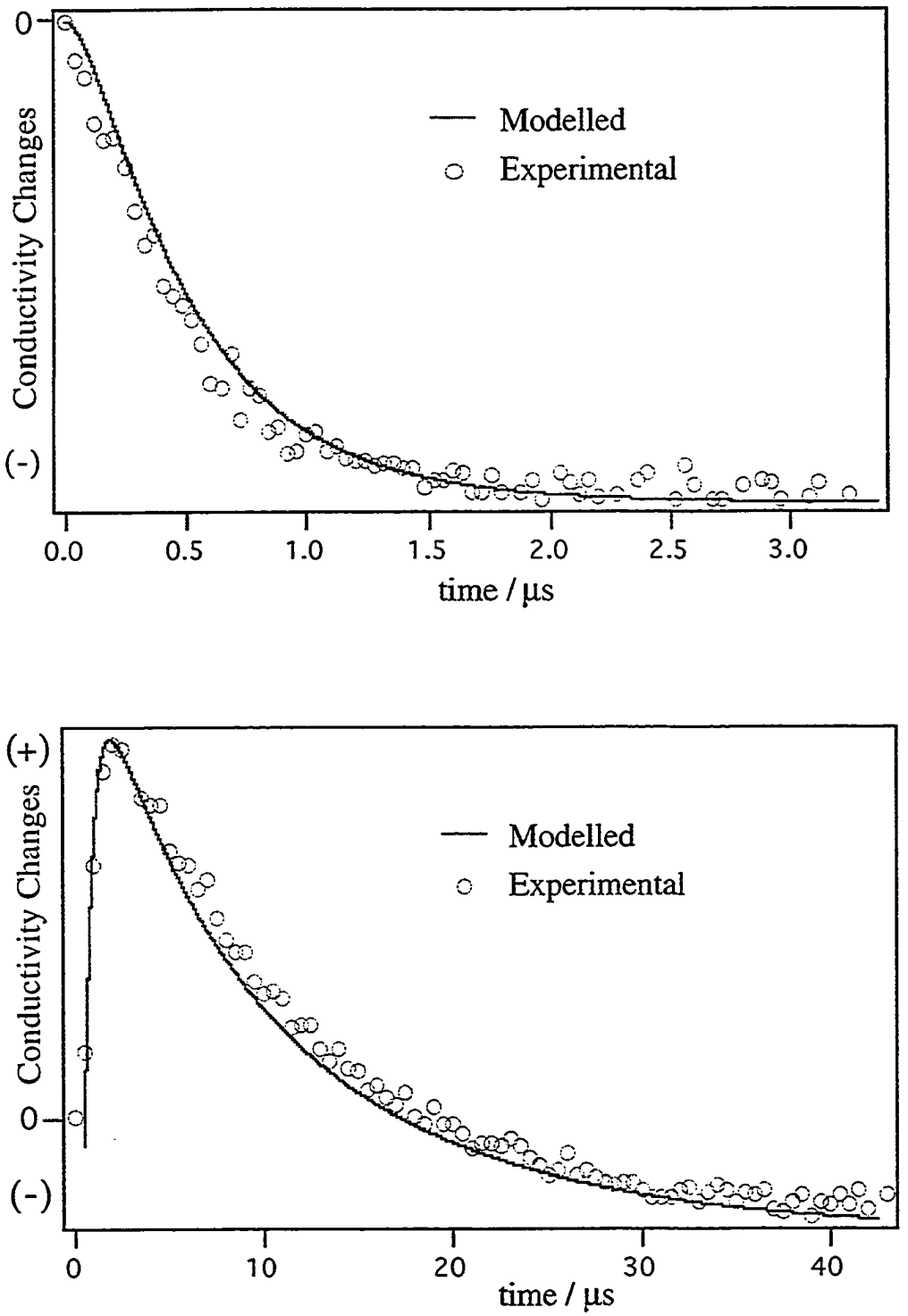

Figure A3.11 Comparison of modelled and experimental conductivity changes for $Cr(sen)^{3+}$ at pH 3.01 and 4.71

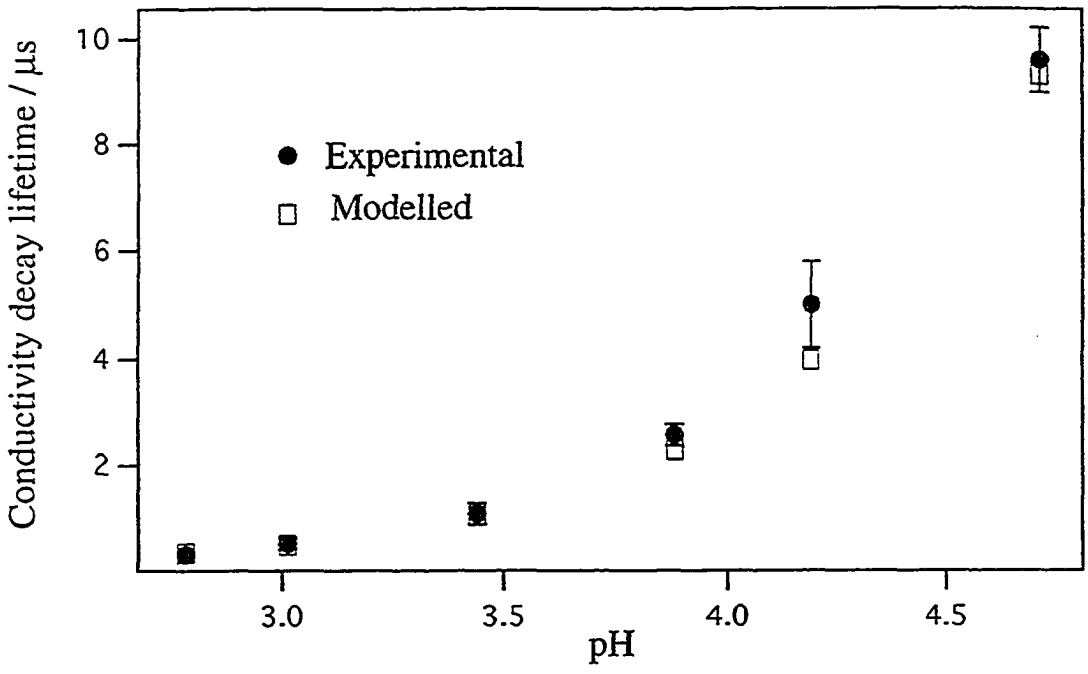

Figure A3.12 Comparison of modelled and experimental decay lifetimes for $Cr(sen)^{3+}$ at various pH values

APPENDIX FOUR

CRYSTAL STRUCTURE OF *cis*-$Cr(cycbH)(NH_3)_2Cl(ClO_4)_3$

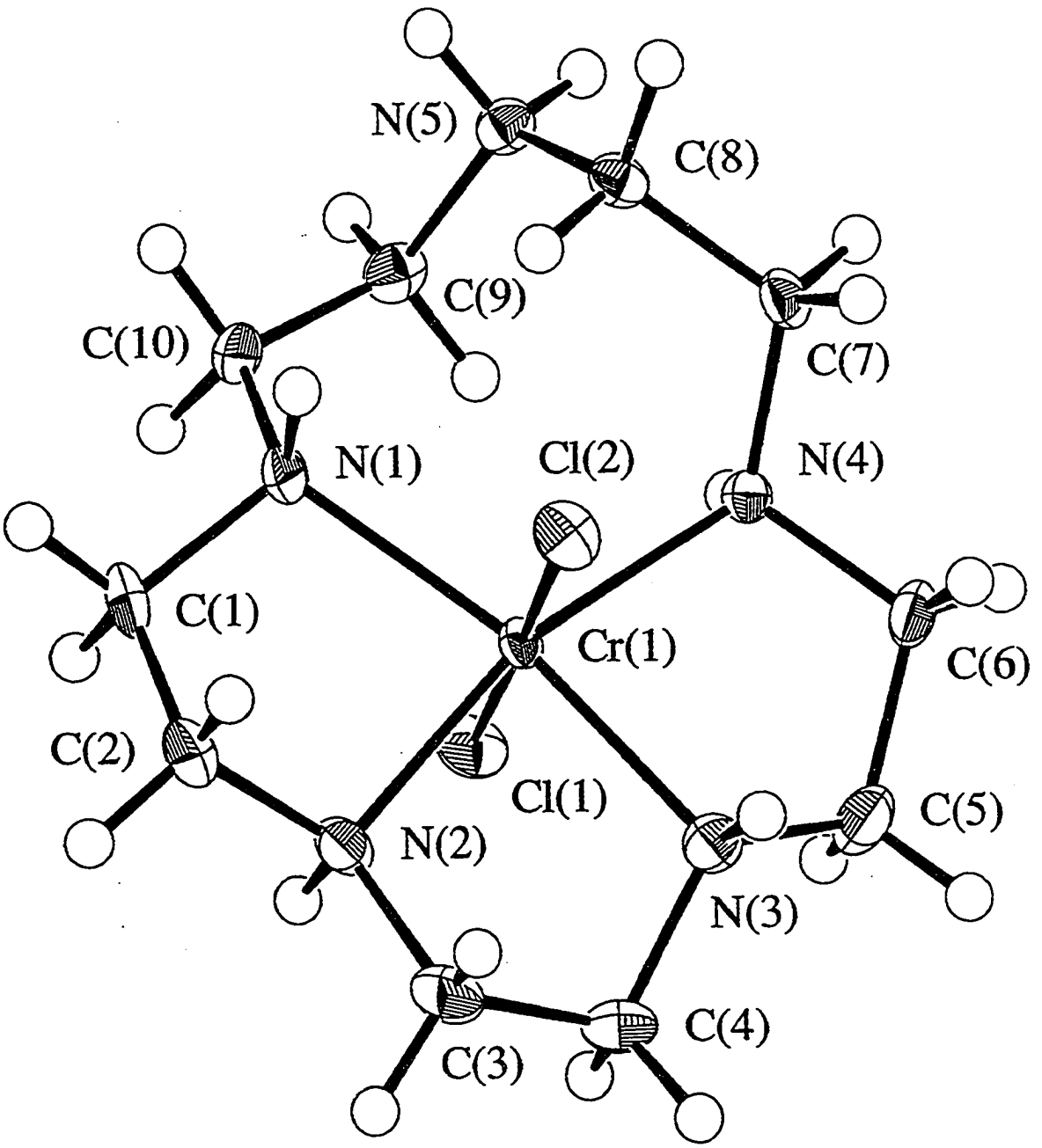

Figure A4.1 X-ray crystal structure of product obtained in attempted synthesis of $[Cr(15aneN5)Cl](ClO_4)_3$